A Three Dimensional Vision System for Industrial Surface Topography Measurement.

by

Matthew C Reynolds

Submitted for a PhD Degree on 27th August 1990 and sponsored by

Thames Polytechnic

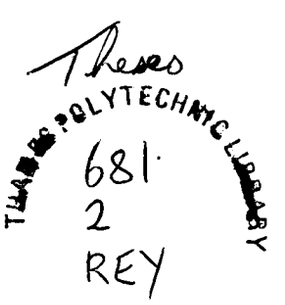

Contents.

A Three Dimensional Vision System for Industrial Surface Topography Measurement.

M.C.Reynolds

This thesis is concerned with a research programme into a triangulation based Surface Topography Measurement (STM) system. The particular system investigated produces a series of three dimensional coordinates of points on a target surface which has been placed in front of the STM system. It is designed for use at long ranges (5m - 20m initially) and onto rough surfaces (a selection of natural materials with particle sizes up to 1cm). The system uses a laser triangulation method with a single spot projected onto the target surface and through movement of the spot over the surface a range map is built up. A simple model which describes the STM system is presented along with an equation which gives the range error, any effects on the model by the physical implementation of the STM system are then described and quantified. Performance tests carried out on the system are described and a second version of the system is then outlined which addresses deficiencies isolated in the original system. A more detailed discussion of how the range errors arise is also given. New hardware enables the received laser spot's distribution to be analysed and processed so that, in certain cases, subpixel resolution of the centre of the laser spot can be obtained. Expansion of the laser spot and varying the parameters of the optical system are examined to assess their effect over different target materials and estimates of the possible range accuracy are also given.

These results presented will be used to assess the applicability of the system for use in an industrial environment. Further work connected to this research area and several industrial applications are also detailed.

Chapter 1: Three-Dimensional Vision Systems and Surface Topography.

This chapter is divided into two main sections. The first will outline the possible optical techniques which have been reported in the technical literature for obtaining the three-dimensional (3-D) coordinates of a surface, or objects, present in a target scene. The second section will describe the characteristics which are deemed important in a 3-D vision system for industrial surface topography measurement and, using these desirable characteristics, one of the techniques will be selected to form the basis of the Surface Topography Measurement (STM) system.

1.1 General Survey of Three-Dimensional Vision Techniques and Systems.

Three-dimensional vision techniques can be divided into two main categories, that of passive and active systems. The difference between the two types of systems are that, in an active system, an external source of light (this is normally a laser since the laser beam has the properties of being monochromatic, coherent and having a small divergence which leads to small beam diameter) is used to project some light energy into a target scene. A light sensing device (e.g. a camera) is used detect this energy and some property of this reflected energy is used to determine the 3-D coordinates of the area, in the target scene, onto which the light energy was projected. In a passive system, although the lighting conditions may be altered to achieve a better signal to noise ratio in the light sensing device, it is 'features' in the target scene that form the measurement objects and it is the 3-D coordinates of these 'features' that are obtained.

A description of the passive and active techniques which have been reported in the technical literature will now be presented. Each

description will be followed by a critical review which will highlight any major drawbacks of the particular technique.

1.1.1 Passive Techniques for 3-D vision.

The passive techniques which are described in this section fall into two main types: those that use a single sensing device and therefore usually require *a priori* knowledge of some properties or characteristics of the objects or surface which is to be measured, and those that use two or more sensing devices. Monocular techniques will be described first and techniques that require two or more views of the target scene will follow after.

1.1.2 Depth from Texture, Occlusion Clues and Focus.

Assuming that the object of interest within the field of view of the camera or sensing device has some texture properties, it is clear that as the object is moved further away from the camera the texture markings on the object will appear closer together, from these texture clues it should be possible to infer relative distances between objects which have similar texture markings (with no more information these inferences can only be of the kind 'object A is behind object B', 'object A is equidistant with object B', etc). If primitive geometric texture elements can be defined or some property of the texture be defined at a known distance from the sensing device the actual range of any similar textured object can now be calculated. The use of texture gradients (obtained from the 2-D Fourier transform using a window which is obtained by segmenting the image into square regions of similar texture, see Jarvis [1]) has been demonstrated but several serious drawbacks must be noted. These are; that the image must undergo initial

segmentation before the texture gradients (and consequently any depth measurements) can be obtained; that prior knowledge of the object texture is needed and only objects that have surface texture can be used and lastly, that certain orientation of objects within the scene can produce apparent texture changes.

Depth from occlusion clues (see Jarvis [1]) is similar to depth from texture due to the use of texture and colour clues to drive the initial segmentation process. As explained in Rosenfeld et al [2] relative distance can be inferred by using six possible occlusion cases (based on the extent to which one region occludes another) and assigning one of these cases to each region (the regions being obtained through the initial colour/texture segmentation) via a scheme of relaxation labelling. Deficiencies identified with this technique are that it produces only relative depths, that colour and texture clues must be present on objects in the scene for the initial segmentation and that if no occlusion is present between two regions of the scene, no depth information can be inferred to link the regions.

The last technique to be considered in this section on monocular depth measurement is depth by focusing. This technique, unlike the previous two described in this section does not require any *a priori* knowledge of the surface or objects whose range is to be determined. This technique requires a lens with a large aperture (to achieve small depth of field) which can be moved so that a sharp focus can be obtained. Using simple lens theory the object distance (range) can be obtained from a measurement of the image distance (provided the focal length of the lens is known). A problem is identified that some measure is needed to indicate that a sharp focus has been obtained, in Jarvis [3] several possible measures are presented. One such measure which is

suggested is to define a square window in the image and calculating the variance with each possible focusing position, a sharp focus is indicated by a maximum being obtained from the variance function. It is assumed that to produce a reliable measure of when a sharp focus has been obtained several simple measures would be combined with appropriate weighting functions and the result of this new function used to decide on which of the possible focusing distances to select. Possible problems will occur with increasing range (an increasingly fine measurement of the image distance, which will be approximately equal to the focal length, will be needed) and the simple sharpness of focus measures will not work in regions which have few features in them (i.e regions of a single colour/luminosity which have no texture markings).

In this section, several monocular techniques, used to obtain the 3-D range coordinates of target surfaces, have been described and appraised. In the following section, binocular techniques for 3-D vision will be considered.

1.1.3 Range from Stereo Disparity and Motion.

Stereo disparity is the process by which the position in an image of a distant point will change if the sensing device is moved laterally to the range axis. Obviously the same information can be obtained with two or more static cameras which have been orientated so that they are viewing the same scene and have been placed a known distance apart from one another. There has been great interest in stereo vision due to its links with the visual mechanism of humans and animals, and there are many papers in the literature which describe the use of stereo disparity (Gennery [4], Marr [5], Grimson [6], Bardy et al [7]) with the

basic principle shown in figure 1.0.

All the texts outline the need for 'interest' points to be present in the two images, these can be low level features such texture or surface discontinuities (large changes in grey level), or high level features such as line segments (derived from edges of objects present in the scene) or regions (of similar colour, texture, etc). These 'interest' points are isolated in one image and then the occurrence of the same 'interest' point is found in the second image so that the disparity can be calculated. This highlights the main problem with the stereo disparity technique which is finding the corresponding 'interest' point unambiguously in both the right and left images. One possible algorithm proposed to solve the problem of the correspondence search are given in Marr [5]. In this algorithm two constraints, which when used produce the simplest (continuous) surface interpretation, were defined, these are:

1. Uniqueness. That each feature can only have a single disparity value.

2. Continuity. For the majority of a real scene, the disparity values change smoothly.

Now this algorithm is best visualised as a three-dimensional graph, illustrated in figure 1.1. In this figure, the z axis of the graph has units of vertical pixel widths and represents stepping vertically up the left and right image sensors. Each z index defines a horizontal strip in the left and right images, now the visual information contained within the horizontal strip in the right and left images form the x and y axis respectively for that particular z index.

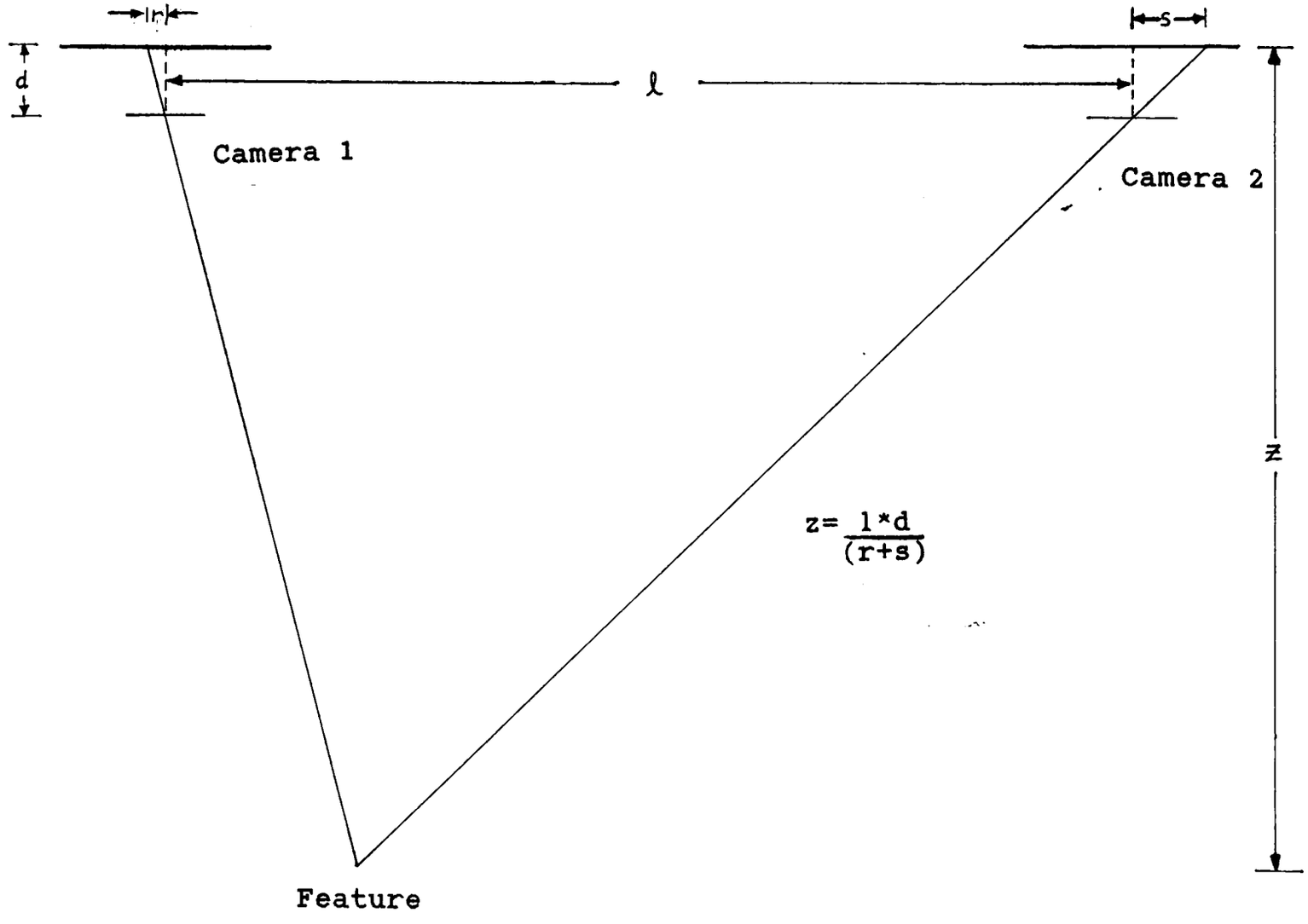

Figure 1.0 An Illustration of the Stereo Disparity Technique.

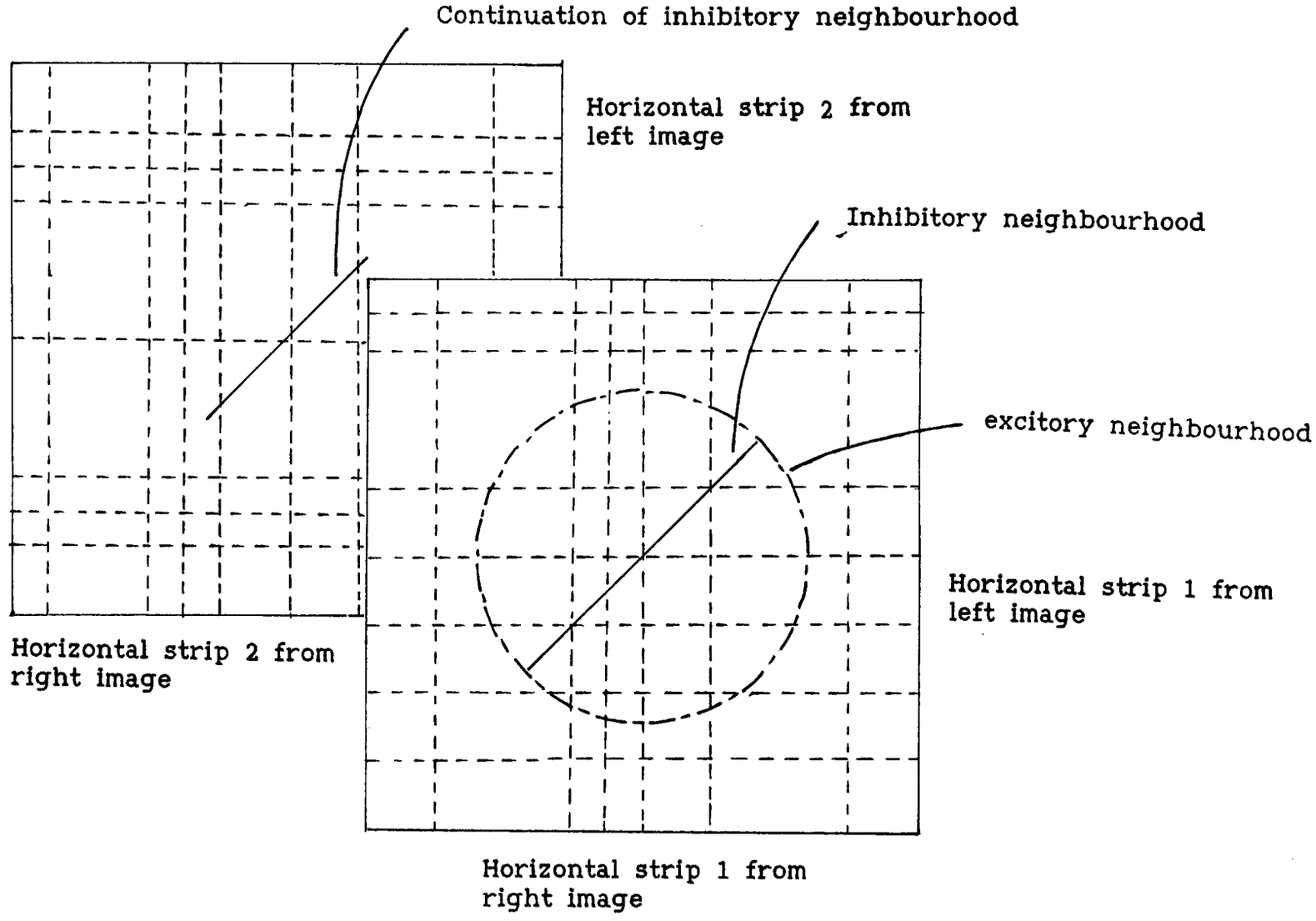

Figure 1.1 An Illustration of the Three-Dimensional Stereo Disparity Algorithm.

Vertical and horizontal lines are now drawn from 'feature' points on the x and y axis respectively (in Marr [5] random dot stereograms were used as the input images and therefore the 'feature' points were just black dots) and the intersection of the horizontal and vertical lines form all the possible matches (and therefore a range of disparity values) for 'features' in the left and right images. Now using condition (1) stated above it is noted that each horizontal and vertical line can only have a single true match, so a target match is selected and a neighbourhood, in the x-y plane of the target match, is defined which contains the all the possible matches (contained within the finite sized neighbourhood) on the same horizontal and vertical lines as the target match. This is defined as the inhibitory neighbourhood. Using the second constraint defined above, that disparity values usually change slowly, an elliptical neighbourhood is defined in the z plane (which appears as a 45 degree line segment in the x-y plane of the target match) with the target match at its centre, this is defined as the excitatory neighbourhood. These two neighbourhoods form the basis of an iterative scheme whereby the number of possible matches in the excitatory and inhibitory neighbourhoods are summed and then subtracted, the resultant value is operated on by a threshold function and this value decides whether the target match is retained as a possible match (assigned a probability of 1) or removed as a false match (assigned a probability of zero). This algorithm is used on all possible matches until each vertical and horizontal line from the features in the left and right images only contain a single match, this convergence is dependent on several factors which include the nature of the threshold function, the size of the inhibitory and excitatory neighbourhoods, the number of iterations of the algorithm

and finally the image content. This algorithm has been shown to work well with random dot stereograms and the two constraints defined above still form some of the central assumptions of any correspondence match algorithm (Grimson [6]).

A different approach was adopted in the system described in Gennery [4] where square match windows are defined in one of the two stereo images and tentative matches are obtained in the second image. The matches are initially obtained from a correlation operation between the window defined in the first image and successive search windows in the second image. Once several matches have been found and their corresponding disparity values calculated, these are used so that tentative search windows can be identified in the second image for areas in the first image which are spatially near to the matched area. This simplification of the search strategy is an implementation of the constraint proposed by Marr [5] (which has been stated above) that in for the majority of most real scenes, disparity values change smoothly. An example of a recent system that has appeared in the literature is that of a trinocular stereo system (Brady et al [7]). This consists of a three cameras unit with the normal two camera stereo set up and a third camera mounted above and between the other two, the disparity calculations are made using high level features extracted from the images (these are linear line segments which are obtained for edges which have been extracted using a simple Sobel edge detector, Gonzalez and Wintz [42] and Fairhurst [52] provide descriptions of Sobel edge operators), the third camera helping with solving the 'feature' matching algorithm.

The main drawback associated with the technique of stereo disparity for 3-D vision is that the scene that is being viewed must

have some definable features which can be used to drive the particular stereo matching / disparity calculating algorithm. Another disadvantage, which is also true of any static vision system that has triangulation as the basic mechanism used for calculating the 3-D coordinates of a image feature, is that since the two images are obtained from different positions the possibility exists that a feature in one image may be occluded in other. This means that any algorithm used for calculating the stereo disparity must include some form of timeout criteria (such as a maximum number of tries to find a match or a maximum amount of processor time to be expended on a single prospective match) so that the present match can be abandoned as unobtainable and a new match attempted.

The last technique to be considered under the category of passive 3-D vision systems is depth via motion, and this can be divided into two main methods. The first method uses a camera mounted on a moving unit which takes several static views at known distances apart and uses the techniques which have already been described in the section on stereo disparity to obtain the 3-D coordinates of objects in the target scene, this is illustrated in figure 1.2. The advantage of using several views instead of just two views is that the problem of occlusion is relaxed. This is because of the probability that the occluded feature will appear in one of the views, and therefore, can eventually be matched. This advantage is offset with increased computation since features now have to be matched in several images rather than just two. Most systems which use this method (see Stephens [8]) use some form of relaxation scheme which operates on each view, increasing the confidence level of features which are matched in several views. Another advantage of this relaxation scheme is that the system becomes

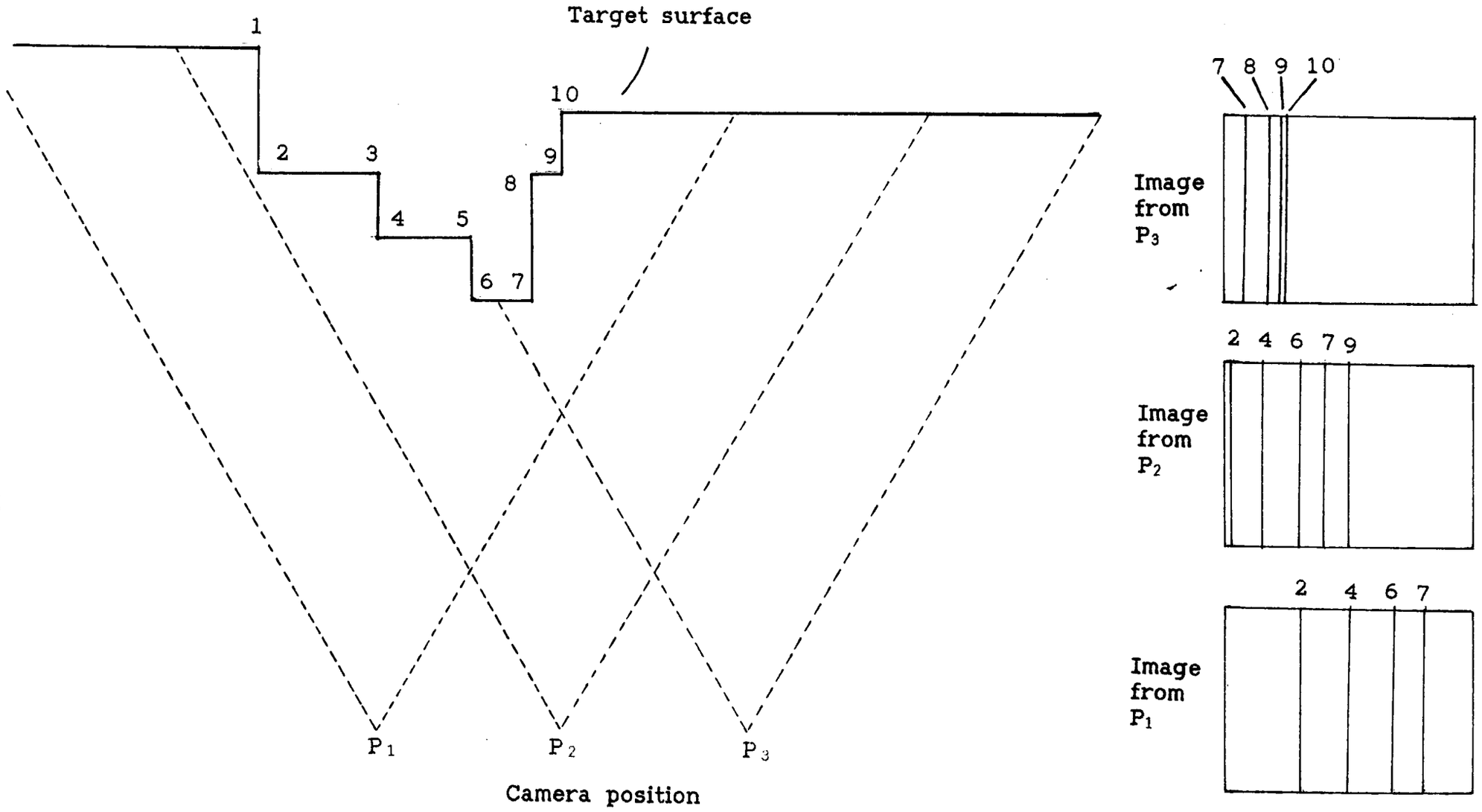

Figure 1.2 An Illustration of the Depth-Via-Motion Technique.

more insensitive to noise present in the image acquisition unit which can cause false matches in simple stereo systems. Since again features must be present in the target scene the disadvantages of this method are the same as described for stereo disparity.

The other main method in the category of depth from motion is that of optical flow, in this method the camera is stationary and the object moving (see Buxton et al [9]). This method will not be considered because the criteria, that the objects in the target scene be must be in motion, is considered too constrictive for a general system.

1.1.4 Active Systems for 3-D Vision.

This section describes the 3-D vision techniques and systems that use active illumination. These techniques fall into two main categories: those that use some form of triangulation measurement and those that use a time-of-flight mechanism for obtaining the range coordinate. The triangulation techniques can use both a single sensing device and stereo sensing device, whereas the time-of-flight techniques use only a single monocular view. The triangulation techniques will be explained first, followed by the time-of-flight techniques and a subsequent section will explain any methods that cannot easily be fitted in the above two categories.

1.1.5 Triangulation Techniques for 3-D Vision using Active Illumination.

The simplest active triangulation technique has a photo sensitive device and a laser light source mounted a known distance apart (Smati et al [10], Livingstone and Rioux [11] and Dremel et al [12]). The laser

light source projects a spot of light into the target scene at known horizontal and vertical angles relative to defined horizontal and vertical reference planes. The horizontal displacement in the image of the laser spot gives an indication of the range. This is shown in figure 1.3 along with a equation which gives the range in terms of the projection angles and an angle derived from the laser spot's horizontal displacement. The above discussion assumes that the laser spot can be distinguished, without ambiguity, from other visual information within the scene. This can be achieved by preventing all the non-relevant information from reaching the sensing device by means of an optical filter which has a passband located at the wavelength of the monochromatic laser used. This means that the output from the sensing device should contain only a signal associated with the laser spot, together with random noise introduced by deficiencies present in the sensing device and any ambient illumination present in the target scene at the laser wavelength. It is evident that to obtain the 3-D coordinates of a whole of the target scene, the scene is spatially sampled by the laser spot. Assuming that a grid of N horizontal and M vertical positions (that is N * M spot positions) are adequate as a sampled representation of the target scene, the time taken to obtain this complete 'range image' is the time for 'range image' acquisition and is equal to N * M * individual frame time (e.g. if N = M = 16, the range image acquisition time is equal to 256 individual frame times).

Moving on to another variation of the triangulation technique, it can be seen (and is shown in figure 1.3) that the horizontal position of the laser spot in the photo sensitive device conveys all the information that is needed to calculate the depth coordinate. This

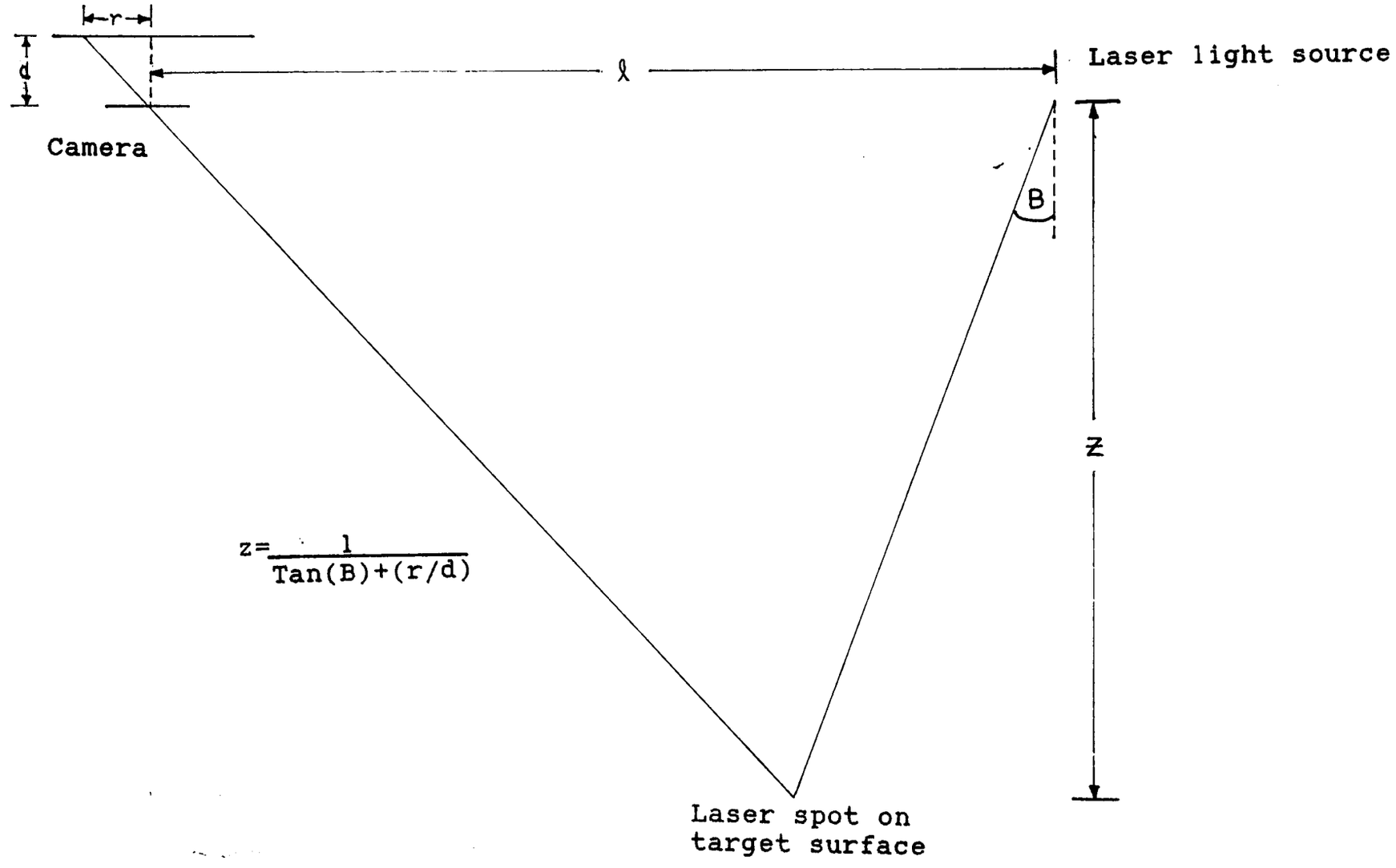

Figure 1.3 An Illustration of the Active Triangulation Technique.

means that a vertical stripe of laser light can be used instead of a single spot (see Kreis et al [13], Reid at al [14] and Nicolas and Hermann [15]) without the introduction of any ambiguity into the measurement needed for the range calculation (z coordinate). The stripe of laser light is moved horizontally across the target scene and this produces a decrease in the time required to acquire the complete sampled 'range image', which was defined in the previous paragraph, since the required horizontal resolution will define the number of individual frame times needed (16 in the above example). Another direct consequence of using the light stripe is that the vertical resolution is increased to the number of picture sensing elements (pixels) defined in the vertical plane of the sensing device (assuming no occlusion of the laser stripe). The horizontal displacement of the light stripe in a video line needs to be obtained to enable the range to be calculated. As described in Reid et al [14], this displacement can be produced by an electronic counter. This counter is set to zero at the start of a horizontal line and then fed with counting pulses of a known frequency. The signal representing the visual information from a horizontal line of the target scene is monitored and when start of the signal representing the stripe is identified the frequency of the counting pulses is halved. When the end of the signal representing the stripe is reached the counter value is stored and forms a direct measurement of the centre of the vertical stripe (horizontal displacement) and therefore the range data for the stripe can be obtained. This technique has found applications in robotic systems (Brady et al [7]) and in industrial quality control situations (Nicolas and Hermann [15]).

The last extension of this technique which again produces a decrease in the 'range image' acquisition time is that of space coding

(Rosenfeld and Tsikos [16] and Vuylsteke and Ossterlinck [17]). In this technique the whole target area is coded Rosenfeld and Tsikos [16], this is achieved by using several different Gray encoded masks which are introduced between the laser light source and the target scene. Each mask has a Grey encoded pattern of vertical stripes and the target frame is stored after each mask is used (Gray coding is used instead of just straight binary coding because points located on the edge of the wedge can assume the binary intensity value of either the preceding or subsequent wedge causing coding errors, with a Grey coding scheme the maximum error is +/- one wedge location). Areas in the frame are identified from the binary intensity (illuminated or dark) and these coded wedges can be associated with a wedge projection angle and therefore the 3-D coordinates found via triangulation. The code of 1 (dark) in all frames must be reserved for occlusion and the code all 0 (illuminated) in all frames is reserved for an erroneous condition in that the ambient light has saturated the sensing device. To aid the problem of finding the threshold between 0 and 1 (illuminated and dark) a procedure is carried out whereby first the whole scene is illuminated and the image captured and stored, then the whole scene not illuminated and again the image is captured. The threshold for each individual pixel is defined as half the sum of the two values of intensity detected at each pixel location. This should make the detection process only dependent on changes of illumination. For maximum resolution the size of the wedges must be the same as the sensing device's horizontal resolution. The decrease in the time to acquire a complete 'range image' is a function of the horizontal resolution but, for the simple grid that was defined in the first paragraph of this section, the acquisition time is decreased to.

$$\text{Time for a 'range image'} = \frac{\text{Ln(horizontal resolution)}}{\text{Ln(2)}} * \text{IFT}$$

Where IFT is the Individual Frame Time and for the 16 by 16 grid mentioned above, the equation has a value of 4 IFT's.

Another variation on the simple triangulation method (Nimrod [18]) is to use a rotating mirror in front of the laser light source and a rotating lens (which is rotating at twice the speed of the mirror) in front of a sensing device (a centre nulling photodetector). This method removes the need for accurate knowledge of the laser projection angles. The range measurement is obtained from the time difference between the laser light passing straight into the detector (the laser beam being directed along the the system's baseline) and the laser energy collected after reflection from the target. The accuracy of this method is dependent on the stability of the unit employed to produce the rotation but using a dynamic measurement of the rotation time reduces this constraint to just one of short term rotational stability. Nimrod [18] does not describe any scene scanning procedure and therefore it is assumed that it must be connected to some autonomous vehicle or the arm of a robot to produce depth information for the whole of a target scene.

The main advantage of the active illumination techniques described above is that very little, if any, *a priori* knowledge is needed of the surface or of objects contained within the target scene (this statement assumes that monochromatic light which is used for the active illumination is of sufficient intensity so that it can be distinguished from any ambient illumination at the monochromatic wavelength). Other advantages are that the depth information can be obtained with great ease, since in most cases, there is no ambiguity contained in the

sensor information (optical filters remove all the visual information apart from the laser light) and that specific objects of interest within the image can be 'ranged mapped' by introducing manual control over the laser projection angles. The decision on which of the above methods (ignoring the rotating scanner due to the complication of the rotational stability) should be used for a particular application is a speed / equipment trade off (though this is only true assuming that, if space encoding is used, the resolution of the masks is the same as that of the sensing device). The simple spot projection triangulation requires the largest acquisition time for a complete 'range image' but the minimum amount of equipment.

The last technique to be considered under the heading of active illumination triangulation methods is that of 'active stereoscopy' (Aryiaeeinia [19] and Faugeras [20]). This technique uses two cameras mounted in the traditional stereo disparity arrangement (that is two cameras a known distance apart in the same vertical planes and in parallel horizontal planes) with a monochromatic light source which projects a 'feature' into the target scene. Usually optical filters are used in front of the two cameras so that the right and left images only contain the monochromatic 'feature' which was projected into the target scene. Obviously this removes the problem of the correspondence search so that, taking [19] as an example where the 'feature' was a laser spot, the horizontal displacement values from each image can be obtained via a pixel counter associated with each image which is stopped and its value stored on the signal, which represents the laser spot, being detected. This process is carried out in the right and left images simultaneously and the disparity value is just the difference between the stored pixel position values. The advantages of this method

are that the mechanism which deflects the laser spot or 'feature' need not be calibrated since all the information to calculate the range value is obtained from the stereo disparity value. The disadvantages are that only a limited field of view is available (this being the intersection of the two camera's individual field of view, see figure 1.0, which is reduced further if the two camera's are inclined toward one another as in Ariyaeeinia [19]) and extensive initial calibration is required on the two cameras.

1.1.6 Time-of-Flight Techniques for 3-D Vision.

This section on time-of-flight techniques comprises two main methods for obtaining three-dimensional coordinates of a target surface. The first method is an interferometric technique which involves detecting the phase shift between the emitted and reflected signals from a laser (see Page and Hassan [21] and Duda et al [22]). The second method is the classical time-of-flight technique in which the transit time of light pulses are measured (see Kaisto et al [23], Heikkinen [24] and Manninen et al [25]). Both these methods have the advantage over triangulation techniques in that the light emitters (lasers in all above papers) and detectors can be mounted approximately co-axial to one another and therefore remove the problem of occlusion (or shading) which is inherent in all contrived illumination triangulation techniques. In the next two sections the two time-of-flight techniques will be described in more detail starting with the phase difference method.

1.1.7 Range using Time-of-Flight Phase Difference Technique.

In the time-of-flight phase difference technique as described in

Page and Hassan [21], sinusoidal amplitude modulation is performed on a continuous wave semiconductor laser which is directed at the target scene. A detector (an avalanche photodiode which has a fast response time), which is mounted co-axial with the laser, is used to collect any reflected laser energy and the phase difference between the emitted and reflected signals is measured. High frequencies are used for the modulation frequency so that the required range resolution is matched to the maximum resolution of the phase difference measurement unit, often the output of the detector is mixed with intermediate frequency so that the phase difference can be measured at a lower more manageable frequency.

The main disadvantages of this method are the limited range (because of only being able to distinguish up to 2π radians phase difference and therefore measure range equivalent to π radians phase shift), and that the return laser beam reflected from the surface can have a very large dynamic range arising from the surface orientation and the reflectance function of the surface (be it Lambertian, specular or more usually a combination of both). This implies that the signal processing must include non-linear functions to reduce this effect (e.g a logarithmic amplifiers). Lastly all the electronic delays and optical path differences must be quantified and their effect taken into account when the phase difference value is produced.

1.1.8 Range using Time-of-Flight Pulse Time Elapsed.

In this method, as described in Kaisto et al [23], a series of finite laser pulses (approximately 5 ns in duration) are produced and projected onto the target surface. As each light pulse is transmitted it is sensed and a START signal is produced and is sent to a Time to

Amplitude Converter (TAC). The detector (which, as in the phase difference technique, is coaxial with the emitter of the laser light) senses the reflected pulse and sends a STOP signal to the TAC. Since, as mentioned above a stream of pulses are emitted, the outputs of the TAC for each individual pulse are averaged to produce the final result (the pulses are averaged over 10 ms period in [23]). Feedback from a return pulse magnitude detector is also used to reduce the inherent large dynamic range (a ratio of 1:100 due to varying distance and surface reflectance) of the return signal.

The advantages of this technique are, that large distance can be measured (1.5 m - 10 m in Kaisto et al [23]), that the range is not defined by a initial design decision (though it may be limited by noise and insufficient amplitude of the reflected pulse) and finally, the small size of the whole range measurement unit. Disadvantages are the increase in complexity of signal processing due to the high frequency nature of the electronics and the wide dynamic range of the reflected pulse and, since averaging of several pulses are used, the time to acquire a spatially sampled scene is large compared with, for example, light sheet methods.

This method has several disadvantages over the phase difference method (which is described in the previous section). The first of these is that the laser diode is turned off or on and any delays associated with these discontinuities are have to be quantified. Other disadvantages are that the pulse edges can be corrupted with noise and therefore effect the range resolution available and that a reduction in complexity of the 'phase difference' signal processing is achieved through the use of intermediate frequencies.

1.1.9 Miscellaneous 3-D Vision Techniques which use Active Illumination.

In this section two techniques will be considered which do not fit into the two main categories of triangulation or time-of-flight techniques. The first of these is described in Blais and Rioux [26] and illustrated in figure 1.4. In this technique a mask, which contains two small apertures, is placed in front of a sensing device (a camera) and a light stripe is then projected onto a reference plane. The light reflected from the light stripe passes through the two small apertures brought to a focus on the detector. Now a target object is introduced into the scene between the reference plane and the camera and illuminated with light stripe, the image formed will consist of two light stripes (the focus point of the light stripe in the scene is behind the detector plane due to the fact that the image distance has been reduced). Now for each line of horizontal pixels a measurement must now be made to find the horizontal pixel which is at the centre of the two stripes produced in the image, also a measurement of the distance between the two stripes is made. From these measurements the 3-D coordinates of the parts of the object illuminated by the light stripe can be obtained (for detail of coordinate equations and signal processing see [26]).

This sensor has advantage that several light stripes could be used increasing the amount of range information obtained from one camera frame (provided that the stripes do not interfere or cross one another), that the device is small and robust and that stripe projector position is not important. The disadvantages are that the small distance between apertures requires subpixel resolution, that a reference plane must be set and all measurements (if they are to be unambiguous) carried out in front of that reference plane which

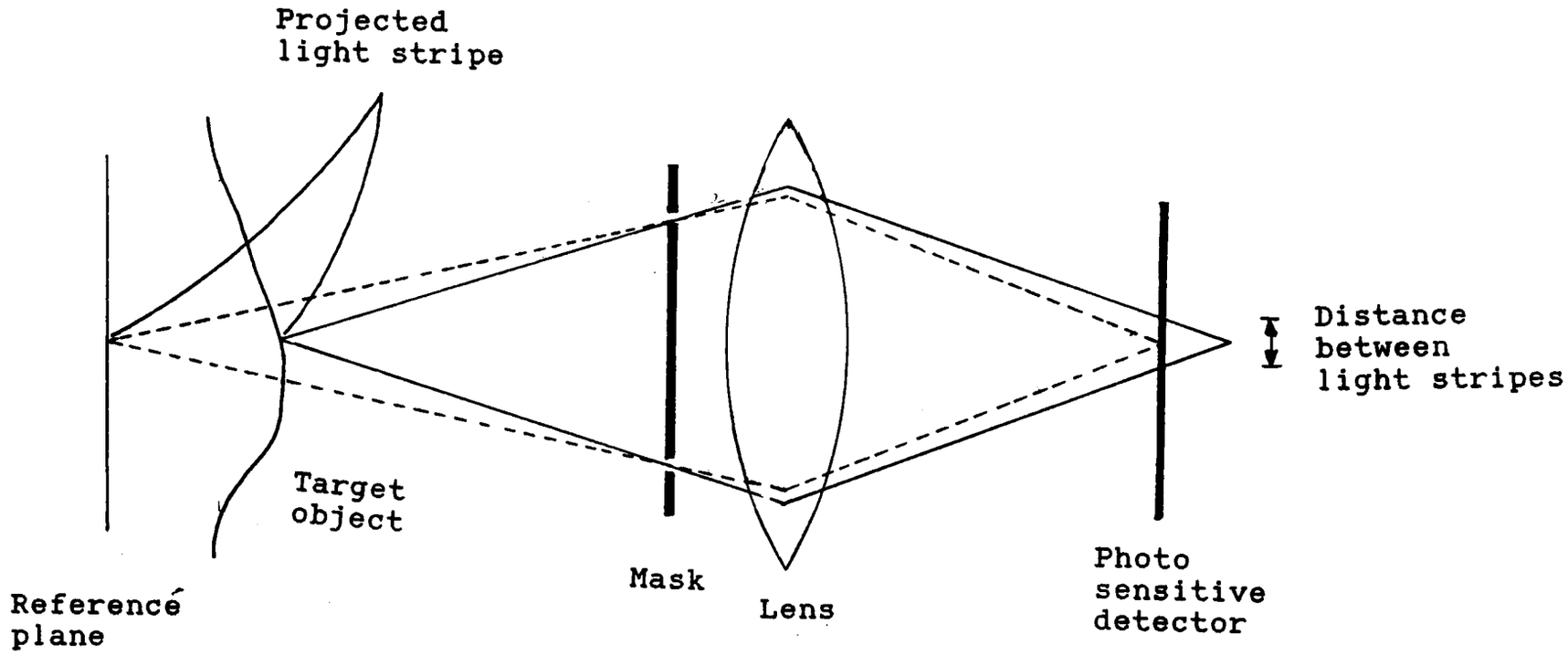

Figure 1.4 An Illustration of the BIRIS Technique.

restricts the possible range.

The second technique in this section is that of digital phase measurement, see Halioua and Hsin-Chu [27], Reid and Rixon [28] and Albert et al [29]. In this method light is projected through a grating onto the target surface, this is then viewed through a second identical grating (in some systems the discrete nature of the camera lines are used as the pseudo second grating, this usually requires some adaptation of the systems optical design). The technique can be visualised by considering a flat horizontal plane (the reference plane) as the target surface, the grating (usually with a sinusoidal structure) will produce regular fringes of light on the surface. These fringes are viewed through the second grating and the image stored. Now the reference plane was removed and a target plane was introduced in its place, the fringes will now be distorted and when this new fringe pattern is compared to the reference stored pattern the resulting image is an interference pattern. It can be seen that this method can be used as a very accurate pass/fail technique for high precision components with the interference fringe pattern from a model component being compared to a component under test. Since the movement in the fringe patterns is proportional to the grating spacing, difference in the region of 10 microns can be detected. TV holography (see Malmo and Løkberg [30] and Ellingsrud and Løkberg [31]) can also be used for this type of quality control situation and in the examination of components under stress but, the literature does not explain how this technique can be used in general 3-D vision system so no detailed study of this method will be presented. In Halioua and Hsin-Chu [27], a method is described which allows range measurements, relative to a reference plane, to be obtained using a device to introduce phase

shifts into the illuminating laser beam and a method of storing the resultant interference images which are taken of both a reference plane and the target surface. Pixels in the stored image change intensity with each change of phase in the input beam and these can be used to calculate the phase difference between the reference plane and the target surface for that individual pixel, this is repeated for all pixels in the image. Provided that the projection angle of the fringes onto the reference plane is known the distance below the reference plane of the target surface can be calculated (the spatial position of this distance in the x-y plane is obtained from the pixels position in the camera's sensing array and the world position of the camera).

The disadvantages of this technique is that several views of the target surface (a minimum of 3) each with different known input beam phase shifts must be obtained (the views of the reference plane can be obtained off line) and that extensive computation is needed to calculate the depth values. Another problem is that all surfaces must not contain large discontinuities since phase changes are restricted to an unambiguous range of 2π.

1.2 Requirements of an Industrial Surface Topography Measurement System.

Now in the previous section (1.1.1 - 1.1.9) most of the optical techniques for 3-D vision have been described. Before the characteristics of an Industrial STM system can be outlined two other possible, non-optical, techniques for obtaining the 3-D coordinates of a target surface will be described. The first of these non optical techniques is ultrasonic ranging Guichard and Renault [32] and Monchaud [33]. This technique is very similar to the time-of-flight Pulsed Time

Elapsed optical technique (see section 1.1.6). Systems incorporating this method usually have a transmitting and sensing device that is often the same unit, ultrasonic pulses are produced and elapsed time between pulses being transmitted and the echo being obtained from the target surface gives an indication of the targets range. The signal processing incorporated in these devices normally uses the average of several pulses to produce a result for the range but, the receiving electronics must only recognise the first echo that arrives since multiple echoes could represent the return from another valid surface in the target scene or a secondary echo of the first return and therefore contain no valid information. The main disadvantages associated with ultrasonic ranging are that the velocity of the ultrasonic pulse (and consequently the range measurement obtained) is temperature dependent, that the beam divergence is large producing coarse spatial resolution and that scanning of the target scene is made difficult by the physical size and rigidity constraints of the receiver/transmitter. The advantages of this method are that the receiver/transmitter is robust and does not require a clear optical line of sight to obtain its range measurements.

The second non-optical alternative to be considered for 3-D 'vision' is to use some form of tactile sensing where contact is actually made with the target surface in the sensing process. A review of some of the available tactile sensors is given in Pugh [34]. Tactile sensing systems are normally used in industrial robotic applications (Taylor et al [35]) where the sensor is mounted on some form of actuator (i.e a robotic arm) which moves the sensor to the object, or part of the target surface, which is to be measured. Since the target surface or object to be measured must be unaffected by the application of the

tactile sensor, the range and accuracy of the 3-D measurements being determined by the actuator on which the tactile sensor is mounted and that, in a complicated scene, the points of interest which are to be range mapped must be identified by some secondary vision system (complete tactile sensing of the scene would involve an enormous time penalty due to the essential small size of the tactile sensor) this technique of 3-D sensing will not be further considered as a possibility for the STM system.

Finally now the desirable characteristics of an Industrial STM system can be outlined and from these considerations the best candidate of the techniques, which have been described above, will be selected and will form the basis of the STM system. These desirable characteristics are now listed

(1) The STM system must be able to obtain 3-D coordinates of a target surface with very little, and preferable no, *a priori* knowledge of that surface.

(2) The STM system should be able to obtain the 3-D coordinates of any desired point in the target scene, subject to horizontal and vertical resolution limits, and not just points that have some visual scene information.

(3) The accuracy of the 3-D depth value should be high, the spatial sampling resolution high (i.e fine resolution possible) and the range should be as large as possible.

(4) The equipment used should be as simple as possible and resilient to the effects of temperature and atmospheric conditions.

The technique selected is that of single spot triangulation, for the following reasons: Criteria (1) and (2) effectively rule out all passive techniques (knowledge of texture, features, etc essential and would form only possible range measurement points) and those techniques presented in section 1.1.7 (in which a smooth change is required in the target surface for unambiguous measurement i.e no range discontinuities). The only *a priori* knowledge needed in single spot triangulation is that the the ambient light intensity is low enough at the laser wavelength so that the laser spot can be distinguished from the background and therefore detected unambiguously and that the surface to be measured is within the minimum range of the system. Criteria (3) removes the possibility of using time-of-flight phase difference (limited range) and ultrasonic ranging (limited spatial resolution due to divergence of beam). Lastly, criteria (4), with its statement of simplicity, removes the techniques of active stereo disparity (limited range and extra camera needed over single spot triangulation), space encoding (complicated pattern projection), time-of-flight pulse elapsed time (high frequency specialist receiving equipment necessary) and the statement of robustness would seem to exclude the rotating scanners. The two techniques left are single spot triangulation and stripe triangulation. Since spatial image acquisition time has not been made a critical factor single spot triangulation can be selected as the simpler of these two systems. Another advantage of the single spot triangulation is that the laser power necessary to produce a good signal illumination to ambient illumination ratio is much smaller with the single spot triangulation than with stripe triangulation, and therefore a less powerful, safer laser can be used.

In this chapter a review of three dimensional vision techniques has been presented and the basis of the STM system defined. In the next chapter a description of the geometry of the STM system will be produced and the system equations will be derived.

Chapter 2: The Geometry of the STM System.

In this chapter an investigation will be made into the geometrical aspects of the STM system. The first task is to produce the system equations which will the relate parameters of the system to the cartesian position of the laser spot on the target surface. This will entail the production of models to represent the components of the system. In the next section an equation will be derived which relates the error introduced into the z (range) coordinate when an error is resident in the measured laser position, which will use the equations and models outlined in previous section. Lastly, the physical implementation of the photo sensitive device and laser light source will be explained along with how these diverge from the ideal models presented in section 2.1.

2.1 The STM System Equations.

As a precursor to the production of the system equations, the geometry of the STM system must be explained. As already stated, this will involve producing models to represent the two major components of the system: the photo sensitive device and the laser light source. In the actual STM system the photo sensitive device and the laser light source are composed of several physical components but, for the geometrical description and consequently the derivation of the system equations, simple functional models will be used to represent these complex units. The functional models developed in this section will be reviewed in section 3.2 where a description of the complex physical units which are used to implement the photo sensitive device and laser light source is presented. Any discrepancies between the simple functional models and the actual physical devices (used to implement

the function of the photo sensitive device and the laser light source) will be quantified and used to modify the system equations which will be derived later in this section. This will enable the goal to be achieved of a simple functional description of the STM system but also, an accurate set of system equations reflecting the non-ideal nature of the physical system.

2.1.1 The photo sensitive device.

The Photo Sensitive Device is used to gather the light energy which has been reflected from a target surface due to a laser spot being projected onto that surface. The photo sensitive device is to produce an indication of the spatial position where the laser spot appeared in the photo sensitive device's field of view. The simple model which will be used in the geometry definition is shown in figure 2.0(a). This model is effectively a pin hole camera, and its operation will now be described. Light passing through the pin hole strikes a series of photo detectors placed in a regular two dimensional array. Each photo detector has a horizontal and vertical index associated with it and, when a particular detector (from now on referred to as a pixel) is illuminated, its horizontal and vertical indices can be obtained. The horizontal resolution of the system is related to the distance between the sensor array and the pin hole at which the light enters, a distance d, and the pixels horizontal width, a distance px.

$$\text{Horizontal Resolution} = \text{Tan}^{-1}\frac{px}{d} \approx \frac{px}{d} \text{ rad since } px \text{ is small}$$

In the discussion of the systems geometry it will be assumed that the pixel's size is small enough so that the horizontal (or vertical)

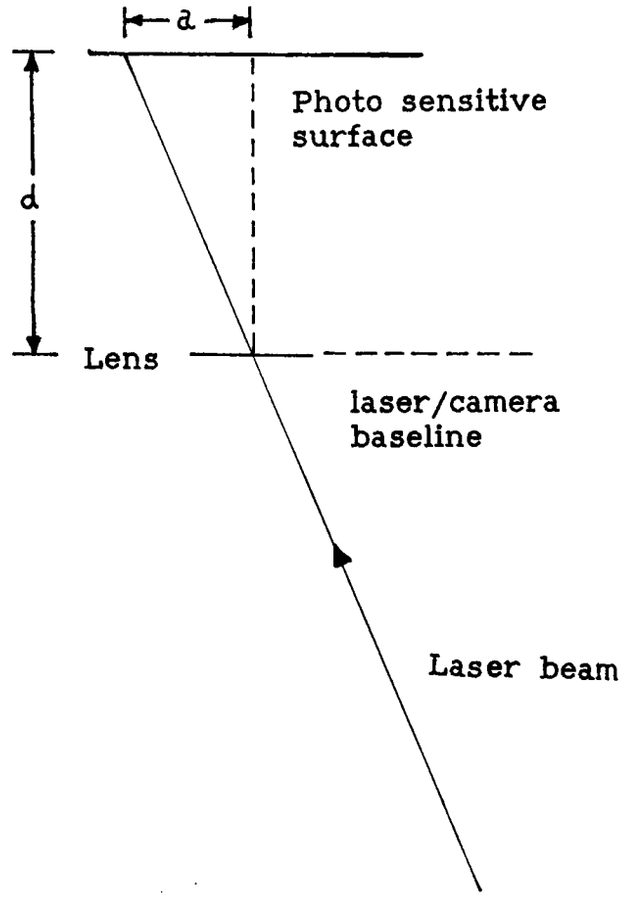

Figure 2.0(a) The Photo Sensitive Device Model.

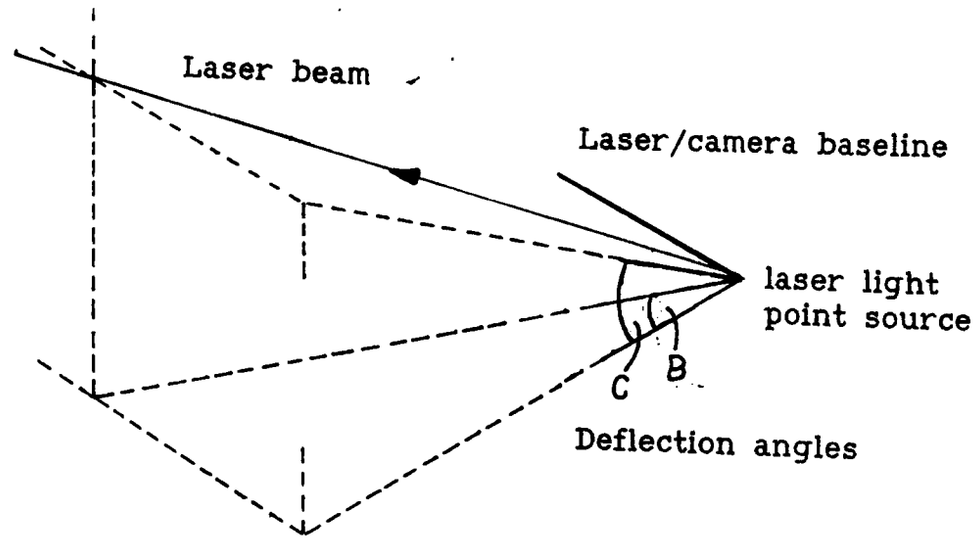

Figure 2.0(b) The Laser Light Source Model.

index obtained represents a continuous, rather than a discrete, measurement of the laser spot's displacement along the sensing array. This displacement value can be converted into a horizontal (or vertical) angle which is measured relative to a line which is constructed perpendicular to the sensing array and with its origin located at the centre of the array, this line is referred to as the 'sight line' of the photo sensitive device.

2.1.2 The laser Light Source.

The model used for the laser light source is shown in figure 2.0(b). The model consists of a point source which produces a narrow beam of laser light, this beam can be deflected in both the horizontal and vertical planes, creating angles B and C respectively relative to the 'sight line' of the laser light source. The 'sight line' of the laser light source is a line constructed to the front of the point source and along the intersection of the vertical and horizontal orthogonal plane which pass through the point source. The beam diameter increases with distance from the source such that the laser beam can always be contained within a single pixel of the photo sensitive device at any distance, that is.

$$\text{Laser Beam Diameter} = \text{distance} * \frac{px}{d}$$

2.1.3 The System Geometry.

Now that models which represent the photo sensitive device and the laser light source have been produced and all the relevant parameters defined, the geometry of a single point measurement to a target surface is described below and shown in figure 2.1. The model representing the

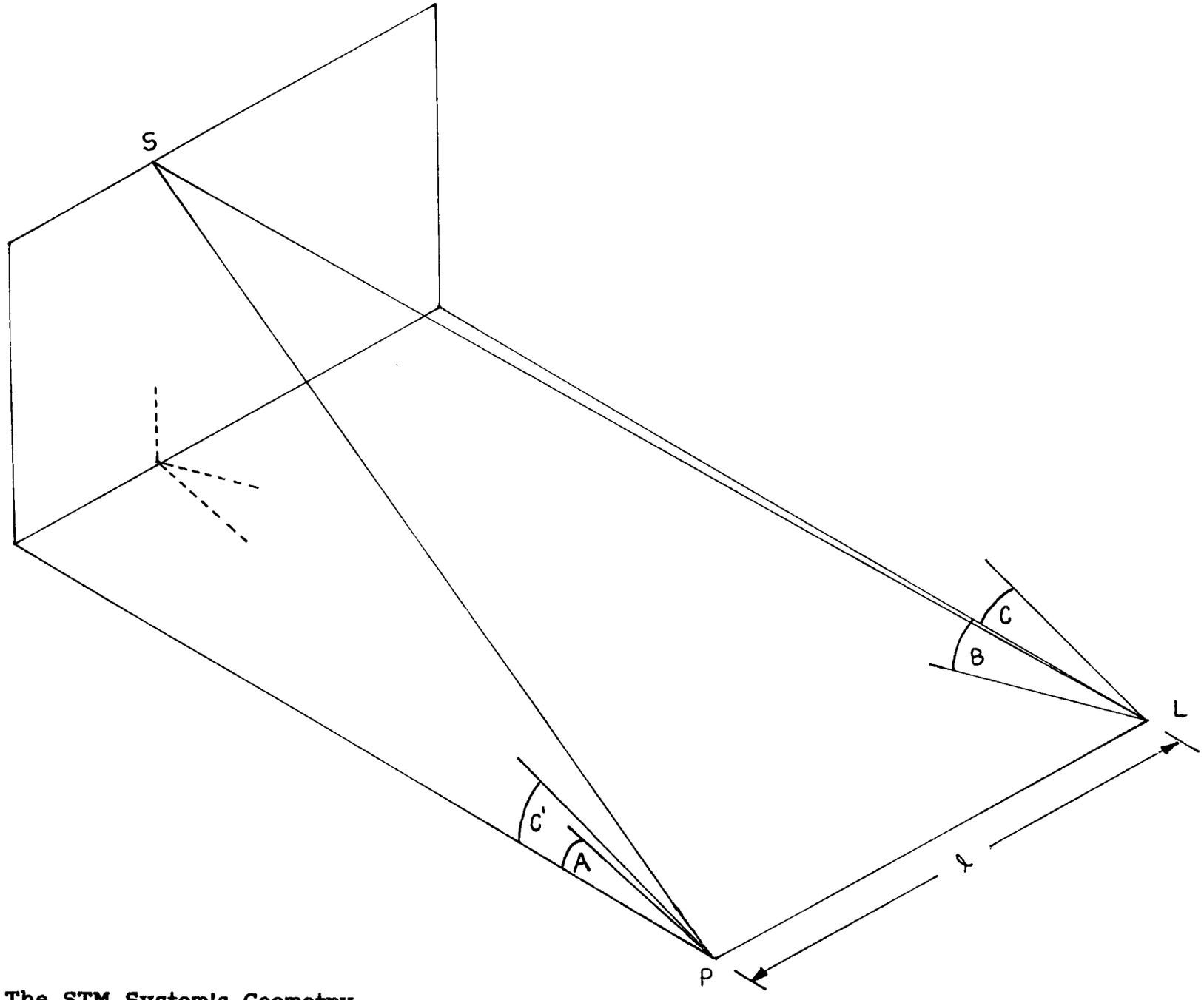

Figure 2.1 The STM System's Geometry.

photo sensitive device (designated P) and the model representing the laser light source (designated L) are placed a distance *l* apart with the 'sight line' of each model parallel and contained in the same horizontal plane. A surface is now defined for the laser beam to strike as a vertical plane perpendicular to the horizontal plane but parallel with the baseline PL, the laser beam is now projected from L with a horizontal angle B and a vertical angle C (these angles are as defined in the laser light source model) to a point S. Some of the scattered laser energy returns to P through the pin hole, the path of this light projected into the horizontal plane makes an angle A with the 'sight line' of the photo sensitive device at P. This angle, along with the vertical angle C', can be obtained from the horizontal and vertical indexes of the photo sensitive device as explained above in the model description.

The cartesian coordinates of the point S are calculated using an origin located at the pin hole of the photo sensitive device. The system parameters used are the horizontal and vertical deflection angles (angles B and C respectively) and the horizontal angle obtained from the horizontal index of the photo sensitive device (angle A). Provided the distance PL (*l*) is known, the following equations provide the cartesian coordinates of the laser spot.

$$z = \frac{l}{\mathrm{Tan}(A) + \mathrm{Tan}(B)} \qquad (1).$$

$$x = (l - z * \mathrm{Tan}(B)) \qquad (2).$$

$$y = z * \mathrm{Tan}(C) \qquad (3).$$

The angle C' which is also obtained from the photo sensitive device is redundant since it has the same magnitude as angle C, however

this angle can be used to check the validity of the received angle A. This application of the vertical angle in error checking will be detailed in a later chapter.

The process described above can be repeated many times with a pre-defined scan pattern for the laser deflectors so that a profile can be built up of the target surface topology.

2.2 Initial Range Accuracy Calculation.

Referring to section 2.1.1 it can be seen that the angle A (or angle C') is not directly produced but an index, relating to the position of the illuminated pixel in the two dimensional photo sensor array, is obtained. The translation of this index into the required angle, or more correctly tangent of the angle, is performed by subtracting an offset equal to half the total number of pixels in that particular direction and then multiplying the result by the resolution in the same direction, therefore for the horizontal angle A.

Tan(A) = (horiz_index - max_horiz/2) * horizontal resolution

Where the horizontal resolution is *px/d*. In section 2.1.1 the simplification of very small pixel size was made so that the general system equations could be produced in terms of continuous measurements, this simplification is now removed so that Tan(A) (as defined in the equation above) is constrained to a finite number of discrete values. The resolution of Tan(A) measurement is, as stated in section 2.1.1, directly proportional to the pixel size.

The angles B and C are actually produced by the STM system as horizontal and vertical deflection angles, the accuracy of the angles depends on the calibration of the deflectors, the resolution of the

deflectors driving signal and their internal stability of both deflectors and drivers. Assuming that the errors occurring in angle A will be far greater than those in either angle's B or C (which can be removed by off-line calibration for a pre-defined scan pattern), an equation will now be defined to quantify the z (range) error associated with an error in angle A.

Referring to figure 2.2(a) where the ideal situation is shown and then to figure 2.2(b) where an error δA has been introduced into the angle A. Substituting the values from figure 2.2 into equation (1) (making the range coordinate equal the correct range 'z' with the addition of an error component 'δz'), equation (4) is now produced.

$$z + \delta z = \frac{1}{\text{Tan}\ (\ A + \delta A\ ) + \text{Tan}\ B} \qquad (4).$$

Since Tan(A) is measured as an index we can replace Tan(A + δA) by (a + δa) * px / d where 'a' represents the modified index (having the offset of half the total number of horizontal pixels already subtracted) and δa is a variable representing the error in horizontal pixel lengths. Now making the substitution into equation (4) produces.

$$z + \delta z = \frac{1}{(\ a + \delta a\ ) * \frac{px}{d} + \text{Tan}\ B} \qquad (5).$$

rearranged (5) and substituting z = 1 / (a * px / d + Tan B)

$$\delta z = \frac{z * d * 1}{z * \delta a * px + d * 1} - \frac{z * (\ z * \delta a * px + d * 1\ )}{z * \delta a * px + d * 1}$$

$$\delta z = -\frac{z^2 * \delta a * px}{z * \delta a * px + d * 1} \qquad (6).$$

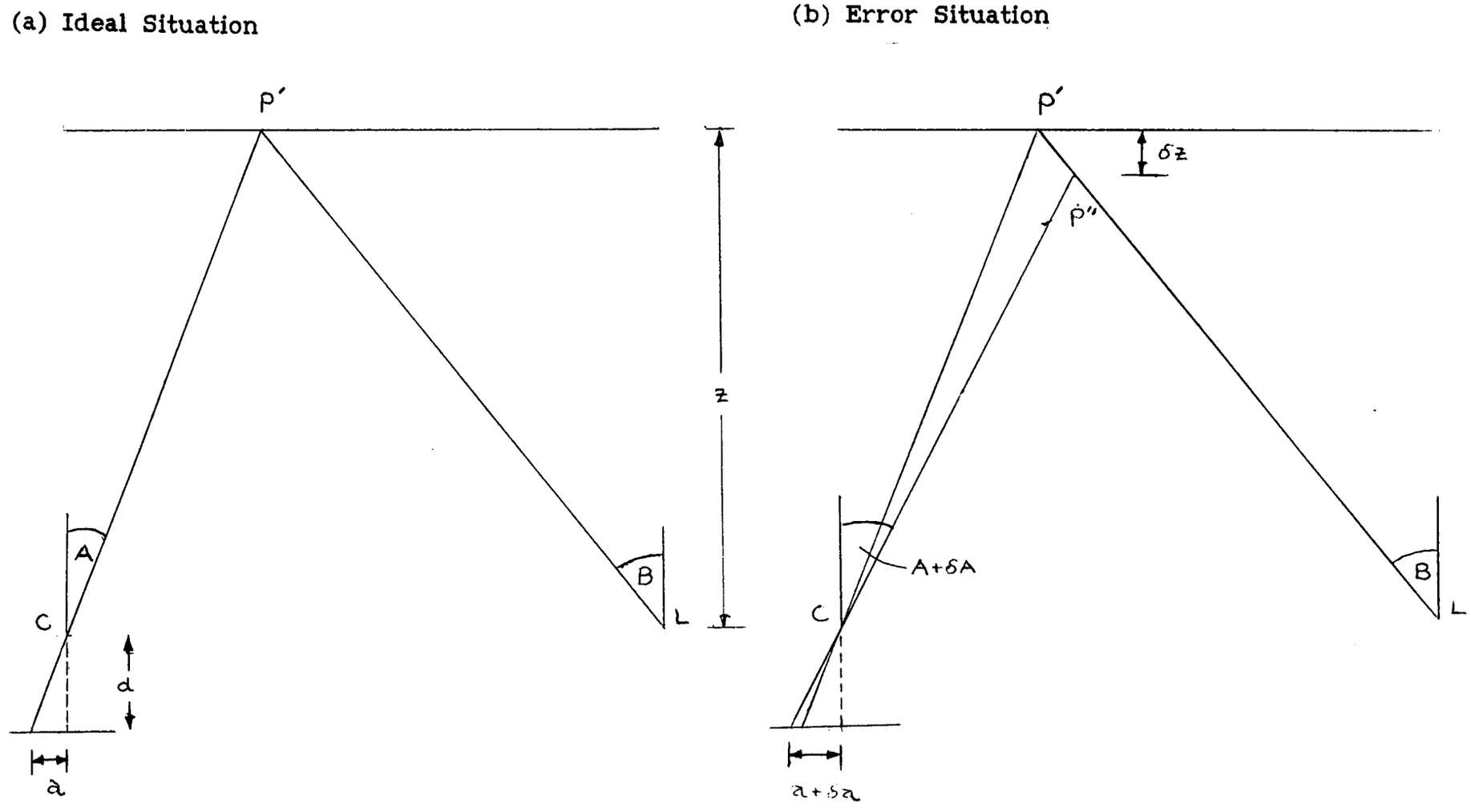

Figure 2.2 Errors in Reading Angle A.

It can be seen from expression (6) that the range error is proportional to the distance squared and the magnitude of the error in angle A (δa). The negative sign indicates that for a positive error (as shown in figure 2.2(b)) the calculated range value is less than the correct value.

Expression (6) provides us with a method of quantifying the range error in the STM system but before any values can be produced several factors arising for expression (6) must be discussed. Firstly, that in using simplifying assumptions in the creation of (6) the expression will accurately reflect the errors obtained with the physical STM system and, if not, what enhancements must be made to the models and expression (6) so that it does. Secondly the mechanism by which the factor δa arises and estimates of its magnitude must also be explained. This can only be done when the physical implementation of the STM system's components have been explained and therefore will be deferred until a subsequent chapter.

2.3 Physical implementation of Photo Sensitive Detector and the Laser Light Source.

In section 2.1.1 and 2.1.2 simplified models of the photo sensitive detector and the laser light source were presented, now the physical implementation of the two modules will be explained. Equations will be produced which describe characteristics of the modules and any deviation from the ideal models will be explained and quantified so that the validity of the equations already produced in this chapter (section 2.1.3) can be assessed.

2.3.1 The Photo Sensitive Device.

The photo sensitive device is implemented with a camera, optical

filter and lens system. The idea of a regular 2-D array of pixels is valid regardless of whether the camera contains a vidicon tube or a CCD (Charged Coupled Device) sensor. The information obtained from the camera is a video stream which contains timing information (field and line sync pulses) so that the temporal video stream can be transformed into a spatial representation used to extract the horizontal and vertical indexes of the laser spot.

The pin-hole has now been replaced by a lens/filter combination which is now described. The lens is a standard 25mm focal length manual aperture lens, the simple pin hole model (which has approximately equivalent properties to the centre of a thin lens) has be superseded by complex lens model (described in Meyer-Arendt [36]) and entails having two focal planes. The two focal planes consist of a Rear Focal Plane (RFP) which is a distance d (the focal length) from the sensing array, and a Front Focal Plane (FFP). The figure 2.3 shows how a light ray enters the front focal plane and exits the rear focal plane in such a way as to seem to have travelled directly from point A to B in perpendicular to the focal planes. The position of the front focal plane is the analogy of the pin-hole in the original model and the position of the front focal plane with respect to the rear focal plane can be obtained by experiment and must be quantified so that the front of the camera's sensor can be set a distance

$$d + \text{distance between FFP and RFP} \qquad (7).$$

back from the camera/laser baseline to maintain correspondence with the equation presented in section 2.1.3. It is assumed that the aberrations in the lens are insignificant, the focus is sharp and the

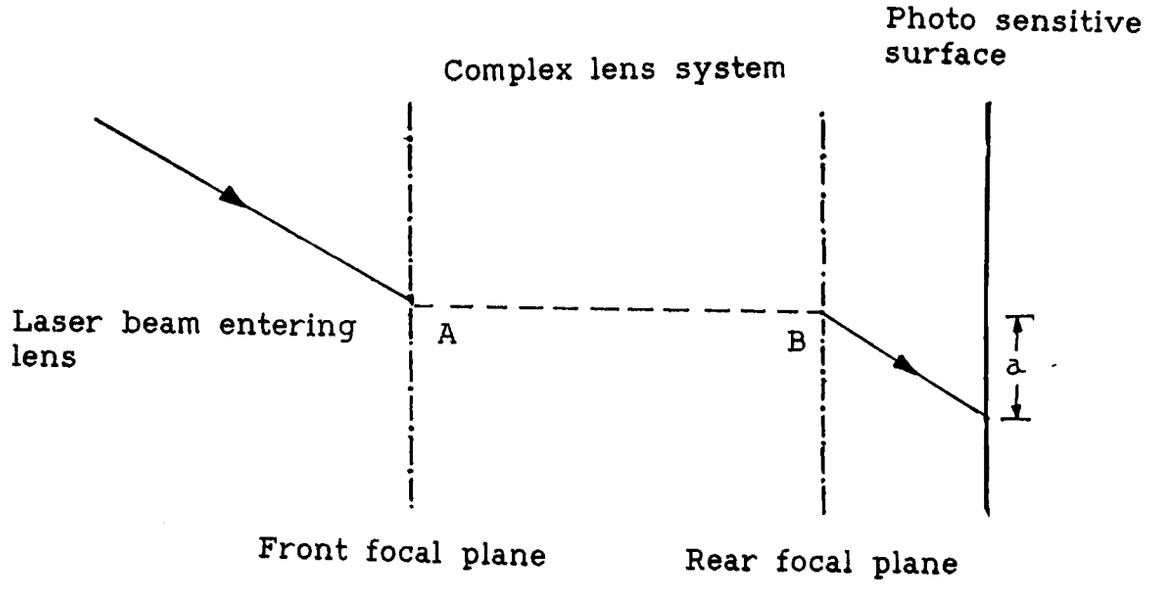

Figure 2.3 Illustration of the Rear and Front Focal Planes.

aperture small.

The camera's horizontal field of view (HFOV) can now be derived, since the sensing array has finite dimensions (hd mm) and the focal length d is known, by the simple equation.

$$HFOV = 2 * Tan^{-1} \left(hd \; / \; \frac{d}{2} \right) \qquad (8).$$

Since in the STM system any other visual information, apart from the laser spot, is not required and could also cause erroneous spot detection, it is removed via a Narrow Band-pass Optical Interference Filter (NBOIF) which is placed in front of the camera's lens. This NBOIF has its passband centred at the helium - Neon (He - Ne) wavelength of 632.8 nm and has a passband which is 10 nm wide. Two problems are associated with using this NBOIF, firstly that only 55% of the incident light energy is transmitted through the NBOIF and secondly, the passband's position is a function of the incident angle of the light. As the incident angle of the light increases the centre of the passband moves to a lower wavelength, this is shown in figure 2.4(a), which also gives the equation which defines this passband movement (from reference [37]). Figure 2.4(b) contains a graph (and associated table) which indicates the magnitude of the incident light transmitted with different incident angles of the laser light. It can be seen that the laser light incident angle at which half the energy is transmitted, compared with that transmitted with light perpendicular to the filter, is 14°. The restriction of the optical systems field of view by the NBOIF limits the use of smaller bandwidth filters which could be used to increase the Signal/Noise (S/N) ratio of the sensing array.

The above description has shown that the photo sensitive device

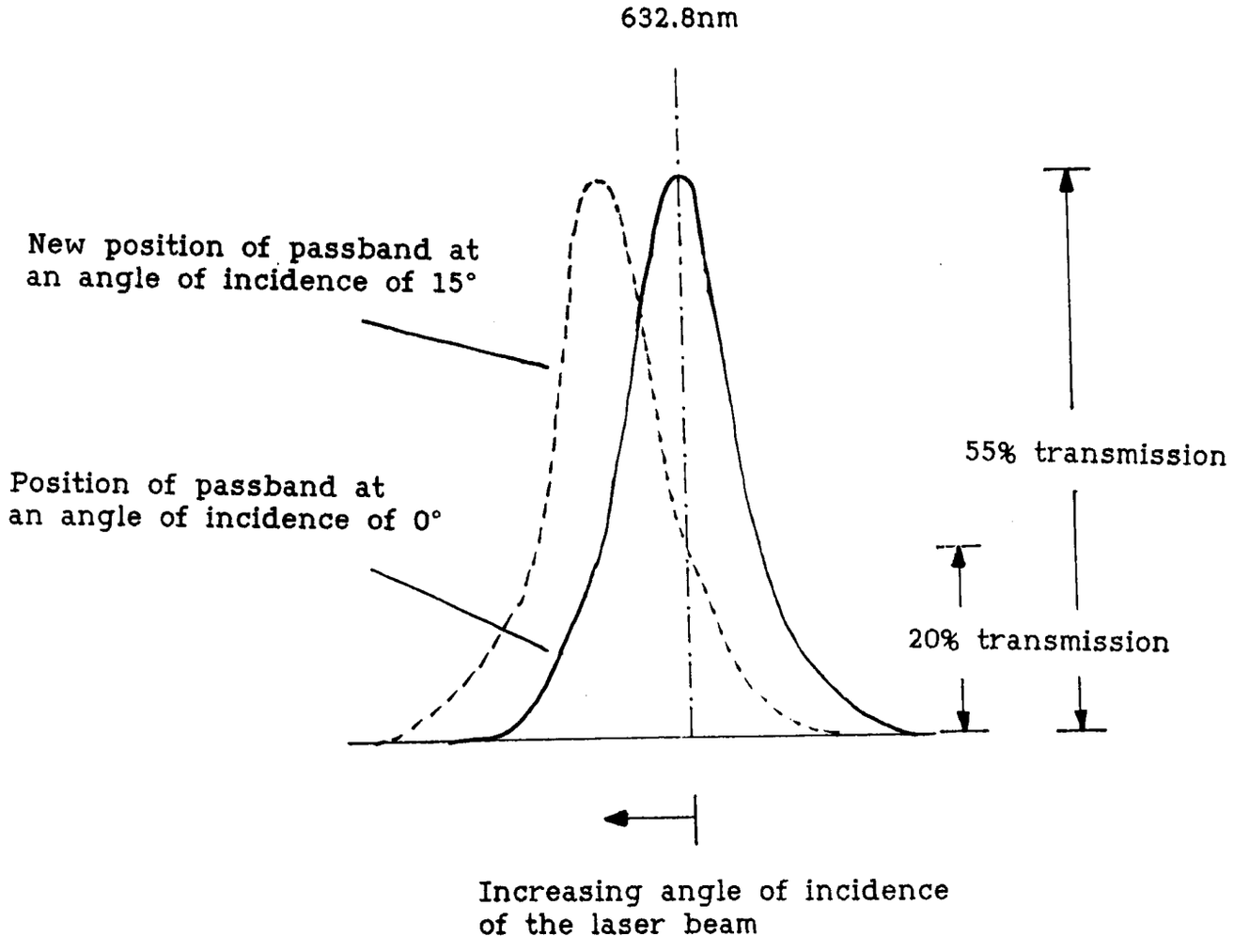

$$\lambda = \lambda_{\perp} \cdot \left(1 - \frac{\sin^2 (\Theta)}{n^2} \right)^{1/2}$$

Where:

λ = new centre passband wavelength

$\lambda_{\perp}$ = centre passband wavelength

ϕ = incident angle of light

n = the index of refraction

Figure 2.4(a) Illustration of Passband Movement due to a Change in the Laser Beam Angle of Incidence to a Narrow-Band Optical Interference Filter.

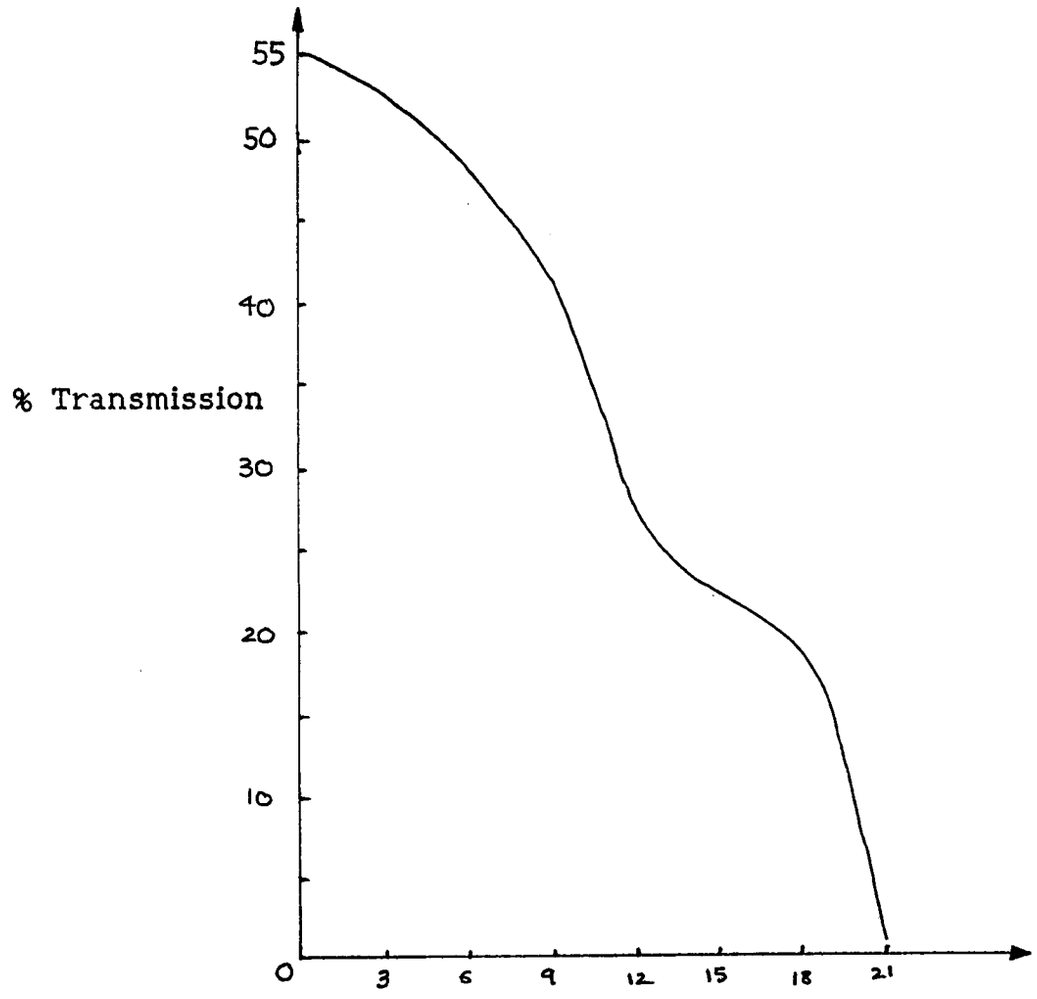

Incidence Angle (Degrees)	Peak Wavelength of Transmission (nm)
0	650.8
1	650.77
2	650.72
3	650.65
4	650.41
5	650.00
6	649.94
7	649.87
8	649.66
9	649.41
10	649.11
11	648.87
12	648.58
13	648.15
14	647.80
15	647.43
16	647.06
17	646.69
18	646.20
19	645.66
20	645.08
21	644.48

Figure 2.4(b) The Response of a Narrow-Band Optical Interference Filter to Non-Perpendicular Incident Light.

model presented in 2.1.1 is valid in describing the actual module used in the physical STM system provided that it is noted the HFOV will be limited either by the equation (7) or by the NBOIF field of view, whichever is smaller, and correct positioning of the camera relative to the camera/laser baseline is observed (equation (8)).

2.3.2 The Laser Light Source and Deflection Mechanism.

The laser light source is implemented via a He - Ne gas TEM_{00} gas laser with a wavelength of 632.8 nm. The laser beam emerges from the laser tube with a certain beam diameter and the diameter of the beam increases, with distance from the exit window, at a rate determined by its divergence. The diameter measurement is based on the fact that a TEM_{00} mode laser has a gaussian beam intensity distribution and the radius is measured between the 'half power' points in that distribution (when the beam amplitude is reduced by a factor 1/e from its maximum value, see reference Harry [38]). The laser divergence is given by the equation below.

$$\text{divergence} = \frac{wl}{\pi * w_0} \qquad (9).$$

Where w_0 is an internal dimension of the laser tube and wl is the wavelength of the laser light, Wilson and Hawkes [39]. For the laser used in the physical STM system the divergence is calculated to be 1.4 mrad (meaning that after the laser beam has travelled a distance of 1 m the diameter has increased by 1.4 mm).

For the above description of the laser light source to resemble the model previously presented in section 2.1.2, ideally, the divergence of the laser spot should be equal to the horizontal angular resolution of a camera pixel. This would force the camera's image of

the laser spot, produced by a surface at any distance from the camera, to have a constant size (measured in camera pixels). If this is not the case, allowance must be made when examining results.

The laser beam is projected into the deflection unit which produces the horizontal and vertical displacement of the laser beam to enable scanning of the target surface. This consists of two precision moving iron galvanometers (MIG) mounted at right angles to one another as shown in figure 2.5. Mirrors are mounted on the shafts of the MIG's and the laser beam is projected onto the first mirror at a point which is perpendicular to the centre of rotation of the MIG. The beam is now reflected up toward the second MIG's mirror striking along a line at its centre of rotation and is then directed out toward the surface to be measured.

The task now is, using the above implementational description, to show how this can be represented by the simple point source deflector model presented earlier and used in the creation of system equations (equations (1), (2) and (3)) which give cartesian position of the laser spot. Any deviations from the simple model must be quantified and appropriate amendments made to the system equations.

Firstly a position for the effective source of the laser beam must be found since this must be located on the camera/laser baseline. Referring to figure 2.6(a) it can be seen that the physical source can be considered as the point where the laser beam strikes the first mirror (point A on figure 2.6(a)). This is because this position does not change regardless of the inclination of the two mirrors, but the source can also be considered to be located at point Q, shown on figure 2.6(b), which is the image of point A behind the second mirror and in the same horizontal plane as the axis of rotation of the second mirror.

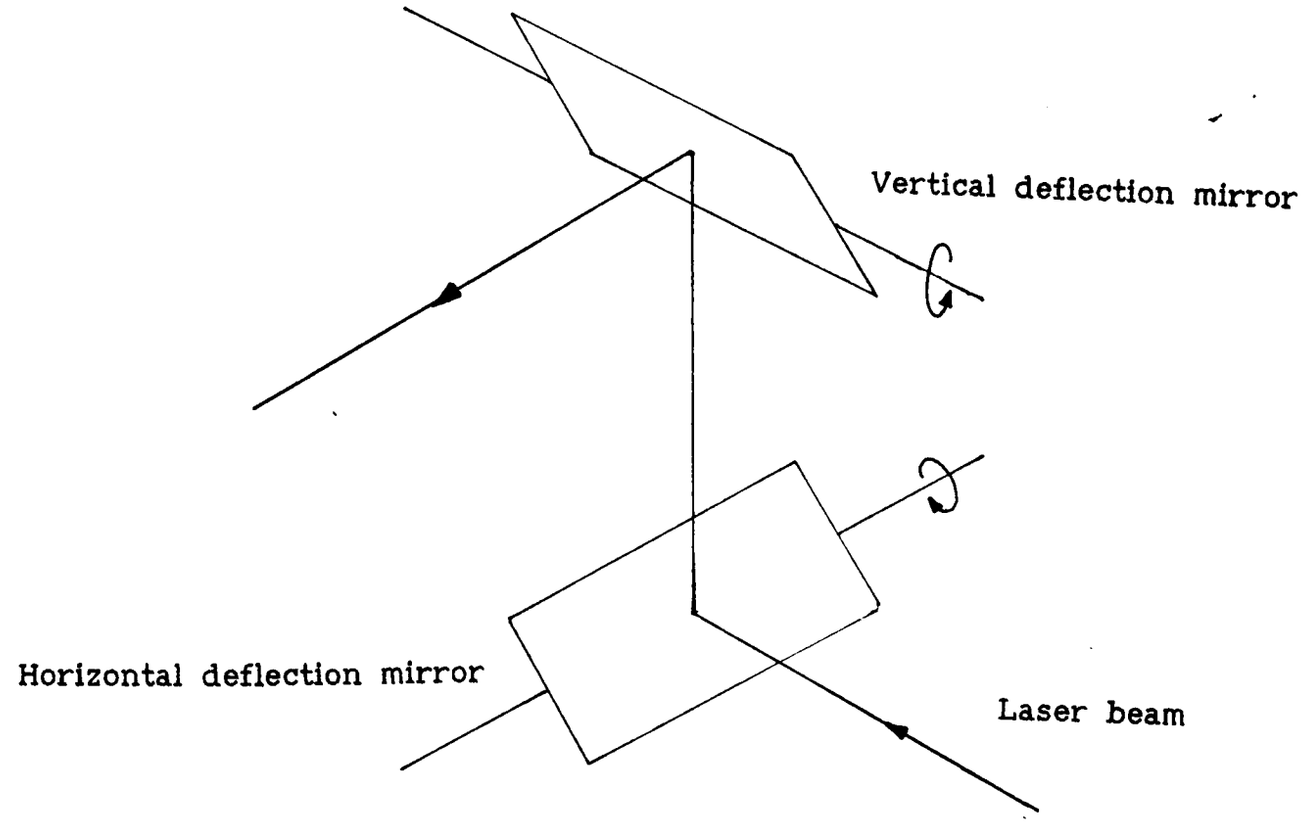

Figure 2.5 Layout of the Moving Iron Galvanometers (Laser Deflectors).

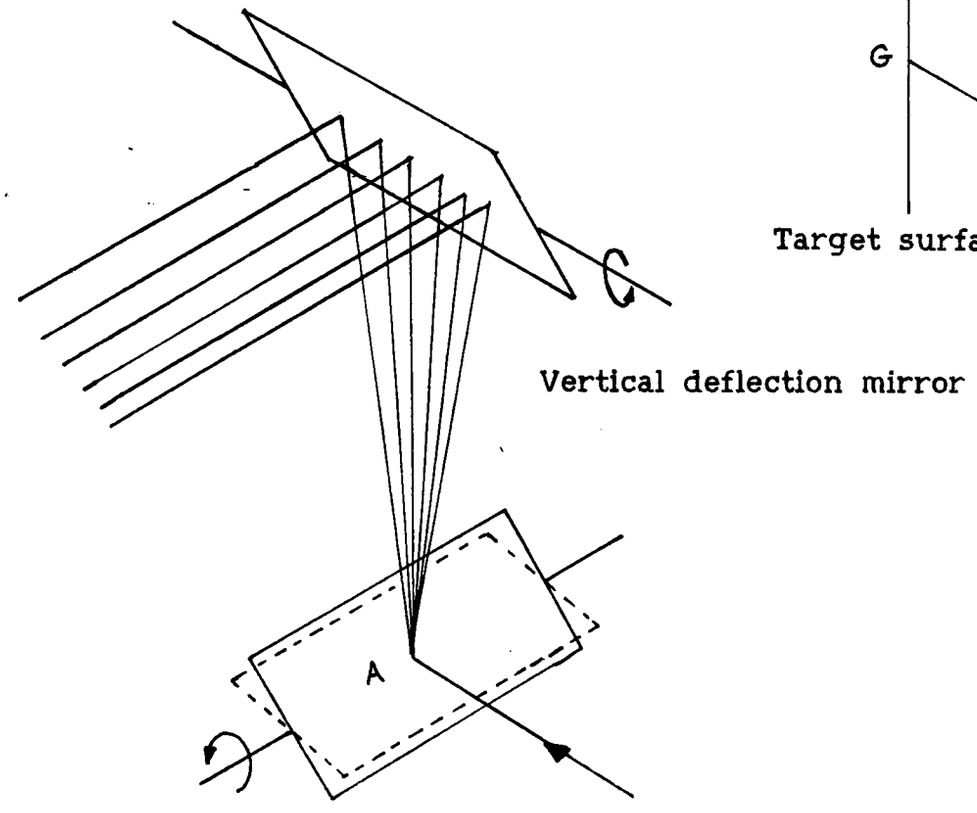

Figure 2.6(a) Apparent Laser Source.

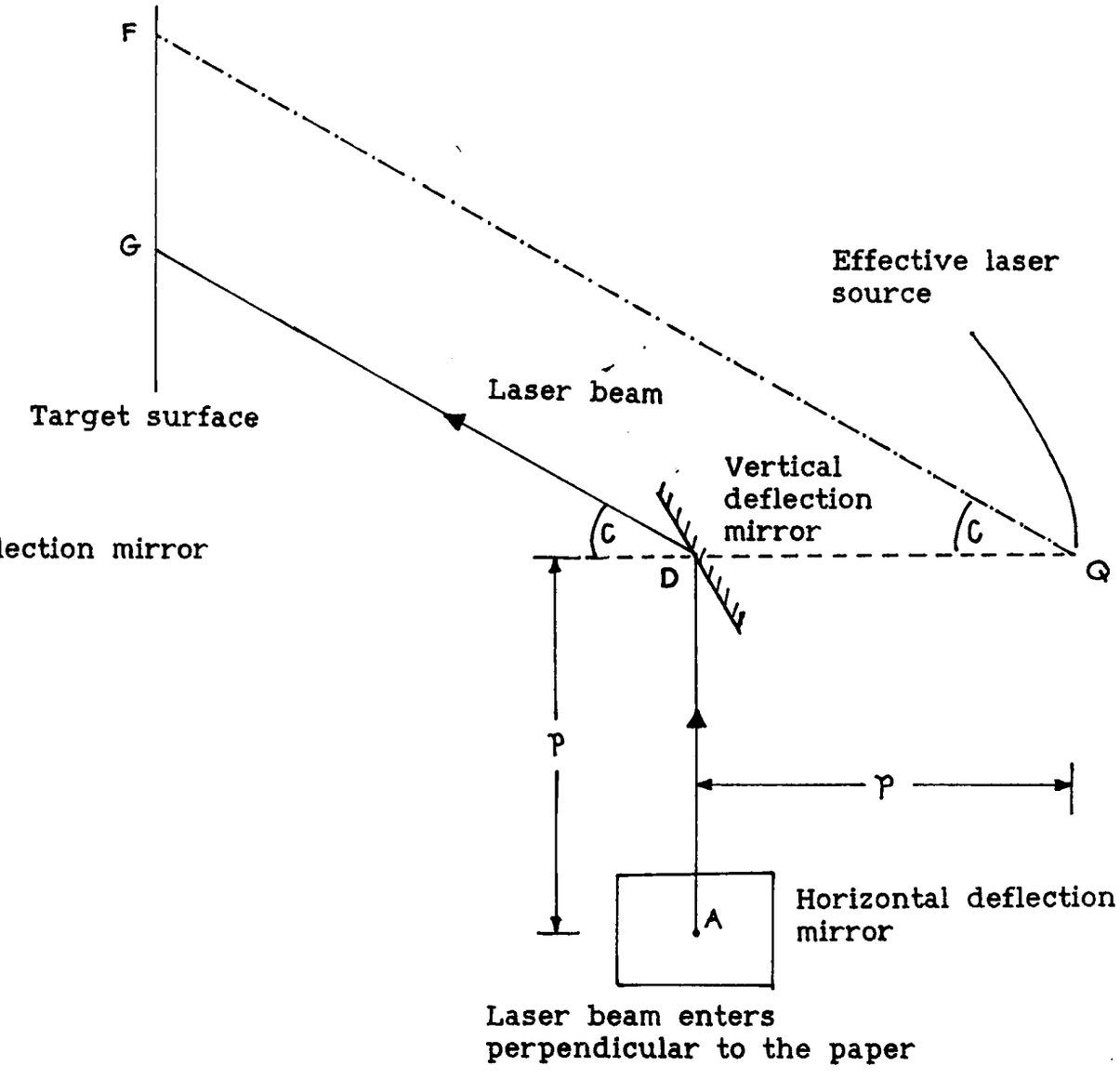

Figure 2.6(b) Equivalent Laser Source (not to scale).

It is now noted, with the help of figure 2.6(b), that when the beam is elevated by the second mirror, an angle C degrees, the position calculated using equation (3) (position F) is incorrect, the correct position being G. This is due to the effective laser source being located behind the point where vertical displacements are introduced, position D in figure 2.6(b). This means that for the correct vertical cartesian value to be obtained equation (3) must be changed to

$$y = \text{Tan}\ (\ C\ )\ *\ (\ z - p\ ) \qquad (10).$$

where p is the distance between the two mirrors. The above description gives the position of the effective source of the laser beam (at position Q a distance p behind the second mirror) and this must be located on the camera/laser baseline to conform to the simple model of the laser light source.

A second deviation from the simple model is explained using figures 2.7(a) and 2.7(b). Referring to figure 2.7(a) the horizontal MIG deflector has been driven to produce an angle B in the horizontal plane (angle YLQ), now in figure 2.7(b) a vertical displacement has been introduced, moving the spot up the vertical target plane YRSV. Using the simple geometry and associated equations presented in section 2.1.3, the position of the laser spot is assumed to be at point U when actually it is at point T. This is because, rather than the magnitude of the angle in the horizontal plane (angle B) being maintained, it is the magnitude of the angle marked D (in triangle VTL) that is maintained when the laser spot is elevated. The angle A from triangle RCW is obtained from the photo sensitive device and using the original equations the value of the range is calculated to be z' instead of z, this is shown in figure 2.7(b). To correct this error it is noted that

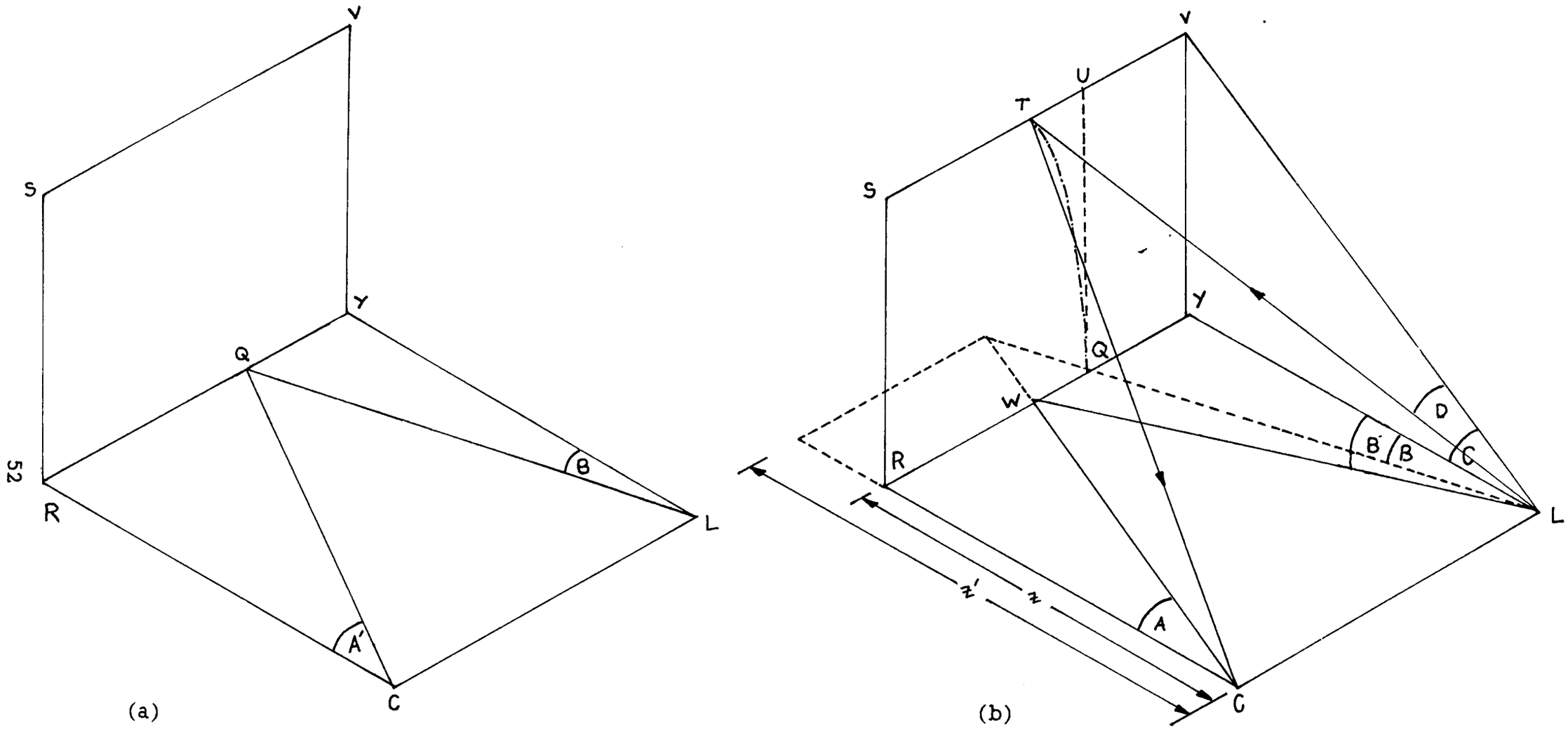

Figure 2.7 Examination of System Equations.

the actual angle, in the horizontal plane, of the laser spot is a function of the elevation angle, using some simple geometry on the triangles LYV and TVL it can be seen that the correct angle in the horizontal plane (referred to as B') has a tangent.

$$\text{Tan}\ (\ B'\ ) = \text{Tan}\ B\ *\ \text{Sec}\ C \qquad (11).$$

Introducing this into equation (1)

$$z = \frac{1}{\text{Tan}\ A + \text{Tan}\ B\ *\ \text{Sec}\ C} \qquad (12).$$

or more correctly, taking equation (5) into account

$$z = \frac{1}{a\ *\ \frac{px}{d} + \text{Tan}\ B\ *\ \text{Sec}\ C} \qquad (13).$$

The equations which have just been derived more accurately reflect the physical implementation of the STM system but do not invalidate the simple models presented earlier provided that the laser deflectors are correctly positioned with relation to the camera/laser baseline, similarly the 'range error' model still retains its validity. Errors in the actual placement of the photo sensitive device and laser light source are detailed in Lin and Zou-Chen [40] and therefore will not be outlined here. Figure 2.8 shows the layout of the actual components representing the photo sensitive device and the laser light source used in the STM system.

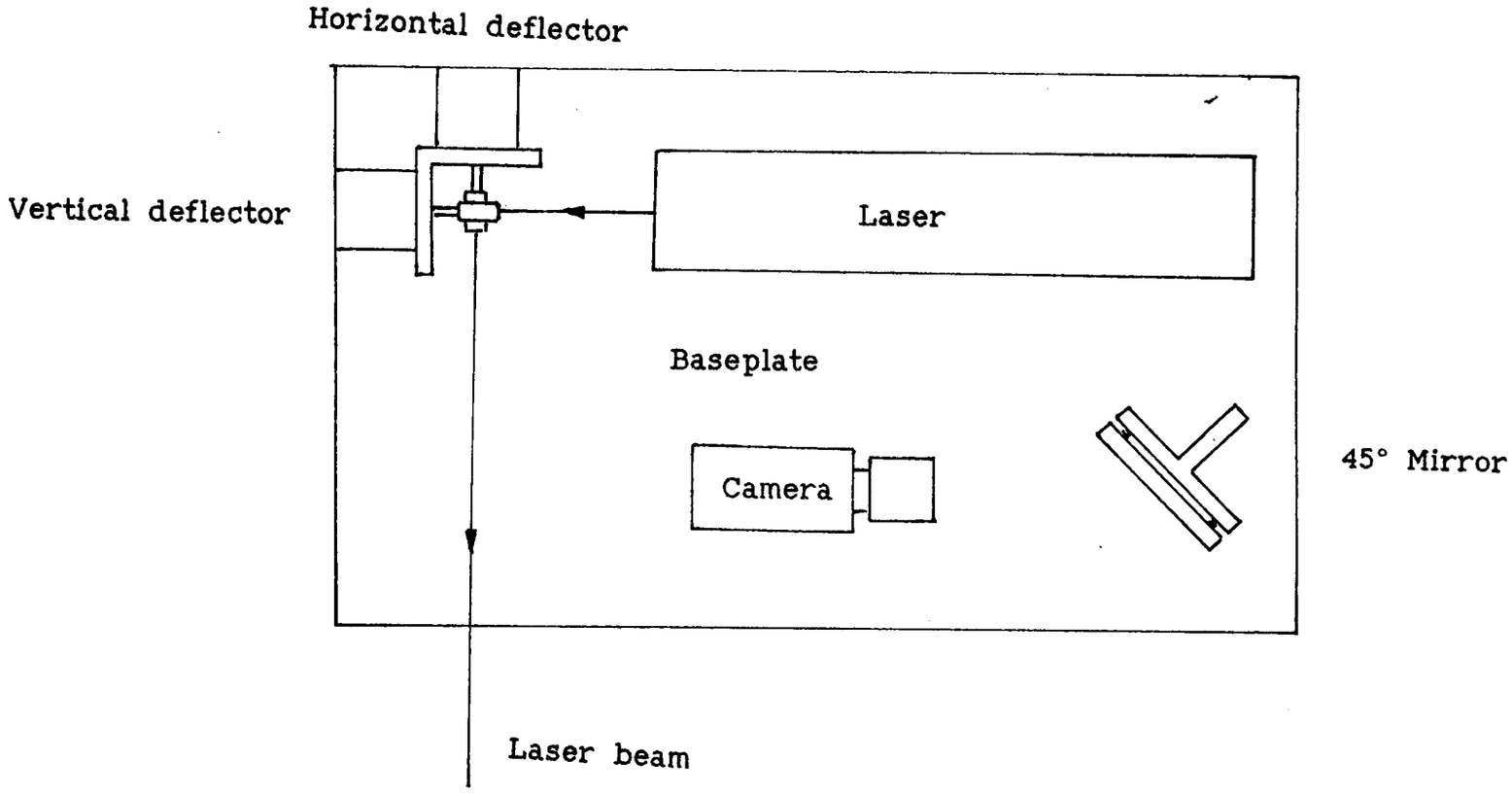

Figure 2.8 The Camera/Laser Physical layout.

Chapter3: The STM System 1.

In this chapter the STM system 1 will be explained. Figure 3.0 shows the general block diagram of the system and in section 3.1 the composition of the individual blocks will be detailed. The next section describes the tests carried out to evaluate the systems calibration and performance. Also included in this section are suggestions for possible enhancements to improve the accuracy of the system and, with these enhancements implemented, new sets of results are obtained so that a qualitative assessment of improvements can be made.

3.1 The STM System 1 Block Diagram.

As already mentioned, figure 3.0 represents the STM system 1 which has been divided into functional blocks. In this section the physical realisation of each functional block will be explained. In section 2.3 some aspects of the physical realisation of the photo sensitive device and the laser light source have been explained. These explanations were to check the validity of the simple models (developed to represent the photo sensitive device and laser light source for use in the production of the system cartesian equations) against the complex physical devices used to implement the photo sensitive device and laser light source functions in the actual STM system. Now any implementational issues that have not been covered in the previous descriptions of these units will be detailed in their block descriptions. The block descriptions presented will not contain any discussions of the effects which these units have on the accuracy of the system, this will carried out in Chapter 4.

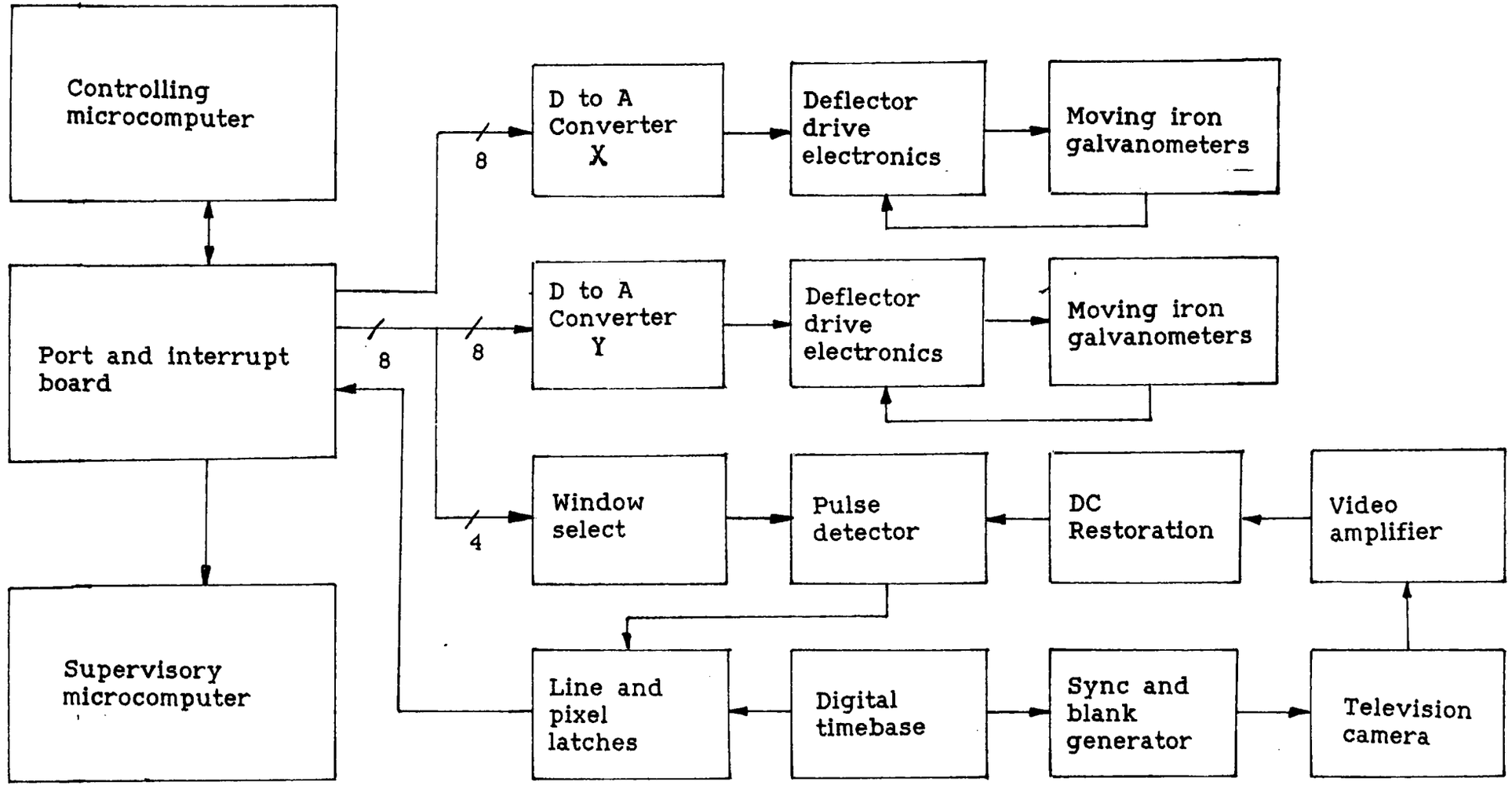

Figure 3.0 Block Diagram of the STM System 1.

3.1.1 The Photo Sensitive Device.

The type of camera used and its associated parameters were not defined in the description of the photo sensitive detector in chapter 2 so this will now be remedied. The camera used in the STM system 1 has a Newvicon tube (this is the same as a standard Vidicon tube but has extra sensitivity in the near Infra-Red region of the electromagnetic spectrum) this has effectively 623 pixels in the horizontal direction and has an active tube diagonal of 11 mm. As detailed in the previous chapter a narrow band-pass optical interference filter and lens system is placed in front of the camera. With the 25 mm focal length lens used, this gives a horizontal field of view (using equation (8) in section 2.3.1) of 20 degrees. In chapter 2 it was stated that the narrow band-pass optical interference filter limits the horizontal field of view to 30 degrees, since this is larger than the camera's horizontal field of view, the horizontal field of view of the system is limited by and equal to the camera's horizontal field of view. The ideal horizontal resolution of the camera (and system) is described by the equation given in section 2.1.1 and is equal to 0.032 degrees or 0.56 mrad.

3.1.2 The Laser Light Source.

The laser light source was described in detail in section 2.3.1 but the output power and initial (exit) beam diameter were not defined since these two parameters did not affect the model of the laser light source presented. Since these parameters are important to the overall operation of the system their values are now quantified. The He-Ne gas laser has an output power of 6 mW and its initial beam diameter at the exit window of the laser is 1 mm.

3.1.3 The Laser Deflectors.

The moving iron galvanometer deflectors (MIG) which produce horizontal and vertical displacements of the laser spot have been described in chapter 2, but their connection with the rest of the system and any specifications which could affect the accuracy of the system will now be described. The horizontal and vertical deflector systems are supplied with a 12 bit binary number which has a maximum value of 4095 and a minimum of 0. This relates to a maximum displacement of 40 degrees optical (20 degrees mechanical) and gives a minimum step of approximately 0.001 degrees or 0.17 mrad. The moving iron galvanometer has a capacitive angular transducer built into its body and this is connected into an electronic feedback loop which drives the galvanometer (The feedback system is described in more detail in section 4.3.1). This feedback loop contains both proportional and integral control giving no steady state error so that the only positional errors are due to thermal changes (which can cause mechanical distortions and electronic offsets) and the inherent instabilities in the MIG at a constant temperature (transducer non-linearities). The thermal drift has a value of 0.4 mrad/°C (1.3 optical minutes per degree Centigrade) and the inherent instability of the MIG and driving electronic system is 0.8 mrad (2.5 optical minutes), both the above quantities have been obtained from experiment on the actual MIG's used in the system.

3.1.4 The Detector Board.

The video signal from the camera is passed to the detector board, here the video signal is DC coupled, amplified and then fed into the

one input of a fast analogue comparator. Since the optical filter has removed all other visual information but that at the laser wavelength the signal will just contain a pulse which corresponds to the laser spot. A variable trigger level is set on the second input of the comparator and when this level is exceeded the output of the comparator goes high, only going low again when the signal level falls below the trigger level (the trigger level must be variable since it is a function of ambient conditions and these can change). This detection signal (the output of the comparator) is sent to the digital time base board so that, on the leading edge of this signal, the values contained in the line and pixel counters can be stored. The detection signal is also sent to the valid data latch thus signifying that the laser spot was detected and that the values contained in the line and pixel counters (in the digital time base board) are valid. This latch is reset after it has been read so as to be ready for the next spot.

3.1.5 The Digital Time Base.

The Digital Time Base (DTB) forms a very important part of the STM system, the stability of the electronics contained in this board and the reproducibility of the measurements have a direct effect on the accuracy of the STM system. The DTB has two main functions, the first is to produce all the sync and blank timing signals for the camera so that its field and line timing can be locked to the stable internal clock of the DTB. The second function is to transform the temporal video signal, from the camera, into a spatial representation of the target surface so that the angles needed for the cartesian coordinate calculations can be identified. The actual position of the laser spot, assuming that it is visible and not occluded, is obtained via the

signal from the detector board which latches the contents from the internal line and pixel counters into storage registers. These stored values will be read by the controlling microcomputer during the field flyback time. The pixels which are mentioned here do not have to correspond to the physical pixels defined in the camera but are just time periods, synchronous with those of the DTB's stable internal clock, which the camera's active line has been divided into. A degree of error is introduced if these time periods are larger than that set by the Nyquist criteria (which is the number of physical camera pixels (623) divided by the active line width (52.14 μs) or $\approx$ 84 ns). This error can be illustrated by assuming that the image of the laser spot resides on a single physical camera pixel. If the DTB's pixel is of a greater magnitude than the physical pixel, any detection mechanism used will experience a temporal reduction in resolution. Assuming there were n physical pixel periods to one DTB pixel period the worst case temporal error obtainable is (n-1)/2 physical pixel periods. This assumes that the horizontal displacement of the laser spot is measured to the centre of the DTB pixel that the spot was registered in. The effect of this temporal error in terms of range accuracy will be examined in a later chapter.

In the STM system 1 it was decided to make the horizontal angular pixel resolution equal to the laser divergence so that the dimensions of the image of the laser spot is one pixel width in diameter and would appear the same size at any distance. This entailed having 382 temporal pixels in the active line period. Since this is less than the physical number of pixels the temporal error mentioned above will be present. Another consequence of making the angular pixel resolution equal to the laser's divergence is that the camera can be run in non-interlaced

mode, (that is only visual information contained within the odd video lines (i.e. 1, 3, 5, etc) is collected) thereby reducing the frame acquisition time by a factor of two.

3.1.5 The Controlling Microcomputer.

The controlling microcomputer was implemented by a proprietary single board microcomputer based round the 8085 microprocessor and was used to control low level activities of the STM system 1. The software, written in 8085 assembler language so that the speed objectives of the system can be met, is initiated by the field sync interrupt every 40 ms (the time for two half interlaced frames). On receipt of this interrupt the values stored from the line and pixel counters of the DTB are read into the controlling microcomputer, provided the valid data latch in the detector board is set, and translated into ASCII characters to be sent down a fast RS232 serial link to the supervisory microcomputer. If the valid data latch is not set, a zero is sent down the serial link to indicate no valid return was obtained. The next software task is to fetch the new horizontal and vertical position of the laser deflectors and then output a new positions to the laser deflectors via a digital port board. The horizontal and vertical position for the laser deflectors can be obtained from two sources, directly entered from the terminal connected to the controlling microcomputer or, from stored horizontal and vertical tables which contain pre-defined scan patterns for the laser spot (the present stored pattern is a horizontal raster). The reason behind using two half interlaced fields is that with the Newvicon camera the video output, for the present screen, is produced as soon as the flyback of the previous field has finished. This means that, supposing a spot has just moved into the top left hand corner of

the screen, enough integration time is not left before the electron beam (which reads the pixels) has reached the spot's position. This causes the spot not to register in the video signal and to be assumed to be occluded from the camera's field of view which is not the case. Allowing two non-interlaced fields, one for the movement of the laser spot to a new position and the second, used as a read out frame, gives all spot positions adequate integration time. The allocation of a laser spot movement frame also solves the problem of a 2 ms settling time of the moving iron galvanometers when large excursions of the laser spot are required (mainly on horizontal and vertical flyback). Since this time is now absorbed into the 20 ms of the first non-interlaced frame, adequate integration time is left regardless of the position in the laser spot's scan pattern.

3.1.6 The Supervisory Microcomputer.

The supervisory microcomputer performs most of the calculations needed to produce the cartesian coordinates of the laser spot. It receives the pixel position values down the fast RS232 serial link from the controlling microcomputer and with a knowledge of the display pattern, and the present position within that display pattern, the x, y and z coordinates of the laser spot can be produced. Once the whole display pattern has been completed, the range map calculated is displayed on the computer screen as a wire-frame (see figure 4.2) using the camera as its origin for all the coordinates.

Several software features have been designed to reduce spurious signals and fill in, if possible, missing data with approximations, these features will now be explained: The first of these features is a neighbourhood range filter which takes the calculated range value and

compares it to its four nearest neighbours, provided one of the neighbours has a range value which is within a specific tolerance of the value obtained from the calculation the value is accepted as 'good'. If it is not similar to any of its four nearest neighbours it is rejected as spurious and not included in the range map. At the edge of the range map each range value does not have four neighbours, therefore only three or two tolerance comparisons can be carried out, this feature can be bypassed if prior knowledge is available that the surface is non-homogenous and that range spikes can occur and must not be assumed spurious. The second feature in the software is a four, three or two point linear interpolation for points where the laser spot was occluded from the camera or the data is adjudged to be spurious. The number of neighbouring points used in the interpolation is dependent on the position of the point in the spatial scan pattern.

The above software is written mainly in the BASIC programming language (with small 'time critical' or 'low-level' input/output sections in 6502 assembler code) on the BBC microcomputer.

3.2 STM System 1 Tests.

In this section the performance and evaluation tests carried out on the STM system 1 will be outlined. The first of these tests are to check the calibration and alignment of individual components of the system and, from the results of these tests, quantify the maximum error possible due to any remaining misalignment. The purpose of the remaining tests are to calculate the accuracy of the system and are carried out over a two static surfaces a known distance away from the camera of the STM system.

3.2.1 Photo Sensitive Device Alignment.

The first task in the system alignment and calibration tests is to check that the camera and related optics that make up the photo sensitive device are orthogonal to the camera/laser baseline. The two important alignment procedures are those that detect and correct any rotation of the sensing device or camera pan (skew of the sensing device in the vertical plane about its centre creating an angle Θ with respect to the camera/laser baseline). Two tests were derived to evaluate these factors and, by adjustment of the camera, minimise them. A description of these test in now given along with an equation defining the maximum misalignment that is, possibly, still present.

Referring to figure 3.1(a), a light source (L_0) is placed on a flat vertical surface (a known distance away) and aligned to the camera centre (that is, on the 'sight line' of the photo sensitive device). Two other light sources (L_1 and L_3) are placed on the same surface and in the same horozontal plane as the centre source. These are on either side of this centre source and a distance G away from it. Similarly, another two light source are placed on the surface but this time in the same vertical plane as the centre source (L_2 and L_4).

Rotational alignment is obtained by adjusting the the camera until all the three vertical light sources (L_0, L_2 and L_4) have the same horizontal pixel position, these are produced by the DTB. With the aid of figure 3.1(b), it can be seen that maximum error, once the alignment outlined above has been achieved, is given below.

$$\text{error} = \frac{\text{sensor horiz size}}{2*\text{Tan}(90°-\Theta/2)/\text{Tan}(\Theta)}$$

Where $\text{Tan}(\Theta)$ = pixel width/sensor vertical size. Substituting the

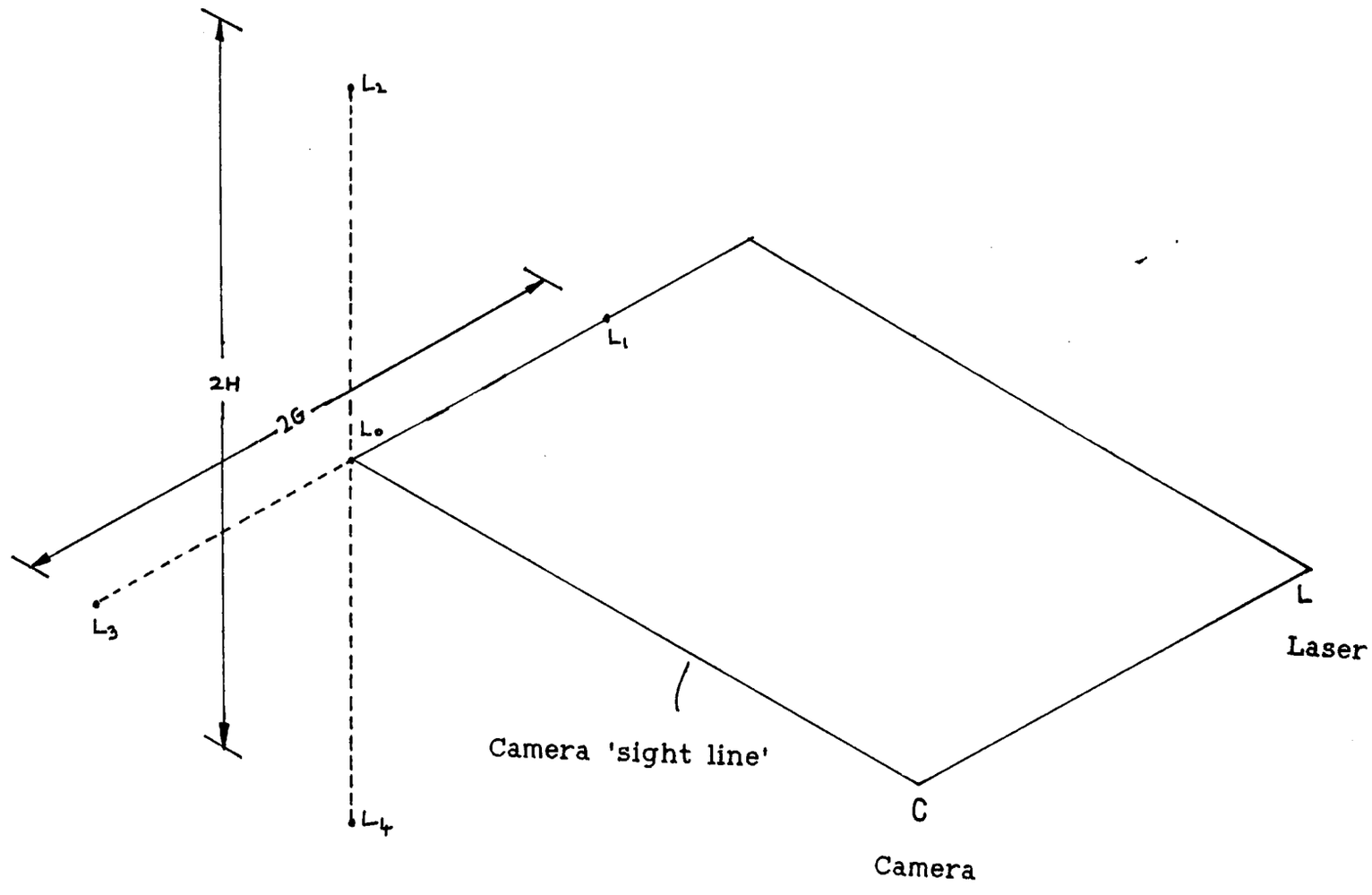

Figure 3.1(a) Camera Calibration Layout.

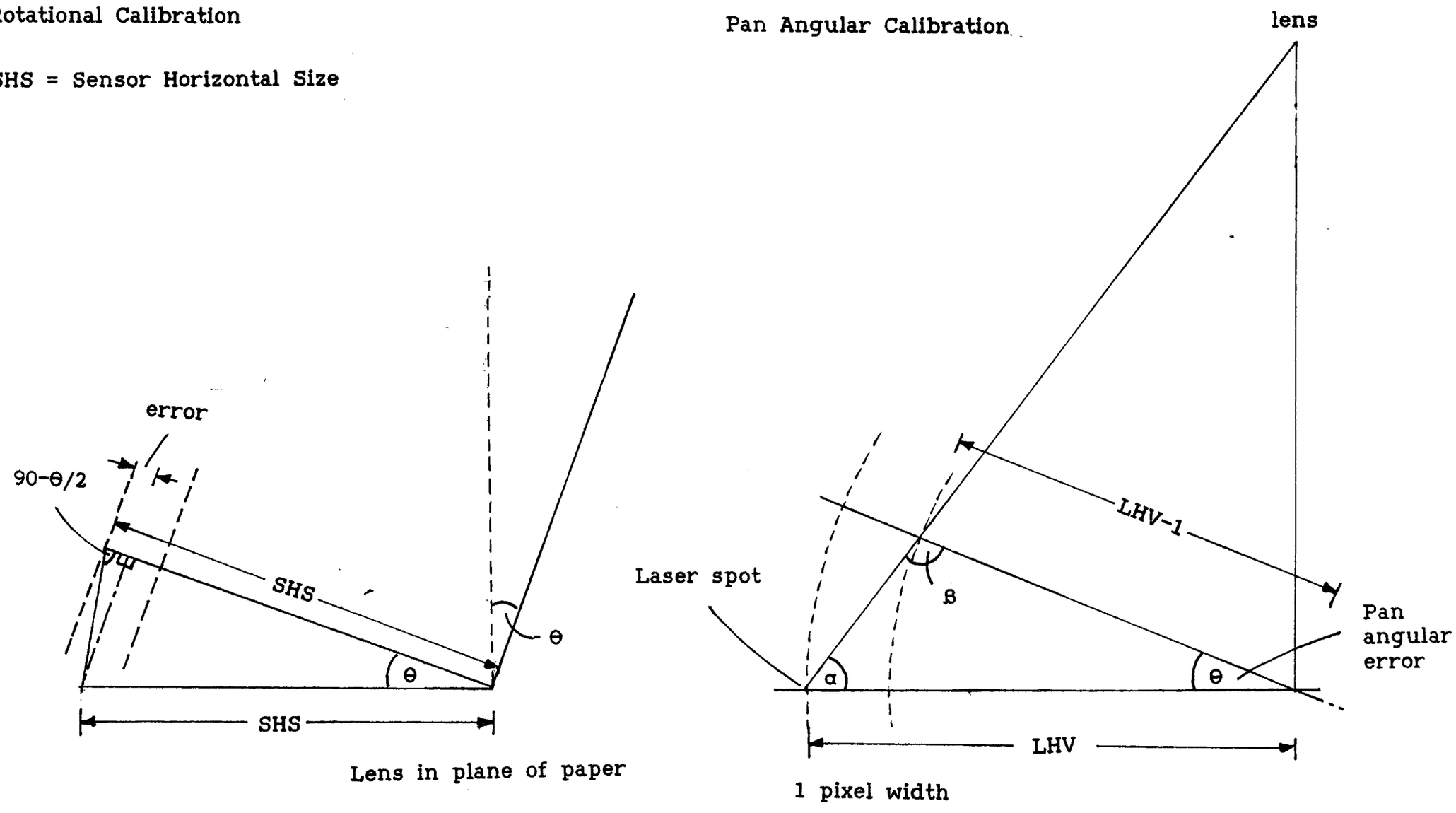

Figure 3.1(b) Rotational and Pan Camera Calibration. (NOT TO SCALE)

systems parameters into the above equation, the result obtained is.

$$\text{error} = 7.4 * 10^{-6} \text{ mm} \quad < \quad 10 * 10^{-3} \text{ mm} \; (= 1 \text{ pixel})$$

The camera pan error is assessed using the three horizontal points, the two pixel values obtained from the two horizontal sources (L_1 and L_3) are subtracted from that obtained from the centre source (which maintains the same value through the test) and the two magnitude obtained are termed the Left Hand Value (LHV) and the Right Hand Value (RHV). Any difference between the values is minimised by adjusting the camera's pan orientation. Once the LHV and RHV have attained the same value the worst case error that can still be present is one horizontal pixel width. This error is illustrated in figure 3.1(b) and can cause a maximum pan angular error of.

$$\text{Pan error} = \Theta = 90^\circ + \alpha - \text{Sin}^{-1}(\text{Cos}(\alpha) * \text{LHV} / (\text{LHV}-1))$$

Where Tan (α) is G divided by the distance from camera to the surface containing the light sources. To reduce this maximum error of 1 pixel a procedure is carried out whereby the camera's pan orientation is adjusted clockwise until LHV and RHV differ by 2. This position is marked and camera's pan orientation is now adjusted clockwise until again RHV and LHV differ by two. This pan angle is marked and a pan orientation chosen which is half way between the two marked angular displacements. This should reduce the pan error to a much smaller value.

The camera tilt error need only be approximately calibrated since the only task of the vertical line value is in error checking and, as will be explained later, need only been known within sixteen lines of the correct value. If its calibration proves desirable, a procedure

similar to that carried out for the pan error could be used with the change that the vertical points and line readings are put into the equation.

Another method of camera calibration would be to produce a transform which, when multiplied by the pixel displacement and line position of a laser spot, will produce the world coordinates of the laser spot. In its simplest form, the coefficients of the transform are obtained by solving two camera calibration equations with the line position and pixel displacements of six points for which the world coordinated are known (see Martins et al [41] and Gonzalez and Wintz [52]). This approach was considered too computationally intensive since all camera's values would have to be operated on by the transform.

3.2.2 Laser Deflectors alignment and Calibration.

In this section the calibration procedure for the laser deflectors will be outlined, the following description is for the horizontal deflector but is just repeated for the vertical deflector. The layout for the calibration is shown in figure 3.2. This shows a horizontal laser deflector mounted on a precision rotating table. This enables any desired mechanical angular offset to be introduced onto the deflector with a precision of 0.0167° or 0.3 mrad. A four quadrant photo diode, mounted on a precision linear displacement device (which can resolve the centre of the laser spot, using a null measure, to 0.0025° or 0.085 mrad) was placed at the same vertical height as the mirror of the laser deflectors and a known distance away. A laser beam was directed onto the mirror of the laser deflectors and aligned on the centre of the photo diode. The precision of the alignment was made available due to the processing of the signals from the four quadrant photo diode, the

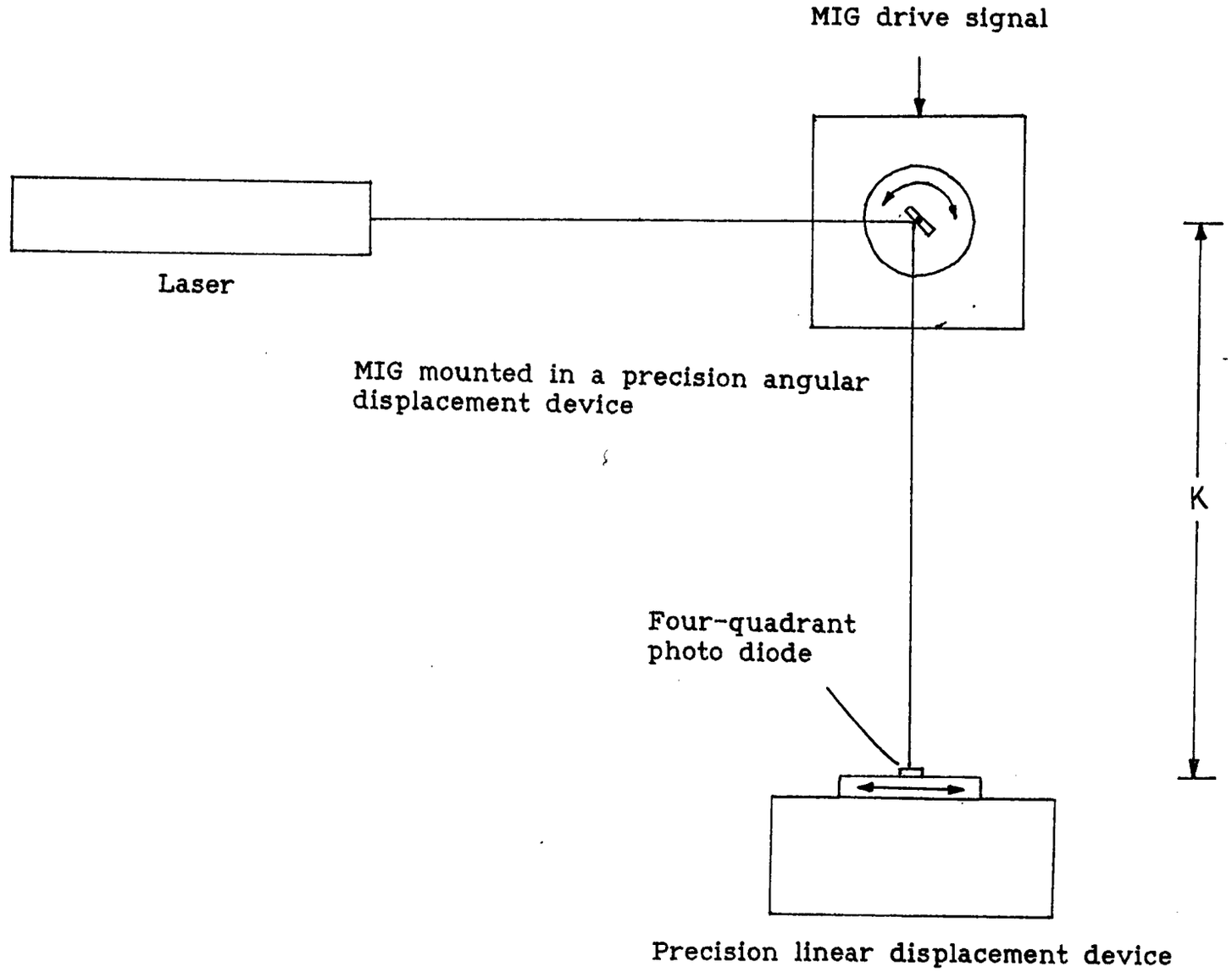

Figure 3.2 Laser Calibration Layout.

return from top and bottom left hand quadrants is summed and subtracted from a signal composed of the summed returns from the top and bottom right hand quadrants. The same procedure was used to give an indication of vertical displacement but the two top and two bottom quadrants were this time summed and subtracted, a null output from the four quadrant diode's electronics indicates that the laser spot is in a centre position on the four quadrant diode. The processing described above is now illustrated in block form in figure 3.3.

Referring to figure 3.2, the procedure for the calibration is now described. Firstly, put the digital representation of zero into the laser deflectors drive unit and then linearly move the photo diode until the laser spot is centred. Then rotate the laser deflector mechanically by a specific number of degrees, using the precision rotation unit, and start increasing the digital number fed into the laser deflectors drive unit until the laser spot was again in the centre of the photo diode. The value fed to the laser deflector's drive unit is noted along with the angle moved from the original start position. This process was carried out for 0.6 degree steps from 0 degrees to 20 degrees (mechanical) and for specific scan positions (16 equal steps between 0° and 20° mechanical). Lastly three more digital displacement values were obtained which would help with the overall system alignment. The first displacement value is the minimum range angle (this is the angle calculated between the edge of the camera field of view at the minimum range and the photo sensitive device's 'sight line') and once the 'sight line' digital displacement value has been found two known angular displacements either side of this position are introduced and their associated digital displacements noted. The stability with respect to time was checked and finally the thermal

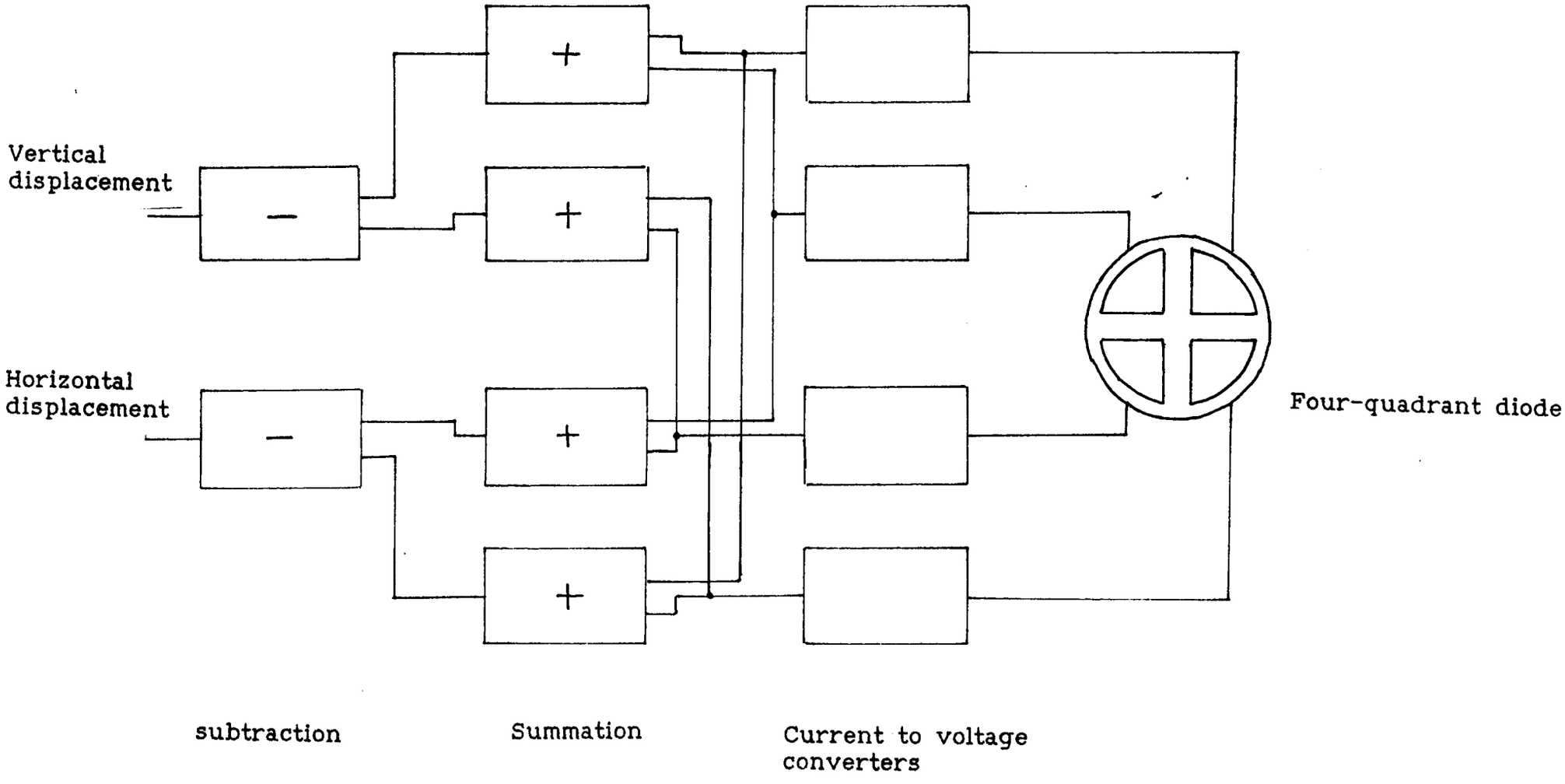

Figure 3.3 Block Diagram of the Four-Quadrant Photo Diode Electronics.

stability was also quantified, these results have already been given in section 3.1.3.

3.2.3 Overall System Alignment.

The layout of the camera, laser, deflectors and associated optical components is shown in figure 2.8. The main problem now is to align the laser with the camera. This is achieved by feeding the value obtained from the minimum range angle into the moving iron galvanometers drivers and altering the position of the laser spot mechanically until it is in the position of the centre light source used in the camera alignment test in section 3.2.1. Now the two digital displacements, obtained from the laser deflectors calibration, are introduced into the moving iron galvanometers drivers, since these represent known angular displacements and the distance between camera and test surface is known all the values can be obtained to solve equation (12) for the value d (initially assumed to be the focal distance but dependent on other factors such as focus and aperture). Since the present system is used at fixed focus only aperture effects need to be examined and d calculated for various values of aperture. The aperture effect on d was found to be negligible with the value of d being within 0.1 mm of the focal length (25 mm).

3.2.4 System Performance tests.

Now that the alignment and calibration have been described, these procedures were implemented and the system was tested using the 256 point pre-defined scan pattern (sixteen horizontal and sixteen vertical deflection angles whose corresponding digital displacement values were obtained from the laser deflectors calibration) over the two test

surfaces. Several scans were obtained and on examination it was noted that several of the range values obtained had an error associated with them of greater that 10 % of the known range value. On close scrutiny of the video output from the camera it was noted that several spot images, of varying brightness and in the position of previous spots, were visible at a instant in time. This problem was due to inadequate re-charging time of the vidicon tube in the camera and was causing false latching of the pixel value in the DTB which, when associated with the laser deflection angle for that scan position, produces erroneous values for the spot's 3-D cartesian position. The solution of this problem was to change the horizontal raster scan presently used to a vertical bi-directional scan pattern and then to restrict spatially the active part of the screen where a return can occur to sixteen lines (with the line with the spot on nominally in the centre of the 16 lines). The registration between the vertical elevation of the laser spot and the camera line position is set during the calibration and alignment procedure so that once an elevation angle has been selected for the laser deflectors the sixteen line active camera window can be obtained by a single integer division and addition operation. Now even if energy from a previous spot has been retained this energy will be outside the active window and therefore cause no false latching of the pixel position. Another enhancement is also achieved by this vertical scan in that all large steps of the laser spot have been removed (horizontal and vertical flyback in the horizontal raster scan pattern) so that the MIG's drivers can have their rise time and settling time optimised for the known step size. One problem that is introduced by the use of the vertical scan, is that the controlling microcomputer must signal to the supervisory microcomputer as to

whether the scan started at the left hand top corner or the right hand top corner.

A second improvement introduced to minimise errors was a hardware spot width detector. As explained in section 3.1.4, a signal triggered by the leading edge of the pulse in the video stream, which represents the laser spots distribution, is used to obtain the pixel position in the DTB. The hardware was now change so that a counter was now started, being incremented by the DTB's clock, when the video pulse magnitude exceeded the trigger level and was stopped when the pulse dropped down below the trigger level (ignoring the small amount of hysteresis introduced into the comparator to aid noise rejection). The value obtained, providing it is greater than one, is divided by two and added to the pixel position to obtain a better estimate of the actual position.

The tests onto the target surface were repeated with each of the above modifications and comparisons of the results are given in the next chapter.

Chapter 4: Analysis of STM System 1 Results and System Enhancements.

This Chapter contains an analysis of the test results that were obtained in the accuracy tests which were detailed in the previous Chapter. As a prerequisite to this analysis, the theoretical errors which are inherent in the system (based on the equation (6) which was defined in Chapter 2) will be quantified so that comparisons can be made to the test results obtained. The next part of this Chapter will outline some of the parameters of the system which have not yet been defined (e.g. the system range and the degree of spatial sampling possible), and finally, the concepts behind the STM system 2 will be introduced along with the physical implementation of these concepts.

4.1 Theoretical Error of the STM System.

To obtain the theoretical error in the range coordinate, equation (6) (which was developed in section 2.2), will be used. Any important system parameters which are used in this equation will be the same as those used in the tests described in chapter 3 so that any error magnitude comparisons made, will be comparable.

In Section 2.2, where equation (6) was derived, the question of whether this equation is truly applicable in the circumstances of the real apparatus was raised. This was because simple models were used to represent the photo sensitive device and laser light source in its derivation. From the discussion presented in Section 3.2 it was shown that the models are indeed a valid representation of the physical devices and therefore, the equations should provide a valid representation of the magnitude of the inherent range error present in the STM system. Another important observation, that was not mentioned in Section 2.3, is that the range error is not dependent on the

projection angle of the laser beam. This is because both the 'target pixel size' and the laser spot size increase in proportion as the projection angle is increased. The last major omission in Section 2.3 is the explanation of the term δa which appears in equation (6), this is defined as being the error present in the measured pixel position and has units of 'horizontal pixel widths'. The first task in rectifying this omission is to describe the mechanism by which this error arises and then, using the known system parameters, estimate its magnitude.

From section 2.3.3, it is known that the laser spot has a gaussian distribution and that the video pulse produced by the camera, which correspond to the distribution of the laser spot, triggers the DTB to produce the pixel position. This is illustrated in figure 4.0. This figure also demonstrates that there may be an error between the recorded position and the actual position of the centre of the distribution. This error comprises two components, the first is, that the signal that triggers the pixel counter is not normally at the centre of the distribution but precedes it. The second component is that, since the pixels are digital quantities, if the trigger signal resides anywhere in a pixel width it indicates a position corresponding to the centre of the pixel. More correctly, the light incident on, and averaged over, a pixel is assumed concentrated at the centre of the pixel, with the horizontal distance from the active edge of the image sensor and the centre of the illuminated pixel being defined as the pixel position. The magnitudes of these two errors differ in that the second component has a fixed maximum value of $\pm$ 1/2 a pixel but, the first has a variable magnitude which is dependent on the size of the laser spot's distribution and the threshold level set for the comparator

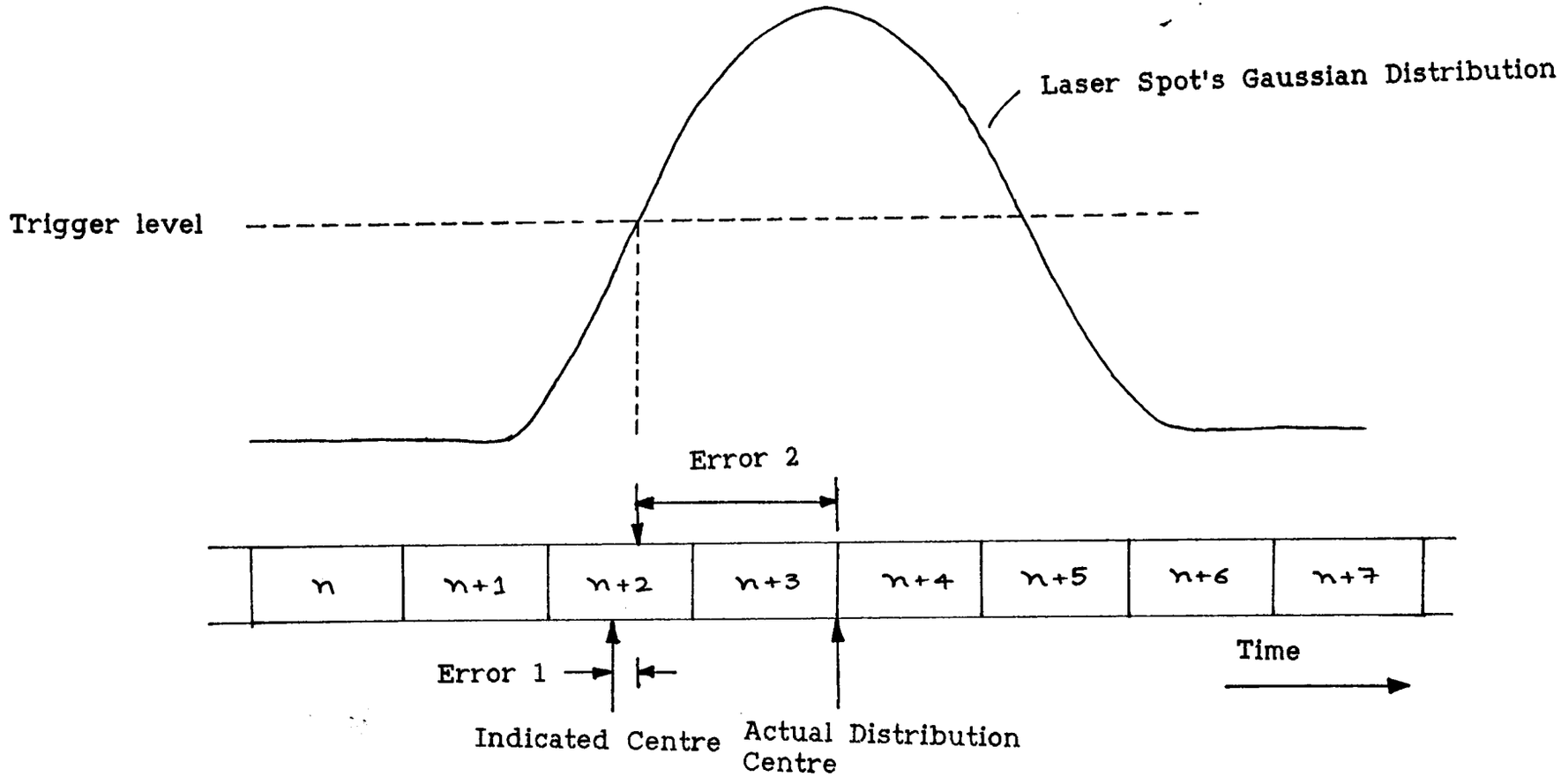

Figure 4.0 STM System 1 Spot Detection Mechanism and Errors.

in the detector board, factors which affect the laser spot distribution size and hence the pixel position will now be examined in more depth.

The size of the distribution of the laser spot is dependent on several factors which include the distance between laser source and surface, the divergence of the laser beam, the emergent diameter of the laser spot and the camera's horizontal resolution. This means that the size of the distribution of the imaged laser spot, measured in units of pixel widths, will not maintain the same size when the distance between the target surface and the STM system is increased. This is because the effective spot size at the target surface is made up of two components, the initial diameter of the spot when it exits the laser tube, and the product of the divergence and the distance to the target surface from the system. With large distances, the laser spot (as imaged in the camera) will become a constant angular size. This is because the contribution to the spot size from the initial diameter is 'swamped' by the contribution from the divergence. In the actual system this not the situation that is observed due to the relatively small system to target surface distance.

Now the possibilities for the relationship between the size of the imaged laser spot (diameter S) and a camera horizontal pixel width (P), will be examined. Assuming that the threshold level of the comparator in the detector board does not change, the possibilities are that the spot's distribution is:

(1). $P = S$

(2). $P > S$

(3). $P < S$

The three situations outlined above are illustrated in figure 4.1 for the worst case position of the laser spot's distribution. These

(a) Spot size = 1 pixel
(error $\leq$ 1 pixel).

(b) Spot size $\leq$ 1 Pixel
(error $\leq \pm$ 1/2 pixel).

(c) Spot Size > 1 pixel
(error $\leq$ 1/2 pixel +
1/2 the distribution size).

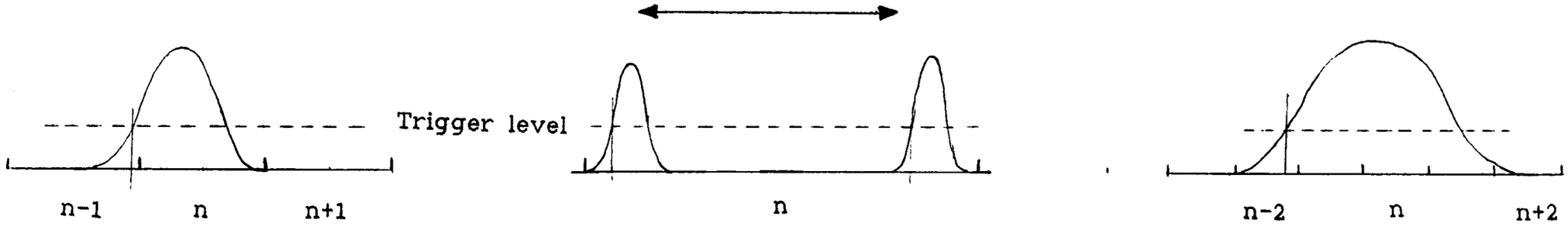

Figure 4.1 An Illustration of Possible Distribution Sizes.

correspond to errors of 1 pixel in case (1), $\pm$ 1/2 pixel in case (2) and half the distribution size + 1/2 a pixel in case (3). The above definitions assume the start and end of the laser spot's distribution is when it exceeds and falls below the threshold level respectively.

Now that the three main possibilities for the distribution of the laser spot have been explained, the task now is to identify which of these situations exist in the STM system's photo sensitive device and quantify the error, so that comparisons can be made with any errors obtained in the test results. The ratio of the laser distribution size to the camera's pixel size is given by the following equation with the distance to the furthest test surface taken into account (a more formal definition of this this equation will be presented in section 4.2.3).

$$(1.4 * 10^{-3} * 5 + 1 * 10^{-3})/(5 * 9.5 * 10^{-4}) = 1.7$$

This means that the laser spot will span more than a single pixel of the camera and therefore it is third case illustrated in Figure 4.1 that applies.

The last two parameters to be obtained are the range error associated with one pixel error (which will form the ordinate of the accuracy test error graph) and the expected error of the system assuming a ratio of 1.7 for the spot diameter to pixel size. Using equation (6) (which is repeated below for convenience), substituting the value 1 for δa (that is a single pixel error) and using the appropriate value for a horizontal pixel width px (where px = 25 * Tan(7°/128) = 23.9 μm) the result is given below.

$$\text{range error} = \delta z = - \frac{z^2 * \delta a * px}{z * \delta a * px + d * l}$$

$$= \frac{25 * 1 * 23.9}{5 * 1 * 23.9 * 10^{-3} + 25 * 0.5} = 47 \text{ mm}$$

The 'worst case' expected error in the system is half the distribution size in pixels + 1/2 pixel producing a result of 1.2 pixels. This value is substituted into equation (6) as shown below.

$$\text{range error} = \delta z = \frac{25 * 1.35 * 23.9}{5 * 1.35 * 23.9 * 10^{-3} + 25 * 0.5} = 64 \text{ mm}$$

Figure 4.2 presents the results from the accuracy tests in terms of their relationship of actual errors to calculated theoretical error, the graph shows the averaged (from 3 runs) results for the original accuracy tests and also the results obtained from the tests performed with vertical scan and hardware spot size detector enhancements implemented. Marked on the graph is also the expected error due to the actual laser spot having a diameter that is greater that a single pixel.

From the results presented in figure 4.2, it can be seen that even with the modifications of the vertical scan, with its associated 16 line active window and the hardware spot size detector, the errors obtained from the accuracy tests were greater that those predicted in the theoretical equation by a factor of 2 or more. Also a significant amount of spurious results were obtained (spurious values are range values with an error which is greater that 10 % of the actual range). On examining the system for the source of these errors the Newvicon tube camera was identified as a major source due to the possibility of a deviation of $\pm$ 3 % between the spatial position of the laser spot and its corresponding position the the output temporal video stream (defined in the camera specification). This translates to a maximum error of 11 pixels in the horizontal pixel position, from the magnitude

(a) Results from the STM System 1 before and after Modification.

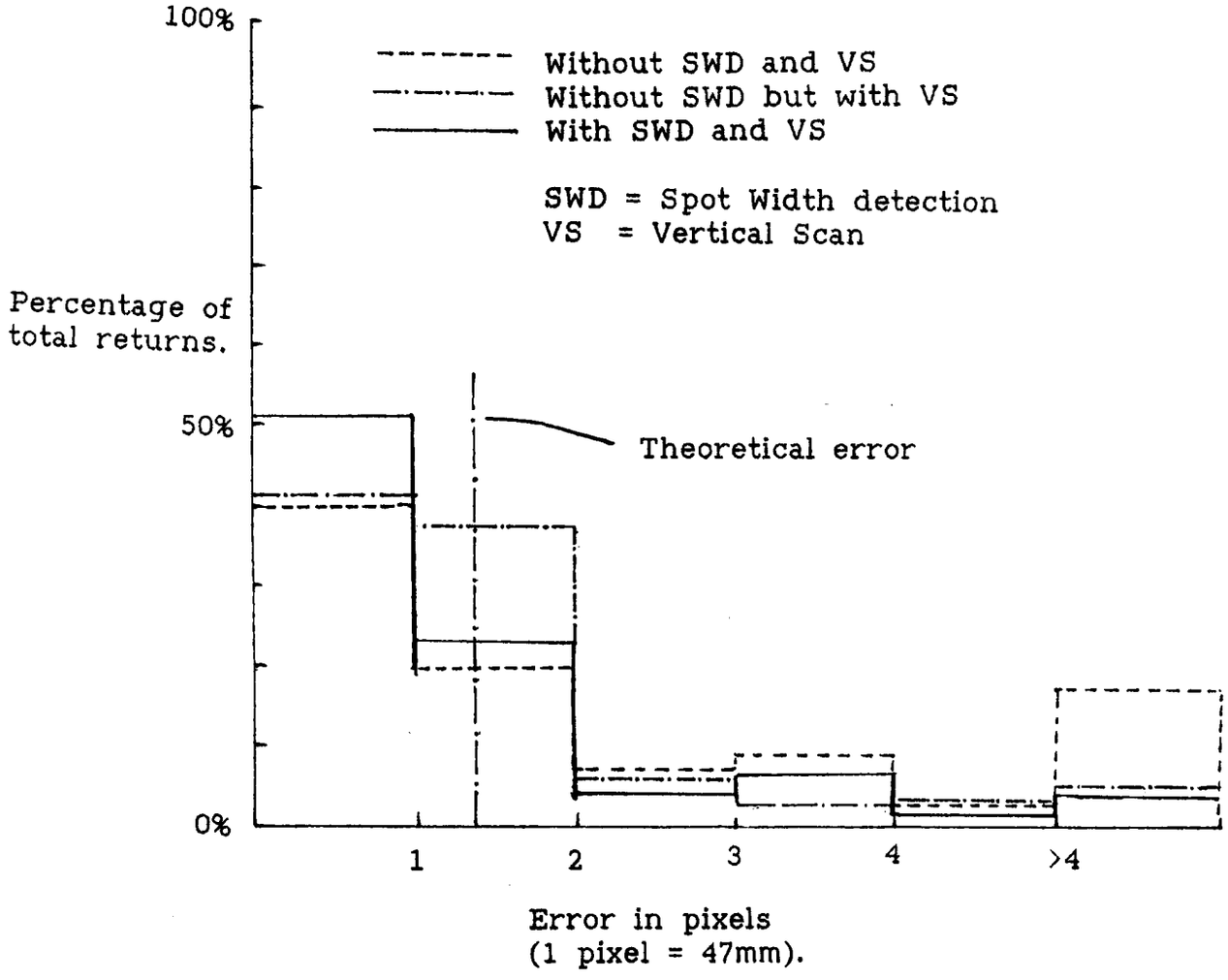

(b) Graphical Output from the STM System 1.

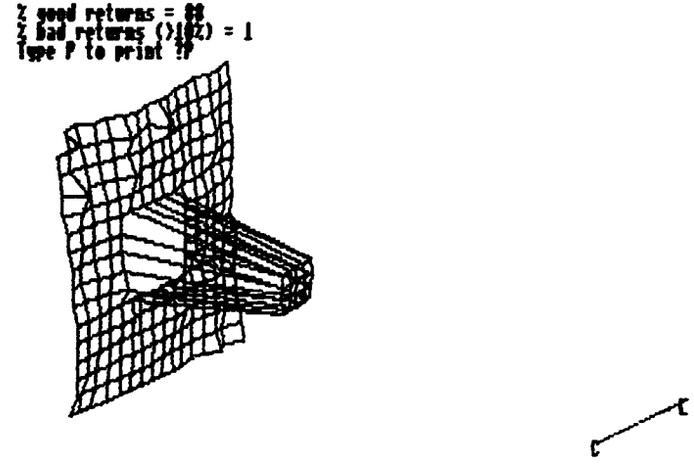

Figure 4.2 Results from the STM System 1 Tests.

of the errors that have been found in the test results this displacement error is evidently occurring and is clearly unacceptable. The above discussion means that the camera must be changed for one with a much more consistent spatial/temporal relationship (greater stability within the sensor geometry and read out electronics).

4.2 Additional Parameters of the STM System.

Several parameters which have not yet been discussed will be outlined in this section. The first of these is the range of the STM system, the next parameter examined is the degree of spatial sampling possible (this is the amount of definable spatial points which can be obtained either, at a specific distance away from the camera, or within a certain range limits). The last parameter is a formal definition of the width of the laser spot as viewed by the camera. This is related to the laser beams' divergence and the allowable range over which the STM system operates.

4.2.1 The Range of the STM System.

An important parameter of the STM system is the minimum and maximum distance, away from the camera/laser baseline, that the system can operate over. This range is bounded by the camera's horizontal field of view and is dependent on the maximum angular extension of the moving iron galvanometer laser deflectors. The method for calculating the range is first to start with deciding a design or application limit for either the maximum or minimum distance that the system may operate over. Once either the maximum or minimum distance has been defined the other can easily be calculated and therefore the range is also defined. For the case of the limit being placed on the minimum distance the

laser deflector must be able to span the camera's horizontal field of view at that distance. Since the moving iron galvanometer laser deflectors have a maximum mechanical excursion of 20° (40° optical), the maximum distance over which the the device can operate is defined by the intersection of the extreme of the cameras horizontal field of view and the laser deflector at maximum extension. This is shown in figure 4.3 where the minimum operational distance (Zmin), the maximum operational distance (Zmax) and the extent of the range (Zrange) are all indicated. Using this figure and equation (1) the minimum operational distance is defined by.

$$Zmin = \frac{1}{Tan\ (\beta) + Tan\ (-\theta)} \qquad (14).$$

In this equation 'α' is an angle equal to half the camera's horizontal field of view. 'β' is the angle made between the laser deflectors 'sight line' (see section 2.1.2 for definition of the laser deflectors 'sight line') and the line projected from the origin of the 'sight line' to the edge of the camera's horizontal field of view. Now, from the argument presented above, this equation is in the wrong form since Zmin has been set and the unknown value is the argument β, therefore, re-arranging equation (14) to make β the subject.

$$\beta = Tan^{-1}\ \{\ 1/Zmin + tan\ (\theta)\ \} \qquad (15).$$

From this equation the maximum operational distance can now be calculated as shown below.

$$Zmax = \frac{1}{Tan\ (\theta) + Tan\ (\beta - MIGmax)} \qquad (16).$$

Where MIGmax is the maximum excursion of the laser deflectors and

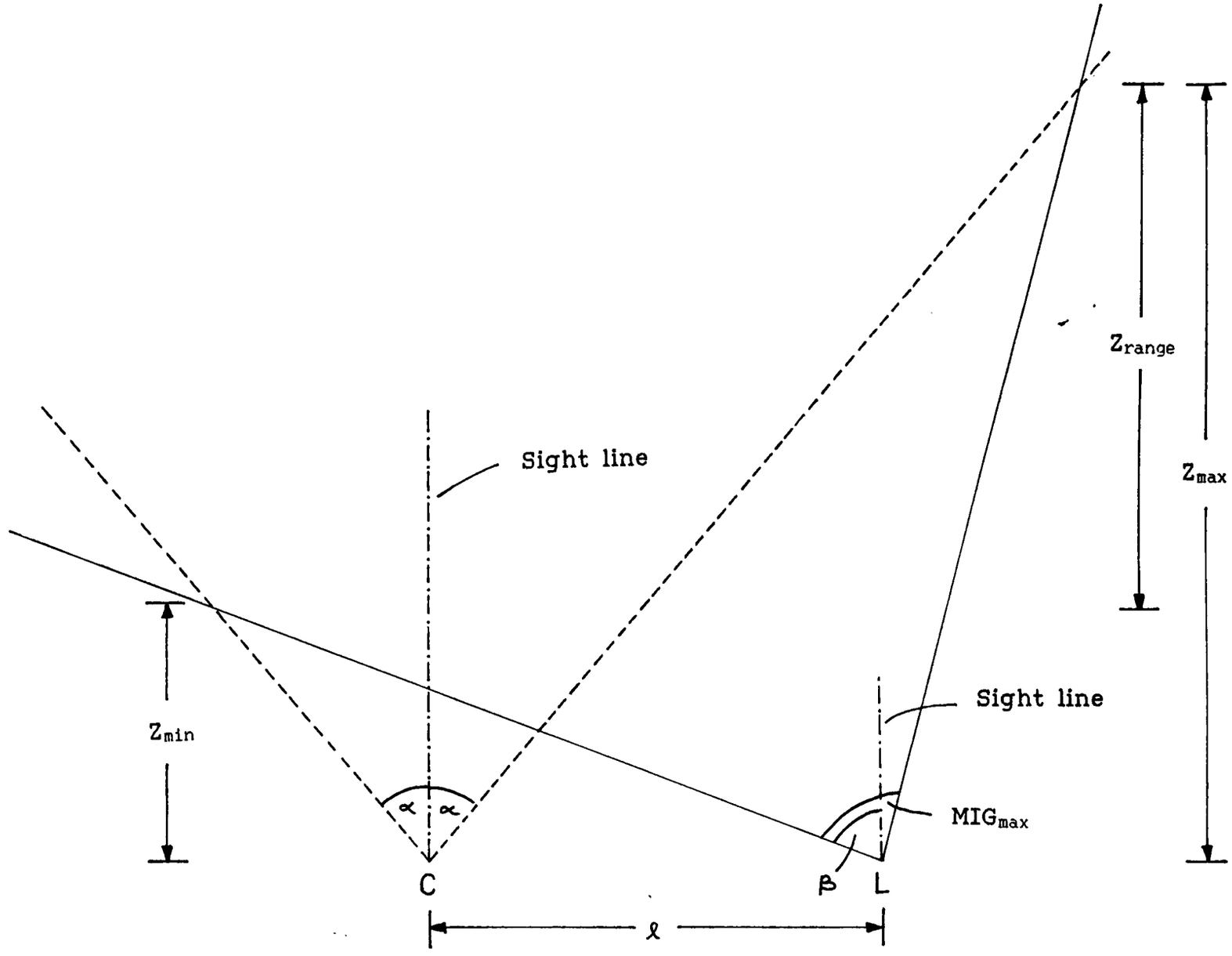

Figure 4.3 The STM System Range.

the condition that $\beta > 40 - \theta$ must hold (that is the extreme of the horizontal field of view of the camera intersects with the line of the projected laser beam with the laser deflector at maximum extension). The combination of equations (16) and (14) gives the range.

$$Z_{range} = Z_{max} - Z_{min} =$$

$$\frac{l}{\tan(\theta) - \tan(MIG_{max} - \beta)} - \frac{l}{\tan(\beta) - \tan(\theta)} \qquad (17).$$

Figure 4.4 shows a graph of Zmin against Zmax, it can be seen that as Zmin -> 2.1 m the maximum value of the range is not limited (that is $\beta > 40° - \theta°$), below this value the minimum operational distance for the particular application should be plotted on the graph and the maximum operational distance read off.

For the STM system the minimum range was set as 2.1 m so that in any application of the system the only criterion to be checked is that the target surface is greater than Zmin away.

4.2.2 Spatial Sampling and the System Range.

As was mentioned in section 3.1.3 the laser deflectors are driven by a 12 bit digital number which allows a possibility of 4096 definable laser spot positions. Referring to figure 4.5 and provided that the distance from the camera is within the range of $Z_{min} \leq Z_{dist} \leq Z_{max}$ the number of definable laser spot positions at distance Zdist is dependent on the angle θ_{dist}. The angle θ_{dist} can be calculated by the equation below since Zdist, l and the angle α are known.

$$\theta_{dist} = \tan^{-1}(l/Z_{dist} + \tan(\alpha)) + \tan^{-1}(1/Z_{dist} - \tan(\alpha))$$

Using the above equation, the maximum number of spatial samples available is given by.

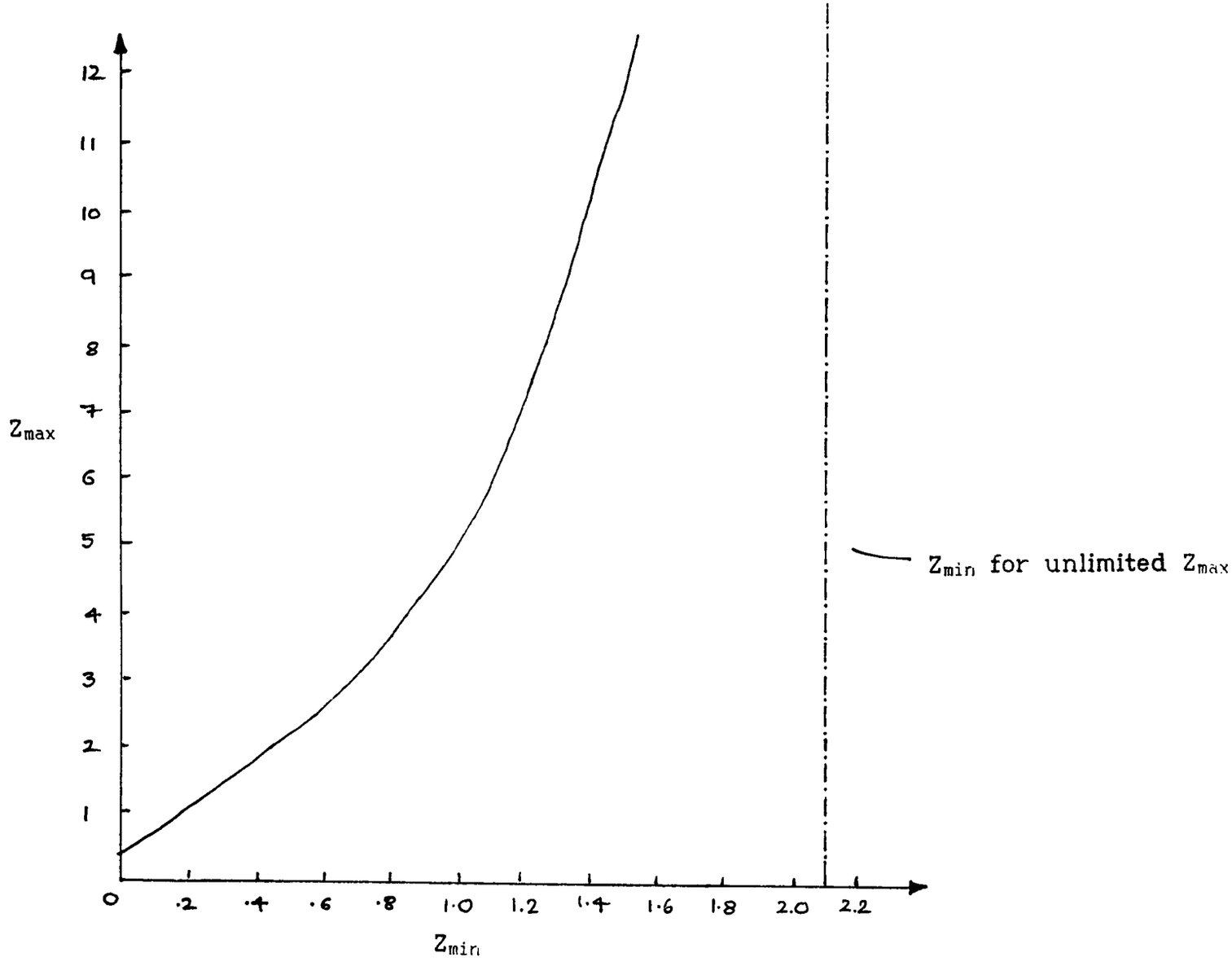

Figure 4.4 The STM system Range (Z_{max} as a function of Z_{min}).

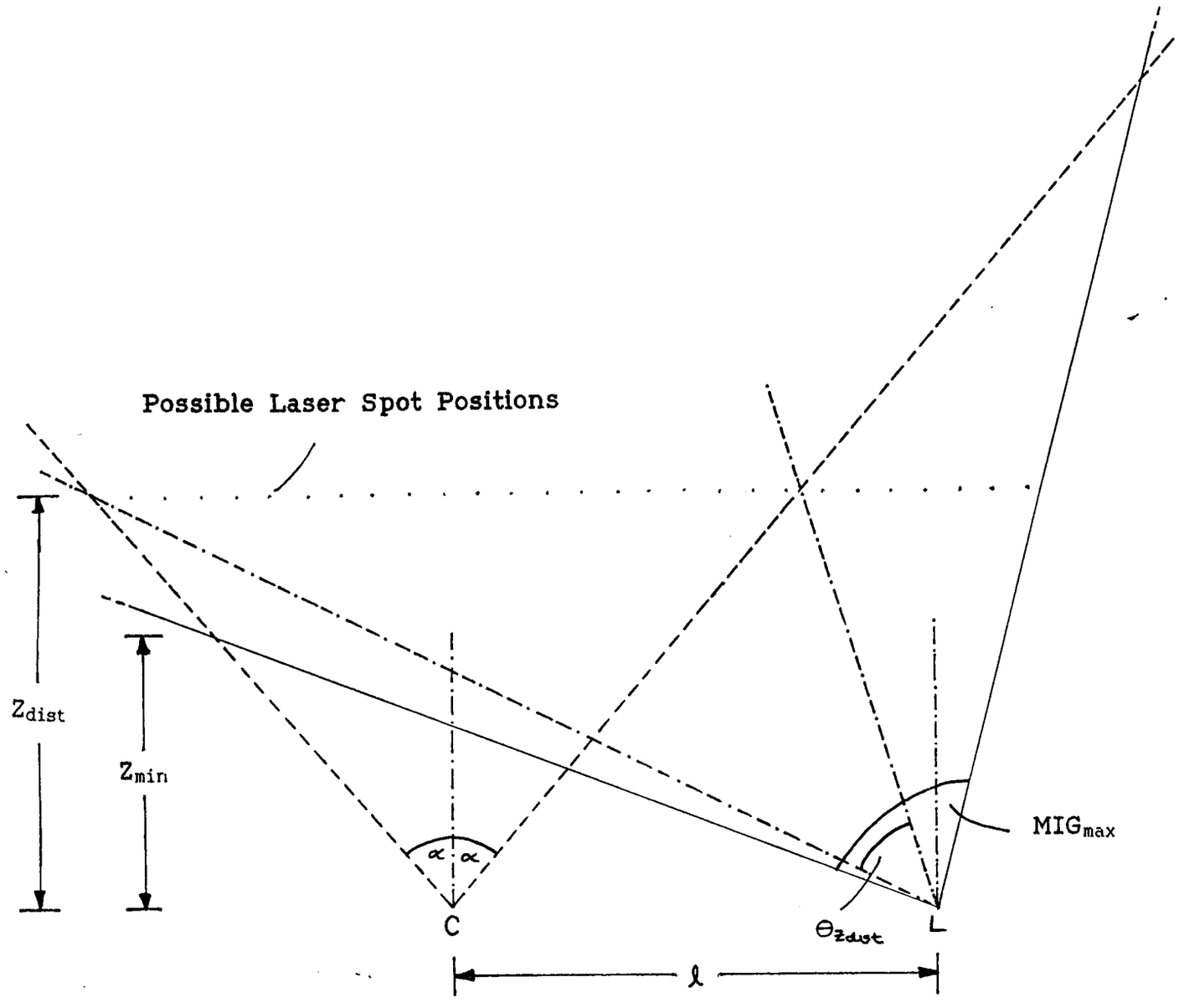

Figure 4.5 Spatial Sampling and the System Range.

$$\text{Maximum number of spatial samples} = \frac{4096}{MIGmax} * \theta dist \qquad (18).$$

This equation represents the maximum ideal spatial sampling. Several conditions may be imposed on the obtainable number of spatial samples by the application (i.e perhaps coarse spatial sampling conveys all the information necessary to characterise the target surface) or errors present in the moving iron galvanometer drivers (inherent errors in D/A converter transfer characteristics and driving electronics can reduce the number of definable positions i.e errors of $\leq$ 0.098 % would mean that only 10 bits of the original 12 are significant reducing the number of definable spot positions by a factor of 4).

With a complex surface the number of spatial samples available is greater than that predicted with the equation defined above provided that Zdist is made equal to the distance of the closest point on the target surface, but the final number of readings obtained will be reduced due to occlusion effects.

In the STM system 1 for the tests described in Chapter 3, 16 horizontal spot positions are defined at a distance of 5 m away from the camera/laser baseline.

4.2.3 Laser Spot Width in the Camera.

The width of the laser spot, as viewed by the camera, is an important parameter which will help with the production of a reliable spot detection mechanism (this analysis will become more relevant when the search for subpixel resolution is outlined in the next Chapter). Assuming that the laser spot must maintain a minimum size (in camera pixel widths), an equation is derived (using simple triangulation) which gives the width of n camera pixels at a distance Zdist away from

the camera/laser baseline.

$$\text{width of n pixels} = Zdist * n * CHR \qquad (19).$$

Where CHR stands for the camera's horizontal resolution which is the tangent of the angle subtended at the lens by one camera pixel and has the same value as px / d ($CHR = 23.9 * 10^{-6}/25 * 10^{-3} = 9.54 * 10^{-4}$). The laser spot has a diameter (as described in section 2.3.2) at distance Zdist of.

$$\text{spot diameter} = \text{divergence} * Zdist + ID \qquad (20).$$

Where ID stands for the laser beams initial diameter. For the laser spot to maintain a minimum size the condition given below must hold.

$$\text{spot diameter} \geq \text{width of n pixels} \qquad (21).$$

Substituting (19) and (20) into (21), this becomes

$$\text{divergence} + ID/Zdist \geq n * CHR \qquad (22).$$

If either the camera's horizontal resolution or the laser divergence are alterable they can be made the subject of inequality (22) and, for a particular value of 'n', a minimum spot size can be guaranteed.

In the present STM system, both the camera's horizontal resolution and the laser divergence have already been set. This means that 'n' is the unknown in equation (22) and its value can be calculated from the equation given below.

$$n \leq \frac{\text{divergence}}{CHR} + \frac{ID}{Zdist} \leq \frac{1.4 * 10^{-3}}{9.5 * 10^{-4}} + \frac{1 * 10^{-3}}{Zdist}$$

From the equation given it can be seen that 'n' will be a minimum when Zdist is equal to Zmax, substituting 5 m for Zdist (maximum operational distance for STM system 1 tests) in the above equation the result is obtained that $n \leq 1.5$. It can also be noted that with the above quantities that after Zdist = 0.068 m (less that Zmin) the effect of Zdist in the above equation is less that 1% and therefore negligible.

4.3 Concepts behind the STM System 2 and their Implementation.

As already outlined in section 4.1, the errors which were present in the system's accuracy tests can be mainly attributed to deficiencies present in the camera used in the STM system 1. In this section, other deficiencies identified in the system 1 will be outlined and remedies to these problems proposed. A major deficiency of the system 1 is the inability to modify the spot detection mechanism, although the hardware spot size detector has improved the system's accuracy, it has not the flexibility required to deal effectively with different ambient lighting conditions and changes in target surface composition (such as roughness and albedo). Another problem is that the present spot size detection mechanism places a limit on the possible resolution to which the centre of the laser spot can be obtained. Other problems found in system 1 are that the system design has made few allowances for the large temperature variation which can be expected when operating in an industrial environment. Also that the limit placed on the complexity and speed of the system by the use of 8-bit microprocessor board for the controlling microprocessor system and the non standard BASIC language for the supervisory computer's software.

What is proposed is to present the ideas and concepts behind the STM system 2. The improvements suggested will reduce or remove the deficiencies, in the STM system 1, which have been highlighted in the proceeding paragraph.

The two major changes which distinguish the STM system 1 from the STM system 2 are, firstly, in the introduction of a camera which uses a Charge Coupled Device (CCD) sensor instead of a Newvicon tube to capture the image of the target scene. In the CCD sensor (see reference [53]) the spatial pixels are defined by gate electrodes etched onto the silicon wafer and not by a scanning electron beam as in the newvicon tube. This gives the CCD a much greater spatial/temporal stability compared with the Vidicon and consequently, a near linear relationship between the input spatial to output temporal position of the laser spot. The second major change is to introduce a hardware unit which digitises and stores the input video stream (between the start and end of the active window, which is normally sixteen video lines wide). This allows the laser spot's distribution to be examined in software which enables complex algorithms to be applied to ascertain the centre of the laser spot's distribution.

Introduction of the enhancements just presented have produced radical changes in the STM system hardware. These changes are now described, along with other minor enhancements which have been introduced, in the following sub-sections. These sub-sections are again based on a functional division of the STM system into blocks and these are shown in Figure 4.6 which is the STM system 2 block diagram.

4.3.1 The Photo sensitive Device and Laser deflectors.

As mentioned in the previous section the Newvicon tube camera has

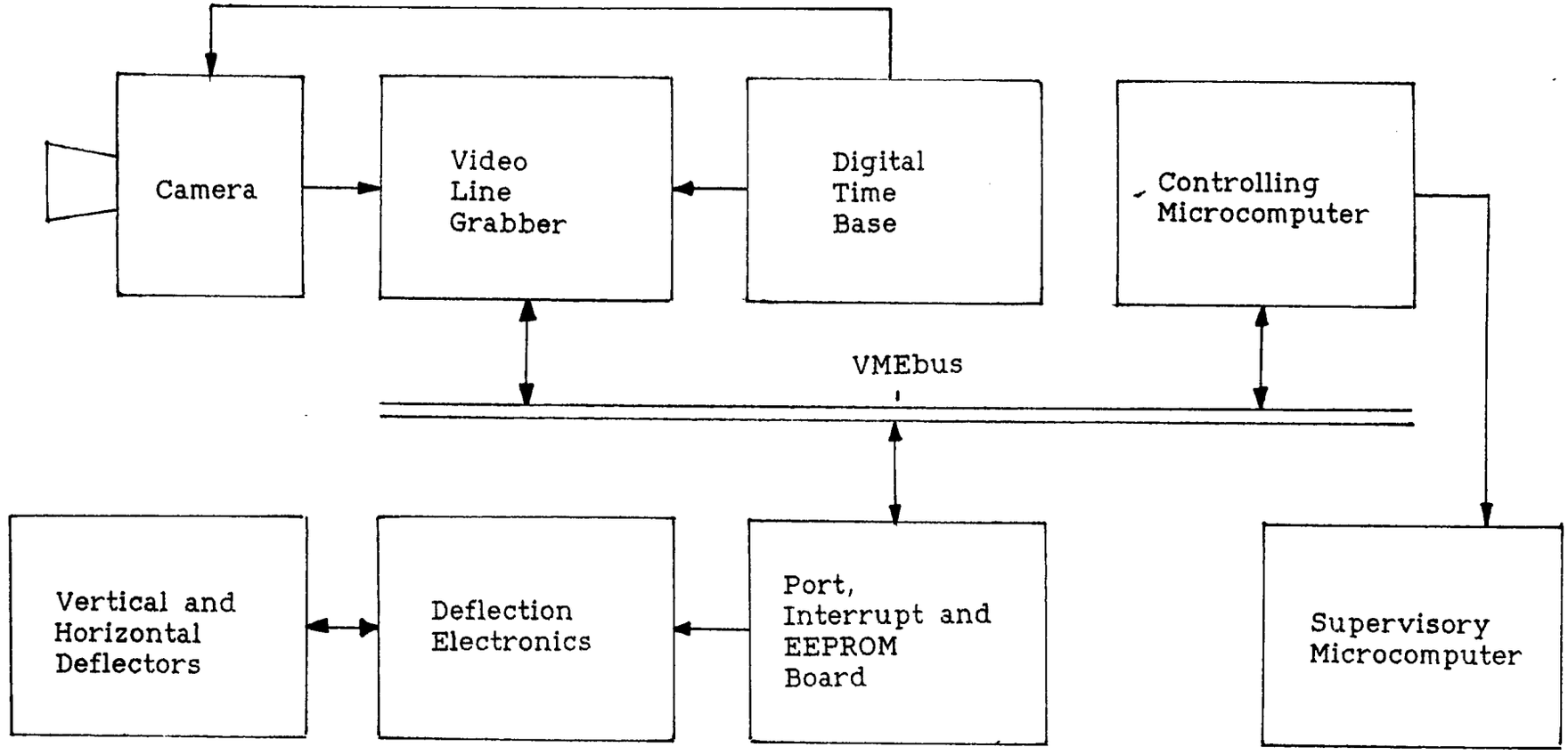

Figure 4.6 Block Diagram of the STM system 2.

been replaced for a camera which uses a CCD image sensor, this camera has other advantages apart from the linear input spatial/output temporal relationship, these will now be outlined. The CCD camera has increased industrial ruggedness (less sensitive than either vidicon or newvicon to E.M. interference) and, since the CCD sensor used has a frame transfer scheme to move the sensed image out of the imaging part of the CCD, each pixel will have a full 20 ms (one half interlaced frame) to register if the spot is present before the whole half interlaced frame is read out. Some disadvantages are associated with the change of camera. These are: that the CCD sensor has smaller dimensions that the Newvicon tube so that a wide angle lens must be used to maintain the the same camera horizontal field of view; another minor disadvantage is that a 20 ms delay is introduced into the system by the frame transfer scheme, this makes repeating a measurement difficult when a predetermined scan is being executed. The narrow band optical interference filter is still placed in front of the camera lens and the new values for photo sensitive device parameters are now given, starting with the horizontal field of view which is obtained from equation (8) noting that the camera has a 12mm lens.

horizontal field of view = $2 * \text{Tan}^{-1}(3/6) = 28°$

The next important parameters to calculate are the number of pixels the laser spot extends over (equation (22)), this equation requires the camera's single pixel angular horizontal resolution to be calculated which is equal to $\text{Tan}(14°/302) = 8.09 * 10^{-4}$ for the CCD camera since it has 604 horizontal pixels. This parameter is now calculated below.

$$\text{number of pixels spanned by laser spot} \leq \frac{1.4 * 10^{-3}}{8.09 * 10^{-4}} + \frac{1 * 10^{-3}}{5}$$

$$\leq 1.7 \text{ pixels}$$

In the above equation Zdist is taken as 5 m. The last parameter to be calculated is the range error due to a single pixel and the range error expected which results from the spread of the laser spot over several pixels, these two results are given below.

$$\text{single pixel range error} = \frac{25 * 1 * 9.71}{5 * 1 * 9.71 * 10^{-3} + 12 * 0.5} = 40 \text{ mm}$$

$$\text{spot size range error} = \frac{25 * 1.35 * 9.71}{5 * 1.35 * 9.71 * 10^{-3} + 12 * 0.5} = 54 \text{ mm}$$

The only change made to the laser and its deflection mechanism was to replace the system 1 moving iron galvanometer deflectors with temperature stabilised moving iron galvanometer deflectors. These maintain the moving iron galvanometer at a predetermined temperature with a small heating blanket attached round them. The temperature chosen for the moving iron galvanometer must be greater than the ambient since the only cooling mechanism is heat lost to the ambient convection. The new moving iron galvanometer has a temperature stability of 20 μrad/°C an improvement of four times the unstabilised galvanometers. More information and additional performance data on the moving iron galvanometer deflectors can be found in reference Montagu [43]. The stability of the moving iron galvanometers was also enhanced by using the same supply for the angular transducers, integral within the galvanometers, and for the D/A converters reference (the D/A converter output forms the input to the galvanometer drive unit). The desired stability is achieved due to fact that any variation in the reference supply will effect both the output of the D/A converters and

the angular transducers output. This will reduces the sensitivity of the whole deflection system to supply variation. A block diagram of this setup is illustrated in Figure 4.7.

4.3.2 The Digital Time Base.

The digital time base has been completely redesigned to deal with the increased number of pixels present in the CCD camera and to provide all the signals needed by the Video Line Grabber. One important new signal produced by the digital time base is Active Window (AW) which is illustrated in Figure 4.8. This signal becomes active indicating that the following video lines are within the AW. The new hardware which produces the AW signal allows for software control of the window start line and the length of the active window (from a minimum of 2 lines increasing by a factor of 2 to a maximum of 16 lines). The digital time base also includes a latch (an 8-bit memory element) which, when provided with a signal from the the spot detection comparator which was described in section 3.1.4, records the horizontal pixel position so that the approximate position of the centre of the laser spot's distribution can be obtained.

The System 2 digital time base, as in the original System 1 digital time base, provides external synchronisation signals for the CCD camera (mixed line blank), this also allows correct registration between the camera and Video Line Grabber. The digital time base also furnishes some of the interrupt sources for the controlling microcomputer.

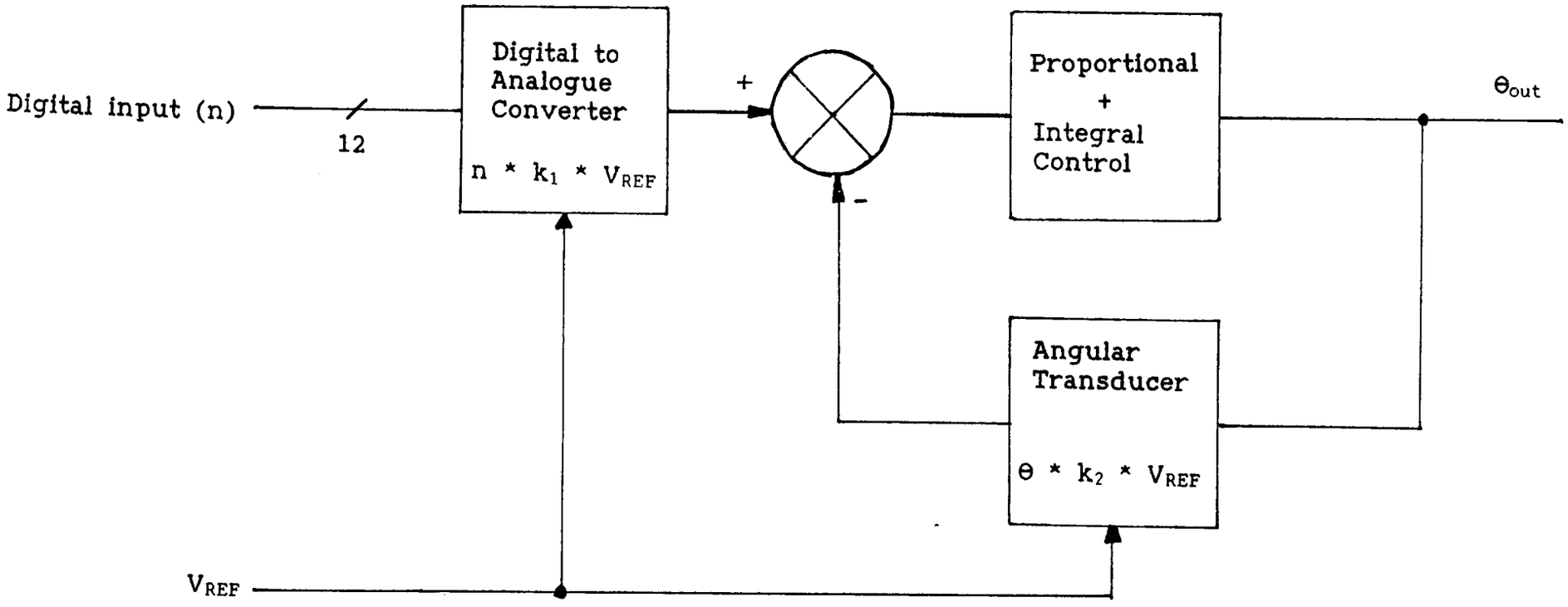

Figure 4.7 Block Diagram of Moving Iron Galvanometers Drive Showing Dual Reference Supply Stability Enhancement.

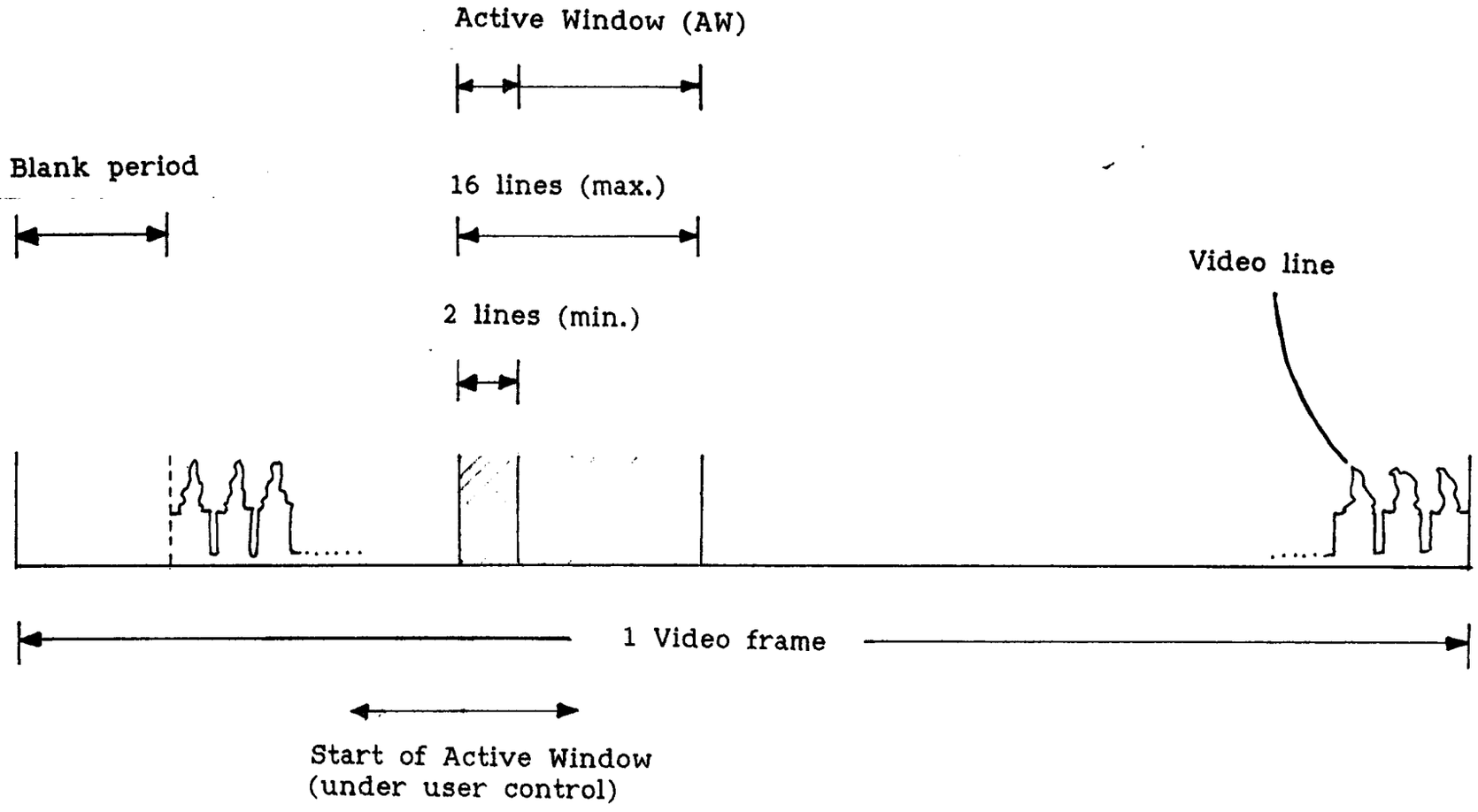

Figure 4.8 Illustration of the Active Window (AW) Signal.

4.3.3 The Video Line Grabber.

The Video Line Grabber is a completely new hardware unit which has been added to the system so that the video lines from the CCD camera, which are within the active window, can be digitised and stored. The video line grabber consists of; analogue signal conditioning circuitry (that is a high frequency amplifier, D.C restoration circuitry and unity gain buffer), an analogue to digital conversion stage (this contains two 6-bit flash ADC which are clocked at half the pixel rate but with clock signals that are 180 degrees out of phase achieving sampling at the pixel rate), the video line grabber memory (64K of fast static RAM), digital address generation logic and a VMEbus interface. The VGL memory is dual-ported so that it can be written to from the ADC's, but also, written to and read from the VMEbus. This allows a method of fast transfer of large quantities of data to and from the video line grabber.

The operation of this unit is as follows; on receipt of an active AW signal from the digital time base, the video signal is digitised and stored with the video line grabber inhibited during the blank period of each line in the active window. When the AW signal goes inactive an interrupt is sent to the controlling microcomputer to indicate that the data in the video line grabber's memory can be operated on. The operations on the video line grabber memory must not take more than 20 - T_{AW} ms or it will extend into the period reserved for the next active window to be digitised and will cause some corruption of data.

4.3.4. Retained System 1 Hardware.

The detector board of the STM system 1 is retained to provide the trigger signal to load the approximate pixel position of the laser spot

into a latch in the digital time base as already explained in Section 3.1.4.

The moving iron galvanometer drivers are retained with the only change being the introduction of more stable chopper stabilised operational amplifiers to increase the long term stability and reduce any temperature dependent drift effects (the chopper stabilised amplifiers offer an improvement of five times, for the parameters of offset voltage temperature coefficient and long term drift of offset voltage, over the original OP07 amplifiers used).

4.3.5 The Controlling Microcomputer.

As mentioned in 4.3.3 the video line grabber has a VMEbus connection, the Controlling Microcomputer is also connected onto the VMEbus so that it can extract data from the video line grabber. The controlling microcomputer is composed of two proprietary VMEbus boards, the first is a Single Board Computer (SBC) and the second is a port/interrupt/ROM board (PIR board). The original 8085 SBC has been replaced by a 16-bit 68000 based SBC, this contains a memory management unit and two serial ports for connection to a local terminal and the supervisory microcomputer. The PIR board contains all the parallel ports used to interface and control to the STM system 2, the prioritised interrupts used by the digital time base and video line grabber and the system ROM which contains the operating software.

The low level software (written in 68000 assembly code) is again interrupt driven for the digital time base's field sync signal which initiates the laser move interrupt service routine (this routine outputs the next 12-bit horizontal and vertical coordinate obtained from either a predetermined scan pattern or from the users terminal,

depending on the mode of operation chosen). The next interrupt to arrive is from the video line grabber to indicate that the lines, which were within the active window, have been acquired and are available; this initiates a service routine that obtains the approximate distribution position from the latch in the digital time base and calculated the addresses of a variable size search window about this approximate spot centre value. This allows only the relevant data (which should contain a digitised representation of the laser spot's distribution) to be moved to the controlling microcomputer for further processing and eliminates the need for a time intensive algorithm which must search the whole of the video line grabber memory for the laser spot's distribution. Data corresponding to the distribution of the laser spot can undergo some processing so that the centroid can be obtained or, can just be passed as raw data to the supervisory microcomputer via the serial RS232 connection or dual-ported RAM parallel link. The controlling microcomputer is now put into wait mode until another digital time base field sync interrupt occurs or the program is aborted by the operator.

4.3.6 The Supervisory Microcomputer and Software.

The supervisory software was completely rewritten in the high level language 'C'. This decision was made because programs written in 'C' are compiled rather than interpreted (as was done with the original BASIC program) and therefore will run much faster. The 'C' language has a ANSI standard and it therefore can be ported with little change to a different supervisory microcomputer if this is required in a later system. Lastly that the "control constructs" and "structured nature" of C enable complex image processing algorithms to be coded quickly and

easily.

There are two main supervisory programs written for the STM system 2. The first is a translation of of the BASIC program described in section 3.1.6 but has enhanced graphics, the ability to re-calculate with the modified system equations (these were presented in section 2.3.2) and a single position calibration procedure. The second program examined the laser spot's distribution in detail, the algorithms used and the results obtained from this program will be explained in the following chapter.

The software was run on an Atari 1040 STFM computer, this contains a 68000 processor, 1 megabyte of memory, a serial port and a cartridge port that is used for the connection to the proprietary dual-ported RAM unit. The dual-ported RAM unit allows many data items to be transferred to the supervisory microcomputer within the 20 ms period between spot movements in the STM system 2 and the serial port allows non-critical messages to be sent to and from the STM system 2.

4.3.7 Circuit Diagrams and Software Listings.

Appendix A contains the circuit diagrams of the STM system 2 hardware described in this Chapter. All the software listings for the STM system 1 and 2 are contained in Reynolds [44].

Chapter 5: Subpixel Resolution and the STM System 2 Tests.

The first part of this chapter will explain the concept of subpixel resolution and how this can be implemented on the STM system 2. Next, the Supervisory microcomputer Laser Spot Distribution Examination Program (LSDEP) will be described and the algorithms which have been developed to locate the centre of the laser spot's distribution will be outlined. The last section details the tests carried on the LSDEP algorithms. These tests used software generated models for the distribution of the laser spot so as to ascertain the performance of the different algorithms under known, controllable conditions.

5.1 Subpixel Resolution: Method and Analysis.

In this section, the resolution available from the STM systems 1 spot detection mechanism will be explored. In the STM system 1 there is no *'a priori'* knowledge of the relationship between the level set as the recognition amplitude (this is the variable trigger level described in section 3.1.4, which operated on the pulse present in the video signal which represents the laser spot's distribution) and the actual amplitude of the laser spots signal (which is a function of the system to target distance, the transmission medium of the laser beam, the target surfaces albedo etc.). Due to this, no estimate of the resolution can be obtained which can be relied upon to reflect the actual situation.

By using the video line grabber hardware a digital representation of the laser spot's distribution is available. In the simplest detection method the spot recognition amplitude can be altered, perhaps as some percentage of the maximum amplitude of the digitised laser

spot's distribution, so that a more consistent resolution, and accuracy, can be obtained. This still does not enable any enhancement in the resolution of the system to be achieved. For subpixel resolution a method must be devised which, instead of just looking at the attributes of single pixels, such as maximum amplitude of any pixel in the laser spots distribution, seeks to find a measure that includes the information contained within sequential pixels. One such multi-pixel measure, which should not have too great a variation between different laser spot positions, is the shape of the laser spot's distribution (although there will definitely be some distortion from the ideal Gaussian distribution theoretically obtained from a TEM_{00} laser). This method of obtaining a greater resolution of the laser spot's position is better that the obvious solution of increasing the number of pixels in the camera (which is both costly and, for large increase in resolution, not yet technically possible) or restricting the system's field of view by using a lens with a greater focal length.

Several papers have described using the the distribution of the laser spot over several pixels to estimate the position of the centre of the distribution to subpixel accuracy. In [45] Young carried out subpixel measurements which are mainly concerned with estimating the length of lines and the location of circles which would form primitives in the identification of the location of industrial parts. This paper also gives good discussion of the errors that can affect whether subpixel accuracy can be obtained (i.e. frame jitter and fixed pattern noise in the imaging device). This problem of errors, which may be present in the laser spots distribution due to deficiencies in the imaging system, will be covered in more depth in a subsequent section when the system software tests are presented.

Tian and Huhns in [46] present an iterative hill climbing algorithm to obtain subpixel resolution but the only source that has been detailed is two successive speckle images (with 3-D coordinates obtained from the stereo disparity technique). The algorithm presented has two main parts. The first which performs a coarse search to locate the positions of the global peak of the cross-correlation function. Once an approximate position for the global peak has been obtained the iterative hill climbing algorithm is used to isolate the global peak of a cross-correlation function to subpixel accuracy. The algorithm yields the disparity between the two images and therefore allows a 3-D representation of the image to be produced.

Two further papers that are directly relevant to the discussion of subpixel resolution and laser spot triangulation are [47] and [48]. In [47] Cielo and Lamontagne describe an astigmatic spot which is projected onto the scene and the resulting image produced by a line array imaging device. This has the property of averaging the astigmatic spot's energy in the vertical direction (the major axis of the spot) and is reported to achieve a more consistent 'near' gaussian distribution. The subpixel resolution is obtained by taking the resultant distribution and performing a centroid calculation (centre of gravity) taking the result to whatever resolution is experimentally verifiable and repeatable. In [48] Lorenz uses an imaging device with conventional pixel shapes but each pixel consists of a photo diode. The resulting image obtained of the laser spot's gaussian distribution is correlated with an ideal gaussian distribution and the peak value from the correlation gives the centre of the distribution to subpixel resolution (provided the ideal gaussian distribution is produced with more that one sample in each pixel position). The horizontal

displacement is then obtained by adding the subpixel displacement, measured from the beginning of the correlation match window, to the pixel coordinate of the start of the correlation match window. The system reported in the paper was tested over several different surfaces and proved to have good repeatability and high resolution (0.002 inches over a 4 inch overall movement).

Several conditions can now be defined for the STM system 2 to be able to achieve subpixel resolution of the centre of the laser spot's distribution:-

(1). That some representation of the laser spot's distribution must be available for examination e.g. stored in a digital memory.

(2). That the laser spot's distribution must extend over more than one pixel because, due to averaging over the surface of each individual pixel in the imaging device, a single pixel conveys no spatial distribution information.

(3). That vertical averaging of the spot's distribution should achieve a better S/N ratio in the resulting distribution even if a non astigmatic spot is used.

(4). That both centroid and correlation methods should be available for locating the centre of the laser spots's distribution.

Since the first two conditions are fulfilled by the existing STM system 2 hardware and conditions (3) and (4) can be implemented in either the controlling microcomputer low level software or supervisory microcomputer high level software, subpixel resolution should be a possibility in the STM system 2. The software, which is implemented at

present in the Supervisory microcomputer and forms the laser spot's distribution examination program, is now described in the following section.

5.1 The Laser Spot's Distribution Examination Program (LSDEP).

The main task of this section is to explain the algorithms, used in the LSDEP, which have the function of locating the centre of the laser spot's distribution to subpixel resolution, before this is carried out a brief description of the rest of the LSDEP will be presented.

5.1.1 A Brief Description of The Program.

The user interface to the laser spot's distribution examination program is a selection menu, this contains options that can be divided into six main categories. The first of these categories are those options which are associated with displaying the input data (which is passed to the Supervisory microcomputer from the STM system 2) and the results produced from this data by the Supervisory microcomputer. The display options include; displaying the STM system 2 data in a wire-frame representation, displaying this data in its raw form as it would have appeared in the VLG's memory (the distribution window), displaying the distribution window after a vertical summation has been carried out, and lastly, displaying the summed data as a graph with the results of the four different distribution centre finding algorithms indicated (also a small section of the summed graph, between specific distribution window pixel values, can be displayed so that any area of interest can be examined in greater detail).

The next category of options are the input and distribution

centre calculation routines (the distribution centre calculation routine produces several estimates of the centre of the laser spot's distribution). These are included together since each time an input is received the distribution centre calculation routine is automatically executed. There are two main input options, the first option is a initiated from the keyboard of the Supervisory microcomputer and the information that is passed from the controlling microcomputer to the Supervisory microcomputer is; all the raw data in the distribution window, the vertical summation of all the lines in the distribution window, an approximate value for the centre of the distribution and various distribution window parameters (distribution window width, distribution window start pixel value and size of the active window in lines). The second option is the remote input option which allows a series of measurements to be obtained and stored to disk. Each individual measurement is initiated from a remote unit. This can be located near the target surface so that a parameter of the target system can be altered and measurements obtained without returning to the supervisory microcomputer's keyboard. Although, as already mentioned, the distribution centre calculation routine is executed each time a new distribution is obtained, it is also available as a separate option which can be used when some LSDEP parameter has been altered. On evoking this option the user is passed to a sub-menu which contains five options, only four of the options are essentially different algorithms the fifth being a 'short cut' method for calculating the fine gaussian correlation (see section 5.1.5 for more detailed description). These four algorithms are discussed in detail in the subsequent subsections.

The third category of options are disk storage and retrieval

routines, this includes a disk storage option which produces a disk data file of all relevant information for a particular distribution. The opposite of this routine is a disk retrieval option which reads all the information stored in the disk data file so that the distribution can be processes further in the LSDEP.

The last two categories of options are for entry to the model sub-menu and LSDEP parameter change option. In the model sub-menu option, models of the laser spot's distribution can be created for centre finding algorithm test and distribution comparison purposes. The LSDEP parameter change option enables parameters referring to the correlation model and display to be modified.

The four individual algorithms, which are available in the distribution centre calculation routine and are used to locate the centre of the laser spot's distribution, will now explained in detail. Some pre-processing is performed on the raw data received from the STM System 2 before it is passed to any of the distribution centre finding algorithms, this will be described in the next section along with a outline of specialised terms which will be used in the descriptions of the four algorithms.

5.1.2 Distribution Centre Finding Algorithms Pre-Processing.

The pre-processing carried out on the raw data, which is produced by the STM system 2, will now be described which the aid of figure 5.0(a) and 5.0(b). The pre-processing consists of first summing the data in the distribution window about the vertical columns with the same horizontal pixel value (required to fulfil condition (2) of section 5.1). The 'distribution window' is defined as being a variable length in pixels (user defined), having a vertical size equal to the

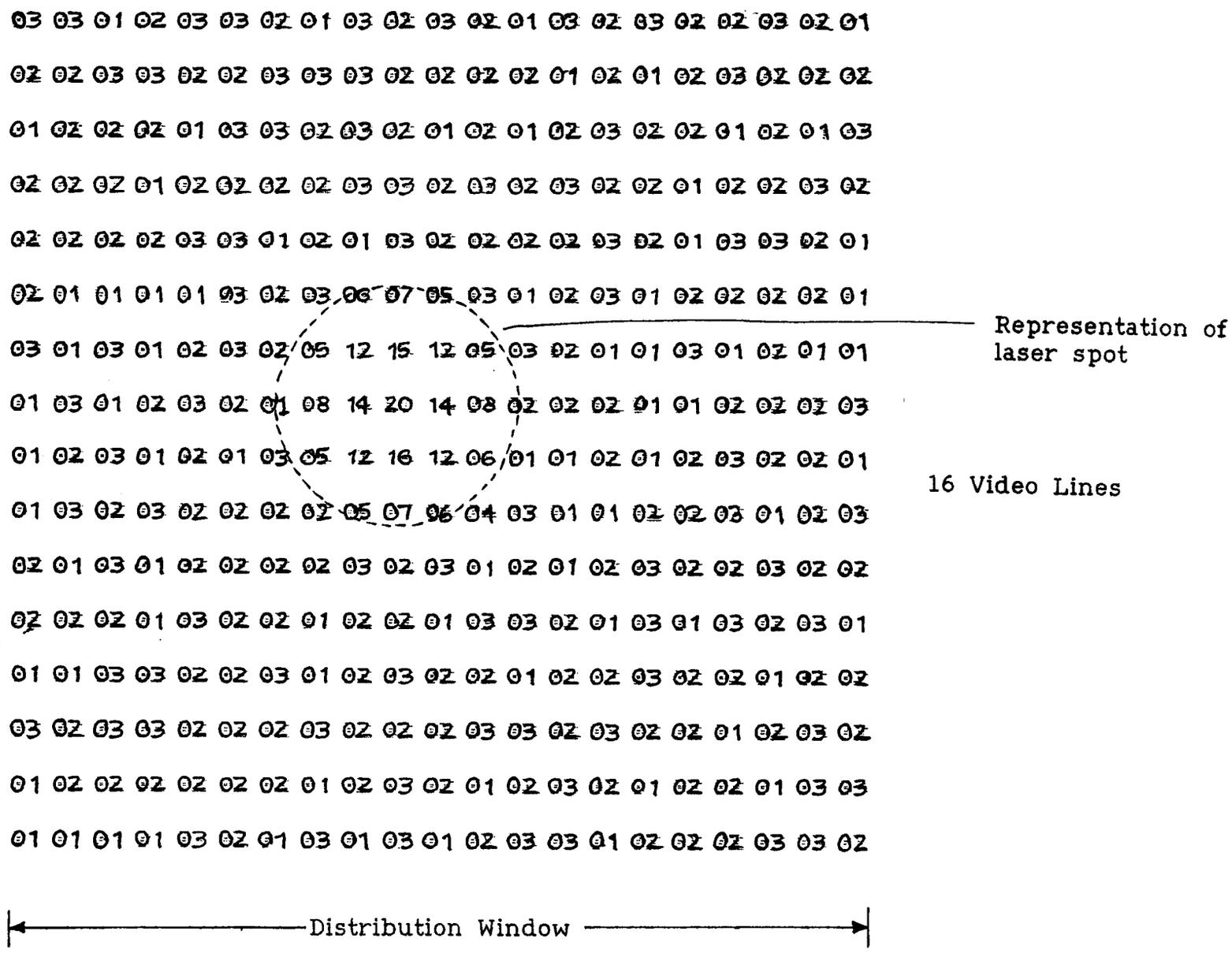

Figure 5.0(a) LSDEP Pre-Processing : Video Line Grabber Raw Data.

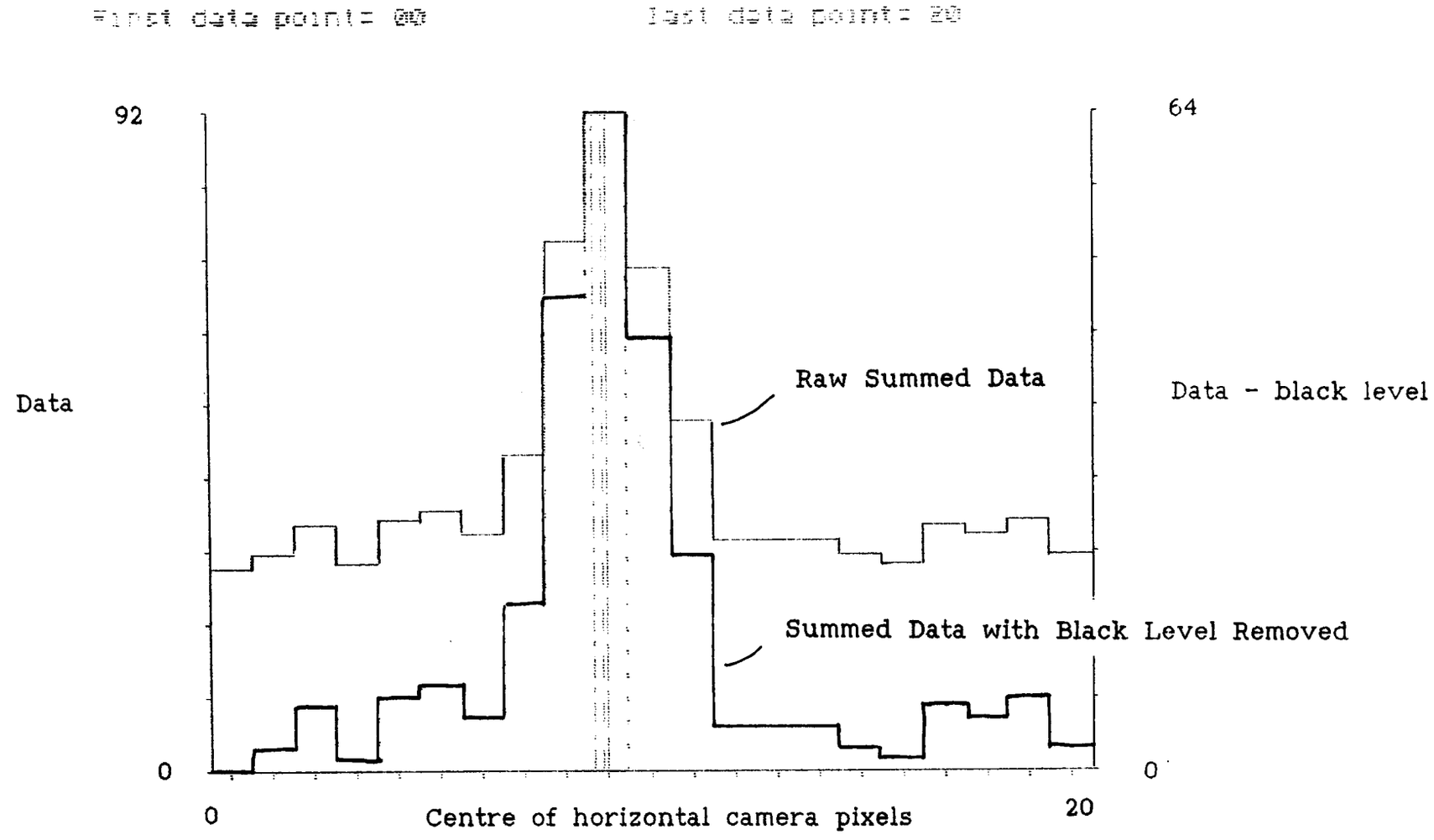

Figure 5.0(b) LSDEP Pre-Processing : Vertical Summation and Black Level Removal.

size of the active window (2 to 16 video lines) and contains a copy of the data present in the video line grabber's memory (see section 4.3.5). The vertical summing of the distribution can be carried out because the TEM_{00} laser beam has a two-dimensional Gaussian distribution. This vertical summation should also reduce the effect of any random noise that may be present in the laser spots signal.

The next operation that is carried out is to remove any 'black level' or zero offset which may have accumulated in the new summed distribution, this is performed due to the fact that an error would be produced if a centroid calculation was carried out and the distribution present was not in the centre of the distribution window. Once the above two operations have been performed the subsequent one dimensional distribution is termed the Vertically Summed Distribution (VSD) and reference will be made to this in the descriptions of the distribution centre finding algorithms. The last term that requires a definition is the calculation window, this is the same size or smaller that the distribution window and defines the limits of the calculation for any of the distribution centre finding algorithms. All the new terms introduced in this section are illustrated in Figure 5.0(b).

5.1.3 Algorithm 1 : Centroid (Centre of Gravity).

In this algorithm the centroid of the laser spot's distribution is obtained, this is illustrated in Figure 5.1. The centroid calculation is performed as follows; the VSD's value at the left hand (LH) edge of the distribution window is multiplied by effective displacement distance (this is the distance from the LH edge of the calculation window to the right hand (RH) edge of the VSD pixel of interest, in this case, it is equal to 1). This value is then added to the

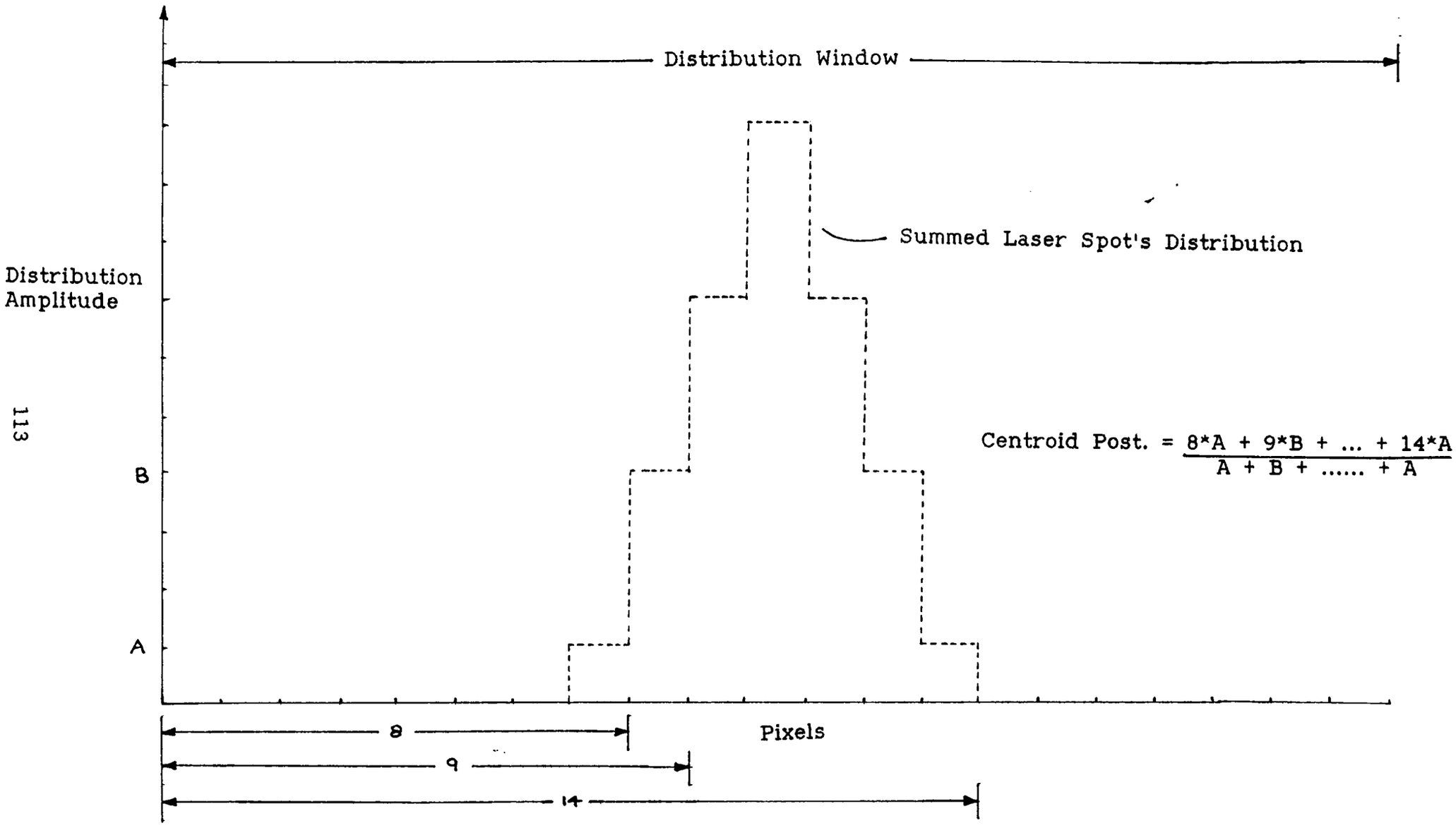

Figure 5.1 An Illustration of Algorithm 1 : A Centroid Calculation.

product of the VSD value located at the position to the right of the last location and its corresponding effective displacement distance (2). This process is continued until the RH edge of the distribution window is reached. The above value is now divided by the sum of all the VSD pixel values and 0.5 is subtracted to correct for the VSD values being nominally located in the centre of each pixel position. The last operation is to add the value created above to the pixel value which corresponds to the start of the distribution window and this produces a value for the horizontal displacement of the laser spot. The equation given below describes this process in mathematical terms.

$$\text{pixel displacement} = \frac{\sum_{i=1}^{m} VSD_{(i)} * i}{\sum_{i=1}^{m} VSD_{(i)}} - 0.5 + DWSPV \qquad (23).$$

Where m is the width of the distribution window (usually 21 pixels), VSD_i is the value of the i^{th} pixel of the vertically summed distribution and DWSPV is the Distribution Window Start Pixel Value, which is a parameter passed from the controlling microcomputer.

5.1.4 Algorithm 2 : Distribution Magnitude Comparison and Centroid.

In this algorithm the maximum VSD value is obtained and the amplitude of the VSD values either side of this maximum are monitored so that a calculation window can be defined, this is illustrated in Figure 5.2. The calculation window is defined as follows; the value in the VSD on the LH side of the maximum value is examined and its amplitude compared to the value on the RH of the maximum value, if it is smaller, it is compared to successive RH values further away from the maximum value until either the new RH value becomes smaller than the LH value, or the edge of the distribution window is reached. If the

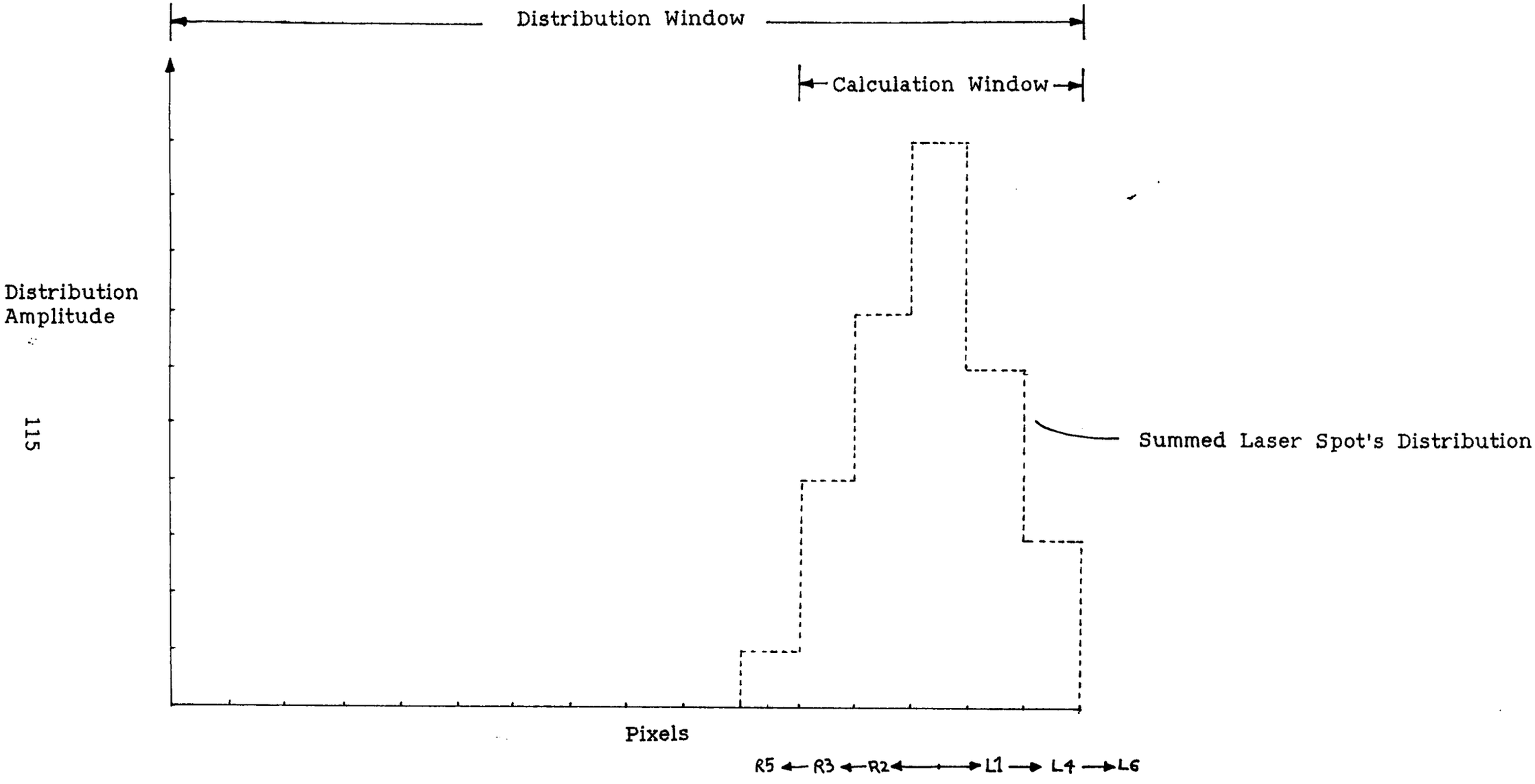

Figure 5.2 An Illustration of Algorithm 2 : Magnitude Comparison and Centroid.

new RH value becomes smaller than the present LH value, successive LH values, further away from the maximum, are tried until the new LH value is smaller that the present RH value or the edge of the distribution window is reached. The algorithm swaps from left to right trying to maintain the VSD pixel values defined by the left and right hand pointers at a similar amplitude. Once either LH or RH edge of the distribution window have been reached the calculation window is produced by finding the smallest distance, away from the maximum value, of either the left or right hand pointers; this value is doubled and centred on the pixel position of the maximum VSD value and this forms the calculation window.

The calculation window is used as the limits of a centroid calculation which has been outlined in 5.1.1. The final displacement value is obtained from taking the result of the centroid calculation and adding this to the pixel value of the start of the calculation window (this is made up of an offset equal to the distance between the start of the calculation window and the start of the distribution window) and the distribution window start pixel value.

The above algotithm is performed to remove the error that would be produced if the laser spot's distribution does not appear in the centre of the distribution window, (due to its size or a small error in the analogue window finding hardware) causing some of the distribution to fall outside the distribution window. In this case the area over which the centroid is calculated should be clipped to achieve an approximately symmetrical distribution . This process stops an error being introduced into the resultant centroid value which would be offset away from the edge of the distribution window where the laser spot's distribution has been truncated.

5.1.5 Algorithm 3 : Coarse Correlation and Centroid.

This algorithm introduces the concept of a correlation being used to isolate the calculation window. This will achieve two objectives, firstly, that the cross-correlation has noise rejection properties ([52] and [45] contain good descriptions of the properties of a cross-correlation and adaptive filters) and that distributions, which are not completely contained within the distribution window, will have their calculation window offset and reduced appropriately.

The correlation is illustrated in Figure 5.3 and is performed by first producing a model of a the laser spot's gaussian distribution using known parameters, such as the laser's divergence and the camera's horizontal resolution, and then making an estimate of the distance between the STM system and the target surface. This estimate is initially taken to be the minimum operational distance over which the system can operate but, once some measurements have been obtained, it is taken as the previous range measurement, provided that it is sufficiently different from the value being used at present to justify re-calculation of the model. The model produced has the form of a quantized representation of an ideal laser spot's distribution with the number of samples used to produce the model under user control. The coarse correlation has a sampling step equal to one horizontal pixel width and the equation used to create the model is given below.

$$\text{distribution amplitude} = \text{maximum\_amplitude} * \exp(-w^2/w_0^2) \qquad (22).$$

In the above equation w_0 is the radius of the beam at the exit window of the laser and w is the a measure of the distance away from the centre of the laser beam's distribution where the distribution

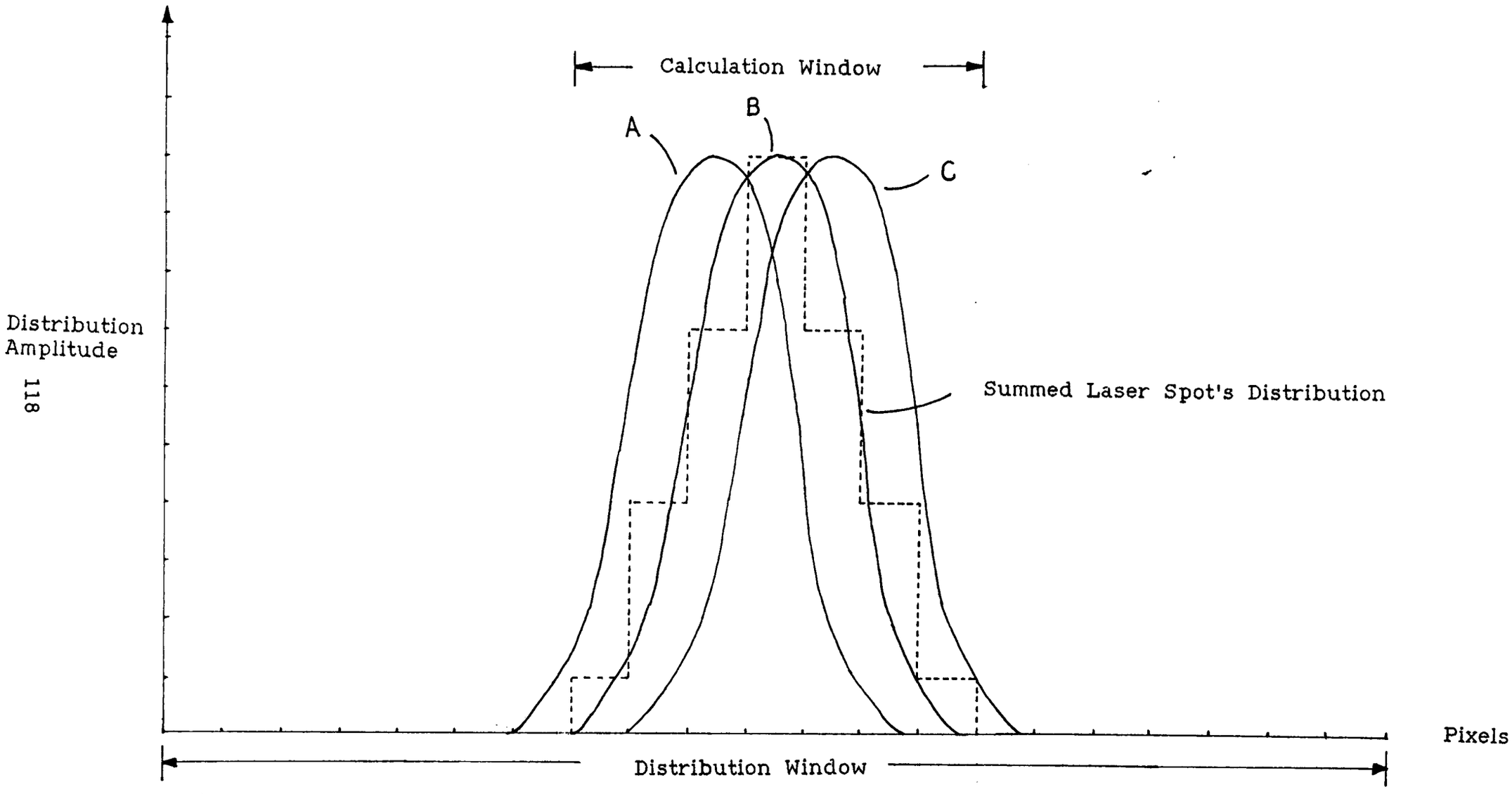

Figure 5.3 An Illustration of Algorithm 3 : Correlation and Centroid.

amplitude is required.

A cross-correlation process is then performed, this entails offsetting the centre of the model distribution to the start of the distribution window and then multiplying together the values in the pixels of the VSD with the corresponding values in the pixels of the model's distribution. All the products are summed and this resulting value is stored, the offset is now reduced by one pixel and the above process performed again. This is repeated until the centre of the model distribution reaches the other end of the distribution window. The stored values are now examined and the offset which is associated with the largest value is taken as the centre of the calculation window. About this centre, the calculation window is made to extend a distance equal to the significant (non-zero) extent of the model's distribution. An equation which describes the cross-correlation (see [52]) is given below where $COR_{(j)}$ represents the correlation value for an offset of the model distribution of j pixels. The classical multiplying factor 1/n does not appear in the equation given since, for the application outlined above, this multiplication does not provide any additional useful information.

$$COR_{(j)} = \sum_{i=0}^{m-1} VSD_{(i)} * MD_{(i+j)}, \text{ for } j = 0 \rightarrow m \qquad (23).$$

In this equation $VSD_{(i)}$ is the i^{th} pixel of the summed laser spot's distribution with m being the number of pixel positions defined in the distribution window, $MD_{(i+j)}$ is the model distribution and the above equation is calculated for values of j from 0 to m (the whole of the distribution window). Now that the calculation window has been defined a centroid calculation is carried out and the horizontal displacement is again the result of the centroid calculation, added to

the offset between the calculation and distribution windows, and the stored pixel value which represents the start of the distribution window.

5.1.3 Algorithm 4 : Fine Correlation.

In this last algorithm a correlation is again used but, in this case, with a model distribution which has many samples defined in a single pixel width (from a minimum of 3 to a maximum of 31 which is set by the need to achieve reasonable calculation time for the result and the subpixel resolution required). The process described in the previous subsection for the cross-correlation is repeated but this time the laser spot's distribution is expanded so that it has as many samples as the model. At present the expanded laser spot's distribution is obtained by just filling the new subpixel samples with a copy of of the present VSD amplitude, that is.

$$SLD_{(k)} = \sum_{j=0}^{m-1} \{ \sum_{i=0}^{n-1} LD_{(j)} \} \qquad (24).$$

Where n is the number of subpixel samples, m is the size (in pixels) of the summed laser spot's distribution, $LD_{(j)}$ is the amplitude of the j^{th} pixel of the summed Laser spot's Distribution and $SLD_{(k)}$ is the Subpixel Laser spot's Distribution which will be m*n subpixel samples in size. Another possible method of producing the Subpixel Laser spot's Distribution would be to use a simple linear interpolation between the present and succeeding pixels summed laser spot's distribution amplitude as shown below.

$$SLD = \sum_{j=0}^{m-1} \{ \sum_{i=0}^{n-1} i * \frac{(LD_{(j+1)} - LD(j))}{n-1} + LD_{(j)} \} \qquad (25).$$

Where all the variables used have the same meaning as in equation

(24).

Now that the subpixel version of the laser spot's distribution has been produced the cross-correlation is carried out but, instead of this just producing a calculation window, the maximum value (or more correctly the offset associated with it) is selected and provides the displacement into the distribution window. This value when added to the stored value for the start pixel of the distribution window, gives the horizontal displacement. This process is illustrated in Figure 5.4.

It can be seen from the algorithm just presented that to calculate the result of for a single correlation value (i.e. a single displacement of the model distribution) the amount of multiplications and additions needed is equal to the product of the distribution window size and the number of model samples per pixel of the model distribution. Obviously this means a great deal of calculation time is needed to produce the fine correlation result. A quick method to produce the fine correlation was developed and will now be described. A coarse correlation is performed, with 1 sample per pixel in the model distribution, and the pixel position that results from this calculation (which is the approximately the centre of the laser spot's distribution) is reduced by one. This value is used as the initial offset for a fine correlation. All the correlation values are now monitored and once a correlation value has been obtained where the previous three values are each of a smaller magnitude than the the one preceding it, this subpixel value minus three is assumed the maximum value, and therefore forms the distribution window offset. This method can reduce the calculation time of the fine correlation to a reasonable value due to only calculating correlation values in the vicinity of the

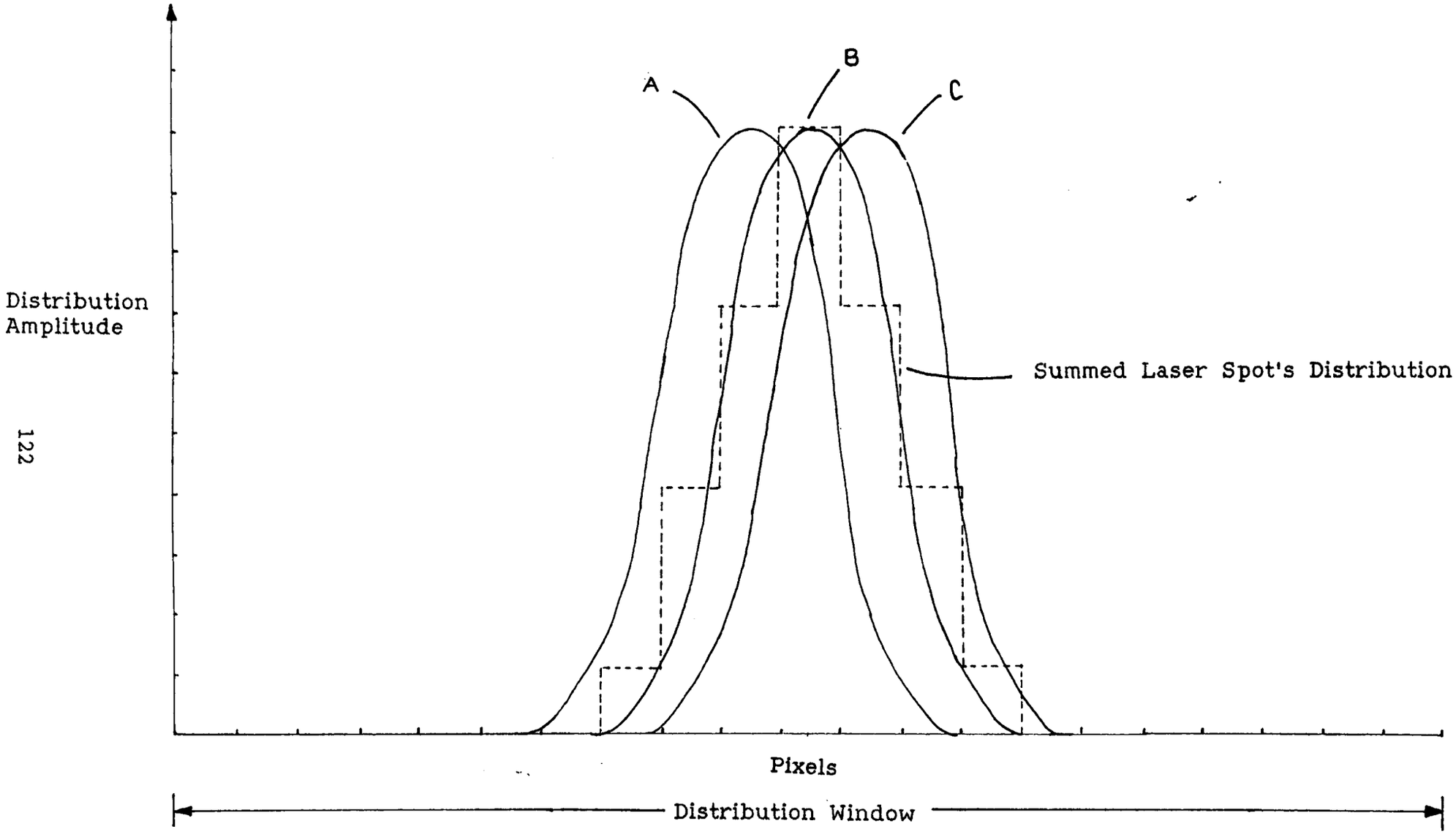

Figure 5.4 An Illustration of Algorithm 4 : A Fine Correlation.

centre of the spot's distribution but, this algorithm can be 'fooled' by noise producing false maximums. The algorithm has been compared to the complete fine correlation on 'real' distributions obtained from the STM System 2 and has produced exactly similar results with a calculation time of approximately 1/20th of that the conventional fine correlation algorithm.

Now that the four distribution centre finding routines have been explained the software testing procedures to test the algorithms will now be outlined, these use the 'model sub-menu' option in the LSDEP to create a distribution with known parameters and user introduced errors.

5.2 Testing the Subpixel 'Distribution Centre Finding' Algorithms.

The software testing involves creating an ideal model of the laser spot's distribution with various known parameters (exit spot diameter, laser beam divergence, etc) and introducing defects into the distribution such as camera saturation, fixed pattern noise, random noise, etc. This distorted distribution is now used as the input to the centre finding algorithms and the results examined .

5.2.1 Algorithm Software Testing: Accuracy.

The model sub-menu, which was described subsection 5.1.1, was used to create a model of the laser spot's distribution. The parameters used in this model were those of the STM system 2 with an imaginary flat vertical plane, situated a distance of 5 meters from the camera/laser baseline, as the target for the laser spot. The model of the laser spot's distribution can have between 3 and 51 samples per pixel. Now using the maximum resolution, 51 samples (of the section of the gaussian distribution which resides in the pixel) are calculated and

these values are averaged over a pixel width to obtain the model pixel value. This means that the centre value of the distribution is known to a resolution of 1/51st of a pixel.

In the first test, the centre of the distribution was moved through half a pixel in steps of 1/51 of a pixel, each time the distribution is moved and calculated it is passed to the centre finding algorithms and the results recorded. These results were compiled for model distributions which represent a 8 mm diameter spot and a 50 mm diameter spot and are presented in Figures 5.5 - 5.8. In these graphs the a least squares best fit line is drawn through the points obtained from the algorithms. Figure 5.5 and 5.6 show the results obtained from the centroid calculation (used in algorithm 1, 2 and 3) and the correlation calculation (used in algorithm 4) respectively for the 8 mm spot. Figures 5.5 and 5.6 show that a deviation occurred in the centre of the graph, this is a function of the truncation of the 'tails' of the model distributions to reduce the time needed to calculate the models. Figures 5.7 and 5.8 show the results for the 50 mm spot, in these figures the truncation has much less effect and therefore the results are much closer to the ideal line. Figures 5.6 and 5.8 highlight the fact that algorithm 4 has a maximum resolution of 1/31st of a pixel, this being the limit of the fine correlation.

5.2.1 Algorithm Software Testing: Signal Defects.

In the next test, the effect of defects that may be present in the signal sent to the centre finding algorithms will be examined. These defects can be introduced by the camera, video line grabber analogue signal conditioning hardware and the ambient condition present when the distribution was obtained. The first of the defects that is modelled is

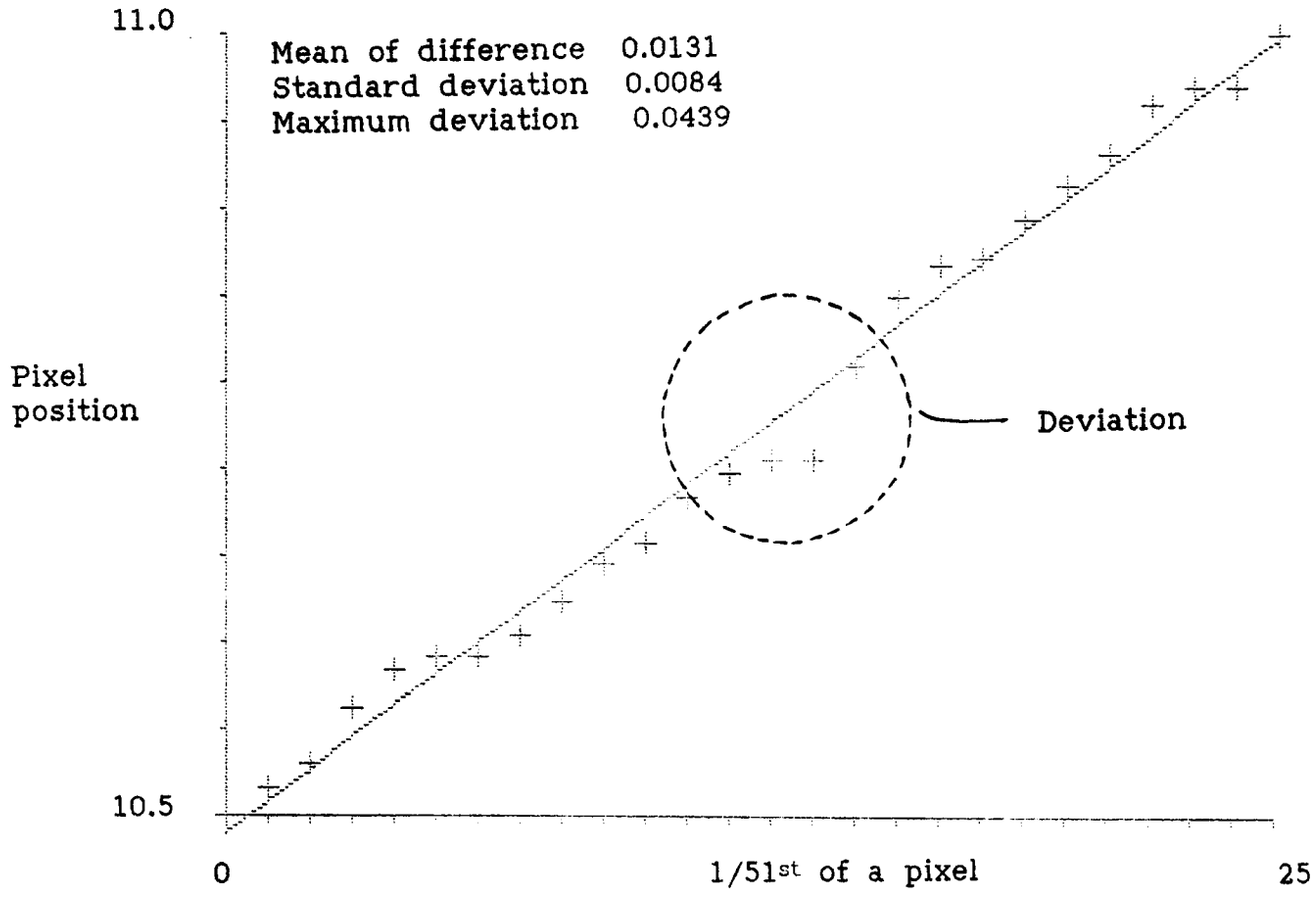

Figure 5.5 Accuracy Test on the Centroid Algorithm using an Idealised Model of a 8mm Diameter Spot.

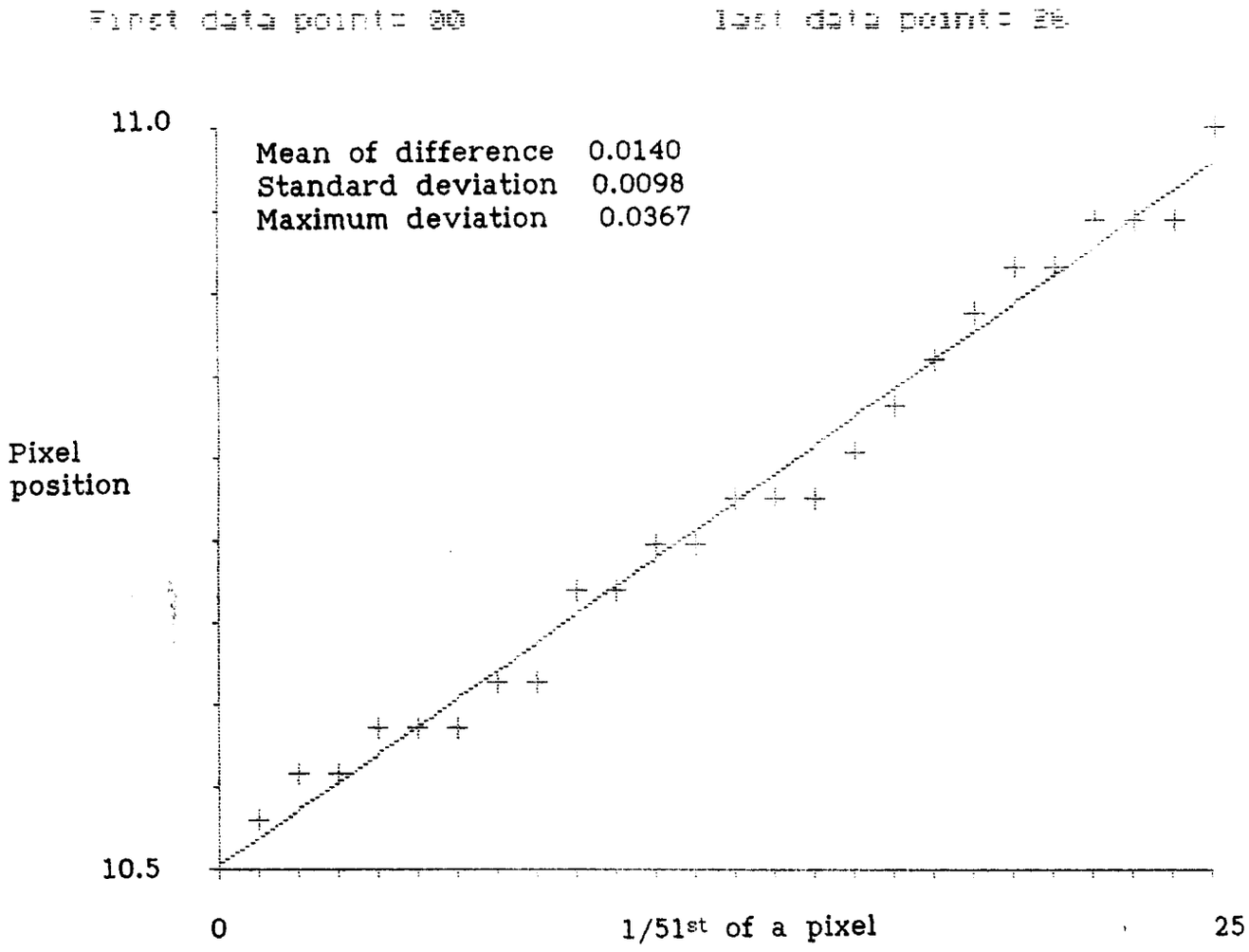

Figure 5.6 Accuracy Test on the Correlation Algorithm using an Idealised Model of a 8mm Diameter Spot.

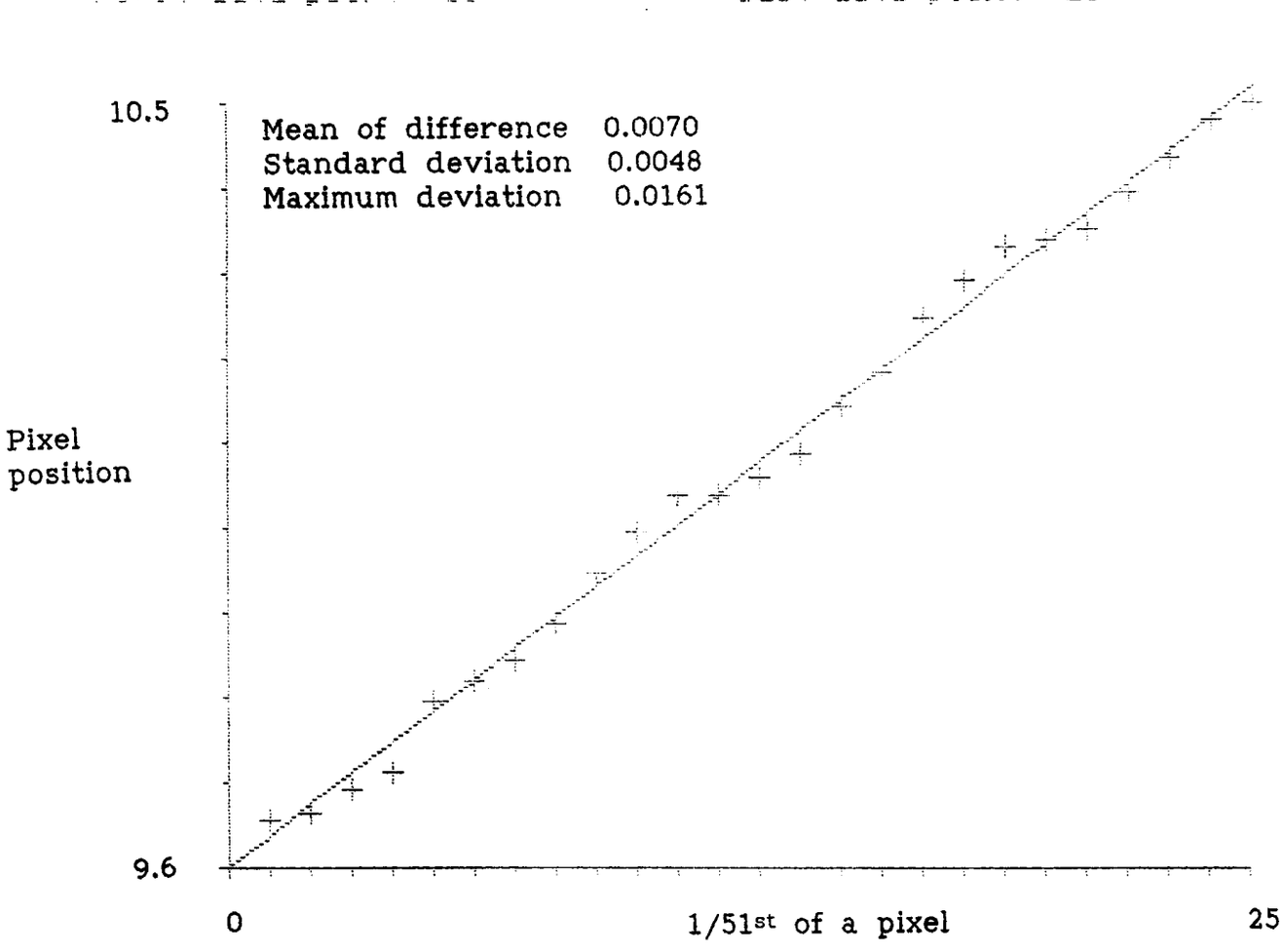

Figure 5.7 Accuracy Test on the Centroid Algorithm using an Idealised Model of a 50mm Diameter Spot.

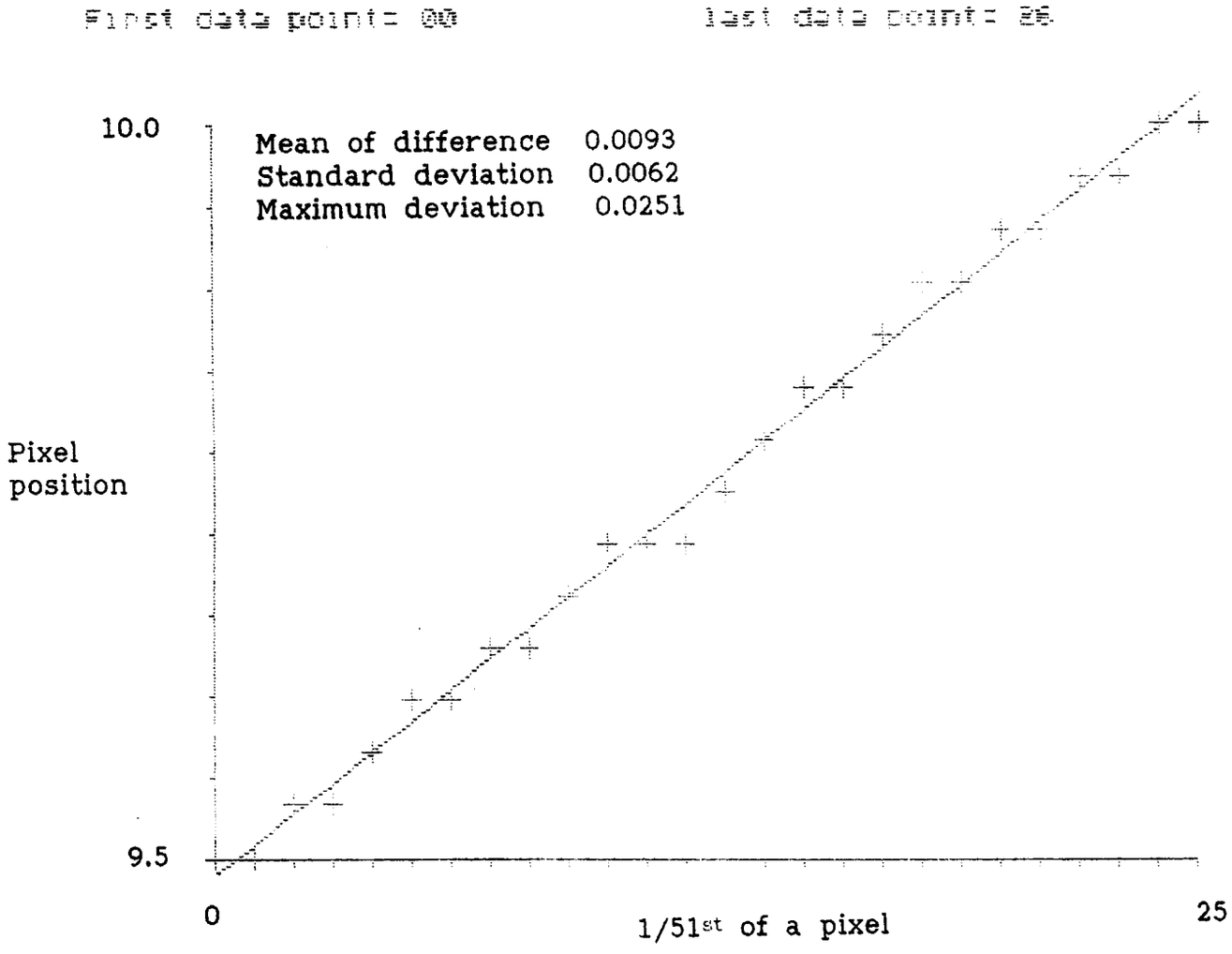

Figure 5.8 Accuracy Test on the Correlation Algorithm using an Idealised Model of a 50mm Diameter Spot.

'Black Level Offset'. This is a constant level that is added to each pixel value and can be produced by high ambient light levels and in the D.C restoration hardware. The next defect is saturation which truncates pixel values to a defined level. This can be introduced by the VLG's amplification stages or the camera. The last defect that is modelled is random noise which adds a random error with zero mean value to each pixel value. This noise can be introduced at any stage of the signals path between camera and A/D converter. Before the combined defect test is outlined fixed pattern noise will now be considered.

Fixed pattern noise (breakthrough of the noise at the camera pixel, line and field frequencies) has not been modelled in the combined defects test since, with both the camera and A/D converter synchronised by the digital time base, it should not occur. For completeness, Figure 5.9 shows a distribution with fixed pattern noise present. With the signal now having a S/N ratio of 20 dB (that is introducing fixed pattern noise which is 10% of the maximum distribution amplitude) it can be seen that the results from algorithms 2, 3 and 4 do not deviate from the correct value of 15.758 by more that $1/20^{th}$ of a pixel (the results of the algorithms are given in the upper left hand corner of the graph with the model centre value given above them). The result for algorithm 1 (the simple centroid calculation with no calculation window), however, has been offset because of the presence of the noise and the distribution not being located at the centre of the distribution window. This shows that the above algorithms, if the restriction is accepted that the distribution must lie in the centre of the distribution window for algorithm 1, are very robust to any fixed pattern noise that may be present in the signal.

The combined defect test will take the form of introducing the

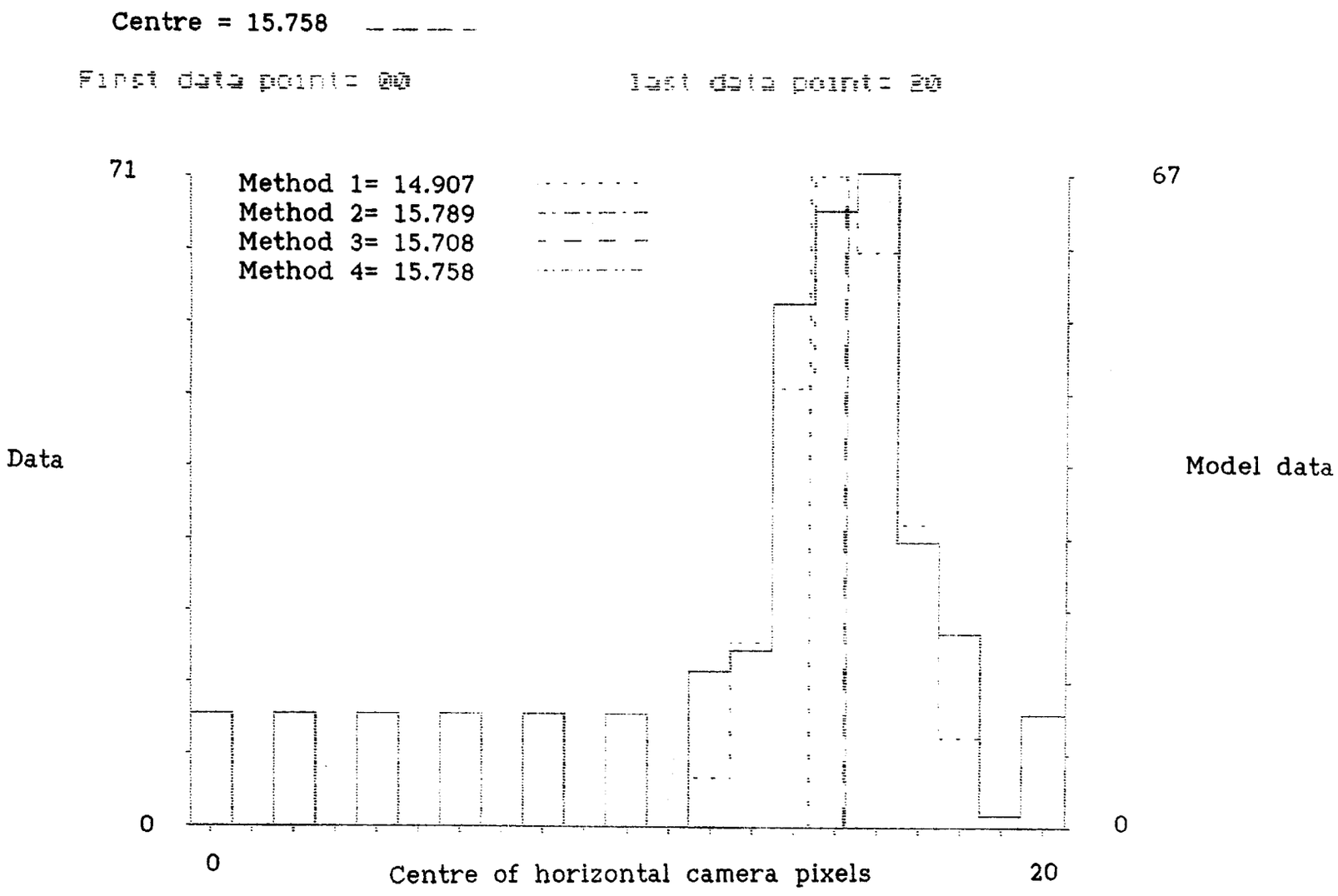

Figure 5.9 Fixed Pattern Noise.

three modelled defects mentioned above into a distribution and then calculating the centre of the resultant distribution. The magnitude of the defects introduced are given below with the values given as a percentage of the maximum distribution amplitude.

Black Level Offset	= 10%
Saturation causes truncation at	70%
Maximum Random Noise Amplitude	= 10%

The test was performed for 10 iterations with the distribution actually centred at 15.758 pixels from the edge of the distribution window. Examples of the distributions obtained for these tests are given in Figure 5.10 for the 8 mm diameter spot and Figure 5.11 for the 50 mm diameter spot. The results for the 8 mm diameter spot show that algorithm 1 produced erroneous results due to a residual noise level (see Figure 5.10). The results for algorithm 2 show that it has a smaller mean error from the correct value that algorithm 1 but, a much larger standard deviation. This indicates an inherent instability of this algorithm when noise is present in the distribution. The results for all 10 iterations are given in Figures 5.12 and 5.13 for the 8 mm diameter and 50 mm diameter spot respectively.

The results for the 50 mm spot have much better values for the standard deviation of the error and the mean error, this is due to the greater amount of signal information that is present in the 50 mm spot model. Algorithm 3 performed better than algorithm 4 (which is the opposite of what happened in the 8 mm spot test) due to algorithm 3 having the facility to create a calculation window when the spot's distribution has been truncated on one side by the distribution window.

The software tests have shown that the two major criteria for the

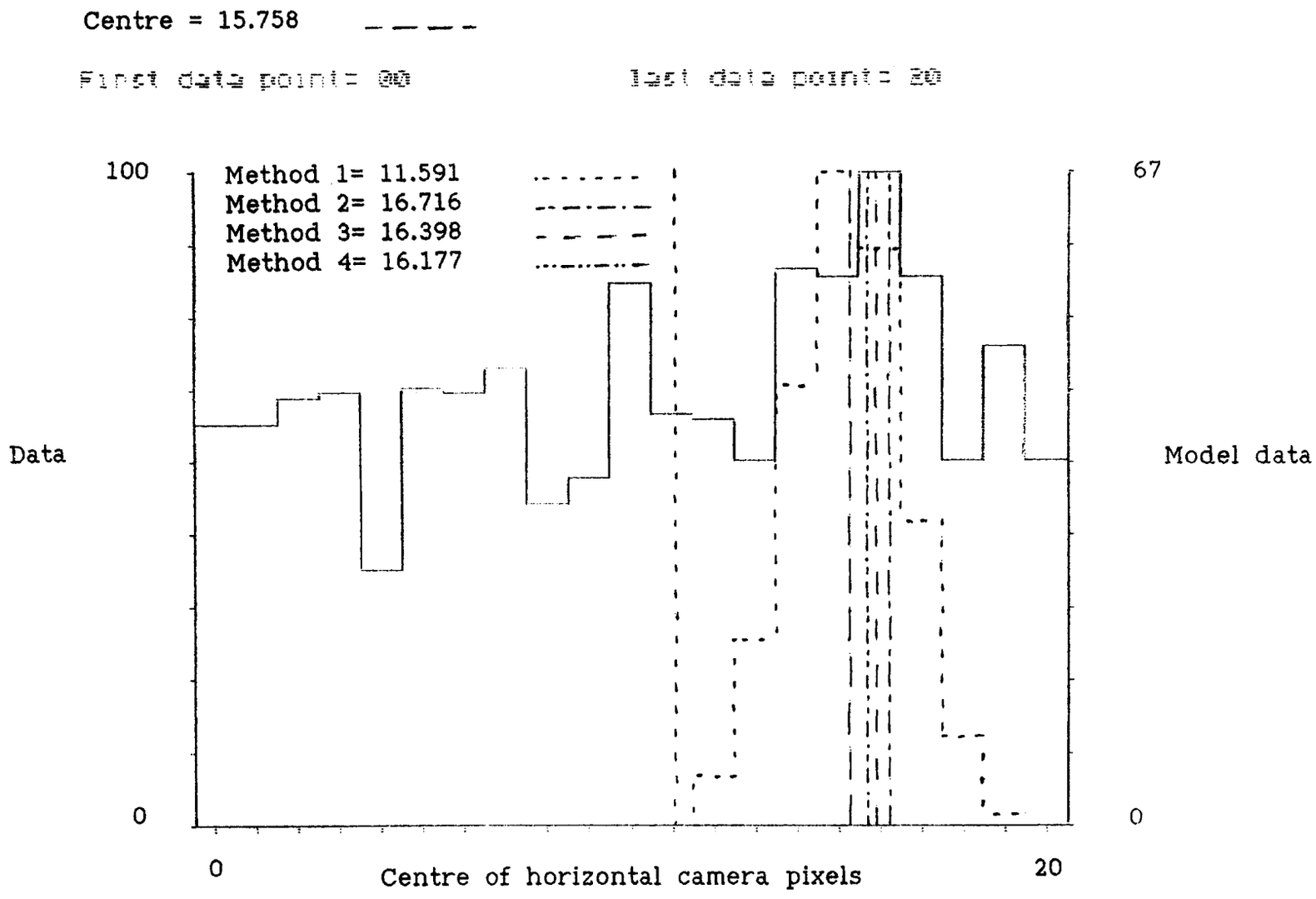

Figure 5.10 An Example of the Distortion Test (8 mm spot).

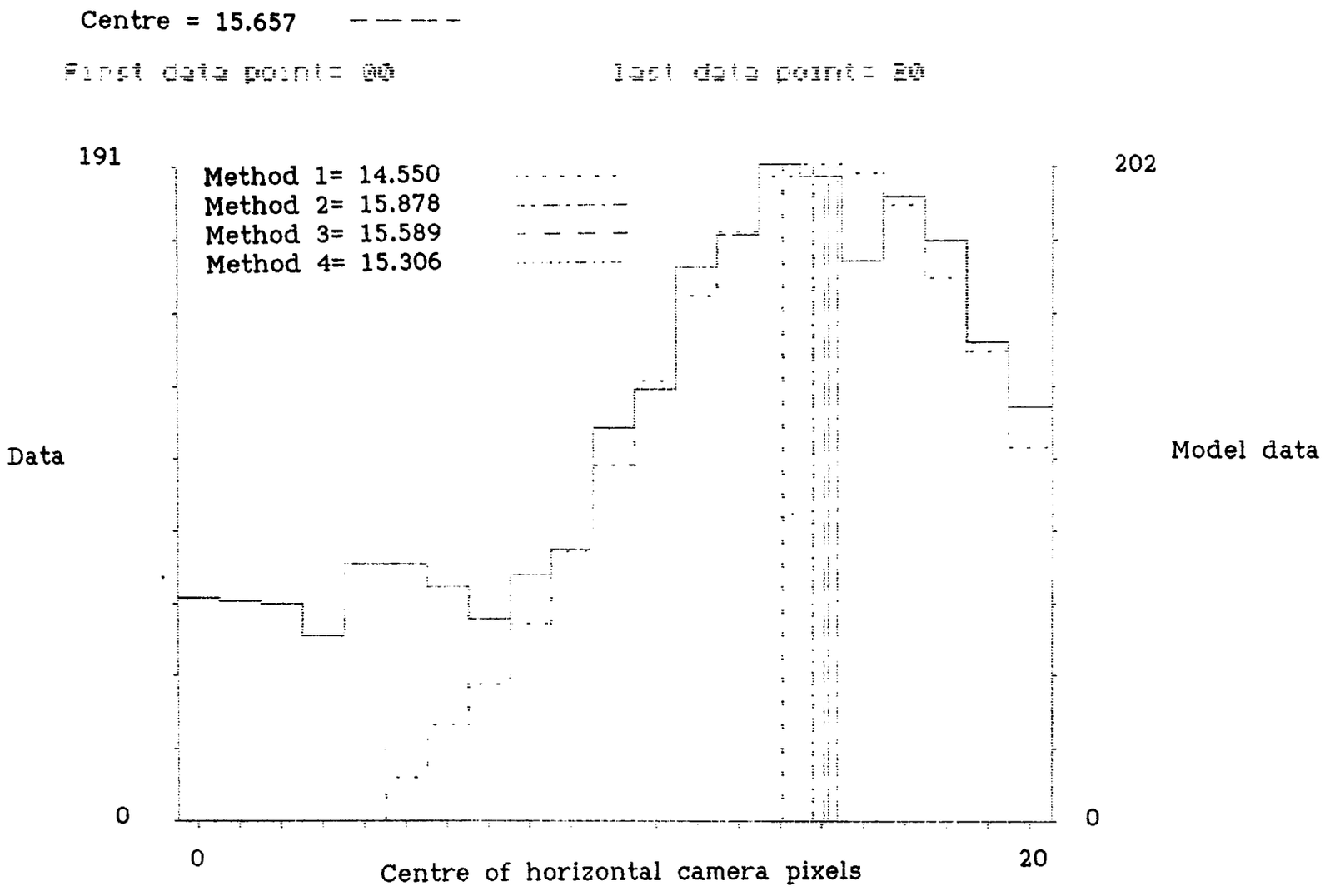

Figure 5.11 An Example of the Distortion Test (50 mm spot).

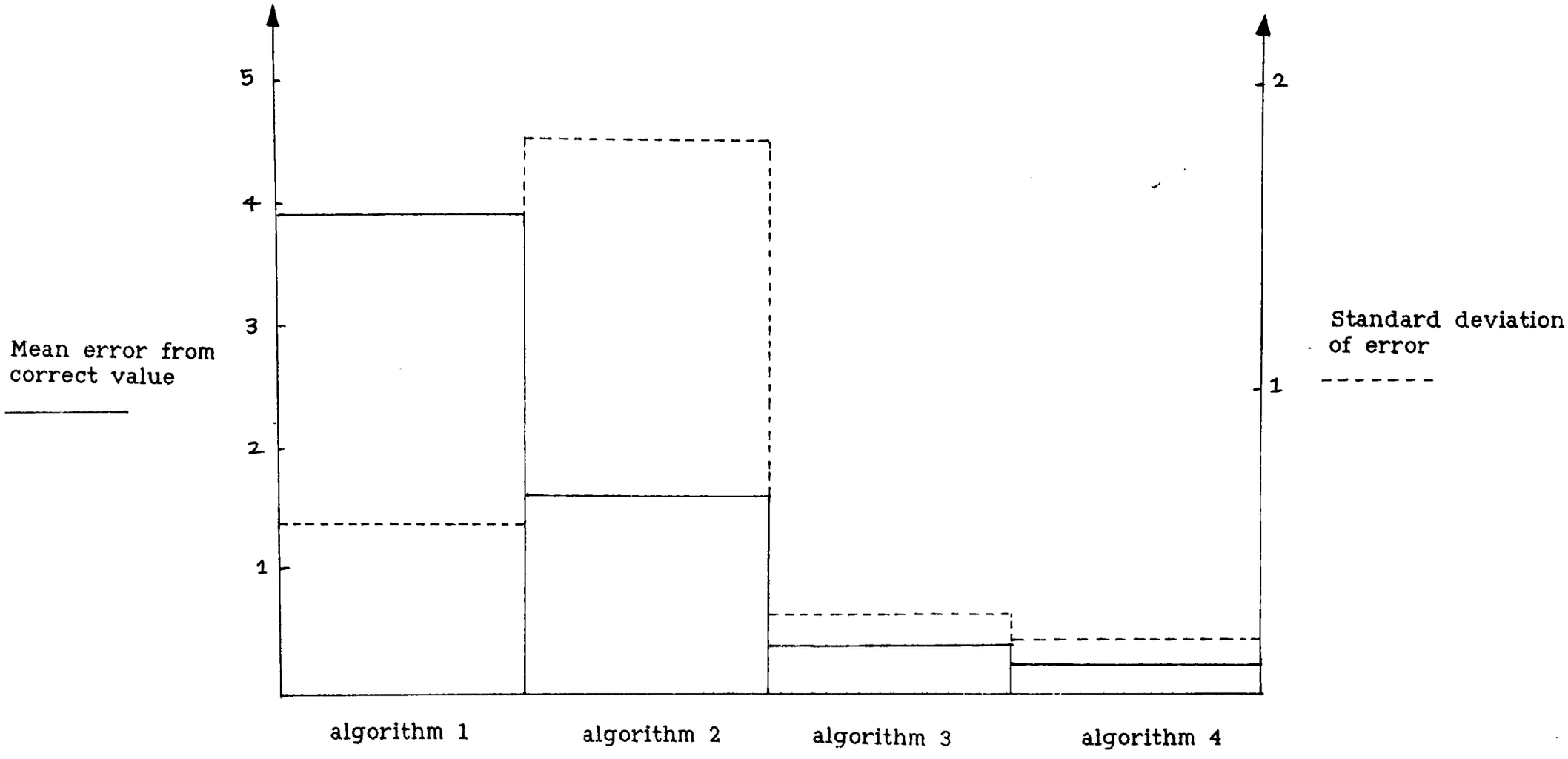

Figure 5.12 Results from the Distortion Tests (8 mm spot).

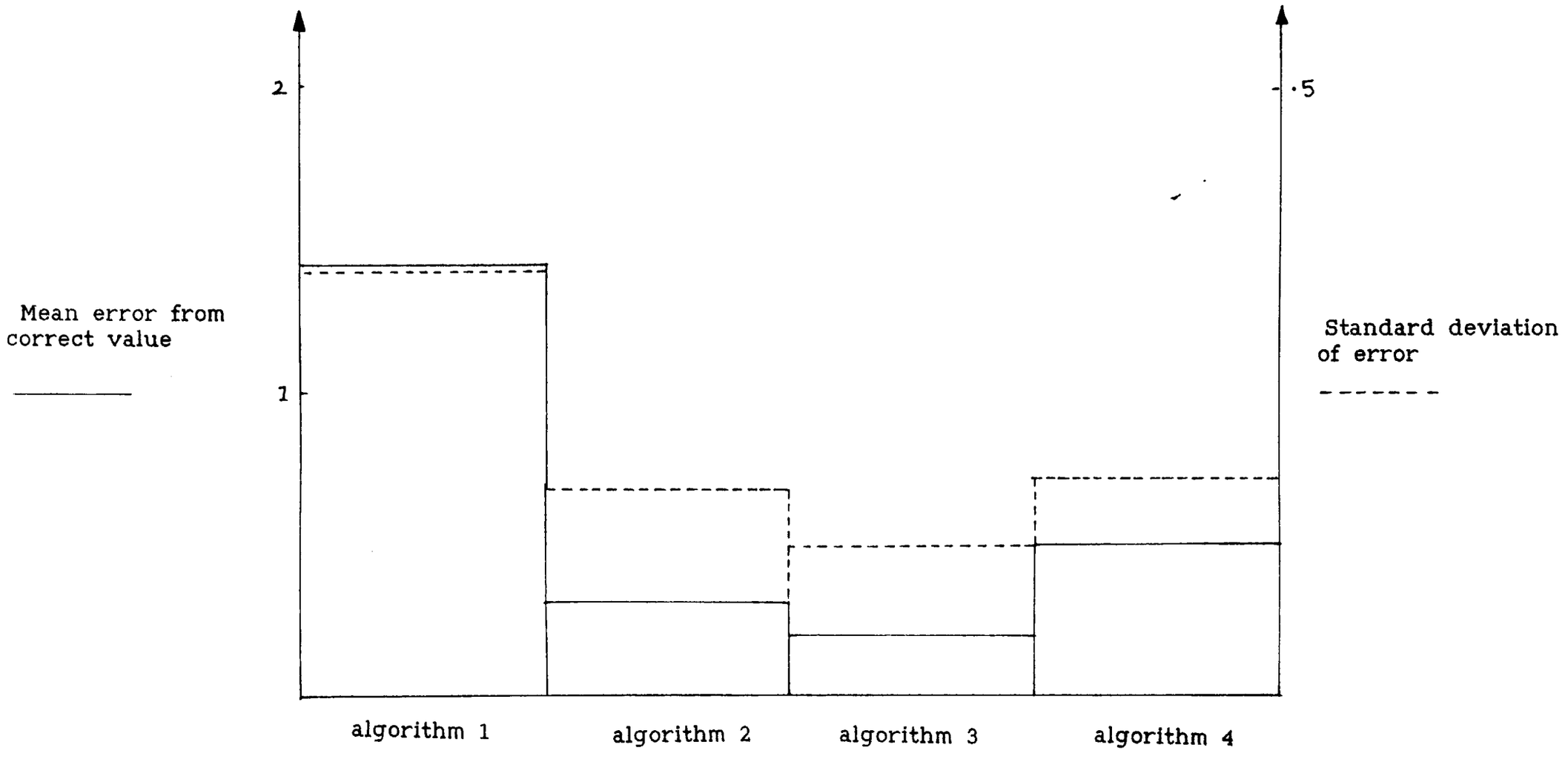

Figure 5.13 Results from the Distortion Tests (50 mm spot).

centre finding algorithms, that of accuracy and robustness to noise, have been fulfilled. With both the 8 mm spot and the 50 mm spot an accuracy of 1/20th of a pixel or better was obtained giving definite subpixel resolution. Considering the robustness of the algorithms to noise, with the combined noise test all the algorithms performed well (especially algorithms 3 and 4 which use a correlation and achieved results of less that half a pixel from the correct result) with the model distribution which had a S/N ratio of 14 dB. The actual system has a S/N ratio of greater that 40 dB (a factor of approximately 20 times better), therefore giving a greater degree of confidence in the resilience of the algorithm to any 'real' noise that may be encountered in the laser spot's distribution.

5.3 Subpixel Version of the Range Error Equation.

In producing the error equation presented in Chapter 2 one main assumption was made. This was that the errors present in the laser deflection angles (angles B and C of Figure 2.2) were much smaller that the error present in the measured horizontal displacement of the laser spot in the STM systems camera. Now that the concept of subpixel resolution has been introduced this assumption must be re-examined and a decision made on whether it is still valid.

The results from the software tests have shown that the algorithms presented can resolve down to at least 1/20th of a pixel (although this will probably not be attainable in the actual system due to noise present in the acquired distribution) this means that an error in the calibration of the laser deflectors must be smaller that 1/20th of a pixel size which corresponds to an angular error of 0.04 mrad or 8.4 arc seconds. Since the calibration error has been defined as 0.17 mrad

and this is greater than the subpixel error which is now present in the horizontal displacement, a new range error equation must be derived to take this into account.

The method of producing the range error equation can be changed because the error quantities are much smaller than when the original error equation was derived (e.g subpixel errors in the laser spots horizontal displacement). The method to be used is partial differentiation (see O'Neil [54]) of the range equation (equation (13) in section 2.3.2) with both the horizontal displacement and horizontal deflection angle as independent values which can contain errors. Therefore the range error equation now becomes for small errors.

$$\text{Range error} = \delta z = -\frac{z^2}{l} * \left(\delta a * \frac{px}{d} + \delta B * \text{Sec}(C) * \text{Sec}^2(B) + \delta C * \text{Tan}(B) * \text{Tan}(C) * \text{Sec}(C)\right) \quad (26).$$

The term $z * \delta a * px$ has been dropped from the denominator of the first term since, with the reduced magnitude of the error, this is insignificant when compared with the other denominator term. The term δB is the angular error in the position of the laser deflector position and this is multiplied by a factor dependent on the magnitude of the deflection angle. A maximum value for this error multiplying factor can be found by substituting the deflection angle associated with the minimum operational range of the system (maximum value = $\text{Sec}^2(35.98°) * \text{Sec}(10°) = 1.55$). The variable δC is the angular error in the position of the vertical laser deflector. The maximum value for this multiplying factor is $\text{Tan}(35.98°) * \text{Tan}(10°) * \text{Sec}(10°) = 0.13$.

Equation (26) will be used in the next chapter to produce an estimate of the theoretical error for the enhanced subpixel resolution STM system.

Chapter 6: Subpixel Resolution Tests and Material Tests.

This chapter contains tests carried out on the STM System 2 for which, at the present time, no similar tests and results have been reported in the technical literature. The first set of tests involve obtaining a reliable value for the subpixel resolution available which a minimum sized spot and then expanding the laser spot and ascertaining what resolution is now available. The reasons for performing this set of tests are two-fold; firstly that an expanded spot may be necessary when the STM system, working in an industrial environment, has a non ideal surface (ideal being considered as having a matt finish and being flat) for which the 3-D coordinates are to be produced. The second reason is that, assuming that a lens with a longer focal length was used (obviously with the subsequent reduction in system field of view) the minimum sized spot would cover a larger area of the charge coupled device and therefore obviously more pixels, which is a analogous to looking at a expanded laser spot. This implies that the results should have some validity in suggesting the subpixel resolution which would be available with the new STM configuration.

The second set of tests are performed on surfaces of different materials, these tests will be referred to as the material tests. These tests explored whether the laser spot was detectable and what resolution could be expected if the spot size were to be increased. The materials used in these tests are materials which may be encountered in possible industrial applications of the STM system (some possible industrial applications of the STM system are discussed in Chapter 7).

6.1 Subpixel Resolution Tests.

The function of the test rig that is shown in figure 6.0(a) is to enable the image of the laser spot to be displaced horizontally, in a controlled manner, along the pixel grid of the camera. These tests differ from those presented in the last chapter because the physical units of the STM system are used to obtain the laser spot's distribution (the tests described in section 5.2.1 used a software model of the laser spots image). An illustration of this displacement of the laser spot that will be achieved by this tests is shown in figure 6.0(b). The results from these tests would give practical and realisable values for the subpixel resolution that can be achieved with the distribution centre finding algorithms and STM system. A description of the test rig used to obtain these results is now given with reference to figure 6.0(a). A separate laser beam and beam expanding optics are placed a distance of 5 m away from the STM system and parallel to the STM system baseline. The laser beam is directed toward a flat black target which has a matt finish, this target is arranged to be at 45 degrees of the vertical axis of the laser beam and mounted on a precision linear displacement device which has a movement positional resolution of 0.01 mm. The known horizontal displacement of the target is compared with the result obtained from the centre finding algorithms of the supervisory computer. The laser beam expanding optics are used to alter the diameter of the laser spot. This can be achieved by two methods, the first of these is to use a simple lens which is mounted in the path of the laser beam. This method produces a rapidly expanding laser beam which will soon disperse the available energy in the laser beam making detection very difficult. The second method is to

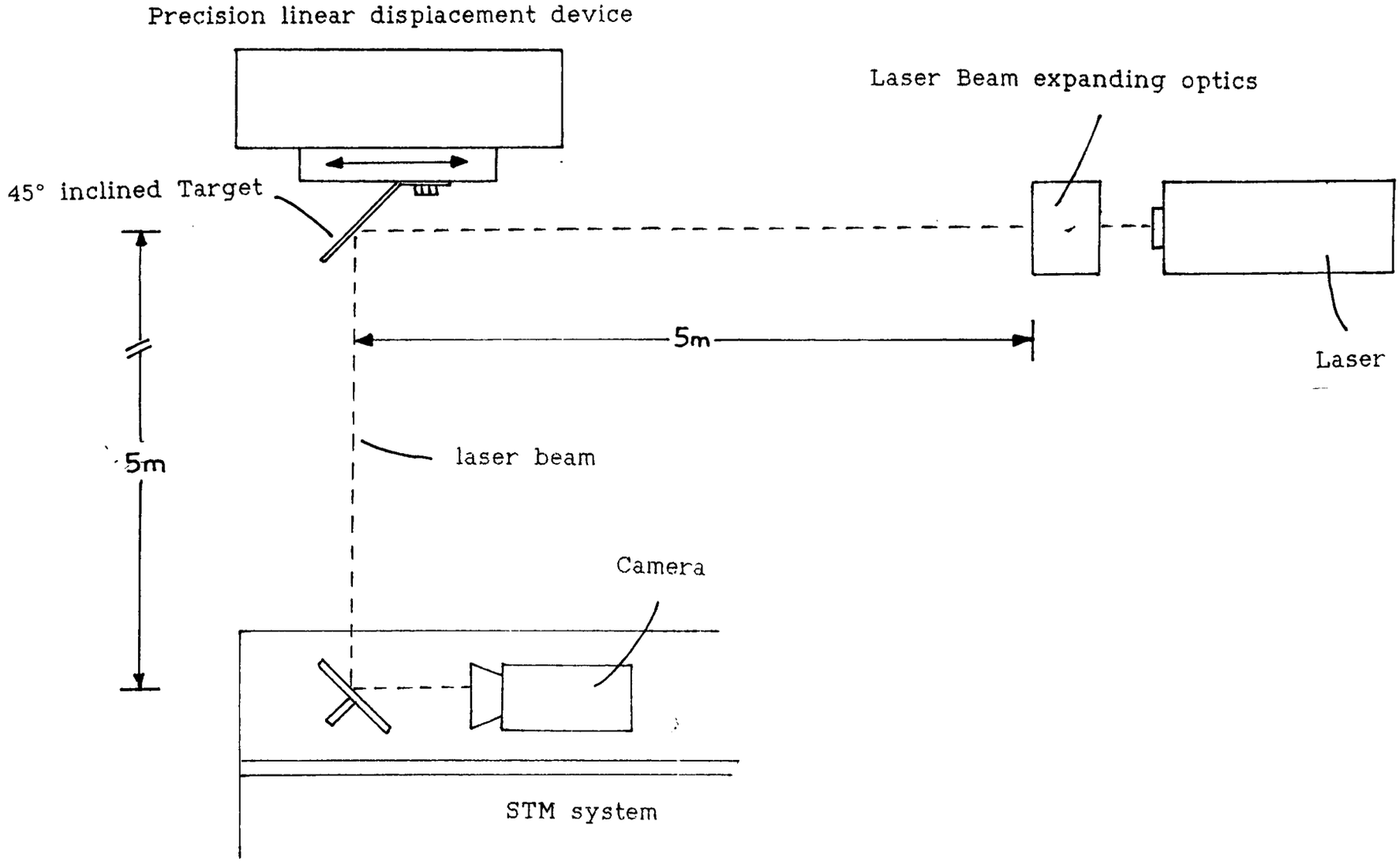

Figure 6.0(a) Test Setup for the Subpixel Tests.

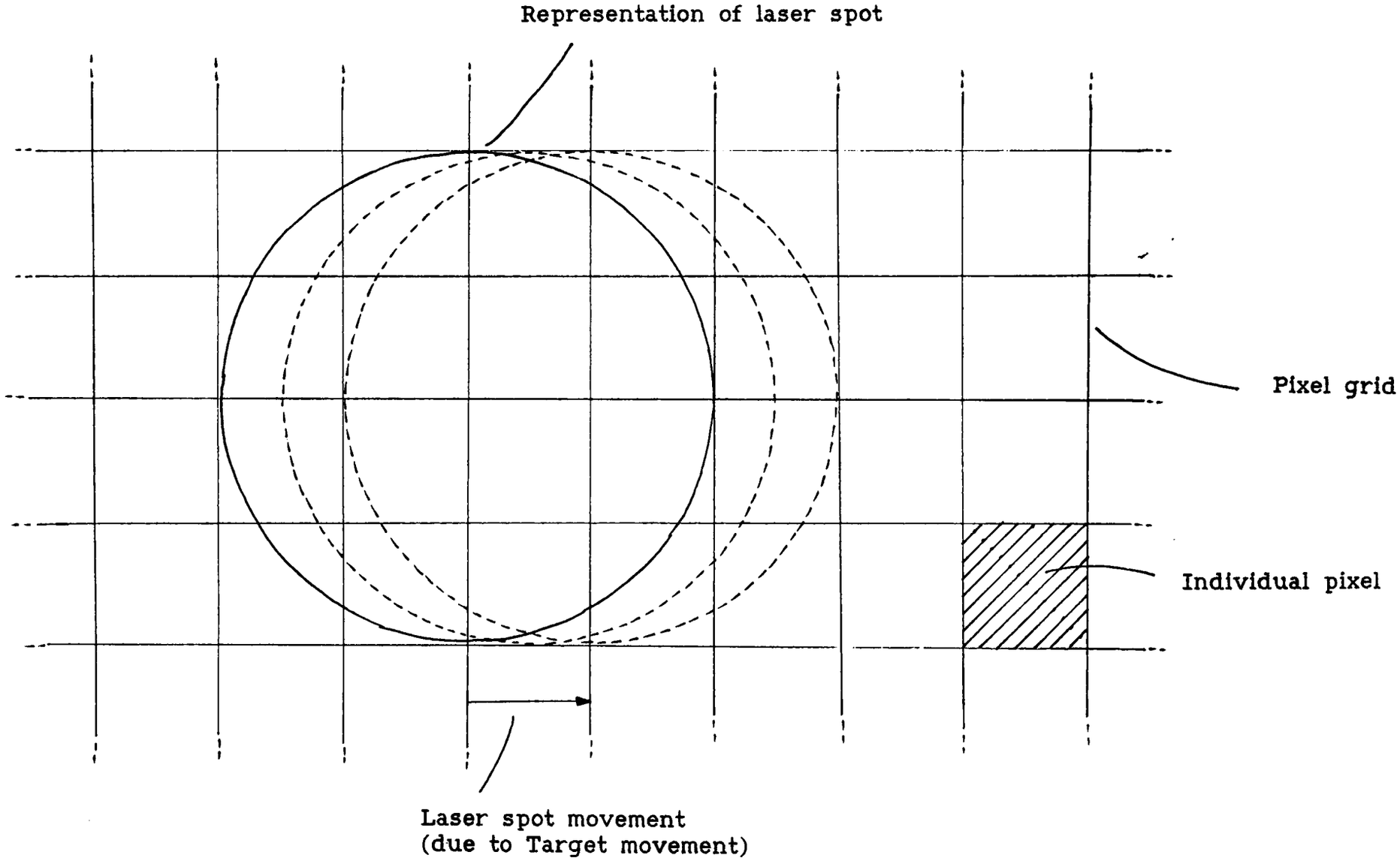

Figure 6.0(b) Illustration of Laser Spot Movement in Subpixel Tests.

use a con-focal beam expander which, although making the beam diameter larger, say by a factor x, reduces the divergence by the reciprocal of this factor therefore, providing a laser beam of approximately consistent diameter.

From the previous results obtained in the software tests which were described in section 5.2.1, it was decided that algorithms 3 (the coarse correlation and centroid calculation) and 4 (the fine correlation calculation) would be used to obtain the results for the subpixel and material tests. This decision was made since, in the software tests, these algorithms produced equivalent results to those obtained by the other algorithms in the subpixel resolution tests and had much superior performance in the combined noise tests. The results for algorithms 1 and 2 were still calculated for all the following tests but on comparison did produced inferior results to those produced by algorithms 3 and 4 which enforced the confidence in the above decision.

The results will be presented in the form of graphs with the horizontal axis representing the lateral movement of the laser spot (the target surface being moved by the precision linear displacement device in steps of 0.2mm which corresponds to a movement of approximately 1/20th of a pixel at the camera) and the vertical axis representing the results for the particular laser spot centre finding algorithm being used. A 'least squares best fit' straight line approximation is drawn through the values obtained for the algorithm used and statistics (maximum deviation from the 'best fit' line, mean deviation from this line and the standard deviation of the error between the values obtained for the algorithm used and those calculated

from the 'best fit' line) are also calculated.

Before these tests can be carried out, the maximum subpixel resolution of the present test set-up must be obtained so that this can form a reference to compare all the results from the subpixel tests against. This maximum resolution was obtained by having a stationary spot and running the centre finding algorithms several times with this as the input. The error that is obtained which is the standard deviation (rms error) from the average value is then calculated. The subpixel resolution obtained is degraded by having to have the source and STM system mounted on different stable surfaces due to the need for a comparatively large source to target distance (5 m). The results of this test are shown in figure 6.1. This figure shows that a maximum deviation of $1/11^{th}$ of a pixel is obtained with a standard deviation of better than $1/40^{th}$ of a pixel from a least squares best fit line drawn through the points. Considering a limit on the available resolution of $1/40^{th}$ of a pixel for the present test set up (this is for the standard deviation measure of the difference between ideal and calculated pixel displacement), this will form a useful comparison measure.

The subpixel tests were carried out using target laser spots with diameters of 8mm and 50mm. The spot would be horizontally displaced, as already described above, by 7mm (this corresponds, approximately, to two camera pixel widths at 5m). The tests for each individual spot size were carried out at two different values of camera aperture. These values were selected as the smallest aperture value where the laser spot was consistently recognised by the STM system hardware (see section 4.3.3 for definition of this hardware) and the largest aperture value for which the video line grabber value was just

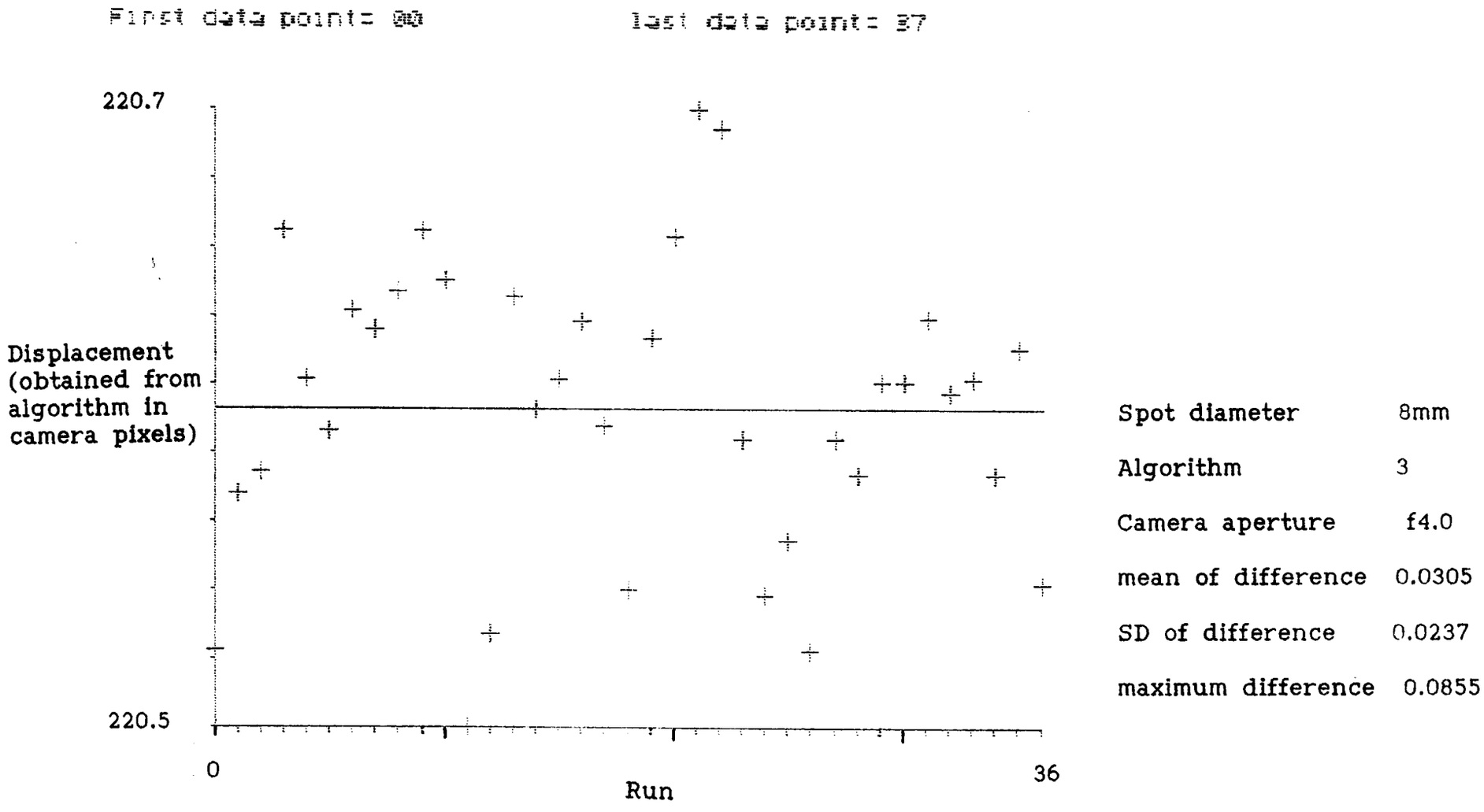

Figure 6.1 Results from the Repeatability Test.

about to enter saturation (a reading of 64 on the output of the A/D converters). These two values of camera aperture represent the limits of the useful aperture range and should provide an insight into the trends at the intervening values for the aperture. The altering of the camera aperture also produces a different value for the maximum summed distribution amplitude in the laser spot's representation in the STM system, this value will be given along with the resolution results from the subpixel tests.

The results for the 8mm spot diameter tests are given in figure 6.2(a) and (b) for the camera aperture of f5.6, and 6.3(a) and (b) for a camera aperture of f2.8 (the (a) and (b) suffix refers to the results from using algorithm 3 and 4, respectively, to obtain the centre of the laser spot's distribution). The summed contents of the video line grabbers memory is shown in figure 6.4(a) and (b). These figures highlight the difference in the maximum amplitudes of the laser spots summed distributions, 114 and 201 respectively (the meaning of summed laser spot's distribution is explained in section 5.1.2). Comparable results for a 50mm spot are given in figures 6.5(a) and (b) for a camera aperture of f2.8 and 6.6(a) and (b) for a camera aperture of f2, figure 6.7(a) and (b) shows a comparison of the summed Video Line Grabber's memory and maximum summed distribution amplitude, 134 and 260 respectively. These results for the two spot diameters, centre finding algorithms and aperture sizes are shown in tabular form in Figure 6.8.

These results show that each time there is an improvement in the results obtained with increasing the camera aperture provided that the system does not go into saturation. This shows the importance having a facility to alter the camera aperture (or camera gain) so as to obtain

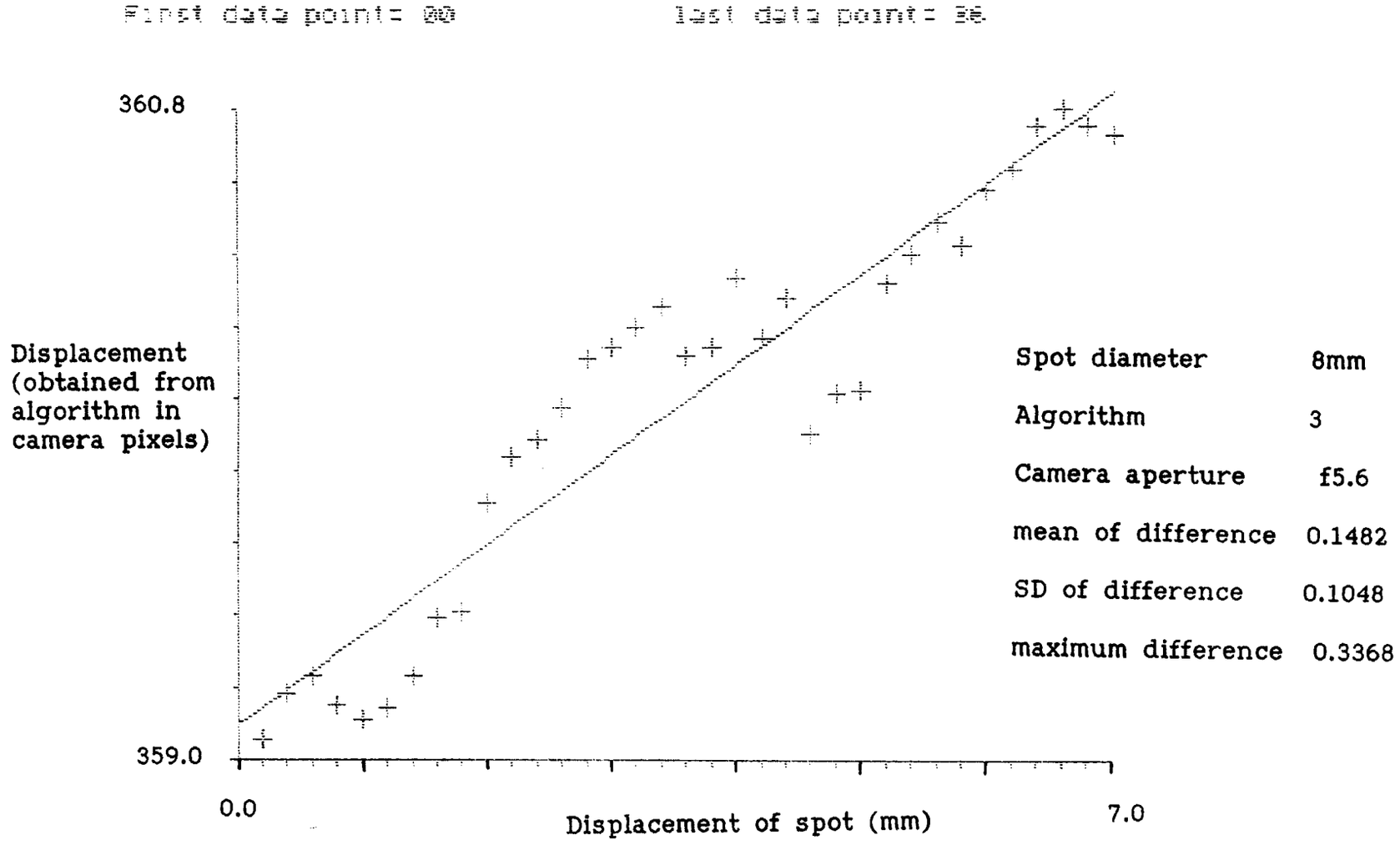

Figure 6.2(a) Results from the Subpixel Test using Algorithm 3, a Camera Aperture of f5.6 and an 8mm Diameter Spot.

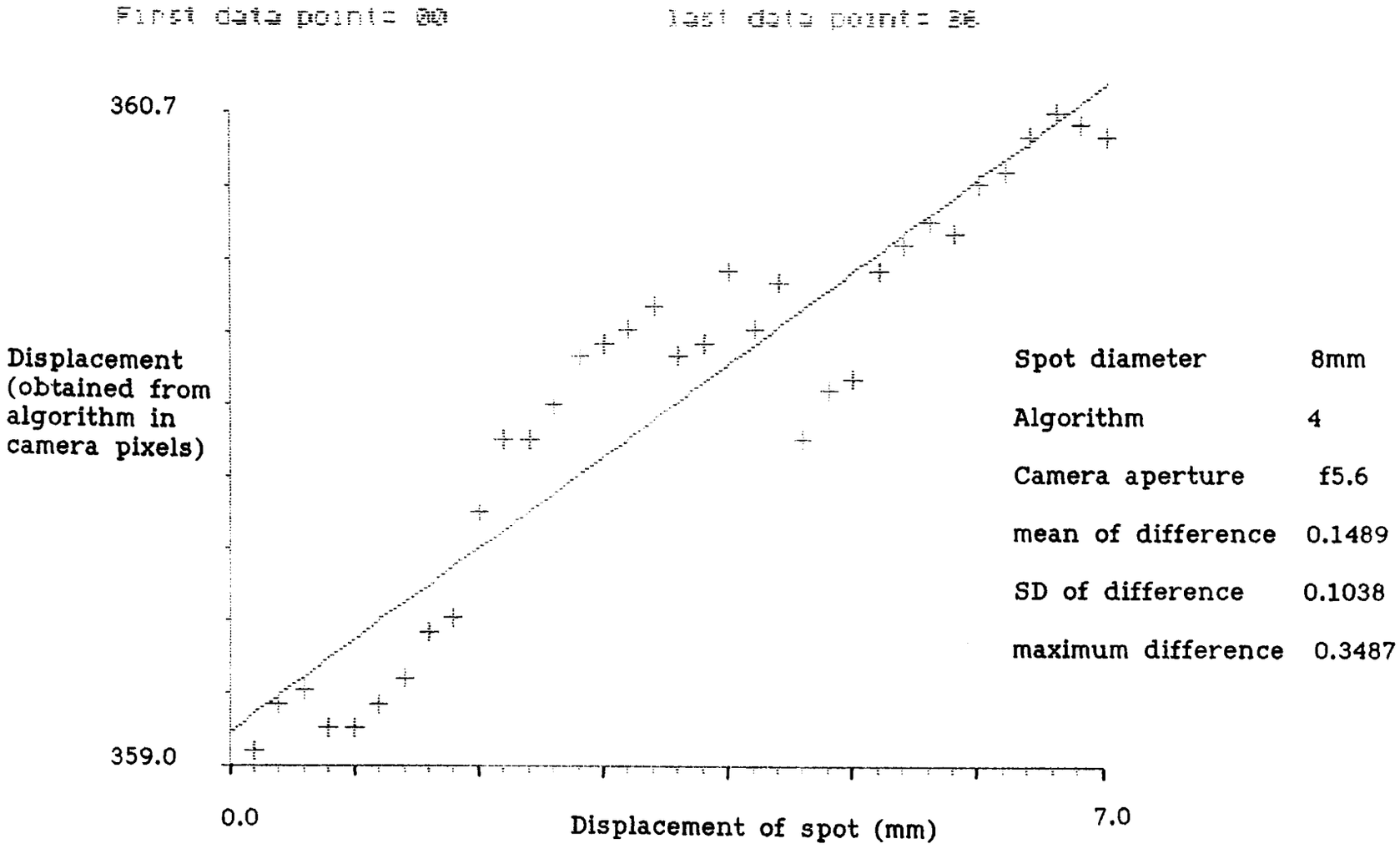

Figure 6.2(b) Results from the Subpixel Test using Algorithm 4, a Camera Aperture of f5.6 and an 8mm Diameter Spot.

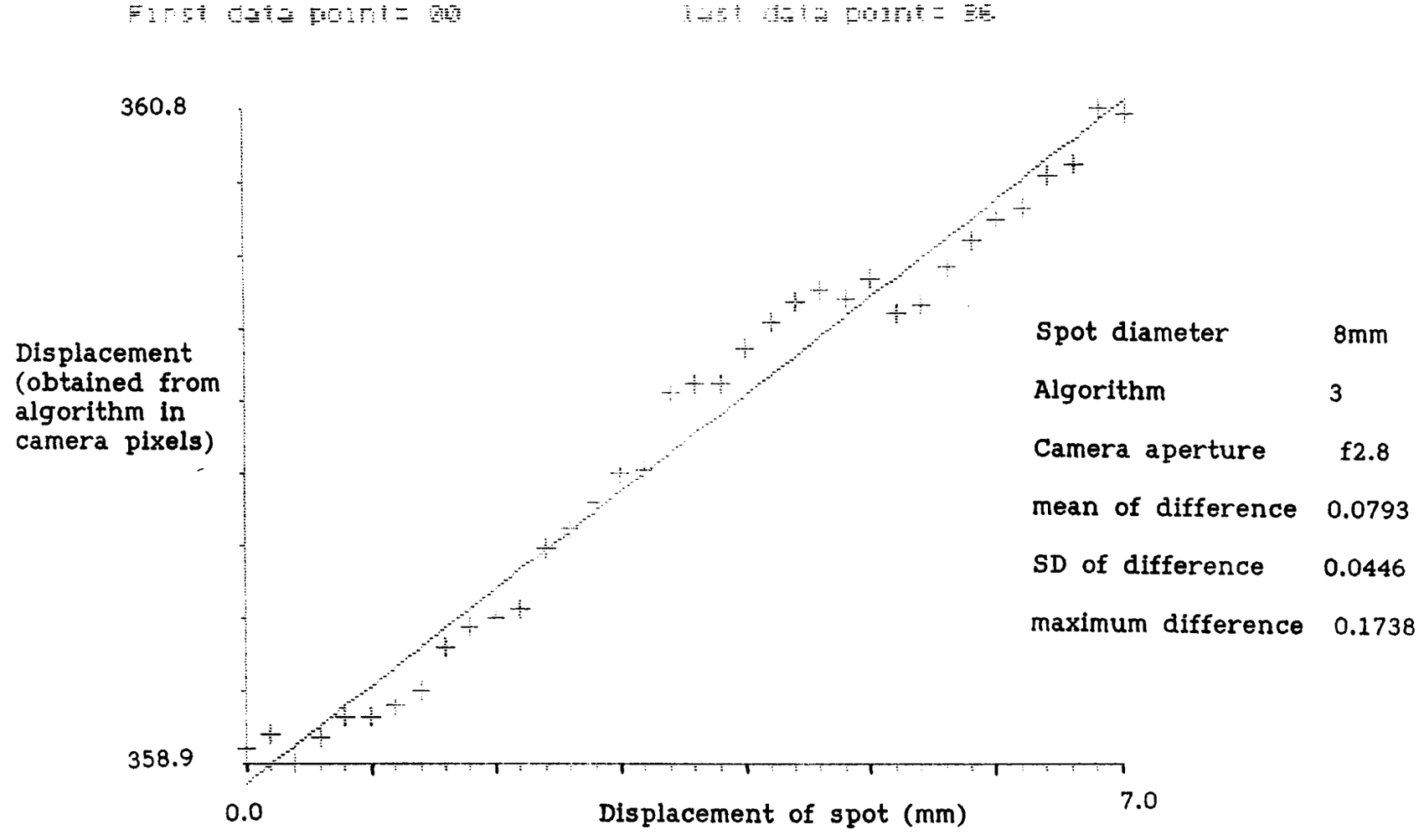

Figure 6.3(a) Results from the Subpixel Test using Algorithm 3, a Camera Aperture of f2.8 and an 8mm Diameter Spot.

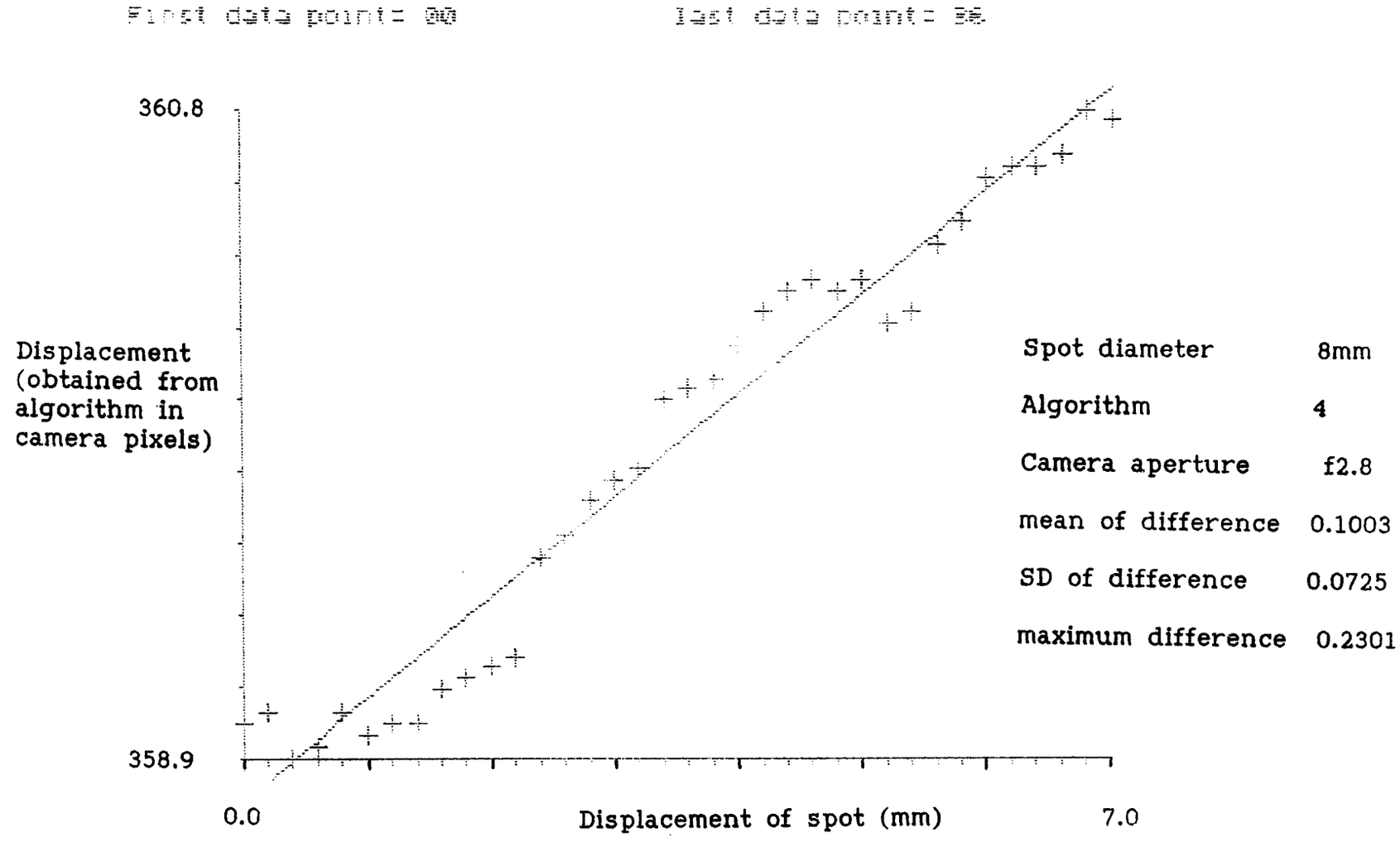

Figure 6.3(b) Results from the Subpixel Test using Algorithm 4, a Camera Aperture of f2.8 and an 8mm Diameter Spot.

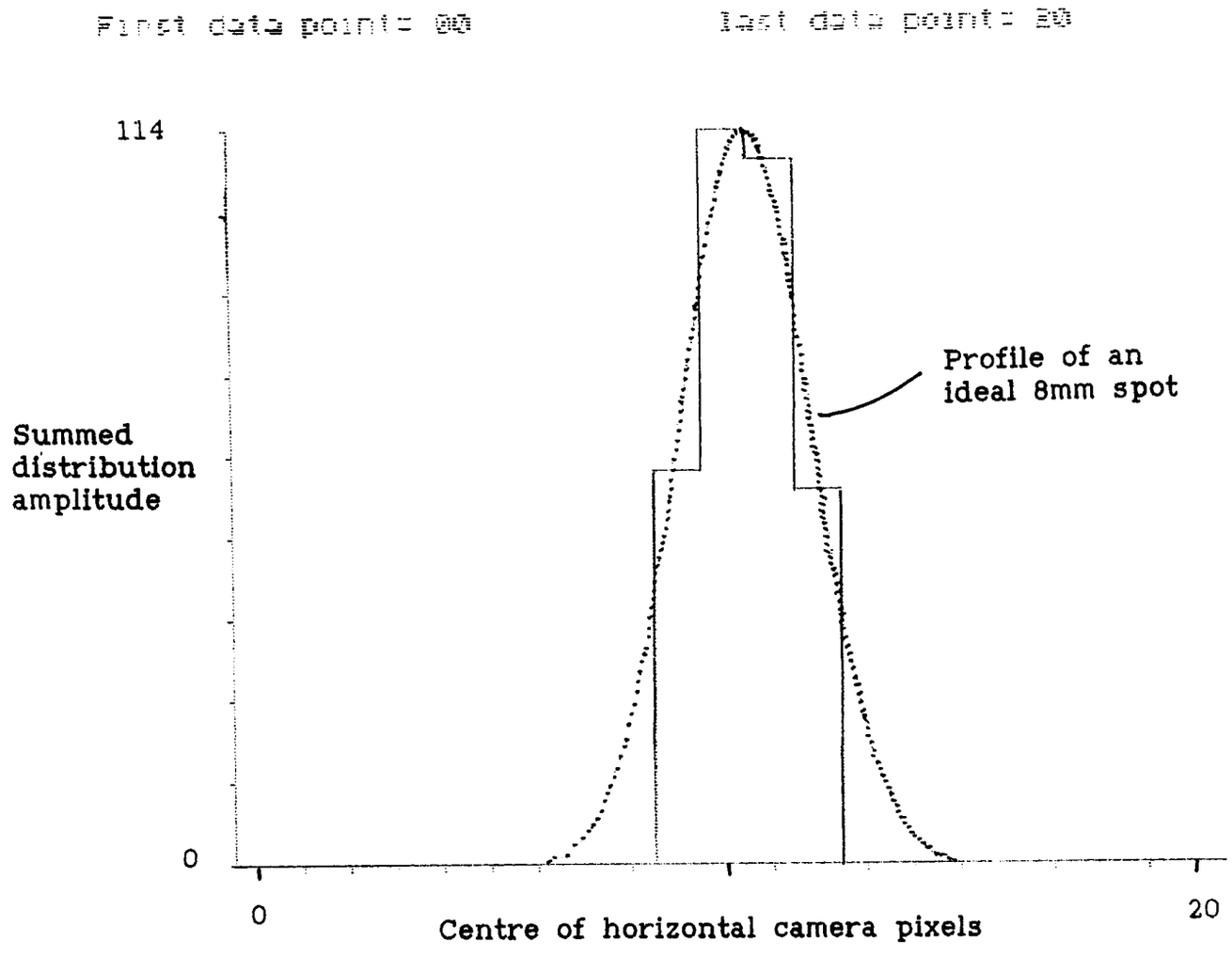

Figure 6.4(a) Sample Vertically Summed 'Near Gaussian' Distribution for an 8mm Diameter Spot with a camera Aperture of f5.6.

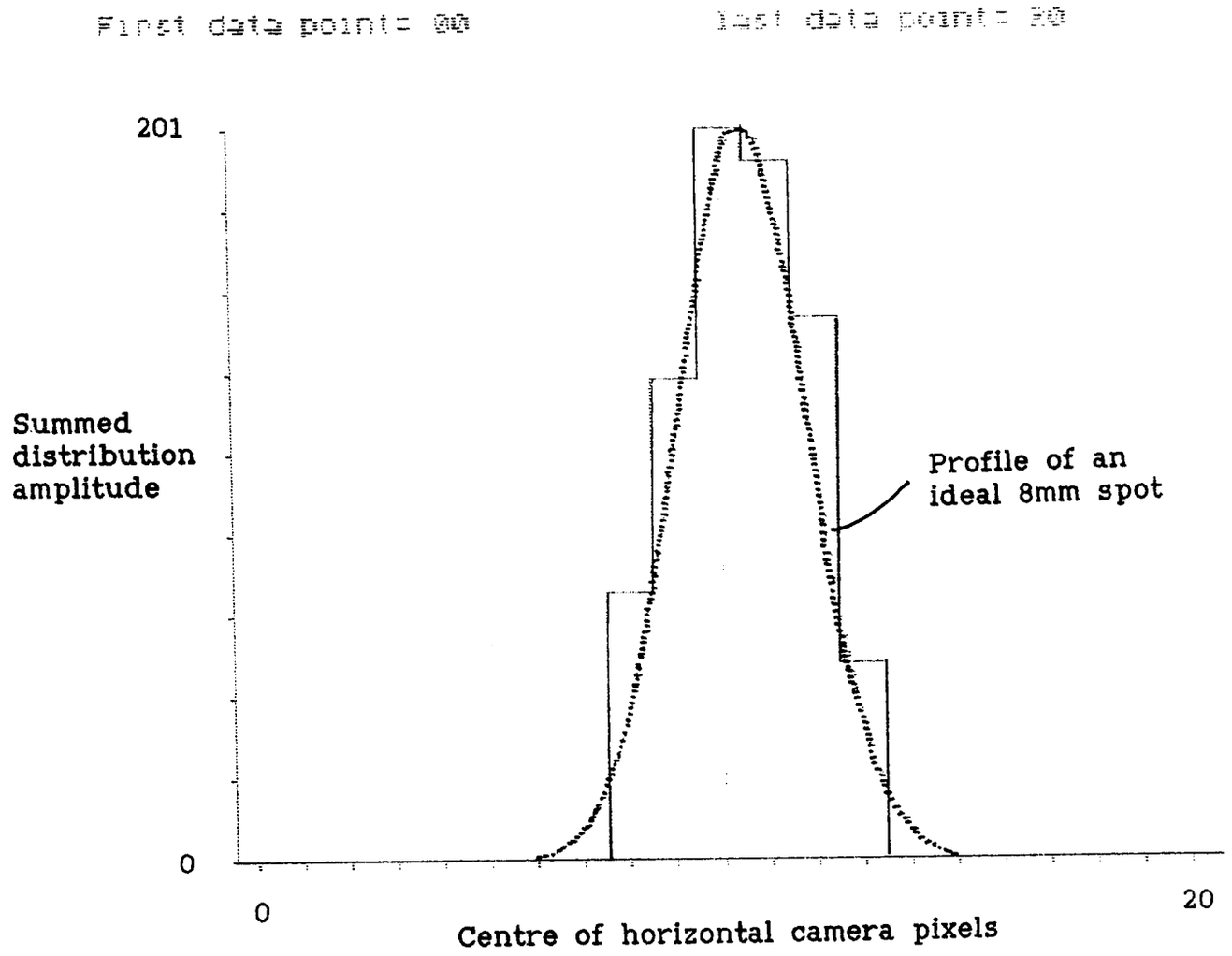

Figure 6.4(b) Sample Vertically Summed 'Near Gaussian' Distribution for an 8mm Diameter Spot with a camera Aperture of f2.8.

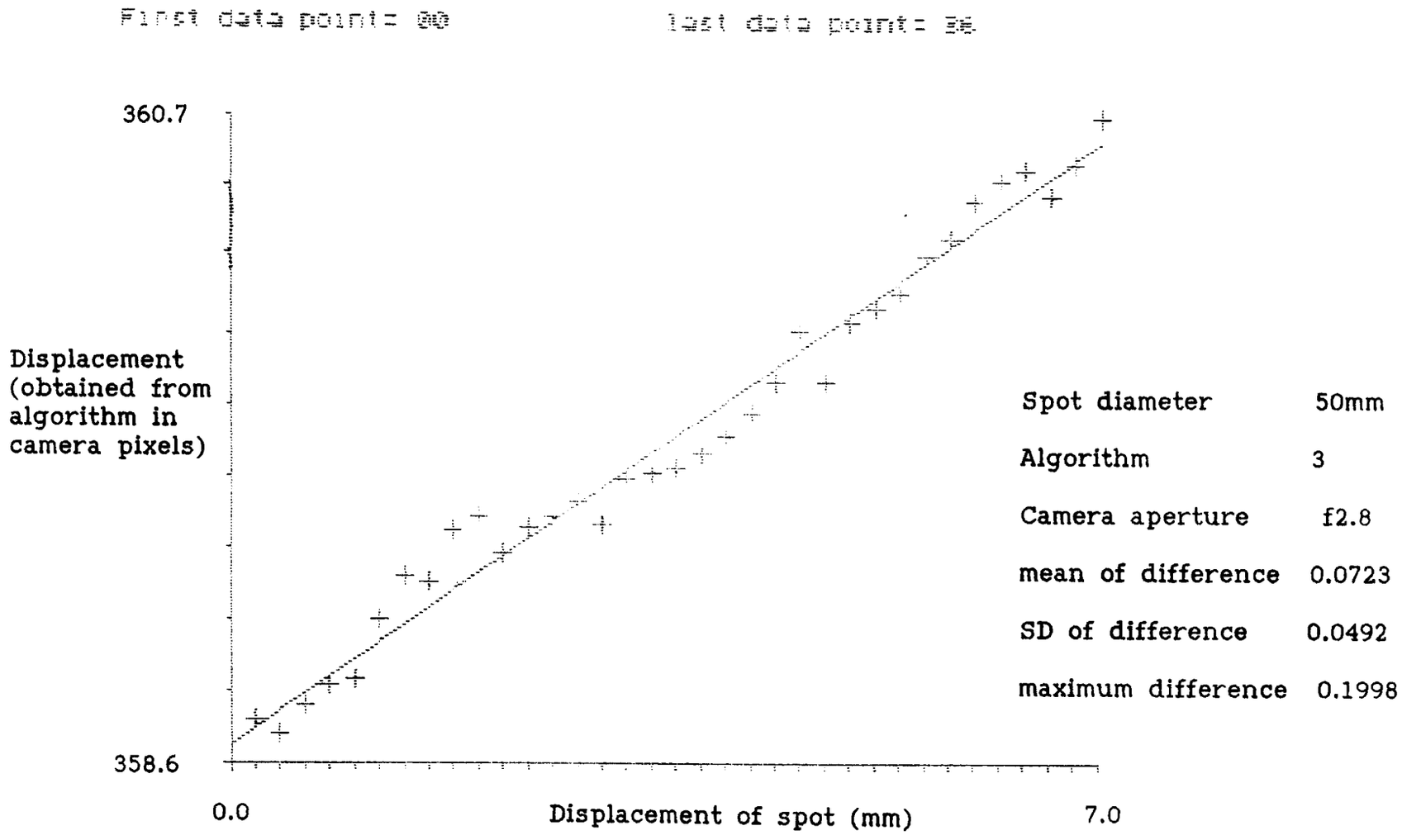

Figure 6.5(a) Results from the Subpixel Test using Algorithm 3, a Camera Aperture of f2.8 and a 50mm Diameter Spot.

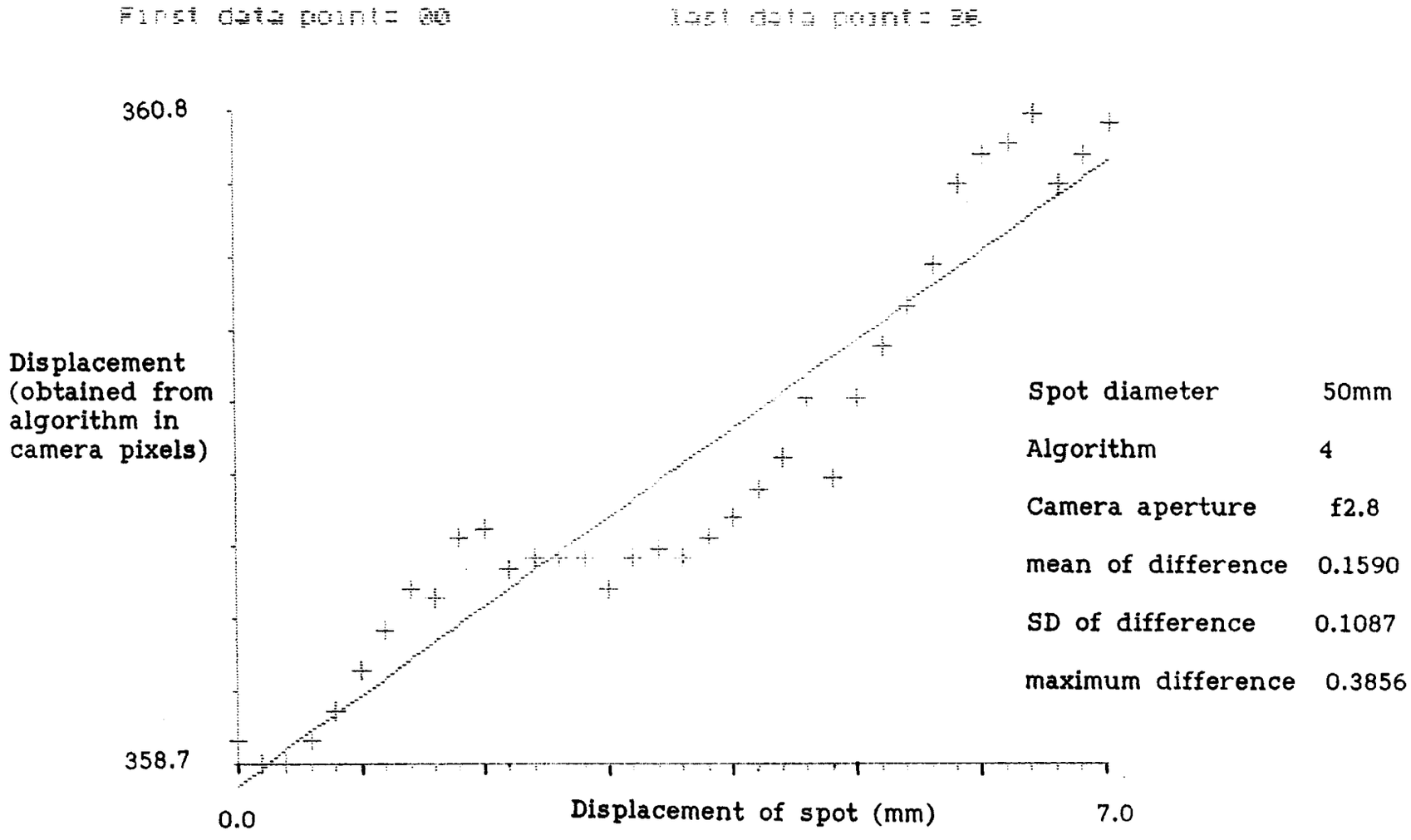

Figure 6.5(b) Results from the Subpixel Test using Algorithm 4, a Camera Aperture of f2.8 and a 50mm Diameter Spot.

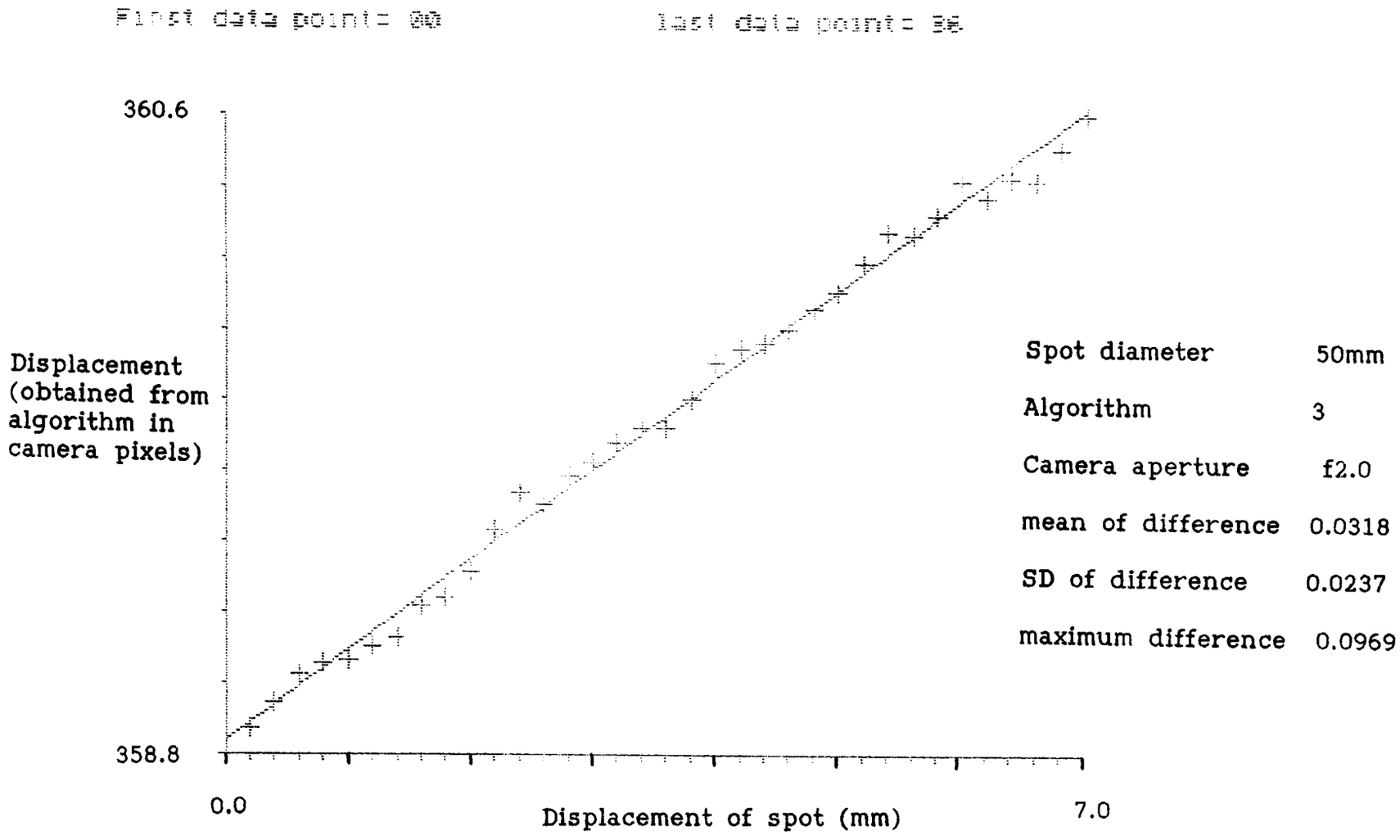

Figure 6.6(a) Results from the Subpixel Test using Algorithm 3, a Camera Aperture of f2.0 and a 50mm Diameter Spot.

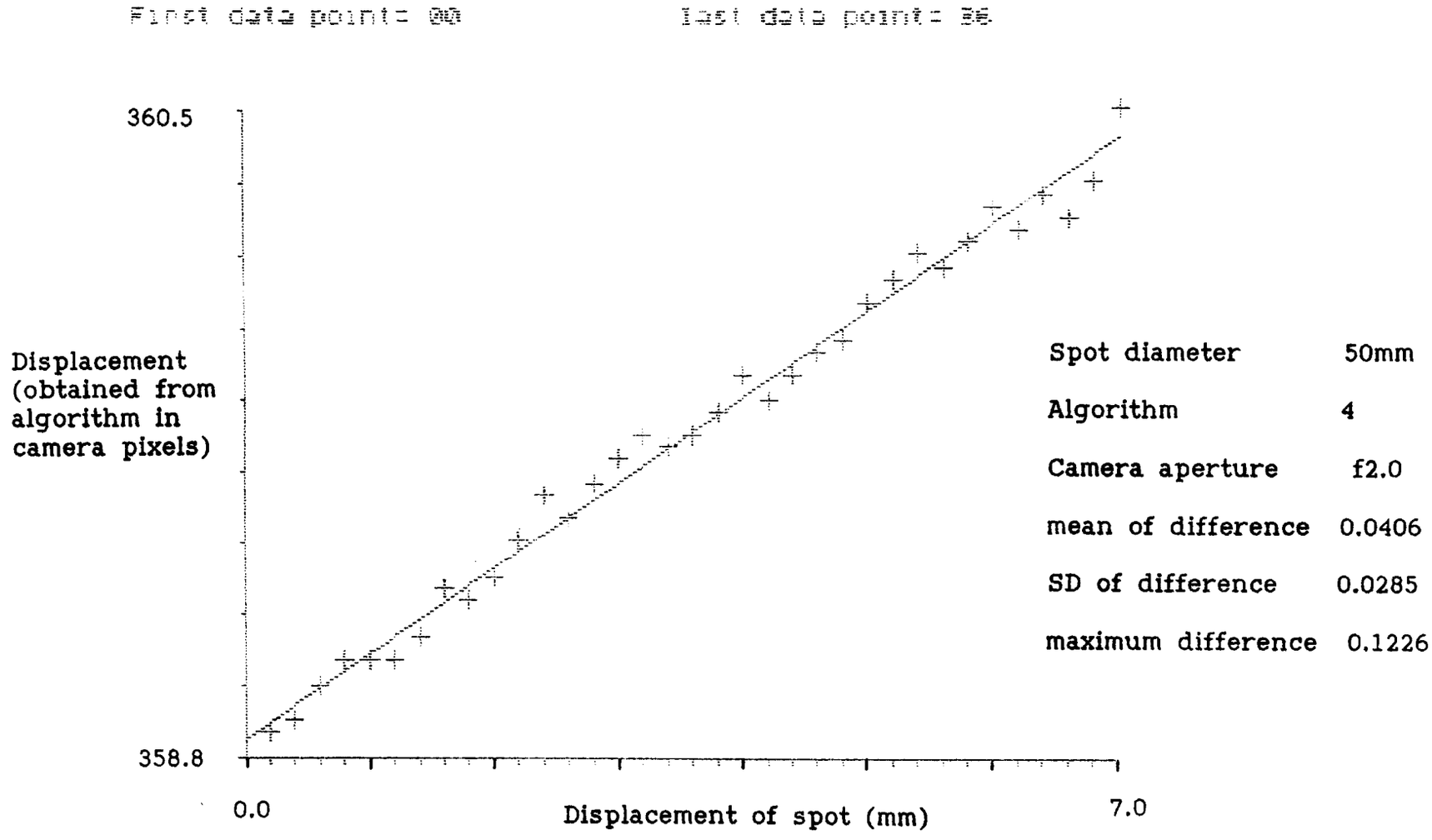

Figure 6.6(b) Results from the Subpixel Test using Algorithm 4, a Camera Aperture of f2.0 and a 50mm Diameter Spot.

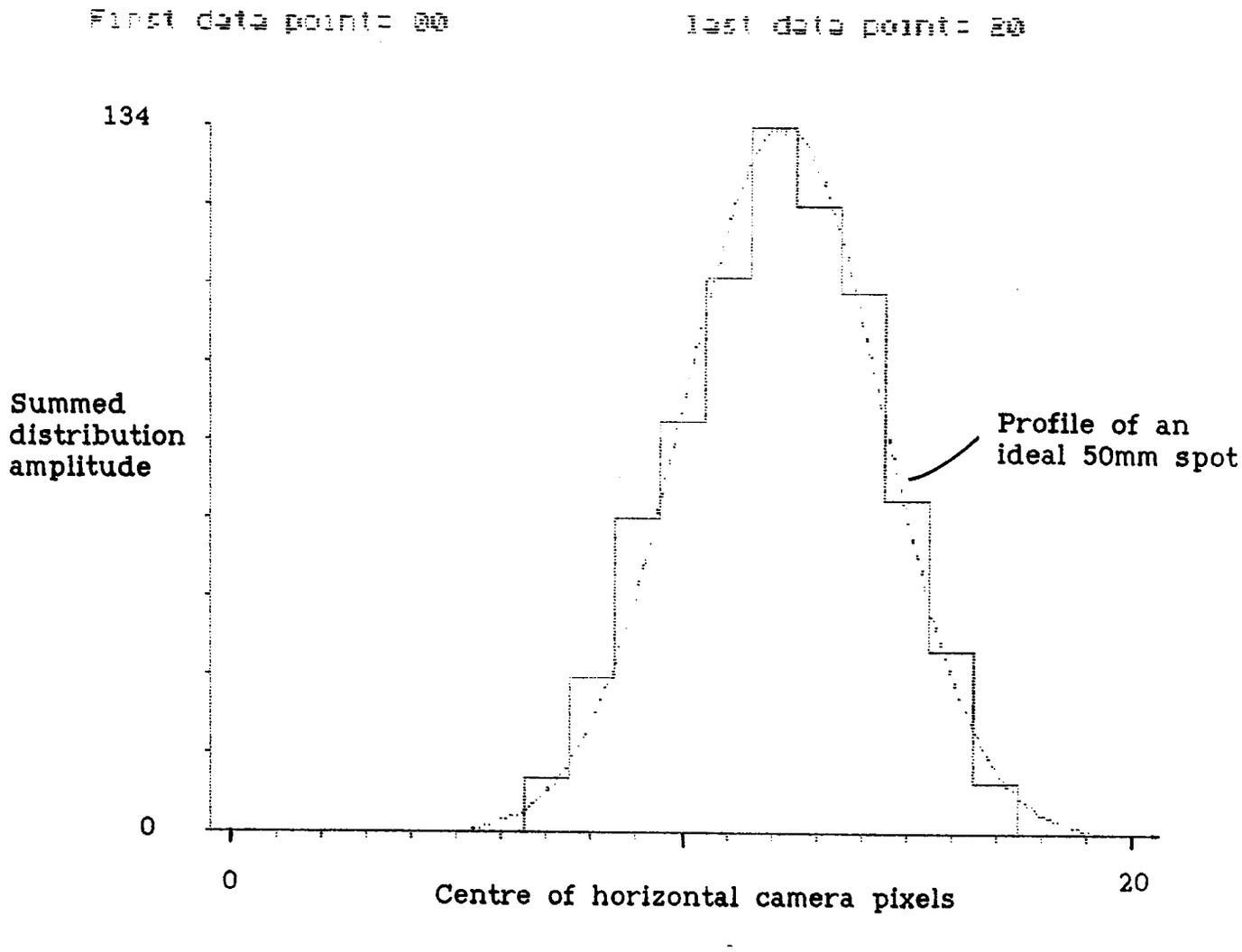

Figure 6.7(a) Sample Vertically Summed 'Near Gaussian' Distribution for a 50mm Diameter Spot with a camera Aperture of f2.8.

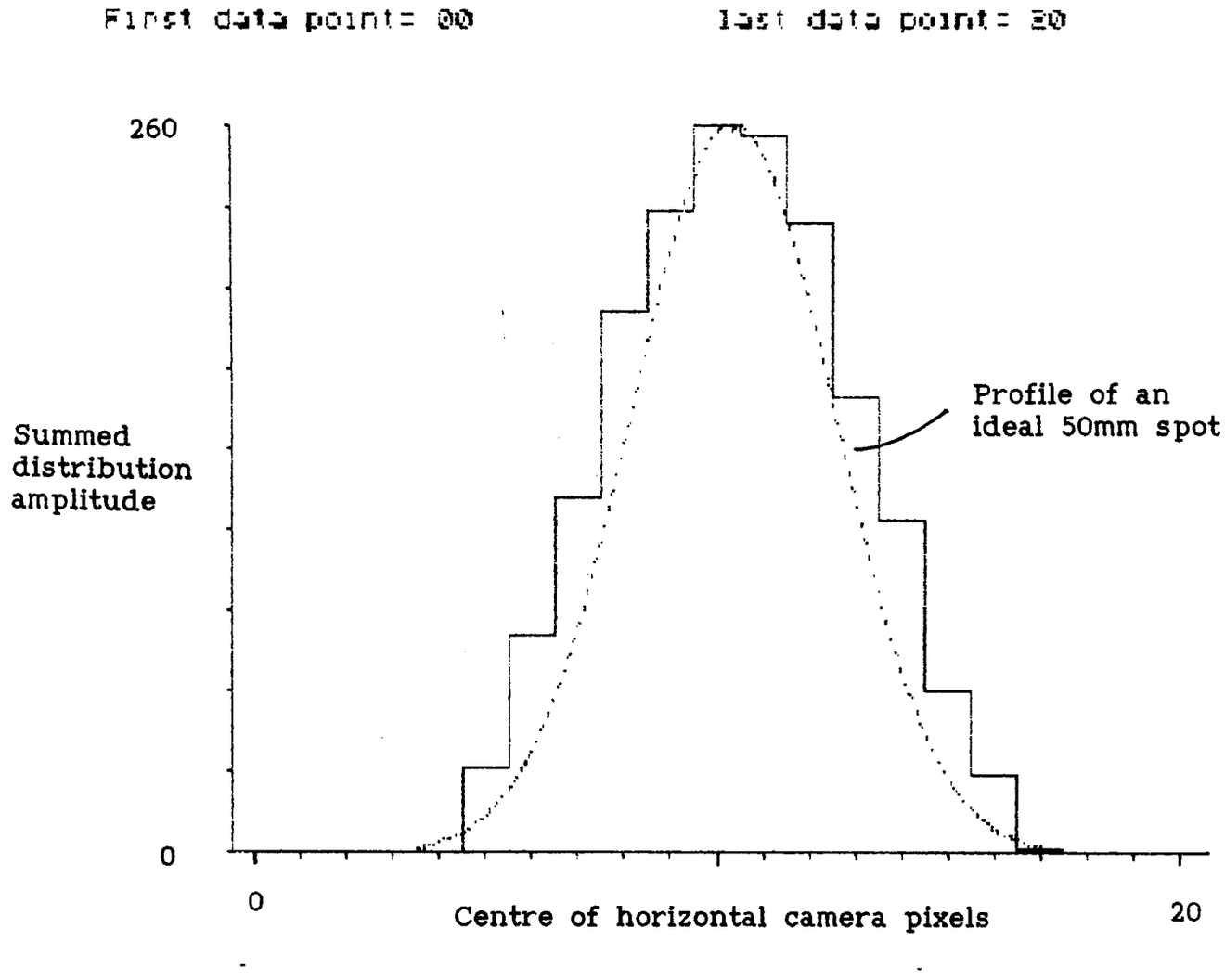

Figure 6.7(b) Sample Vertically Summed 'Near Gaussian' Distribution for a 50mm Diameter Spot with a camera Aperture of f2.0.

Spot diameter	Camera aperture	Standard Deviation (pixels)	
		Algorithm 3	Algorithm 4
8mm	f5.6	1/10	1/10
8mm	f2	1/22	1/13
50mm	f2.8	1/20	1/10
50mm	f2	1/43	1/35

Figure 6.8 Tabulated results from the sub-pixel tests.

the best results from the STM system. The results show, even with a non optimum aperture setting and taking the standard deviation of the error from the best fit straight line through the data, that a subpixel resolution of 1/9th of a pixel is obtainable with an 8mm spot and 1/9th to a 1/20th of a pixel (using algorithm 4 and 3 respectively) with a 50mm spot. The standard deviation error obtained when near optimum apertures (in terms of maximum summed distribution amplitude before any saturation effects are noticed) are used are an improvement, the results now become 1/13th to 1/20th of a pixel for the 8mm spot and 1/35th to 1/43rd of a pixel for a 50mm spot. The results for the 8mm spot also show that the STM systems's internal representation of the laser spot (Figure 6.4(a) and (b)) spreads over more than the two pixels widths which was predicted. This is because the value for the theoretical spot diameter is derived from the distance to the two half power points of the distribution rather that the actual point where the amplitude of the distribution reduces to the background level. A second contribution to this effect is obtained from charge leaking from one CCD well to adjacent wells and the de-focusing action of a wide camera aperture (decrease in the depth of field).

The conclusions that can be drawn from these tests are that subpixel resolution can be obtained with the STM system which, even with non-ideal system parameters, produces a resolution nine times that of a conventional laser triangulation system (i.e. the STM system 1). The results also show that, excluding the fact the the minimum detectable feature size is much greater with a 50mm spot diameter that with a 8mm spot, that both 8mm and 50mm spot diameters achieve as resolution of at least 1/9th of a pixel, provided a centre finding

algorithm is used. In fact, from the table of figure 6.8 it can be noted that in subpixel resolution terms the 50mm spot had superior performance to that of the 8mm spot. A second observation is that the results from algorithm 3 had a smaller magnitude of error that the results from algorithm 4. Possible reasons for these observations are that firstly, any small defect which may be present in the laser spots distribution will have, proportionally, a much greater effect in the 8mm diameter spot than in the 50mm diameter spot. This is because the 50 mm spot covers a greater number of pixels and therefore the estimate of the spots position is based on a larger number of observations. A possible explanation for the superior performance of algorithm 3 over algorithm 4 is that the model used for the correlation cannot be accurately known, since this would entail knowing the distance from the system to the target surface. This uncertainty reduces the obtainable accuracy of the fine correlation.

6.2 The Material Tests.

The tests to be to be described were performed to ascertain the performance of the STM system over non-ideal surfaces (with ideal being considered as matt black flat surfaces). These surfaces consist of material (i.e grain, coal and various types of gravel) that may be encountered in the industrial applications that have been considered for the STM system.

The two criteria for which comparisons will be made between the different material tests are:

(1) The resolution that is available over these non-ideal surfaces.

(2) The maximum amplitude of the summed laser spot's distribution.

The test layout which is shown in figure 6.9 will now be described. The test surface material is made to adhere to, and cover half of, a target metal plate. This plate is mounted a distance of 5m away on an optical bench by a fixture which allows the target plate to be displaced laterally with respect to the laser/camera baseline. The laser beam from the STM system passes through beam expansion optics before reaching the horizontal and vertical moving iron galvanometer deflectors.

For each material the tests were run using the material coated half of the of the plate, and then using the control half. The plate is displaced laterally a distance of 12 mm to produce a control for the tests performed over the material of interest. For all the control tests, the results of less that a $1/10^{th}$ of a pixel spread were obtained. Each test over a material was conducted at three spot diameters, 8, 25 and 50 mm and different values for the camera aperture were used to produce a varying signal/noise ratio. The material tests used the same 12 mm lateral displace as the control tests.

The following four materials were used in the material tests, grain, two different sizes of gravel and coal. These materials were chosen because of their different properties and since they could be encountered in applications envisaged for the STM system. The properties that the materials exhibit are that the grain has a specular surface with dense packing of the individual grains. The small diameter gravel (approximately 6 mm diameter) is multi-faceted but non-specular, with the large gravel (approximately 12 mm diameter) having similar

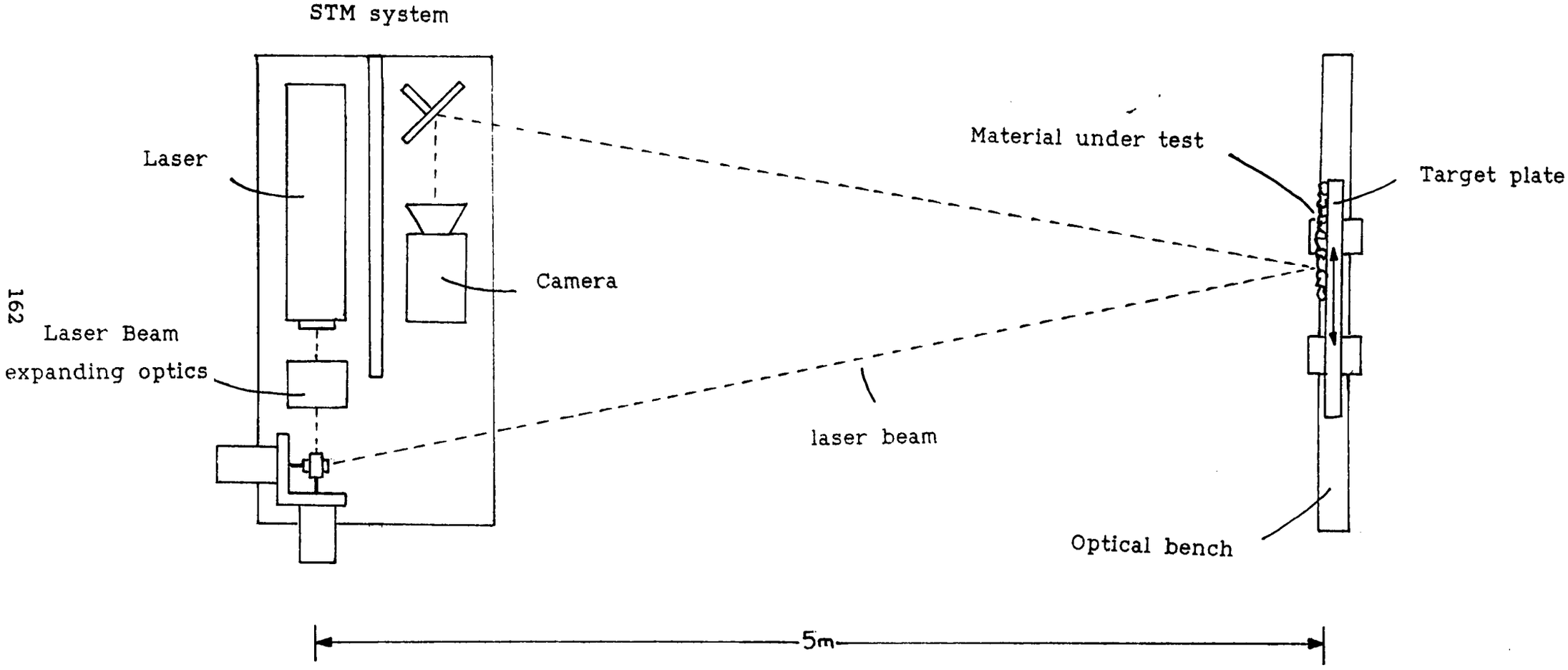

Figure 6.9 Test setup for the material tests.

characteristics, but a much looser packing, allowing a small diameter laser beam to be 'absorbed' in one of the holes in this loosely packed structure. Lastly the coal combines the problem of the loosely packed structure, variable size of the component coal pieces and a very varied surface albedo characteristic.

The complete results for all the tests are presented in Appendix B, in this section graphs are presented that contain the two criteria that were defined at the start of this section (that of resolution and maximum distribution amplitude). The measures that were devised to show if these two criteria were met are:

(1). For resolution, looking at the standard deviation of any of the readings taken from the average value of the data obtained from the results of the distribution centre finding algorithms (for a specific spot diameter and camera aperture setting).

(2). The maximum distribution amplitude was obtained from the pre-processing stage of the distribution centre finding algorithms calculation.

Measure (1) was chosen since the 'correct' deviation is impossible to obtain, from any other test, due to the finite and irregular thickness of the material covering the target surface. Measure (2) was used since it indicates the amount of energy from the laser spot that is reaching the camera.

The results from the large gravel, are shown in Figures 6.10(a), (b) and (c) for spot diameters of 8mm, 25mm and 50mm respectively. It is assumed that the small diameter laser spot will not exhibit as good a performance as the large diameter laser spots due to the feature size

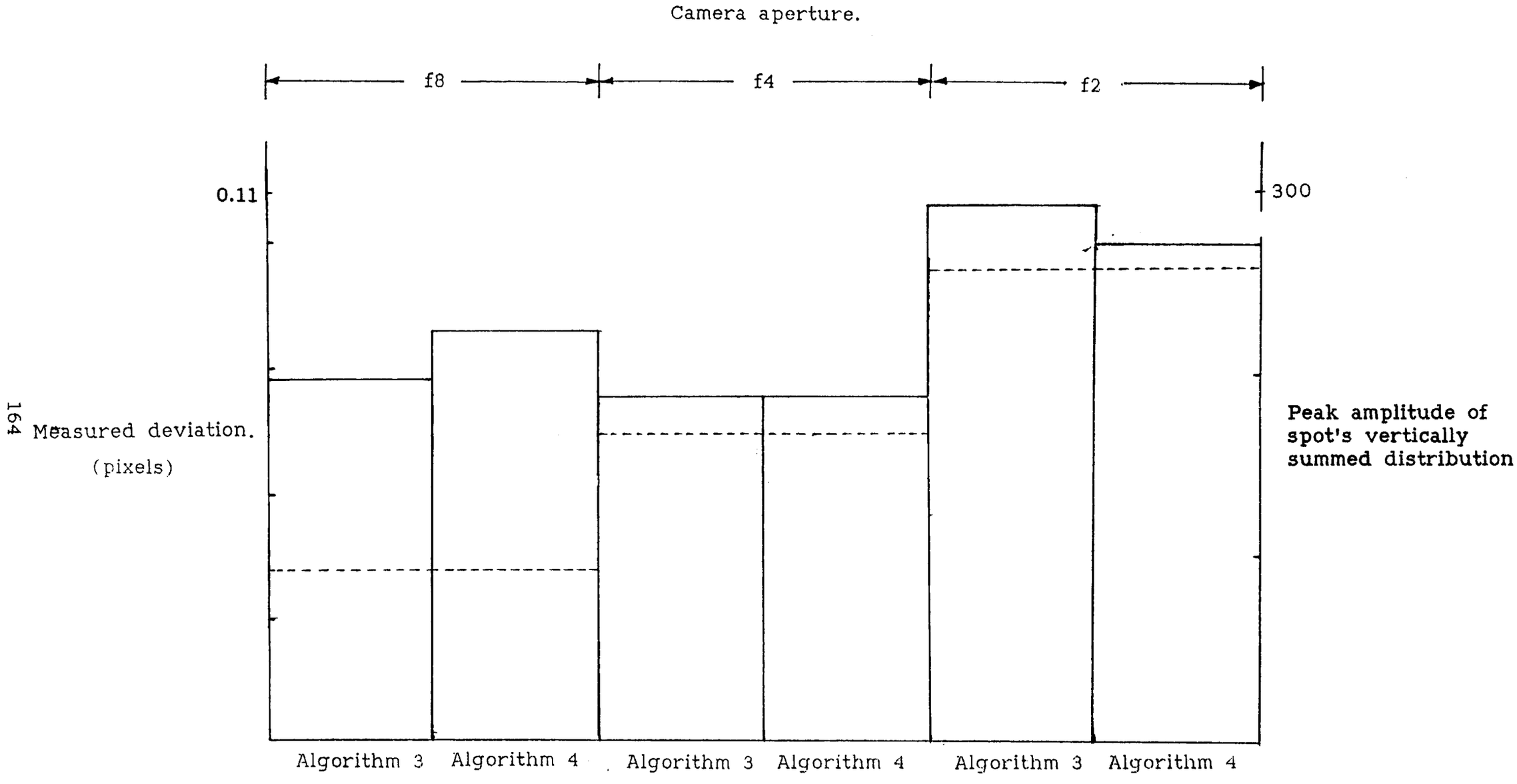

Figure 6.10(a) Results from the Material Tests using the Large Gravel and an 8mm Diameter Spot.

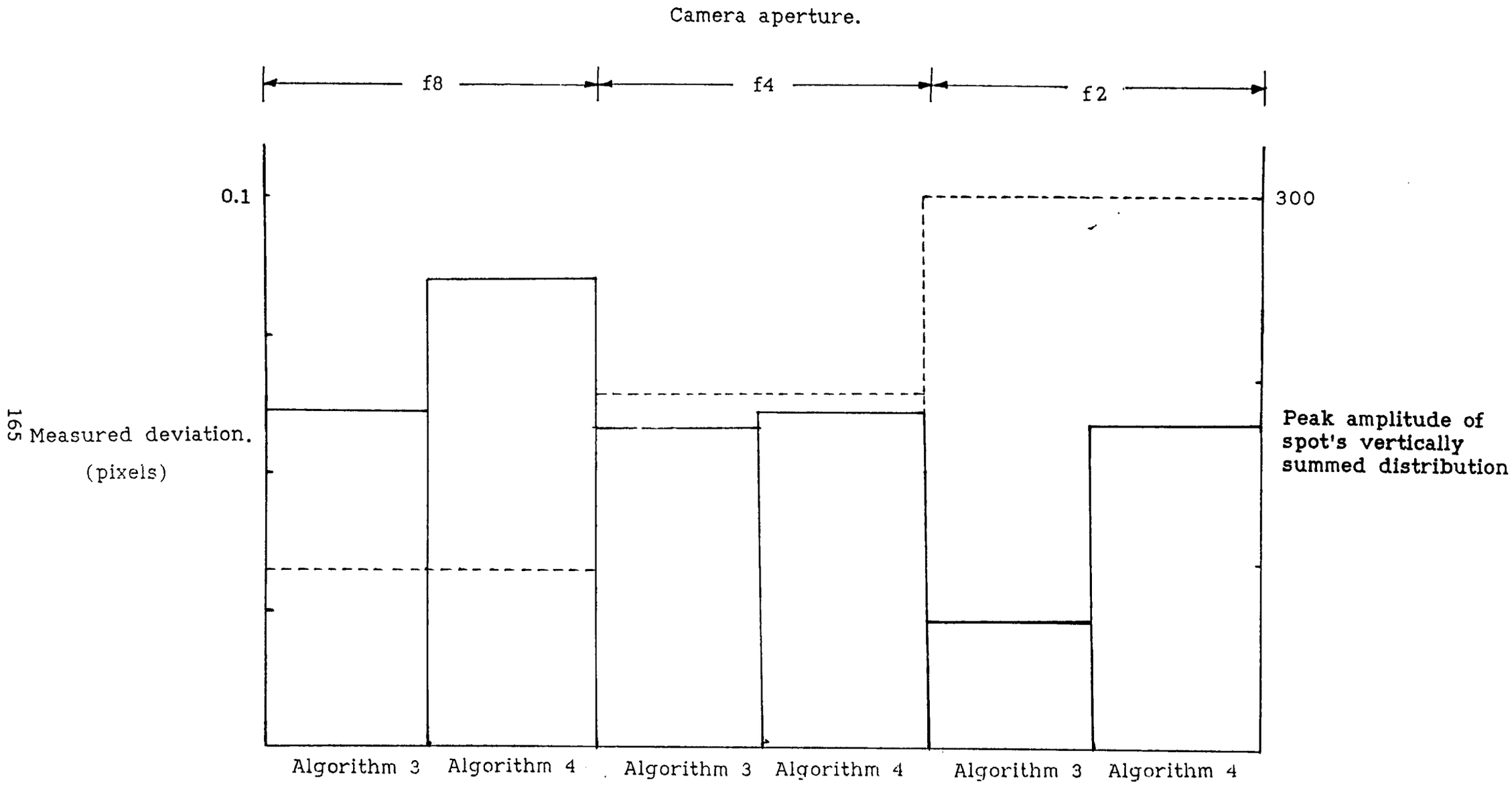

Figure 6.10(b) Results from the Material Tests using the Large Gravel and a 25mm Diameter Spot.

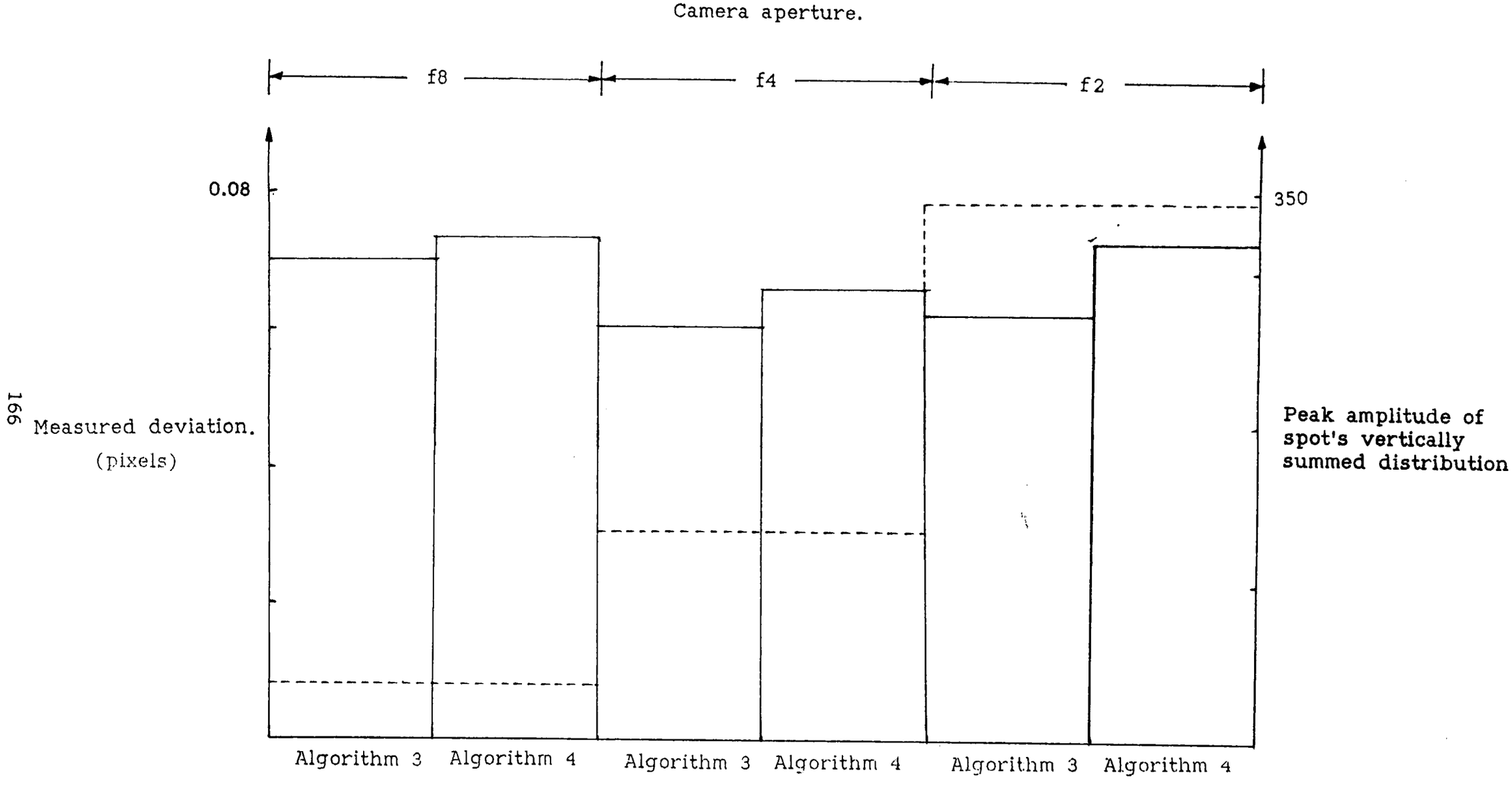

Figure 6.10(c) Results from the Material Tests using the Large Gravel and a 50mm Diameter Spot.

of the material being similar to the size of the smallest laser spot. This is reflected in the results with the 8mm diameter laser spot achieving a marginally worse resolution than that of either the 25mm or 50mm diameter spots although the effect is not very prominent. It can be seen that the results remain constant at better than a 1/10th of a pixel for all laser spot diameters and any change in camera aperture. The 8mm diameter spot however does shown the onset of saturation with a camera aperture of f2 which consequently degrades the results. The best overall performance was obtained from the 25mm diameter spot, but all the results had a spread, over a real material, of less than 1/10th of a camera pixel.

The next set of results are for the small gravel, the results are presented in Figure 6.11(a), (b) and (c) for the varying spot diameters. It can be seen that the maximum summed distribution amplitude (for equivalent spot diameters) have a smaller amplitude that those obtained from the large gravel, this implies that the surface's albedo properties are less specular that those of the large gravel and therefore saturation effects in the laser spot's distribution do not occur. The 8mm and 25 mm diameter spots have very similar results which remain around the 1/10th of a pixel level for all the camera aperture settings. For the 50mm diameter spot the very low value maximum distribution amplitude was obtained in the test with the camera aperture at a f8 setting and consequently, results with a standard deviation of approximately 1/3rd of a pixel. With a more realistic value of summed distribution amplitude (between 100 and 300) the resolution results produced had a standard deviation of around the 1/10th of a pixel level. The 25mm spot produced the most consistent

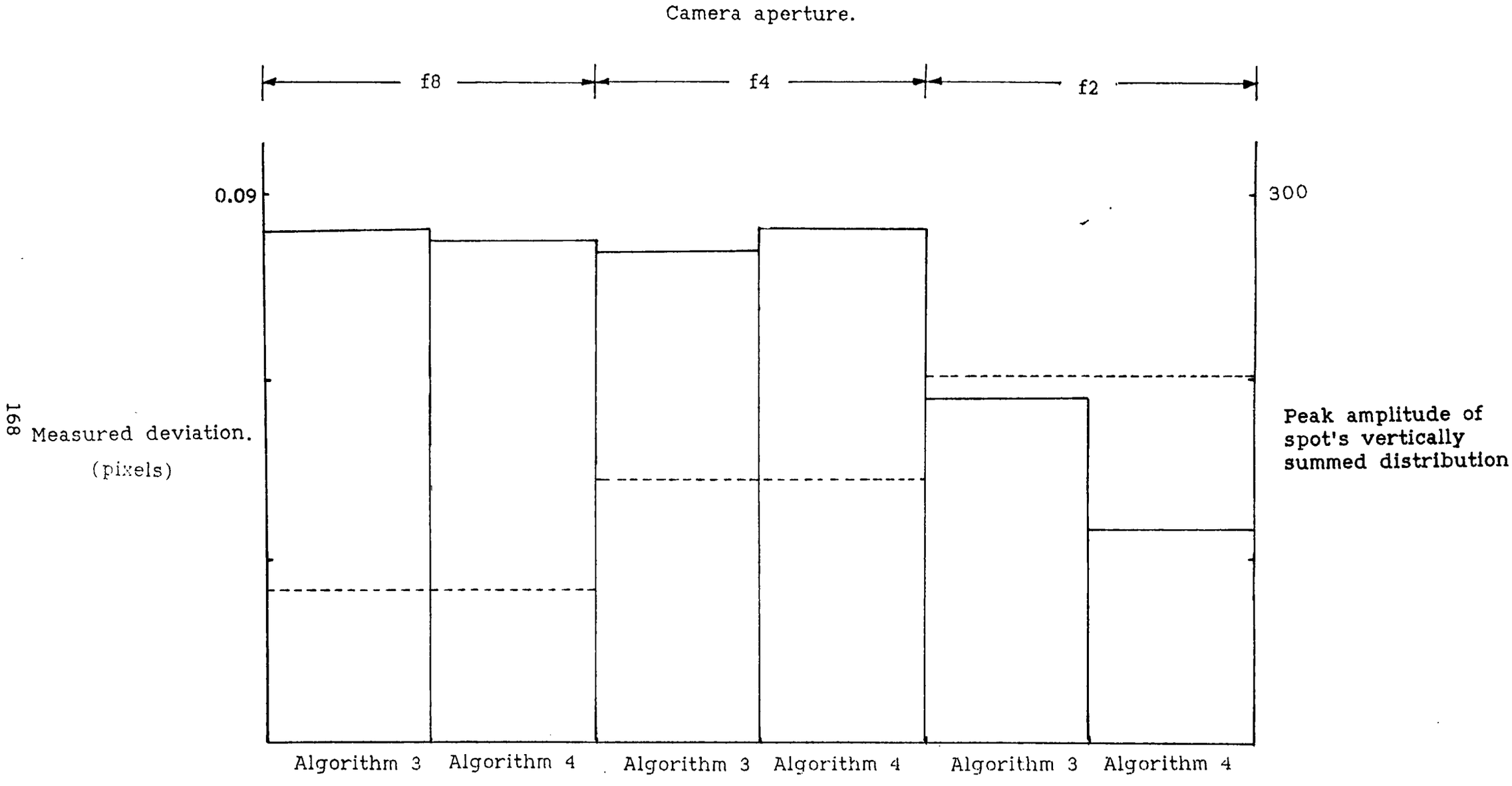

Figure 6.11(a) Results from the Material Tests using the Small Gravel and an 8mm Diameter Spot.

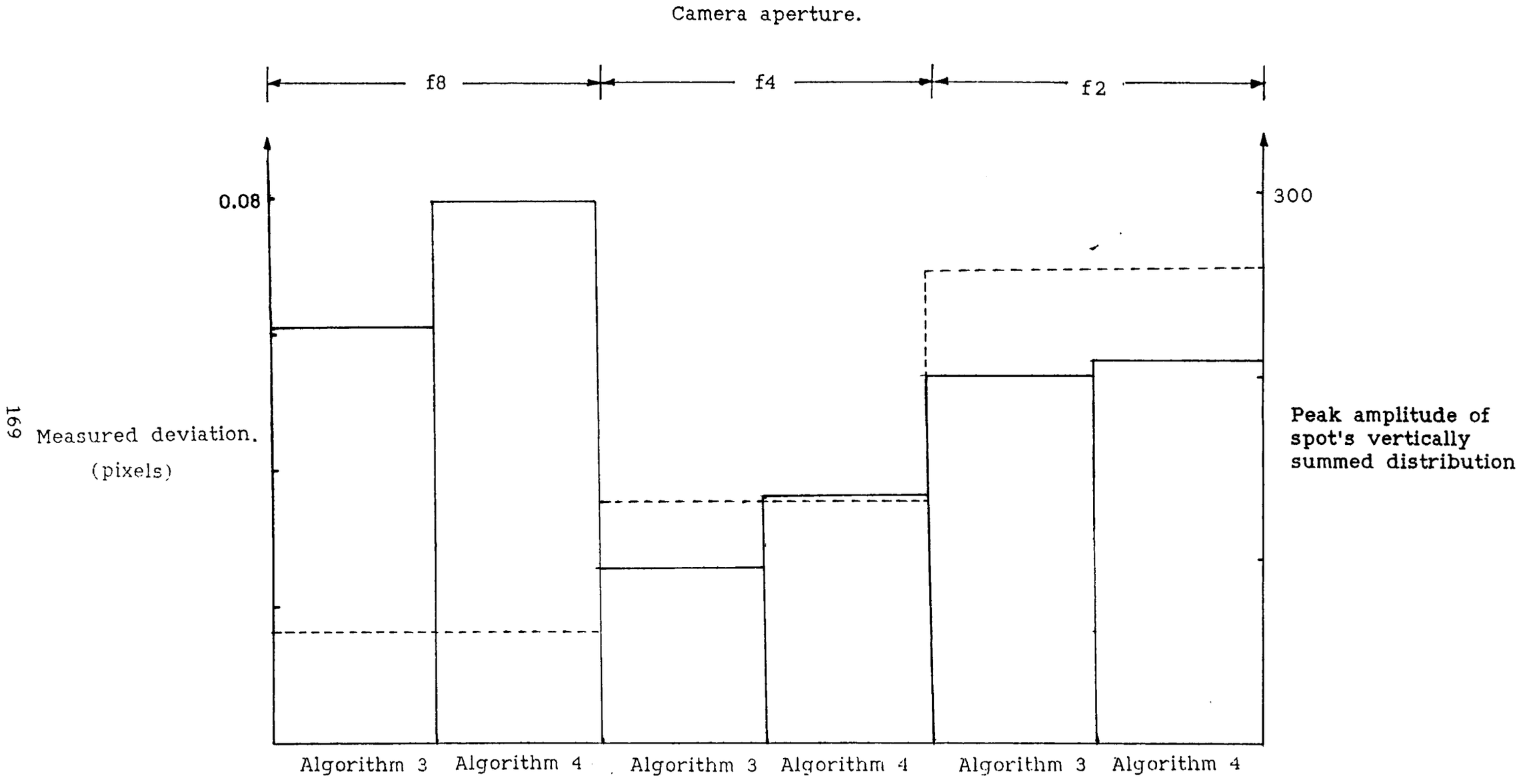

Figure 6.11(b) Results from the Material Tests using the Small Gravel and a 25mm Diameter Spot.

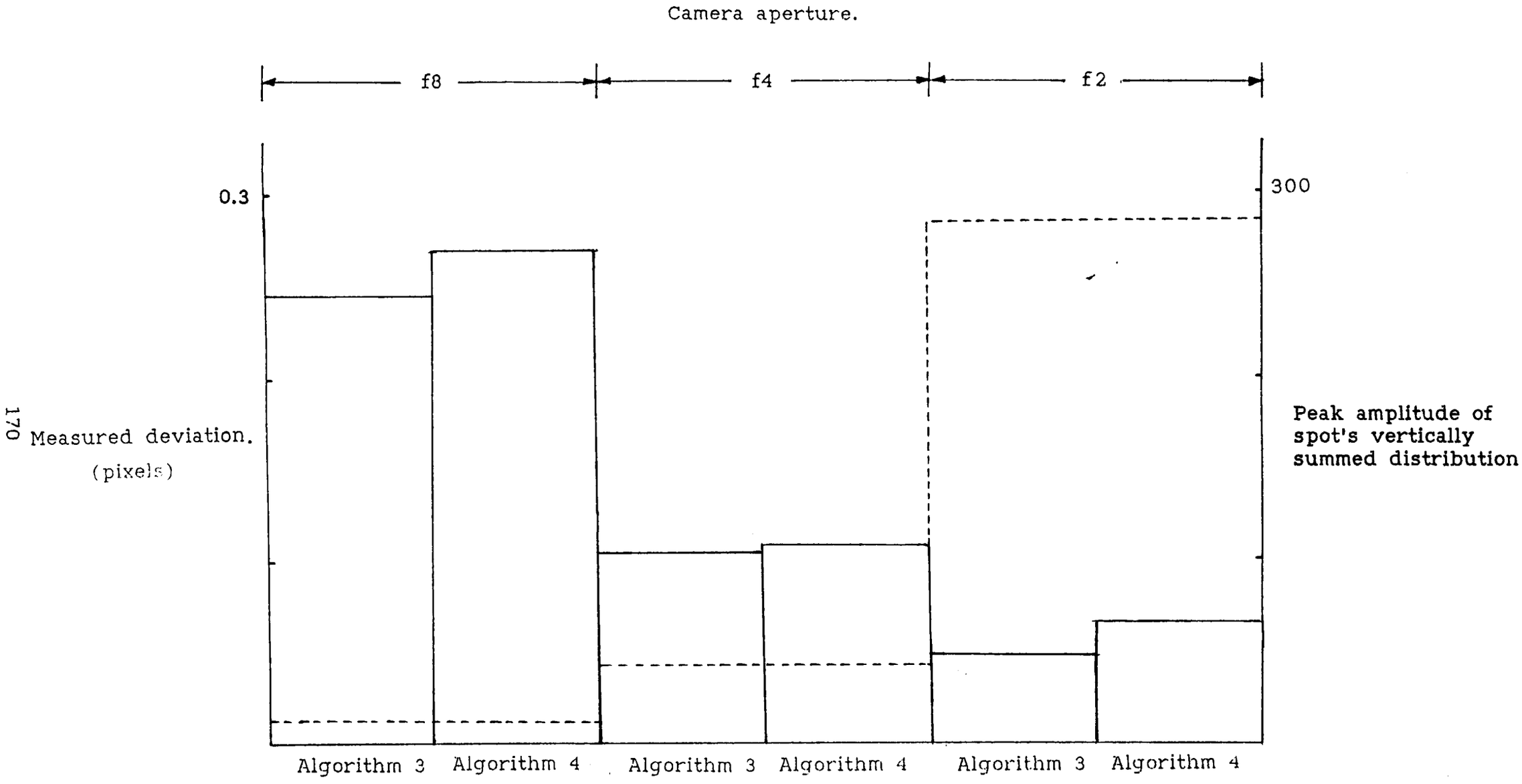

Figure 6.11(c) Results from the Material Tests using the Small Gravel and a 50mm Diameter Spot.

results with the greatest spread of resolution results being better than a 1/12th of a pixel at all camera aperture settings.

The results for the grain are presented in Figures 6.12(a), (b) and (c). It would be expected that this material would produced large maximum distribution amplitude values because of its specular surface and densely packed structure of the grain. This means that the results for three different spot diameters should not be significantly different, this was confirmed by the observations. The 25mm diameter spot again produced the best results with the resolution measure having a standard deviation of less that 1/12th of a pixel at any of the camera aperture settings.

The results for the coal are presented in figures 6.13(a), (b) and (c) for ascending spot diameters. The coal is envisaged as the most difficult material because of is very irregular surface and varying albedo. The results from the 8mm spot show, contrary to expectations, little variation in the resolution measure. For the f4 and f2 camera aperture settings the results observed were approximately a 1/10th of a pixel. The results from the test with a camera aperture value of f8 did show a degradation in the resolution yielding results in the region of a 1/5th of a pixel. The results for the 25mm diameter spot showed a very poor resolution of approximately 3 pixels. When the camera aperture was adjusted to produce an optimum value (between 100 and 300) for the summed distribution amplitude, the results improved to a value of 1/10th of a pixel or better. The 50mm diameters spots results were unobtainable until the camera aperture was increased to f2 with the results again improving to better than a 1/10th of a pixel with the largest camera aperture of f1.2.

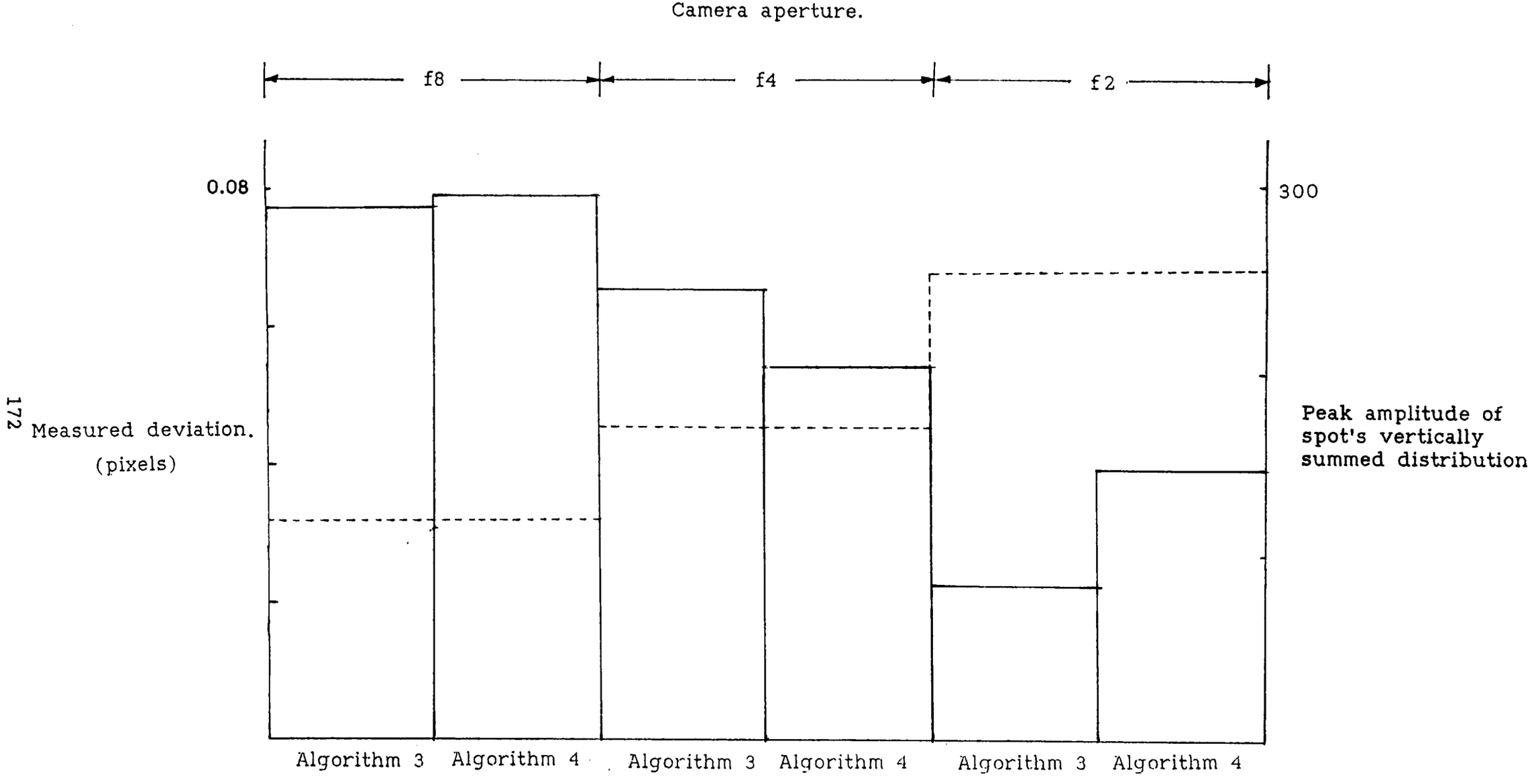

Figure 6.12(a) Results from the Material Tests using Wheat and an 8mm Diameter Spot.

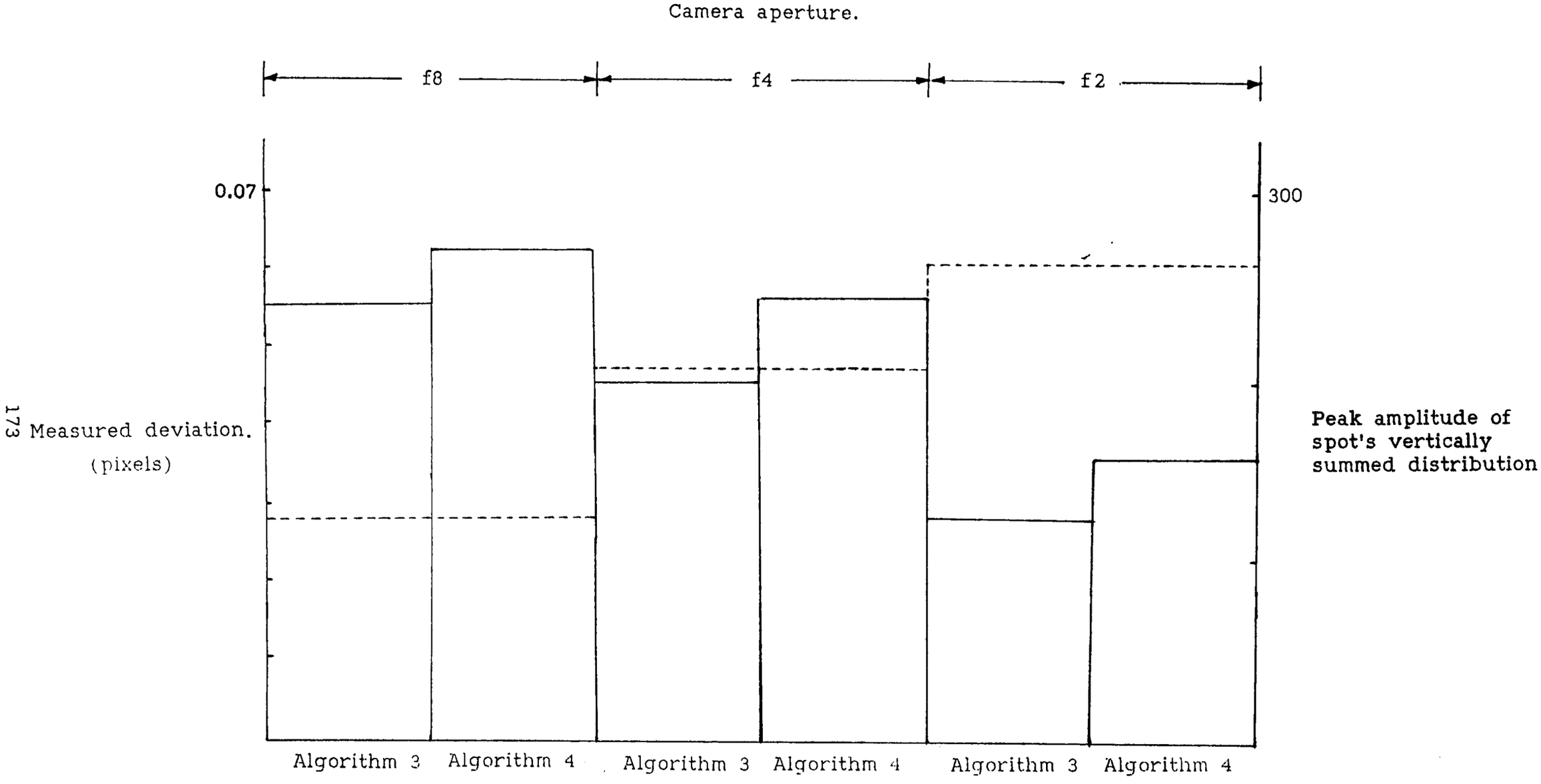

Figure 6.12(b) Results from the Material Tests using Wheat and a 25mm Diameter Spot.

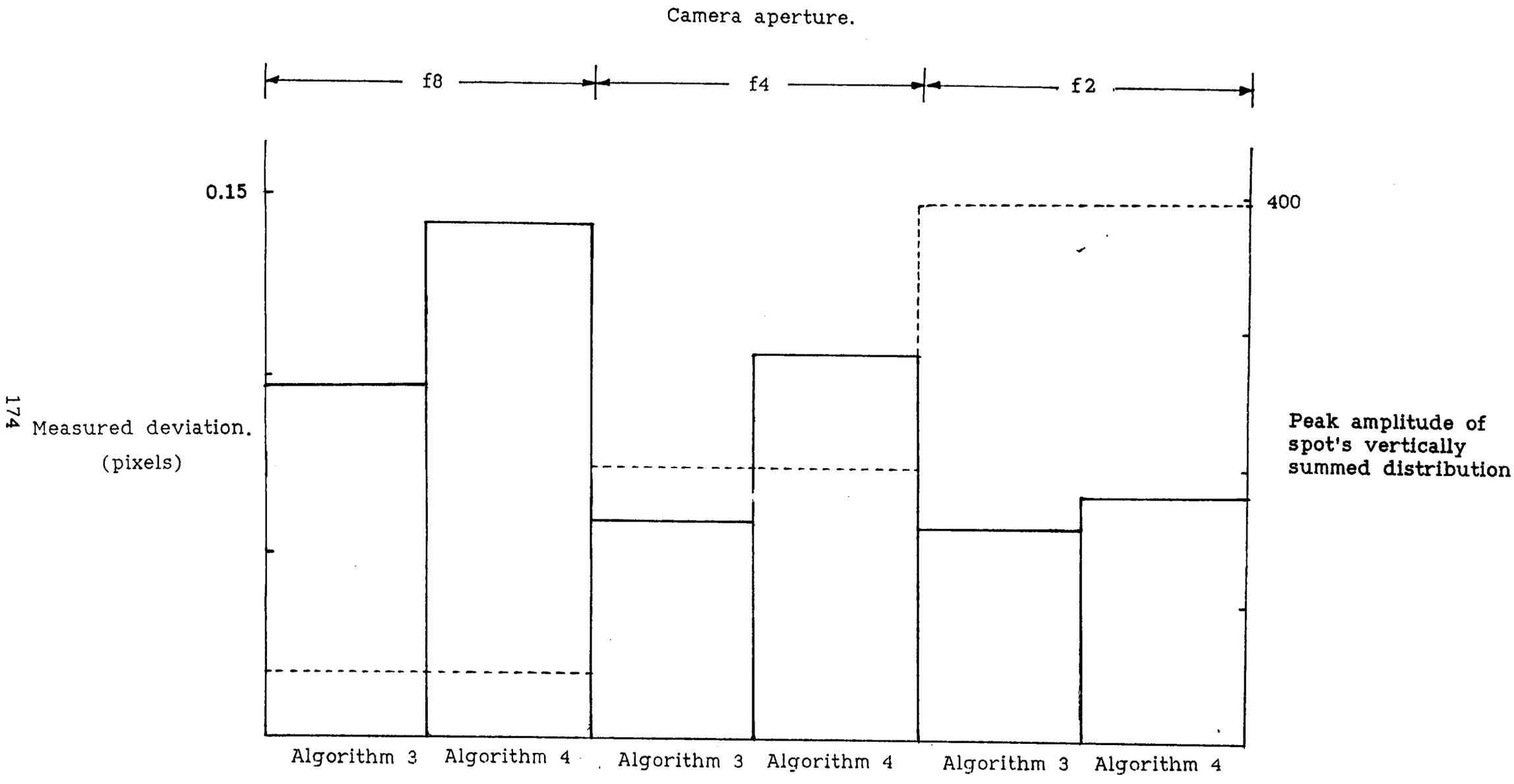

Figure 6.12(c) Results from the Material Tests using Wheat and a 50mm Diameter Spot.

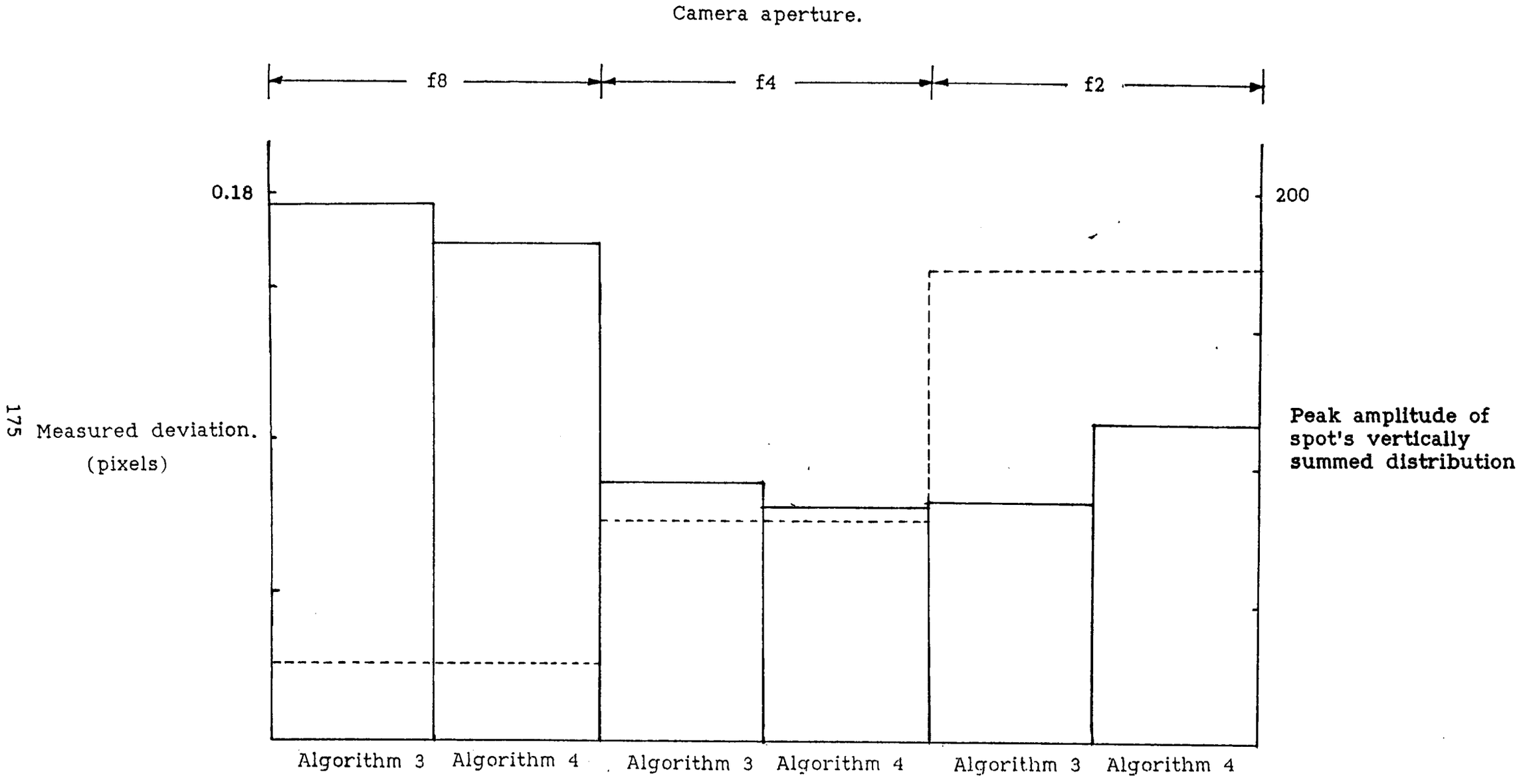

Figure 6.13(a) Results from the Material Tests using Coal and an 8mm Diameter Spot.

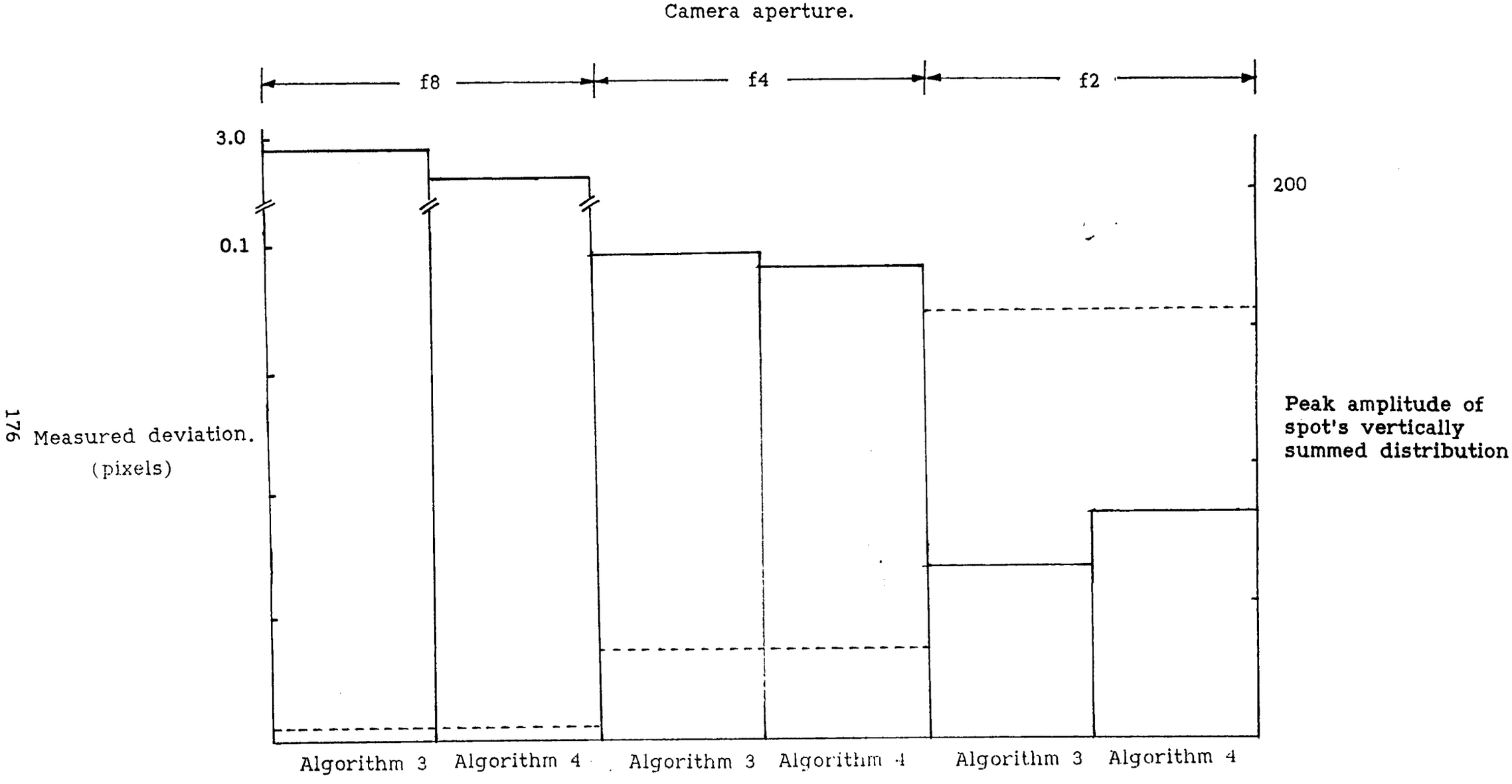

Figure 6.13(b) Results from the Material Tests using Coal and a 25mm Diameter Spot.

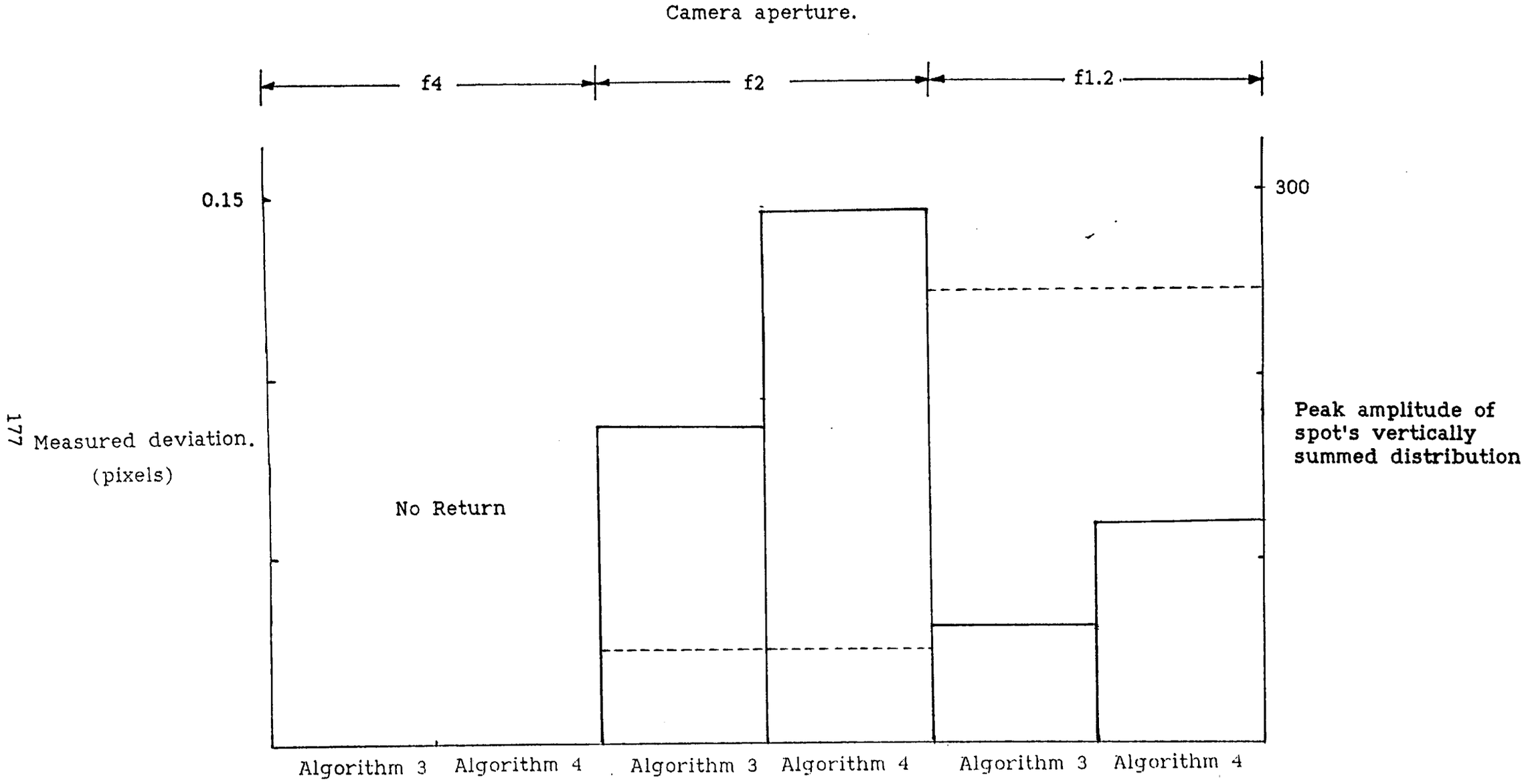

Figure 6.13(c) Results from the Material Tests using Coal and a 50mm Diameter Spot.

6.3 Conclusions

The conclusions that can be drawn from these results are; that the effect of maximum signal amplitude (and consequently camera aperture) is highly significant when non-ideal materials are used as the target surface if the best interpolation of the centre of the laser spots is to be obtained. The amplitude of the summed distribution obtained from image of the laser spot captured by the the STM system's camera must be as high as possible without saturation effects becoming significant. This will require elaborate control of the camera aperture, and camera gain, in a practical system. A second important point is that, a large laser spot diameter makes a reasonable maxiumum distribution amplitude only obtainable at a large camera aperture setting (assuming that the same laser is used for all spot diameters) and the large apertures can cause focusing problems (since the depth of field decreases with increasing aperture).

From the results it may be inferred that the choice of a 25 mm laser spot diameter gives results which are equal to or better than those for a spot of 8 or 50 mm diameter, and has the added advantage over the 8mm diameter spot of reducing of the laser hazard if the STM system is used in situations where people could come into direct eye contact with with the laser beam (see [50] for a definition of laser hazards). A problem that must be considered with the use of a 25mm spot as standard in the STM system is that, assuming it is produced from a 1mm diameter beam by a confocal beam expander, the divergence has been reduced by a factor of 24.7. This will definitely dictate a maximum value for the range obtainable for the system (from equation (22)) because of the stipulation that the laser spots image must spread over

more that one pixel for the centre finding algorithms to operate correctly. For a 25mm diameter laser spot (measured at 5m), the maximum distance over which the system will operate, using equation (22), is given by.

$$Z_{max} = \frac{24.7*10^{-3}}{(1.5 * 8.09*10^{-4} - 1.4*10^{-3} / 24.7)} = 21 \text{ m}$$

In this equation the maximum number of camera pixels that the image of the laser spot must cover assumes a value of 1.5, which is value observed in the present system. This is a conservative estimate. The laser spot's image will normally cover more that 1.5 camera pixels because the theoretical equation uses the half power points as the edge of the laser spots distribution.

The requirement for accuracy, range and the ability to operate under a diversity of target materials conflicts with the specification of an optimum spot size. This situation can be alleviated by using a laser with a larger divergence or a greater initial beam diameter, which would give a larger ratio of spot size to camera pixel width at the target surface.

The availability of the resolution enables the theoretical intrinsic range error to be calculated. This is the variable δa in equation (26) and the value of δa is taken as the worst case value of $1/10^{th}$ of a pixel which was obtained for all of the materials tested provided a reasonable camera aperture was used (i.e a maximum distribution amplitude of between 100 and 300). The equations gives the range error at a target distance of 5m as.

$$\delta z = \frac{-25}{0.5} * (0.1 * 8.09*10^{-4} + 2.44*10^{-4} * (1.55 + 0.13)) = 25 \text{ mm}$$

This equation uses worst case values and offers an improvement of 100% over the STM system 1 and this improvement should be available over any of the materials tested.

6.4 Summary of Findings.

In this thesis an industrial surface topography measurement system has been presented and the equations describing its performance have been derived. After examination of test results from the STM system 1 a second STM system was produced which addressed major deficiencies of the first system. This new system, the STM system 2, had radical enhancements which enabled it to achieve subpixel resolution of the laser spot's displacement in the camera (and therefore increased accuracy in the three dimensional measurements obtained from the system). This was achieved through the use of centre finding algorithms which operated on the camera's image of the laser spot obtained by the new STM system 2 hardware. The equations defining the parameters of this system have been produced and examined and the system tested. The tests, carried out to ascertain whether subpixel resolution is achievable under practical conditions and the observe the performance of the system over 'real' materials, have produced results which indicate a consistent ten-fold improvement in resolution obtainable over the STM system 1 for a range of target materials.

The next chapter will briefly outline further work that can be carried out on the STM system and will outline some possible industrial applications of the STM system.

7.0 Further Work and Possible Applications.

In this chapter the further work to be carried out on the STM system in both the research and development fields will be described. These major enhancements have come to light during the course of this research and are also are needed to tailor the system to specific industrial applications. The second section will contain an outline of the proposed industrial applications.

7.1 Proposed Further Work on the STM System.

From the results of the previous chapter it is proposed that the camera's aperture and gain come under the direct control of the STM system's controlling microprocessor. This would enable a fine/coarse adjustment of the magnitude of the laser spot's distribution so that a good S/N ratio could be obtained and any saturation effects avoided. Before this can be achieved some measure of the distribution size must be proposed which is both robust (i.e. resistant to noise) and computationally fast. For initial tests, a simple magnitude comparison between the maximum value of the laser spot's distribution and a pre-defined minimum level could be used. If problems were encountered, because of the presence of noise in the laser signal, a more robust method which used the result of correlation to assess the magnitude of the distribution could be used. This has the advantage that the correlation would have already been performed in the centre finding algorithms, and is therefore available at very little extra computational cost. The gain control algorithm would assess whether an increase in gain was required and alter the camera gain by producing a 6 - 12 Volt signal via a D to A Converter and associated offset and amplification electronics. If the gain was still considered incorrect

the aperture would be altered by one stop via an electrically controlled iris and the fine adjustment process, using variation of the camera gain, would be repeated. The possibility exists that no satisfactory combination of gain exists because the spot was occluded, or because of unfavourable lighting conditions. If this were to be the case the best results obtained is used and the data marked to indicate that its reliability was questionable. A watchdog timer would also have to be used to stop the gain algorithm spending too much time searching for the correct gain when one may not be available for the specific laser spot position .

A problem that can be identified arises from the use of a conventional camera for the photo sensitive device. The results for a gain tests can only be obtained every 20 ms which implies a trade-off between time required to locate the correct gain/aperture combination and any error introduced by using a non-optimum gain/aperture combination. One solution would be to introduce a concurrent method of assessing the correct gain aperture combination. This would entail the use of a large area photo diode (which was sensitive at the laser wavelength) mounted on the camera with a lens which affords the same field of view as the camera (this is shown in Figure 7.0). This would allow, once the relationship between the photo diode output and camera output has been experimentally obtained, a fast reading of the intensity of the laser spot and therefore a quick attainment of the correct camera gain/aperture setting. This could be implemented as a separate hardware process with its own processor. This would take input from the STM systems timing information and provide as outputs the drive signals for the gain and aperture control systems. The processing power may also be needed if the relationship between the output of the

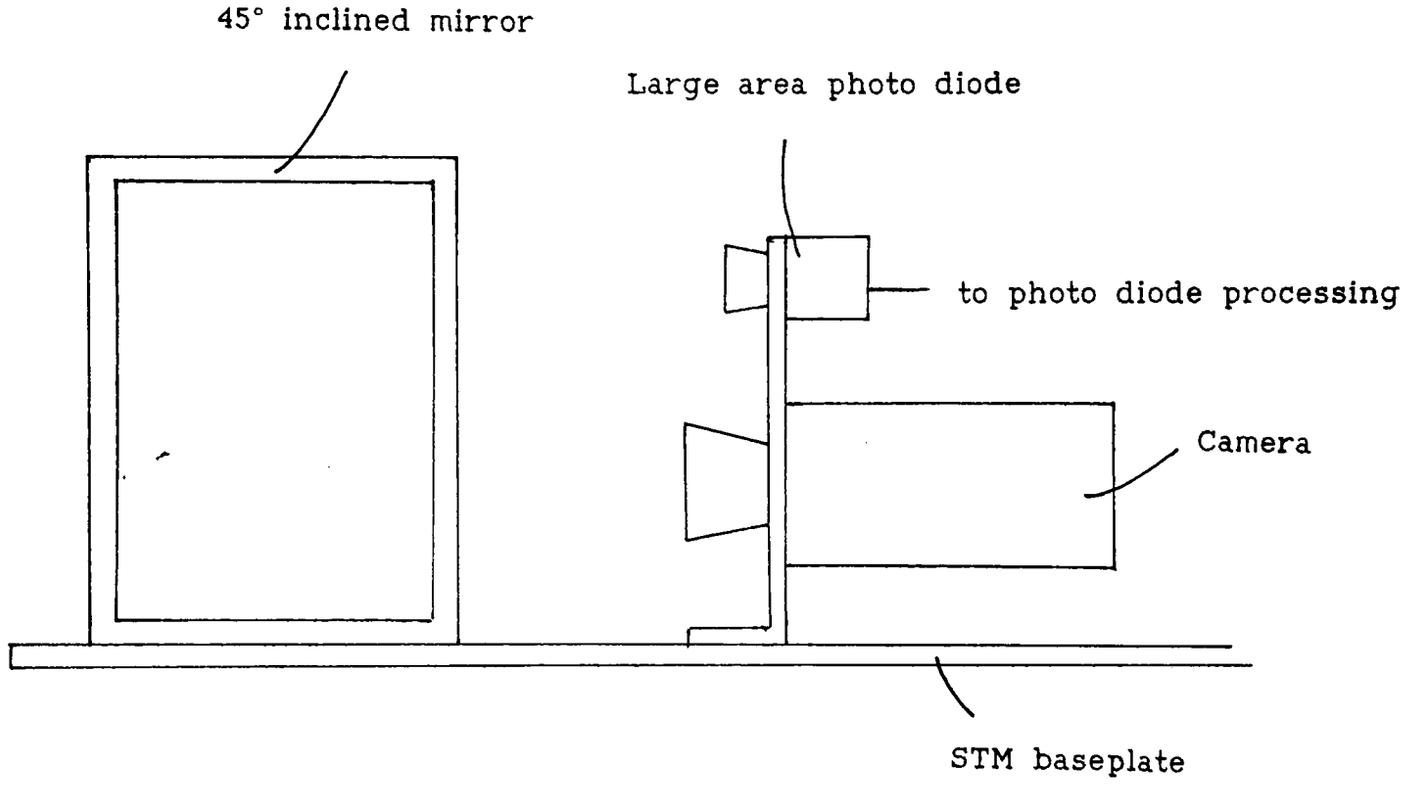

Figure 7.0 Possible camera / aperture control setup.

photo diode and the camera is not a simple relationship and therefore some form of experimentally obtained software 'look-up' table may be needed to define this complex relationship.

In the present STM system the hardware for the fine camera gain control has been implemented as a simple D to A converter with 6 bit resolution but, the camera aperture control and gain control algorithm have not been implemented. The software task of implementing the gain control algorithm and then integrating this into the present software structure is not a trivial operation and would require careful coding so as not to slow down the major task of obtaining 3-D coordinate points.

Another area which requires further work is the possibility of enhancing the STM accuracy by the introduction of a second camera fitted with an electronically adjustable zoom lens. This would only been a viable possibility in an instrument or application where very high accuracy was a priority i.e a automatic surveying device, the accuracy requirements of which have been reported in Freeman [50]. The addition of a second camera, as illustrated in Figure 7.1, produces a 'two tier' STM system where a camera with a conventional wide angle lens would be used to locate the position of the laser spot from a preliminary calculation. This calculation, although having a limited accuracy, would be used to produce a drive signal for a field of view deflection mirror mounted in front of the camera which has the zoom lens attached to it. The camera with the zoom lens would then view the laser spot which would extend over several camera pixels as a result of using the zoom lens. The displacement, therefore, would be obtained with a much greater resolution due to the increase in angular resolution of each camera pixel provided that a subpixel centre finding

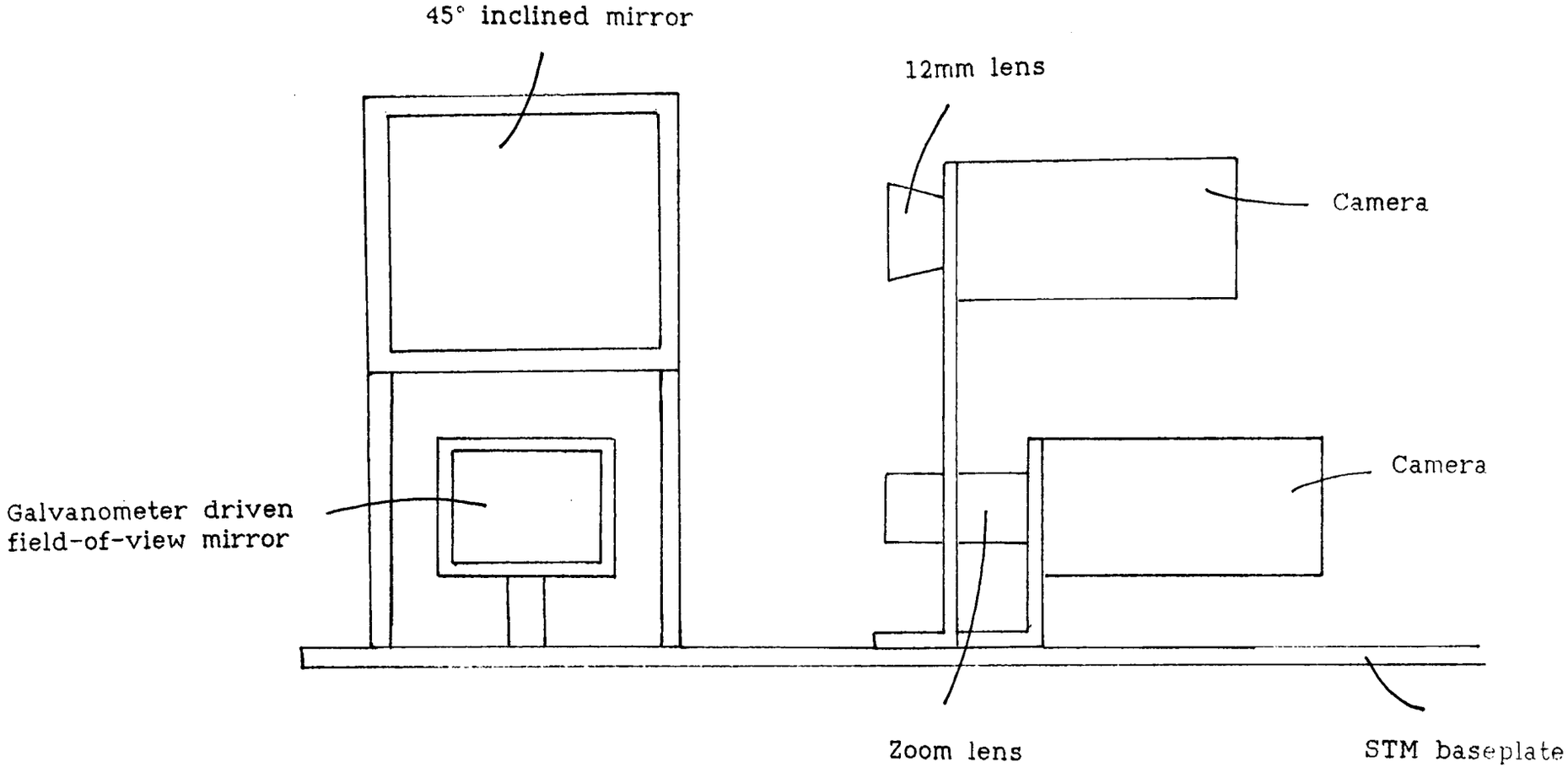

Figure 7.1 The 'Two tier' high accuracy STM system.

algorithm is used. The accuracy of the measurement would now rely, as in the STM system 2, on the error in defining the exact angular offsets of the horizontal and vertical laser projection moving iron galvanometers. A new possible error source has been introduced, this is in the form of defining the angular error resident when a specific angular offset is required for the 'field of view' moving iron galvanometer. This error can be treated in a similar fashion to that present in the horizontal and vertical laser deflectors which has been described in this thesis. The range error would also be a function of solving the non-trivial problem of selecting the correct focal length for the zoom lens (to achieve optimum spot diameter), an optimum aperture setting and a sharp focus.

It is assumed that the next stage of the development may include the above two major design enhancements but a specific industrial application should be identified first so that the specification for this application can be examined to indicate whether either enhancement is necessary. The next section will outline two such industrial applications.

7.2 Sample Industrial Applications.

The two main industrial applications that have been considered for the STM system are as an automatic surveying instrument or as a device for measuring the amount of material contained within a stockpile, ship's hold (for automatic unloading) or a silo. In the first application the modification to a 'two tier' system is essential so the the required accuracy can be obtained. Also in this application the photo sensitive device will most probably not be mounted on the same physical unit as the laser light source and deflection galvanometers

(to increase the accuracy by increased baseline, see equation (26) which indicates that the error is proportional to the reciprocal of the baseline). This requires that some method of obtaining the position of one platform relative to the other has be devised, along with the ability to then relate this position to some external reference to give the measurements some relative to world coordinates. The results obtained from this project would be helpful in assessing the accuracy that could be obtained with the increased spot size.

The second application would definitely require the introduction of some form of camera gain/aperture control. For the stockpile measurement application the STM system would be mounted on an overhead gantry and move across the stockpile until all of it had been measured and then produce a value for the amount of material present, as shown in figure 7.2. The silo application would have the system mounted permanently in the roof of the silo, the suitability of the STM system over a ultrasonic system would depend on the material being stored (excessive dust would negate the use of the STM system) and the regularity of the silo being filled. The ship's hold application would require that the system be attached to the unloading unit and be linked to a system which would control the unloading (see reference Barnes [51]).

For any of the above applications the results and insight into the STM system given in this thesis would be essential to produce a working and fully defined industrial system.

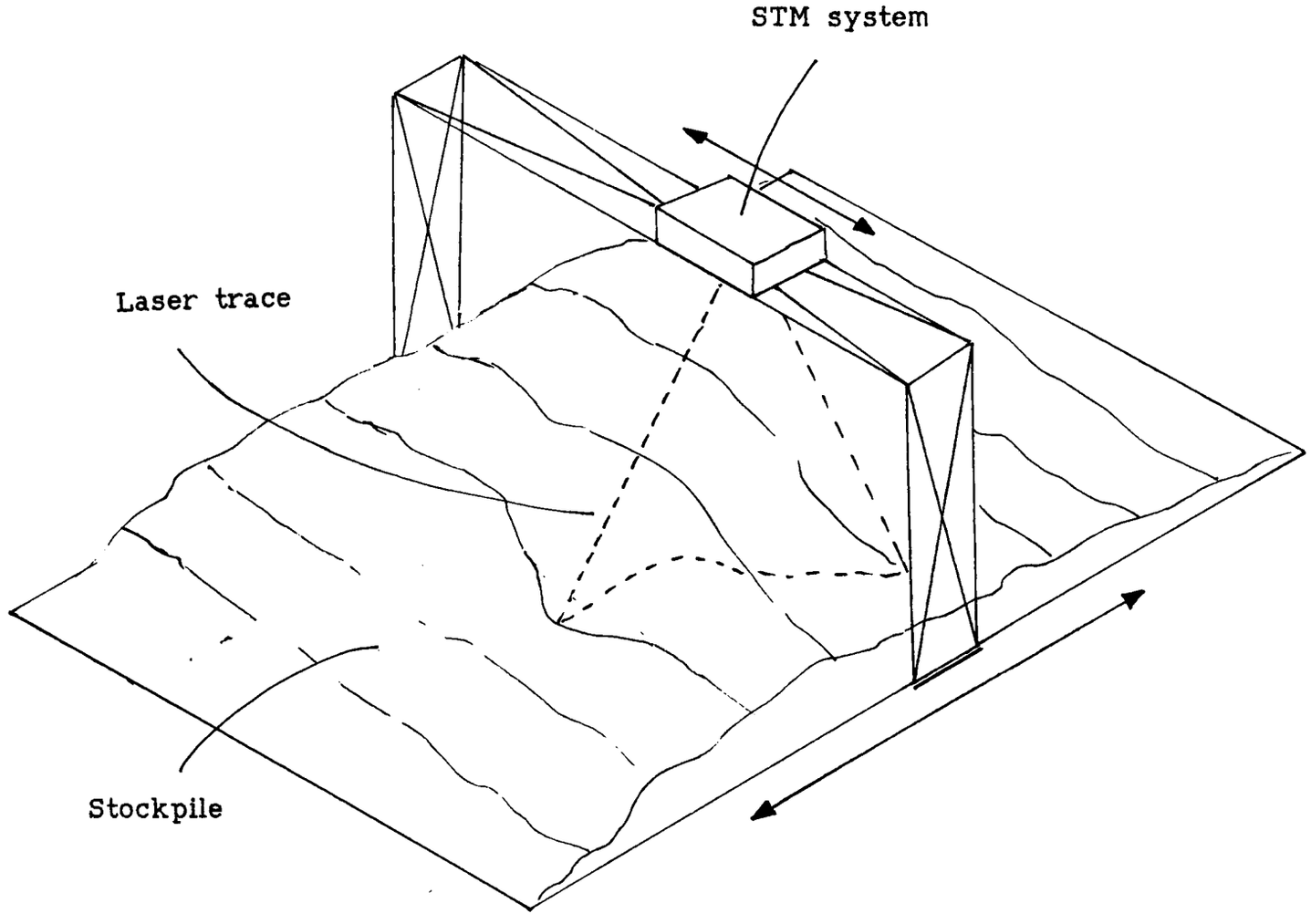

Figure 7.2 STM System in stockpile measurement application.

Glossary.

DTB	-	Digital Time Base
FOV	-	Field of View.
HFOV	-	Horizontal Field of View.
LSDEP	-	Laser Spot's Distribution Examination Program.
STM	-	Surface Topography Measurement.
VLG	-	Video Line Grabber.
VSD	-	Vertically Summed Distribution.

References.

[1] Jarvis, R.A. " Perspective on range finding techniques for computer vision ". IEEE transactions on Pattern Analysis and Machine Vision. Vol. 5, pp 122-139, 1983.

[2] Rosenfeld, A. et al. " Scene labeling by relaxation operations ". IEEE trans. Syst., Man, Cybern. Vol. SMC6, pp 420-443 , 1976.

[3] Jarvis, R.A. " Focus optimising criteria for computer image processing ". Microscope. vol. 24, pp 163-180, 1976.

[4] Gennery, D.B. " A stereo vision system for an autonomous vehicle". Proceedings of the joint conf. on artificial intelligence. pp 576-582 , Aug. 1977.

[5] Marr, D. " Vision ". 1982. W.H. Freeman, New York, U.S.A.

[6] Grimson, W.E.L. " From images to surfaces ". 1981. MIT press.

[7] Brady, J.M. et al. " Vision and the Oxford AGV ". Computer Vision for Robotics. IEE colloquium 1989.

[8] Stephens, M.J. " Toward 3D vision for mobile and grasping robots " Computer Vision for Robotics. IEE colloquium 1989.

[9] Buxton, B.F. et al. " Machine perception of visual motion ". The GEC Journal of Research. Vol. 3, No. 3, pp 145-161, 1985.

[10] Smati, Z. et al. " Laser Guidance System for Robots ". Proceedings of Robot Vision (4th Int. Conf.). pp 91-101, 1984.

[11] Livingstone, F.R and Rioux, M. " Development of a large field 3-D vision system ". SPIE Optical techniques for Industrial

Inspsection. Vol. 665, pp 188-194, 1986.

[12] Dremel, W. et al. " triangulation with large dynamic range " SPIE Optical techniques for Industrial Inspsection. Vol. 665, pp 182-187, 1986.

[13] Kreis, Th. et al. " Detection of edges by video systems ". Proceedings of Robot vision and sensory control (2nd Int. Conf.). pp 9-17, 1982.

[14] Reid, G.T. et al. " A laser scanning camera for range data acquisition ". Journal Phys. D: Appl. Phys. Vol. 21, No. 10S, pp S1-S3, 1988.

[15] Nicolas, G. and Hermann, J.P. " Inspection of moulds by 3-Dimensional Vision ". Proceedings of Robot Vision and Sensory controls (6th Int. Conf.). pp 99-104, 1986.

[16] Rosenfeld, J.P. and Tsikos, C.J. " High-Speed space encoding projector for 3-d imaging ". SPIE Optics, Illumination and Image Sensing for Machine Vision ". Vol 728, pp 146-151 1986.

[17] Vuylsteke, P. and Oosterlinck, A. " 3-D perception with a single binary coded illumination pattern ". SPIE Optics, Illumination and Image Sensing for Machine Vision ". Vol 728, pp 195-202, 1986.

[18] Nimrod, N. et al. " a laser based scanning range finder for robotic applications ". Proceedings of Robot vision and sensory control (2nd Int. Conf.). pp 241-252, 1982.

[19] Ariyaeeinia, A.M. PhD thesis " An active co-ordinate imaging

system for robot vision ". 1985. Trent Polytechnic.

[20] Faugeras, O.D. " Toward a flexible vision system ". Proceedings of Industrial Robots (12th Int. Symp. on Ind. Robots). pp 67-78, 1982.

[21] Page, C.J. and Hassan, H. " Non-contact inspection of complex components using a rangefinder vision system ". ROVOSEC 1 pp 245-254, Aprl 1981.

[22] Duda, R.O. et al. " Use of range and reflection data to find planar surface regions ". IEEE transactions on Pattern Analysis and Machine Intelligence ". Vol. PAMI-1, No. 3, pp 259-271, 1979.

[23] Kaisto, I. et al. " Optical range finder for 1.5-10 m distances ". Journal of Appl. Optics. Vol. 22, pp 3258-3264, 1983.

[24] Heikkinen, T. " Recent results of the performance analysis of a 3-D sensor based on time-of-flight measurement ". SPIE Optical techniques for Industrial Inspsection. Vol. 665, pp 168-173, 1986.

[25] Manninen, M. et al. " Design of a scanning laser range finder for 3-D robot vision ". Proceedings of Image science 85. pp 122-125 1985.

[26] Blais, F. and Rioux, M. " BIRIS: A simple 3-D sensor ". SPIE "Optics, Illumination and Image Sensing for Machine Vision ". Vol 728, pp 235-242 1986.

[27] Halioua, M. and Hsin-Chu Lui " Optical sensing techniques for 3-D machine vision ". SPIE Optical techniques for Industrial

Inspsection. Vol. 665, pp 150-161, 1986.

[28] Reid, G.T. and Rixon, R.C. " Automatic inspection of quasi-cylindrical objects by phase measuring Moire topography ". SPIE Optical techniques for Industrial Inspsection. Vol. 665, pp 162-167, 1986.

[29] Albert, J. et al. " Adaptation of a parallel architecture computer to phase shifted Moire interferometry ". SPIE Optics, Illumination and Image Sensing for Machine Vision ". Vol 728, pp 183-194 1986.

[30] Malmo, J.T. and Løkberg, O.J. " TV holography in adverse environments ". Journal Phys. D: Appl. Phys. Vol. 21, No. 10S, pp S8-S10, 1988.

[31] Ellingsrud, S. and Løkberg, O.J. " Analysis of high frequency vibrations using TV holography ". Journal Phys. D: Appl. Phys. Vol. 21, No. 10S, pp S11-S13, 1988.

[32] Guichard, M. and Renault, A. " Industrial use of ultrasonic ranging sensors in robotics ". Proceedings of Robot Vision and Sensory controls (6th Int. Conf.). pp 157-164, 1986.

[33] Monchaud, S. " Calibration and Interpretation problems for range pictures in a wide field scanning triangulation range finder for machine vision ". SPIE Optical techniques for Industrial Inspsection. Vol. 665, pp 174-181, 1986.

[34] Pugh, A. " Vision sensors ". Computer Vision for Robotics. IEE colloquium 1989.

[35] Taylor, P.M. et al. " A multisensory approach to shoe sole assembly ". Proceedings of Robot Vision and Sensory controls (6th Int. Conf.). pp 117-125, 1986.

[36] Meyer-Ardent, J.R. "Introduction to Classical and Modern Optics". 2nd Edition. Prentice Hall Int. 1984.

[37] The Ealing Optical Components Catalogue. 1977.

[38] Harry, J.E. " Industrial lasers and their Applications ". McGraw-Hill, U.K. 1974.

[39] Wilson, J and Hawkes, J.F.B. "Lasers Principles and Applications". Prentice Hall Int. 1987.

[40] Lin, J.C. and Zou-Chen Chi. " Accuracy analysis of a laser/camera based 3-D measurement system ". Proceedings Robot Vision. pp 179-191, Nov. 1983.

[41] Martins, H.A. et al. " Camera models based on data from two calibration planes ". Computer Graphics and Image Processing . pp 173-180, Vol. 17, Mar. 1981.

[42] Fairhurst M.C. "Computer Vision for Robotic Systems. An Introduction". Prentice Hall, U.K. 1988.

[43] Montagu, J. "Galvanometeric and Resonant Low Inertia Scanners ". Laser Beam Scanning Opto-Mechanical Devices, Systems and Data Storage Optics ". Editor G.F. Marshall. 1985.

[44] Reynolds, M.C. " The STM system Software Report " Internal Thames Polytechnic. 1989.

[45] Young, R.A. "Locating Industrial Parts with Subpixel Accuracies". SPIE. "Optics, Illumination and Image Sensing for Machine Vision". Vol. 728, pp 2-9, 1986.

[46] Tian, Qi and Huhns, M.N. "A fast iterative hill-climbing algorithm for subpixel registration". Proc. 7th Int. Conf. on

Pattern Recognition. pp 13-15, 1980.

[47] Cielo, P. and Lamontagne, M. "Improvement os subpixel resolution in triangulation ranging by astigmatic spot projection and wide-aperture line array imaging". Optics and Laser Technology. Vol. 20, No. 1, pp 19-24, 1988.

[48] Lorenz, R.D. "A novel, high range-to-resolution, optical sensing technique for high speed surface geometry measurements". SPIE, "Optics, Illumination and Image Sensing for Machine Vision ". Vol. 728, pp 152-159, 1986.

[49] BS 4803 : Part 3 : 1983.

[50] Freeman, S. "Remote Measurement of Plant Structural Coordinates" Process Engineering Jan. pp 45, 1985.

[51] Barnes, R. "Surface Topography Measurement of Bulk Solid Material Stockpiles". Bulk Solids Handling. Vol. 7, No. 5, 1987.

[52] Gonzalez, R.C and P. Wintz. " Digital Image Processing ". 2nd Edition. Addison Wesley. 1987.

[53] Philips Technical Publication 211. "The Frame Transfer Sensor". 1986.

[54] O'Neil P.V. "Advanced Engineering Mathematics". 2nd Edition Wadsworth, California, U.S.A. 1987.

Acknowledgements.

I would like to thank all the teaching staff and technicians of the Engineering School at Thames Polytechnic, especially Len Parrish, John Tabor, Jeff Allwood for there help and comments. A special vote of thanks to my long suffering supervisor Roger Barnes for all his help and advice.

I would also like to thank my family, especially my parents Rex and Bunty, Yvonne and all friends for their help, support and encouragement.

Appendix A.

Selected circuit diagrams from the STM system 2 are given in this Appendix.

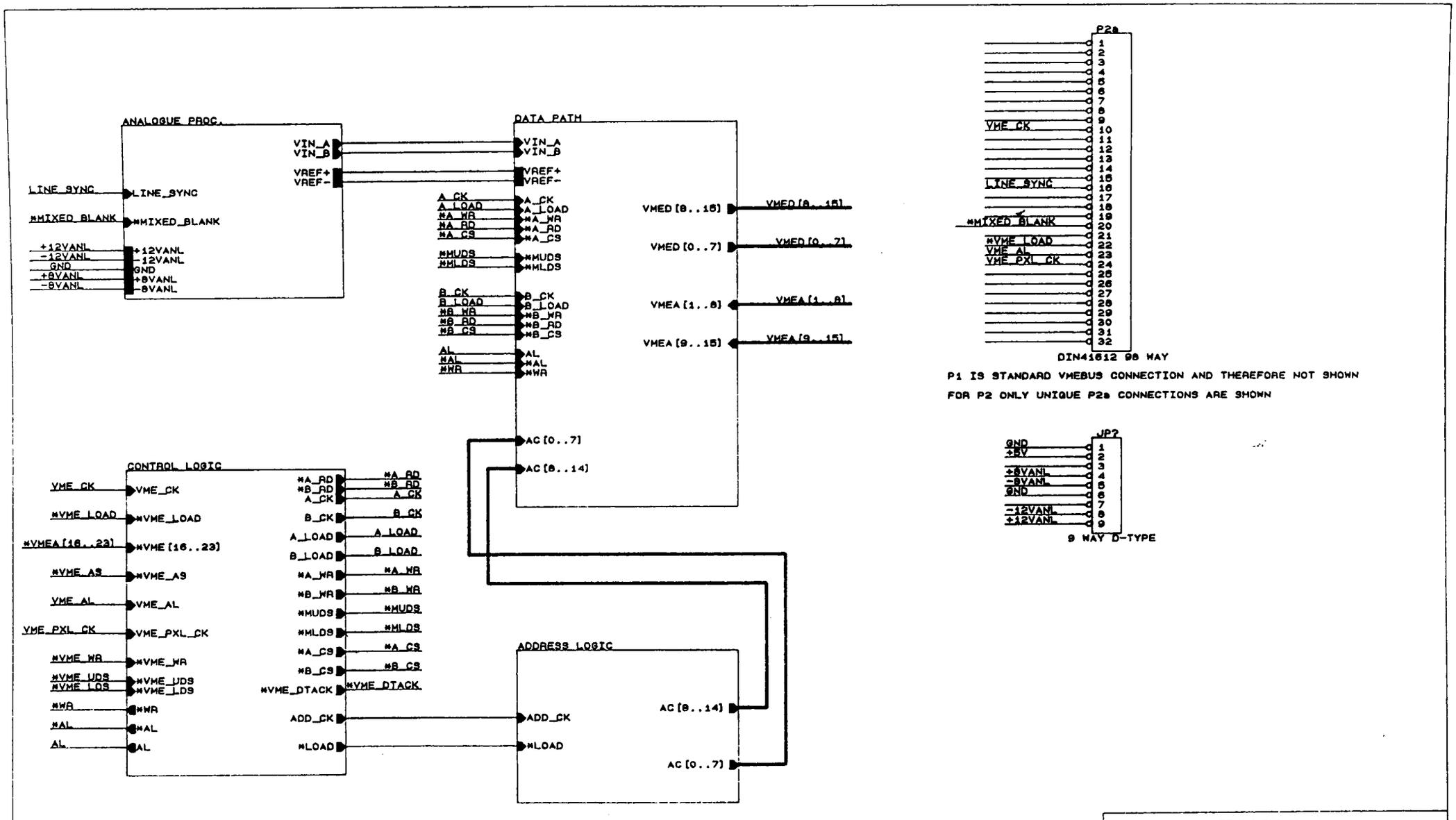

2

MATTHEW REYNOLDS
THAMES POLYTECHNIC

Title: VIDEO LINE GRABBER

Size	Document Number	REV
B	MCR/01	2.0

Date: August 20, 1990 Sheet 1 of 5

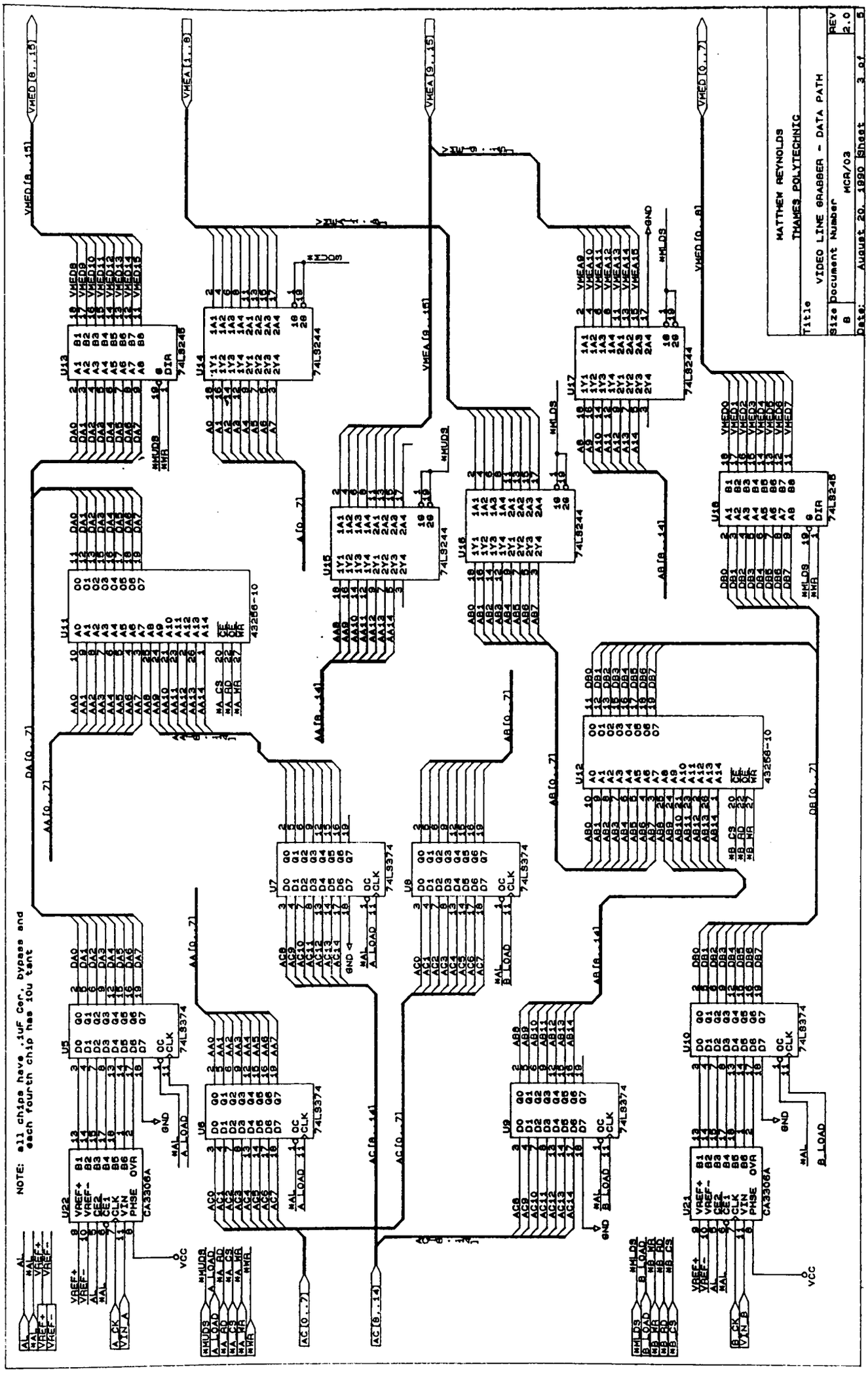
MATTHEW REYNOLDS
THAMES POLYTECHNIC
Title
VIDEO LINE GRABBER - DATA PATH
Size
B
Document Number
MCR/03
REV
2.0
Date:
August 20, 1990
Sheet
3 of
5
NOTE: all chips have .1uF Cer. bypass and each fourth chip has 10u tant
VMED[0..15]
VMEA[1..9]
VMEA[9..15]
VMED[0..7]
VMED[8..15]
VMEA[8..15]
DA[0..7]
AA[0..7]
AA[8..14]
AB[0..7]
AB[8..14]
AC[0..7]
AC[8..14]
DB[0..7]
74L8248
74L8244
74L8374
43256-10
CA3306A
A_LOAD
B_LOAD
VCC
GND

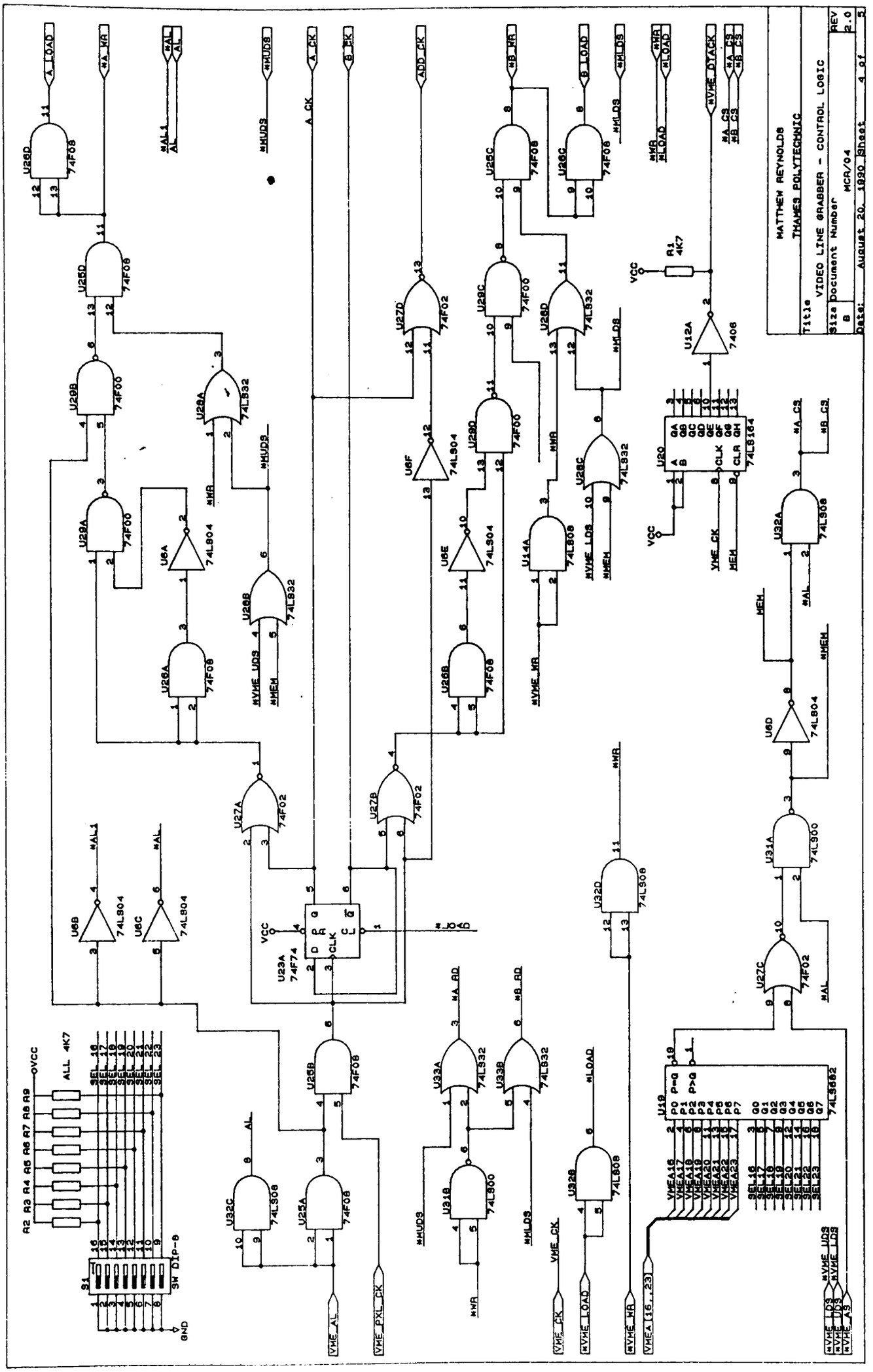
MATTHEW REYNOLDS
THAMES POLYTECHNIC
Title VIDEO LINE GRABBER - CONTROL LOGIC
Size B Document Number MCR/04 REV 2.0
Date: August 20, 1990 Sheet 4 of 5
A_LOAD
#A_WR
MAL1
MAL
#MUDS
A_CK
B_CK
ADD_CK
#B_WR
B_LOAD
#MLDS
#WR
#LOAD
#VME_DTACK
#A_CS
#B_CS
VCC
R1 4K7
U12A 7406
U26D 74F08
U25D 74F08
U29B 74F00
U28A 74L832
U29A 74F00
U6A 74L804
U26A 74F08
U28B 74L832
#VME_UDS
#MEM
U27A 74F02
U6B 74L804
U6C 74L804
U23A 74F74
D Q CLK
U25B 74F08
U32C 74L808
U25A 74F08
U33A 74L832
U33B 74L832
#A_BD
#B_BD
U31B 74L800
U32B 74L808
VME_AL
VME_PXL_CK
#VME_CK
#VME_LOAD
#VME_WR
VME[16..23]
U27D 74F02
U27B 74F02
U6F 74L804
U6E 74L804
U26B 74F08
U14A 74L808
U29C 74F00
U29D 74F00
U28C 74L832
U28D 74L832
U25C 74F08
U26C 74F08
U20 74L8164
QA QB QC QD QE QF QG QH
A B CLK CLR
U6D 74L804
U31A 74L800
U32A 74L808
U27C 74F02
U19 74L8682
P0 P1 P2 P3 P4 P5 P6 P7 P=Q P>Q
Q0 Q1 Q2 Q3 Q4 Q5 Q6 Q7
SEL16 SEL17 SEL18 SEL19 SEL20 SEL21 SEL22 SEL23
VMEA16 VMEA17 VMEA18 VMEA19 VMEA20 VMEA21 VMEA22 VMEA23
S1 SW DIP-8
R2 R3 R4 R5 R6 R7 R8 R9
ALL 4K7
GND
#VME_UDS
#VME_LDS
#VME_AS

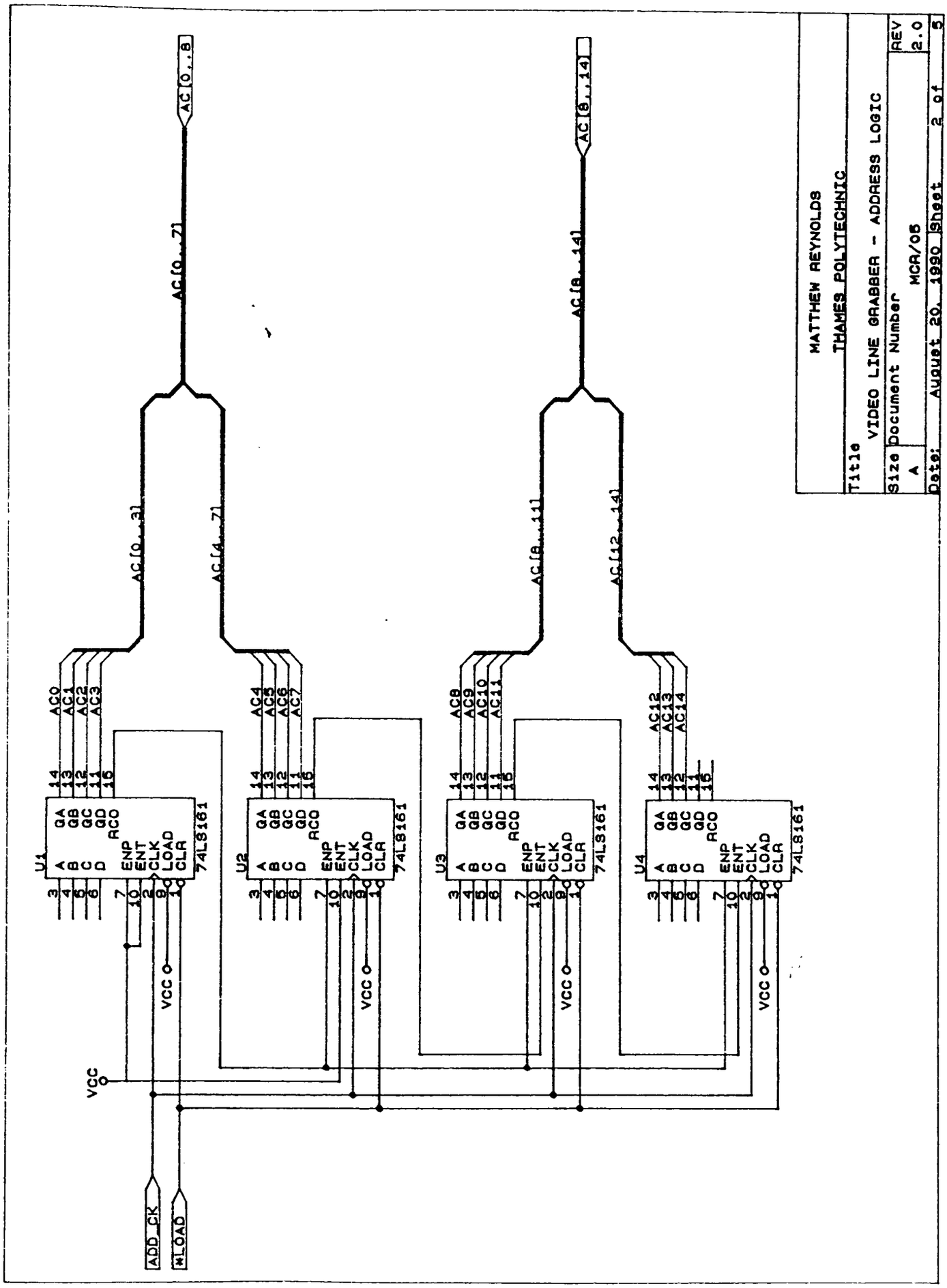
MATTHEW REYNOLDS
THAMES POLYTECHNIC
Title
VIDEO LINE GRABBER - ADDRESS LOGIC
Size
A
Document Number
MCA/05
REV
2.0
Date: August 20, 1990
Sheet
2 of
5
AC[0..8]
AC[0..7]
AC[8..14]
AC[0..3]
AC[4..7]
AC[8..11]
AC[12..14]
U1
U2
U3
U4
74LS161
VCC
ADD_CK
*LOAD

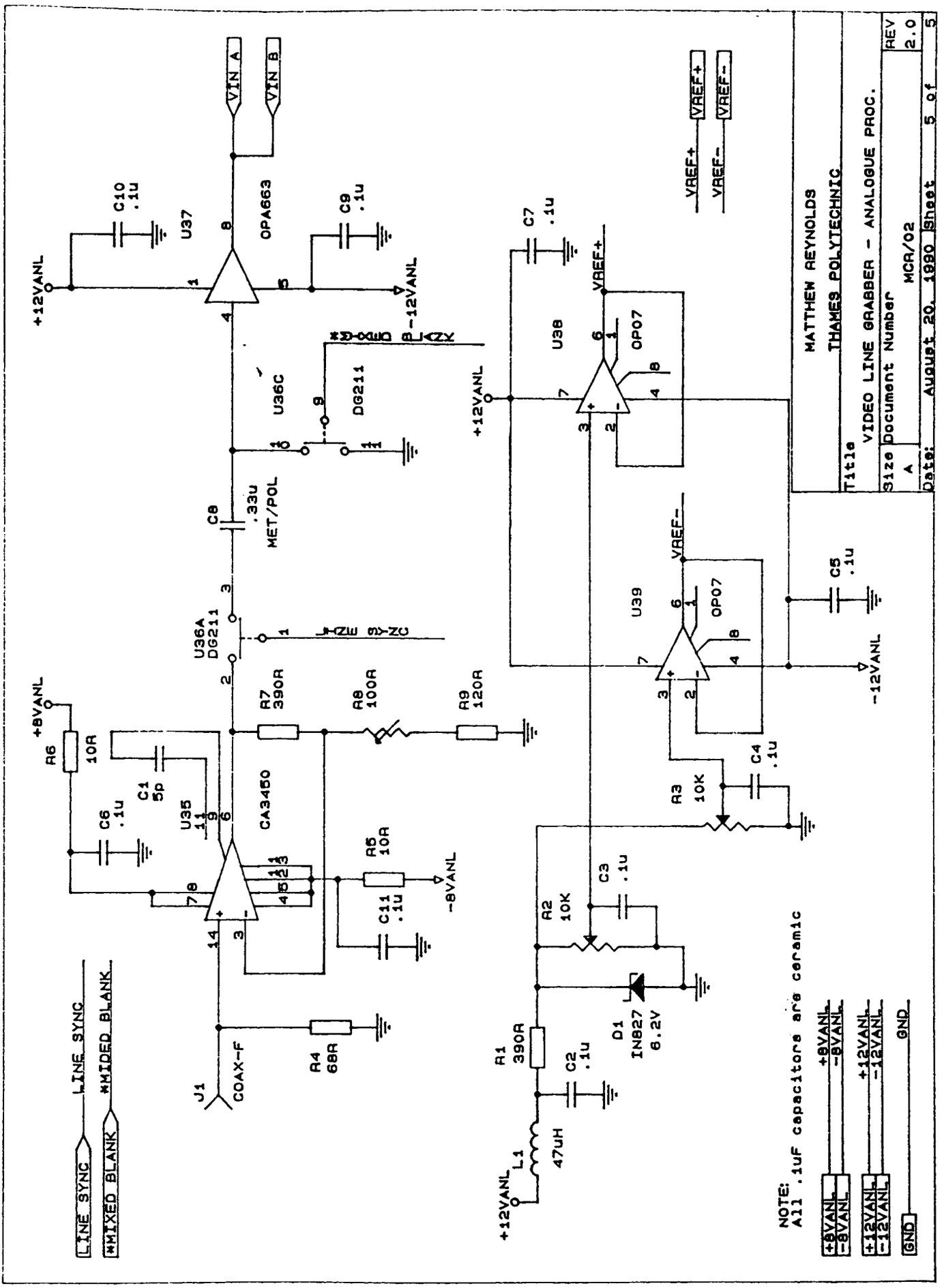
MATTHEW REYNOLDS
THAMES POLYTECHNIC
Title
VIDEO LINE GRABBER - ANALOGUE PROC.
Size A
Document Number MCR/02
REV 2.0
Date: August 20, 1990 Sheet 5 of 5
VIN A
VIN B
VREF+
VREF-
U37
OPA663
U36C
DG211
U36A
U38
U39
OP07
CA3450
U35
C1 5p
C2 .1u
C3 .1u
C4 .1u
C5 .1u
C6 .1u
C7 .1u
C8 .33u MET/POL
C9 .1u
C10 .1u
C11 .1u
R1 390R
R2 10K
R3 10K
R4 68R
R5 10R
R6 10R
R7 390R
R8 100R
R9 120R
L1 47uH
D1 IN827 6.2V
J1 COAX-F
+12VANL
-12VANL
+8VANL
-8VANL
LINE SYNC
*MIXED BLANK
NOTE:
All .1uF capacitors are ceramic
+8VANL
-8VANL
+12VANL
-12VANL
GND

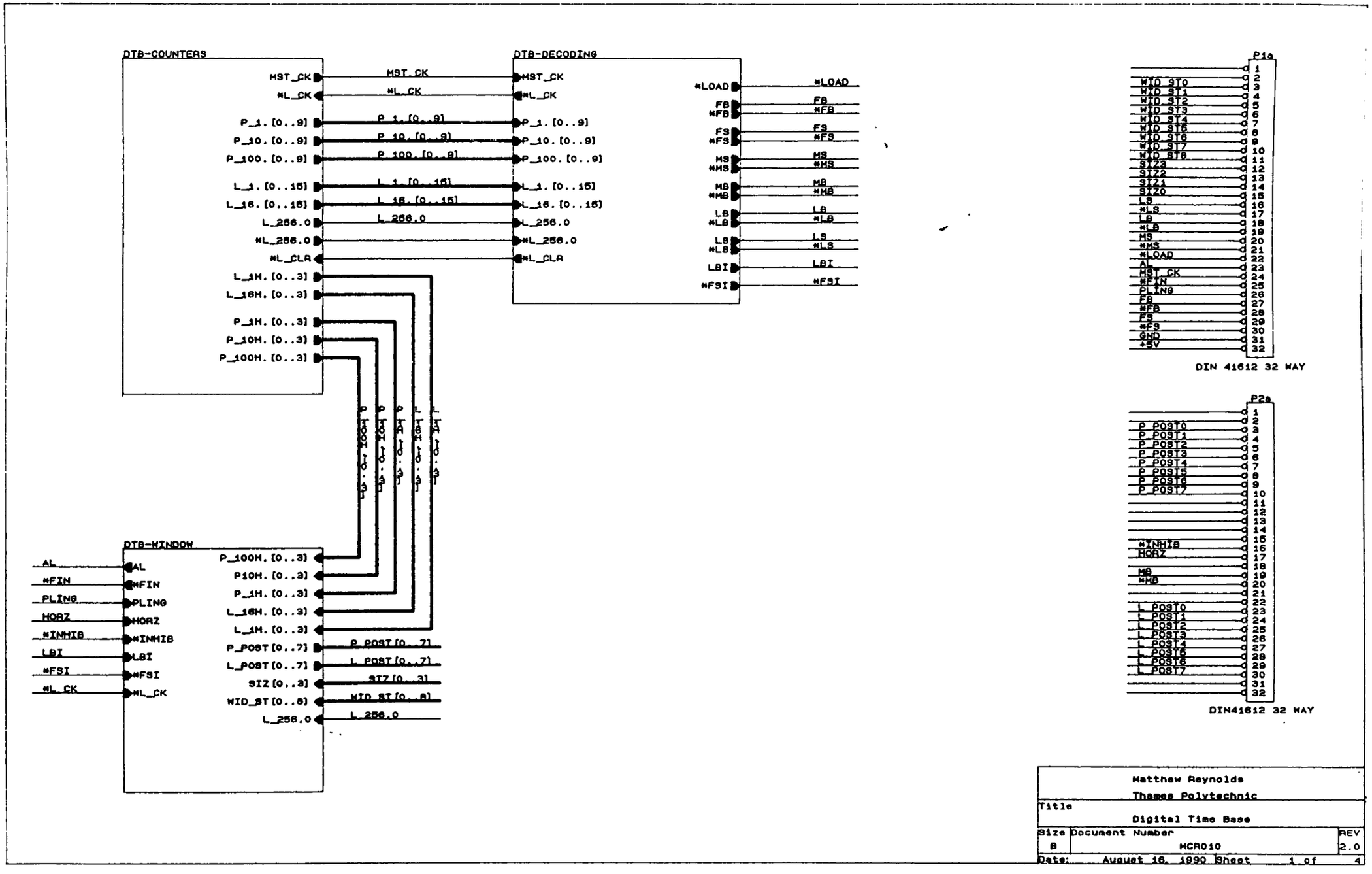
DTB-COUNTERS
MST_CK
ML_CK
P_1.[0..9]
P_10.[0..9]
P_100.[0..9]
L_1.[0..15]
L_16.[0..15]
L_256.0
ML_256.0
ML_CLR
L_1H.[0..3]
L_16H.[0..3]
P_1H.[0..3]
P_10H.[0..3]
P_100H.[0..3]
DTB-DECODING
MST_CK
ML_CK
P_1.[0..9]
P_10.[0..9]
P_100.[0..9]
L_1.[0..15]
L_16.[0..15]
L_256.0
ML_256.0
ML_CLR
MLOAD
FB
MFB
FS
MFS
MS
MMS
MB
MMB
LB
MLB
LS
MLS
LBI
MFSI
MLOAD
FB
MFB
FS
MFS
MS
MMS
MB
MMB
LB
MLB
LS
MLS
LBI
MFSI
P1a
MID_ST0
MID_ST1
MID_ST2
MID_ST3
MID_ST4
MID_ST5
MID_ST6
MID_ST7
MID_ST8
SIZ3
SIZ2
SIZ1
SIZ0
LS
MLS
LB
MLB
MS
MMS
MLOAD
AL
MST_CK
MFIN
PLING
FB
MFB
FS
MFS
GND
+5V
DIN 41612 32 WAY
P2a
P_POST0
P_POST1
P_POST2
P_POST3
P_POST4
P_POST5
P_POST6
P_POST7
MINHIB
HORZ
MB
MMB
L_POST0
L_POST1
L_POST2
L_POST3
L_POST4
L_POST5
L_POST6
L_POST7
DIN41612 32 WAY
DTB-WINDOW
AL
MFIN
PLING
HORZ
MINHIB
LBI
MFSI
ML_CK
P_100H.[0..3]
P10H.[0..3]
P_1H.[0..3]
L_16H.[0..3]
L_1H.[0..3]
P_POST[0..7]
L_POST[0..7]
SIZ[0..3]
WID_ST[0..8]
L_256.0
P_POST[0..7]
L_POST[0..7]
SIZ[0..3]
WID_ST[0..8]
L_256.0
Matthew Reynolds
Thames Polytechnic
Title
Digital Time Base
Size
B
Document Number
MCR010
REV
2.0
Date: August 16, 1990 Sheet 1 of 4

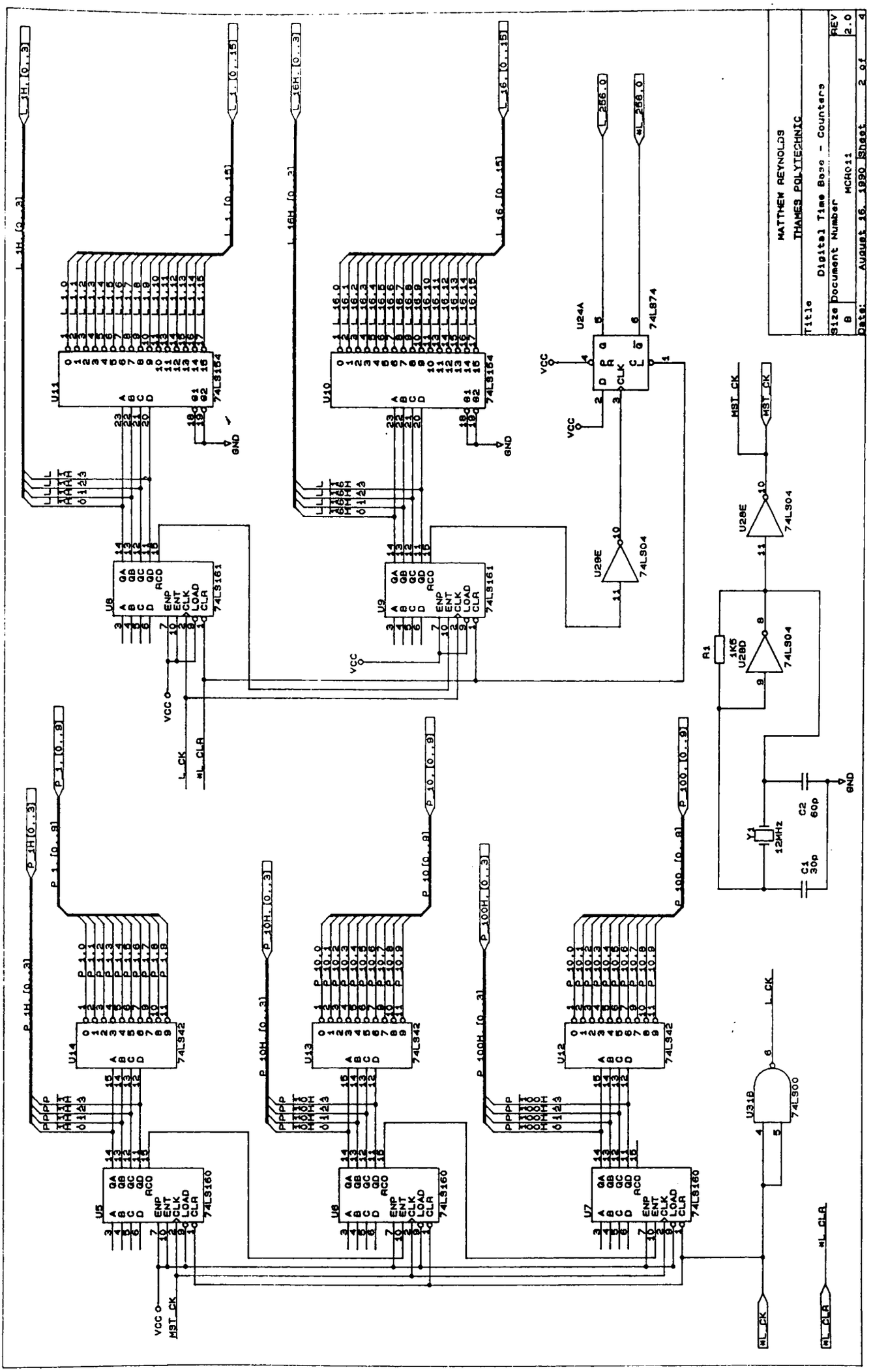
MATTHEW REYNOLDS
THAMES POLYTECHNIC
Title
Digital Time Base - Counters
Size Document Number REV
B MCR011 2.0
Date: August 16, 1990 Sheet 2 of 4

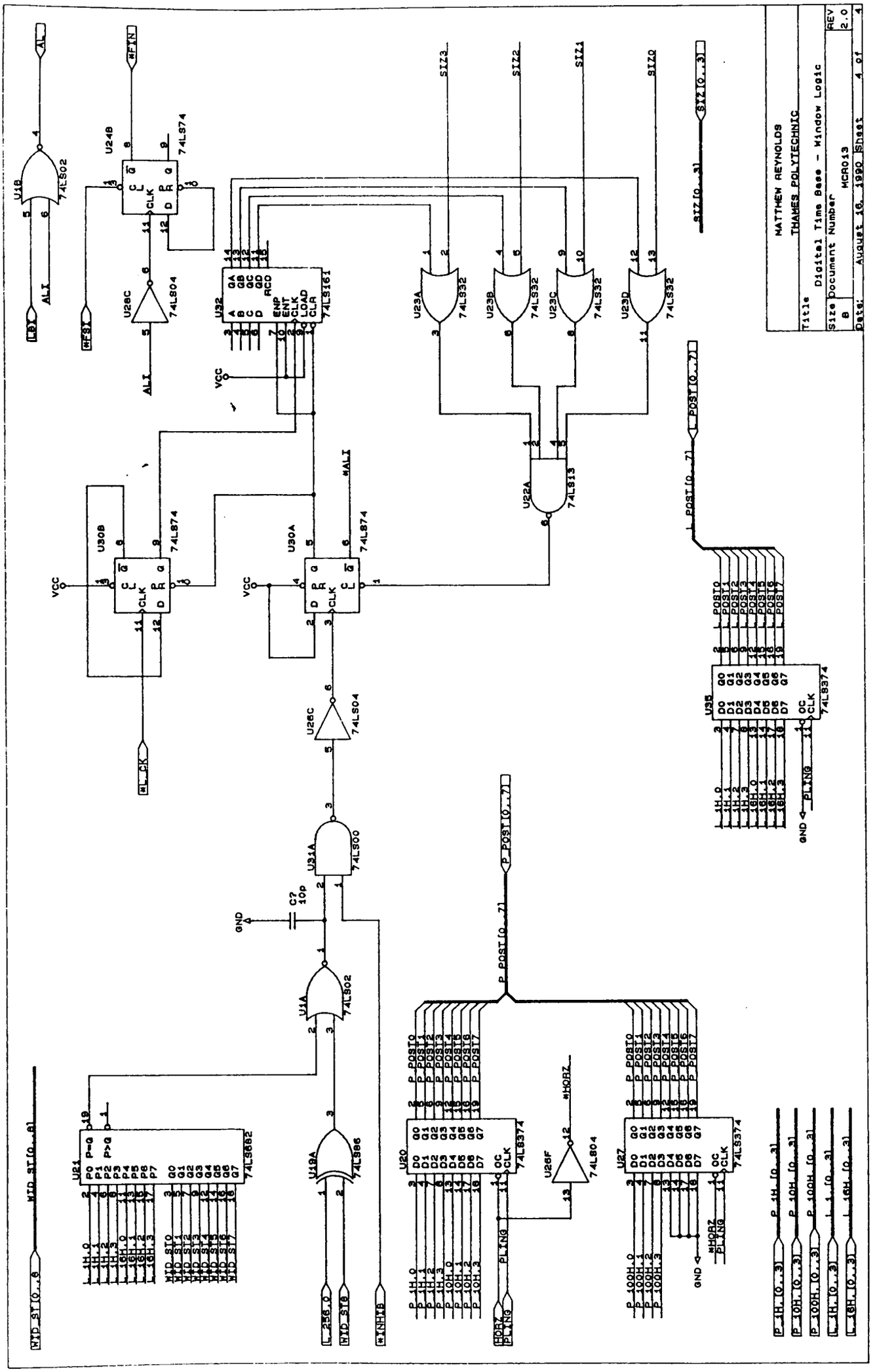
MATTHEW REYNOLDS
THAMES POLYTECHNIC
Title
Digital Time Base - Window Logic
Size
B
Document Number
MCR013
REV
2.0
Date:
August 16, 1990
Sheet
4 of 4

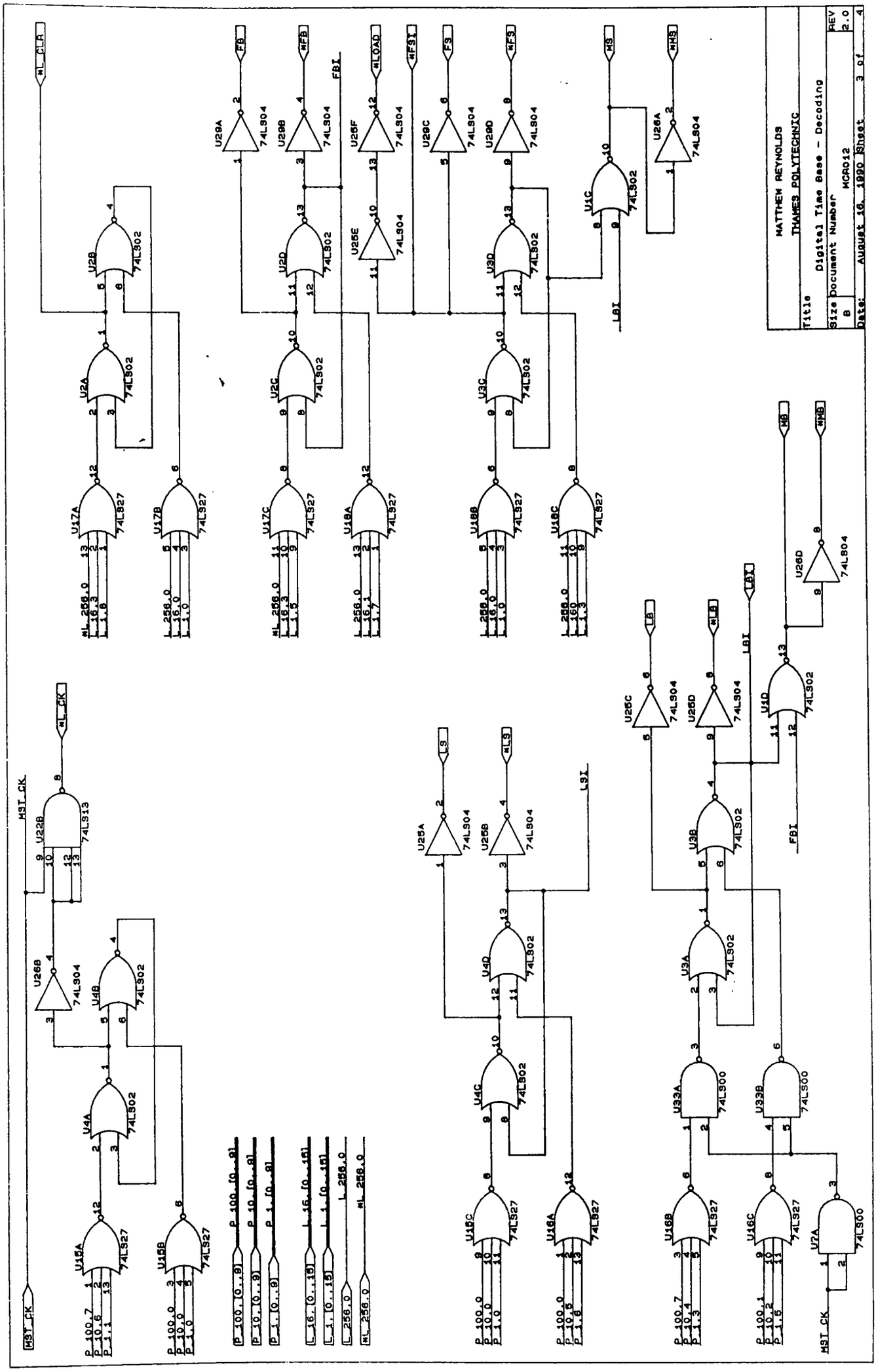
MATTHEW REYNOLDS
THAMES POLYTECHNIC
Title
Digital Time Base - Decoding
Size
B
Document Number
MCR012
REV
2.0
Date:
August 16, 1990
Sheet
3 of 4
MST_CK
ML_CLR
ML_CK
FB
MFB
FBI
MLOAD
MFST
FS
MFS
MS
MMS
LBI
L9
ML9
L9I
LB
MLB
MB
MMB
U2A
U2B
U2C
U2D
U2E
U2F
U3A
U3B
U3C
U3D
U4A
U4B
U4C
U4D
U1C
U1D
U7A
U15A
U15B
U15C
U16A
U16B
U16C
U17A
U17B
U17C
U18A
U18B
U18C
U22B
U25A
U25B
U25C
U25D
U25E
U25F
U26A
U26B
U26C
U26D
U29A
U29B
U29C
U29D
U33A
U33B
74L902
74L904
74L927
74L813
74L900

Appendix B.

The following figures are the actual data obtained in the material tests. Each figure contains the data for both the centre of gravity calculation (mthd 3 in the title) and the fine correlation (mthd 4 in the title).

B1: Results from an 8mm diameter spot using a camera aperture of f8 and with the large gravel as the target material.

B2: Results from an 8mm diameter spot using a camera aperture of f4 and with the large gravel as the target material.

B3: Results from an 8mm diameter spot using a camera aperture of f2 and with the large gravel as the target material.

B4: Results from an 25mm diameter spot using a camera aperture of f8 and with the large gravel as the target material.

B5: Results from an 25mm diameter spot using a camera aperture of f4 and with the large gravel as the target material.

B6: Results from an 25mm diameter spot using a camera aperture of f2 and with the large gravel as the target material.

B7: Results from an 50mm diameter spot using a camera aperture of f8 and with the large gravel as the target material.

B8: Results from an 50mm diameter spot using a camera aperture of f4 and with the large gravel as the target material.

B9: Results from an 50mm diameter spot using a camera aperture of f2 and with the large gravel as the target material.

B10: Results from an 8mm diameter spot using a camera aperture of f8 and with the small gravel as the target material.

B11: Results from an 8mm diameter spot using a camera aperture of f4 and with the small gravel as the target material.

B12: Results from an 8mm diameter spot using a camera aperture of f2 and with the small gravel as the target material.

B13: Results from an 25mm diameter spot using a camera aperture of f8

and with the small gravel as the target material.

B14: Results from an 25mm diameter spot using a camera aperture of f4 and with the small gravel as the target material.

B15: Results from an 25mm diameter spot using a camera aperture of f2 and with the small gravel as the target material.

B16: Results from an 50mm diameter spot using a camera aperture of f8 and with the small gravel as the target material.

B17: Results from an 50mm diameter spot using a camera aperture of f4 and with the small gravel as the target material.

B18: Results from an 50mm diameter spot using a camera aperture of f2 and with the small gravel as the target material.

B19: Results from an 8mm diameter spot using a camera aperture of f8 and with wheat as the target material.

B20: Results from an 8mm diameter spot using a camera aperture of f4 and with wheat as the target material.

B21: Results from an 8mm diameter spot using a camera aperture of f2 and with wheat as the target material.

B22: Results from an 25mm diameter spot using a camera aperture of f8 and with wheat as the target material.

B23: Results from an 25mm diameter spot using a camera aperture of f4 and with wheat as the target material.

B24: Results from an 25mm diameter spot using a camera aperture of f2 and with wheat as the target material.

B25: Results from an 50mm diameter spot using a camera aperture of f8 and with wheat as the target material.

B26: Results from an 50mm diameter spot using a camera aperture of f4 and with wheat as the target material.

B27: Results from an 50mm diameter spot using a camera aperture of f2 and with wheat as the target material.

B28: Results from an 8mm diameter spot using a camera aperture of f8 and with coal as the target material.

B29: Results from an 8mm diameter spot using a camera aperture of f4 and with coal as the target material.

30: Results from an 8mm diameter spot using a camera aperture of f2 and with coal as the target material.

B31: Results from an 25mm diameter spot using a camera aperture of f8 and with coal as the target material.

B32: Results from an 25mm diameter spot using a camera aperture of f4 and with coal as the target material.

B33: Results from an 25mm diameter spot using a camera aperture of f2 and with coal as the target material.

B34: Results from an 50mm diameter spot using a camera aperture of f2 and with coal as the target material.

B35: Results from an 50mm diameter spot using a camera aperture of f1.2 and with coal as the target material.

mat.1 8mm f8 mthd 3

Mean of differences= .1056

Standard deviation= .0737

Maximum deviation = .2315

First data point= 00 last data point= 12

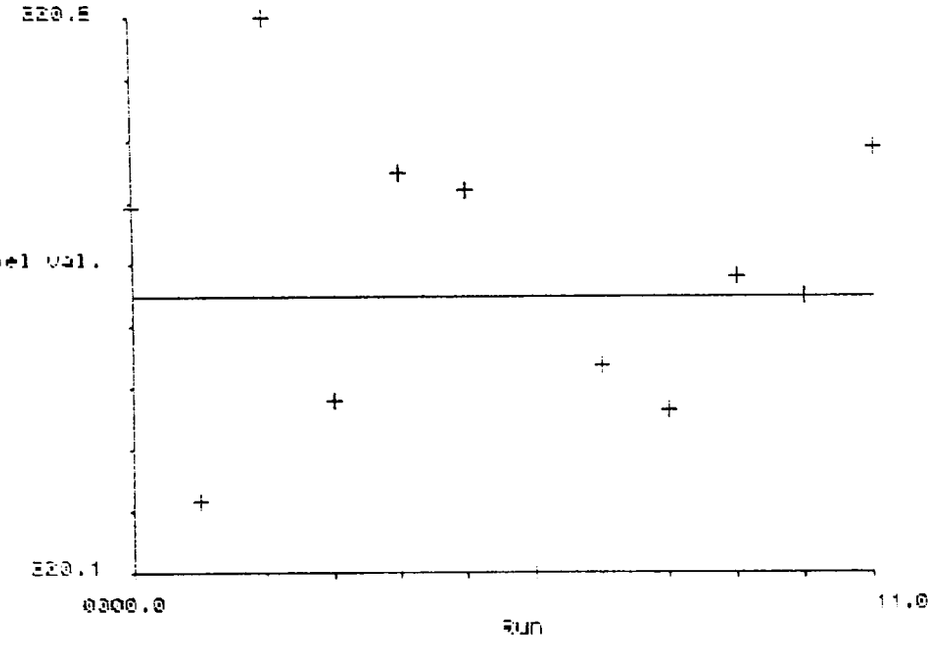

mat.1 8mm f8 mthd 4

Mean of differences= .1053

Standard deviation= .0831

Maximum deviation = .2554

First data point= 00 last data point= 12

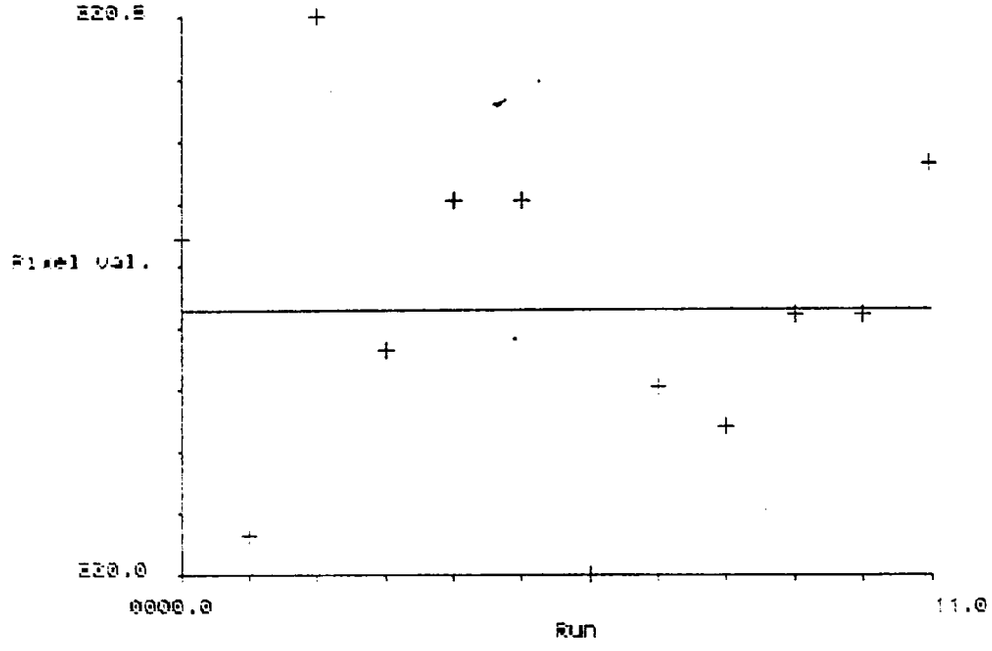

B1

mat.1 8mm f4 mthd 3

Mean of difference= .0031

Standard deviation= .0702

Maximum deviation = .2147

First data point= 00 last data point= 12

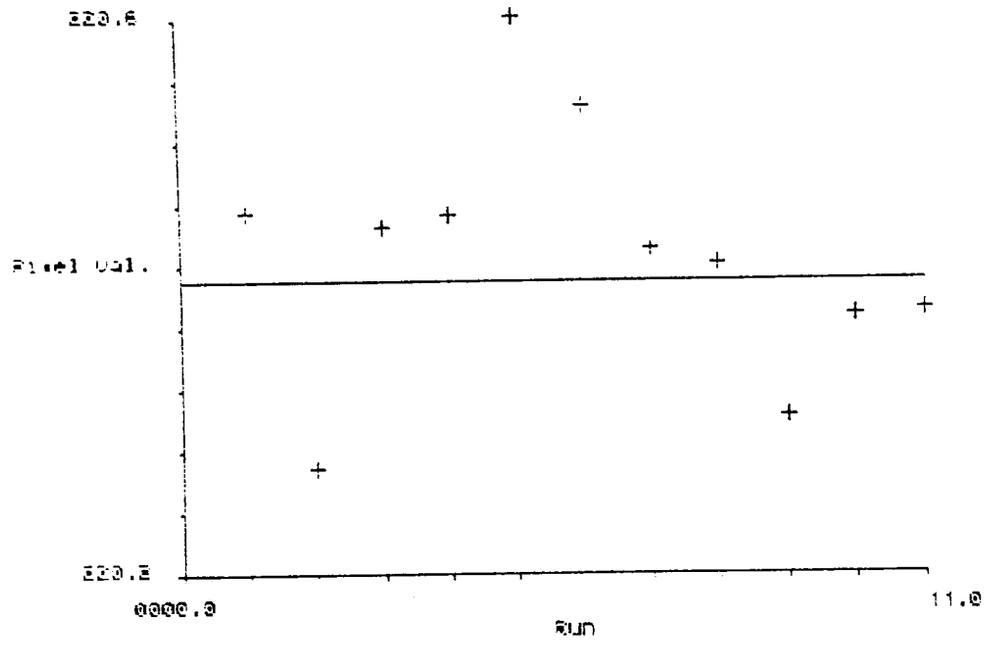

mat.1 8mm f4 mthd 4

Mean of difference= .0856

Standard deviation= .0705

Maximum deviation = .2446

First data point= 00 last data point= 12

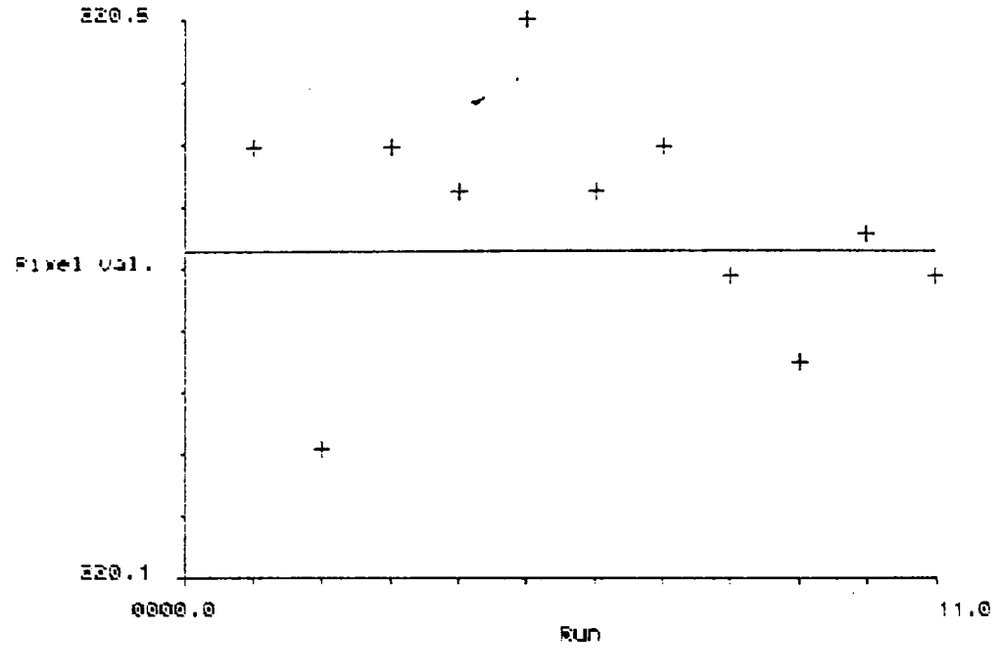

mat.1 8mm f2 mthd 3

Mean of differences= .1673

Standard deviation= .1061

Maximum deviation = .3532

First data point= 00 last data point= 12

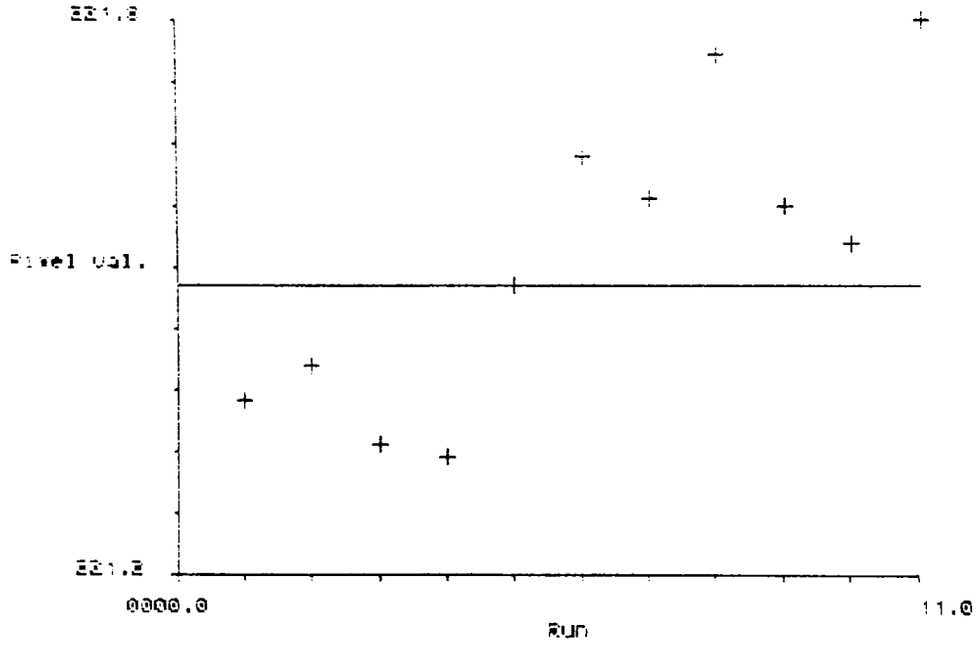

mat.1 8mm f2 mthd 4

Mean of differences= .1478

Standard deviation= .1002

Maximum deviation = .3952

First data point= 00 last data point= 12

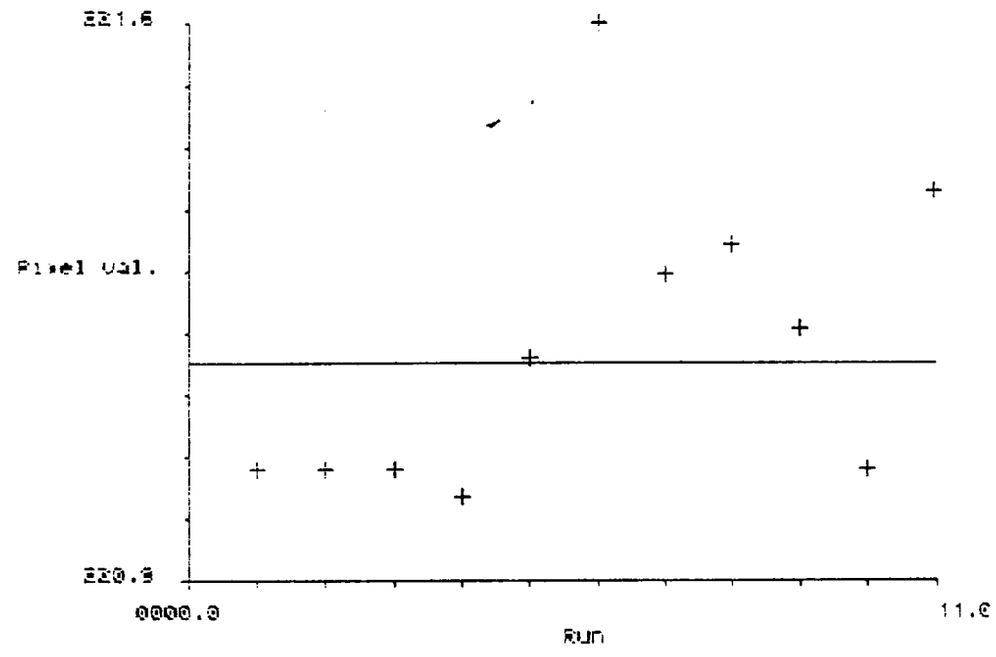

mat.1 35mm f8 mthd 3

Mean of difference= .1135

Standard deviation= .0613

Maximum deviation = .2072

First data point= 00 last data point= 12

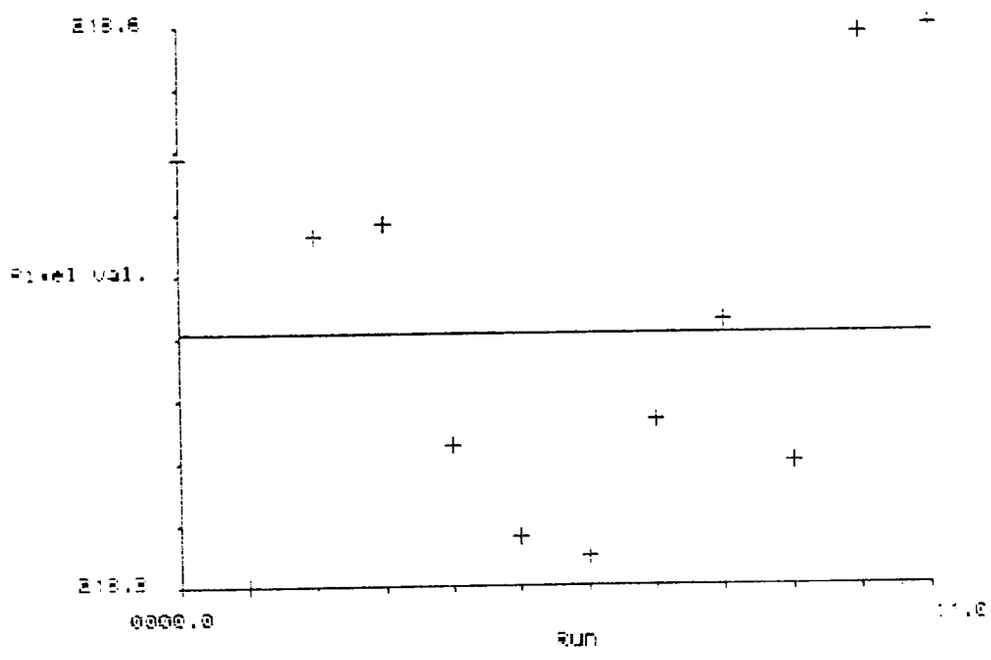

mat.1 35mm f8 mthd 4

Mean of difference= .1603

Standard deviation= .0351

Maximum deviation = .2769

First data point= 00 last data point= 12

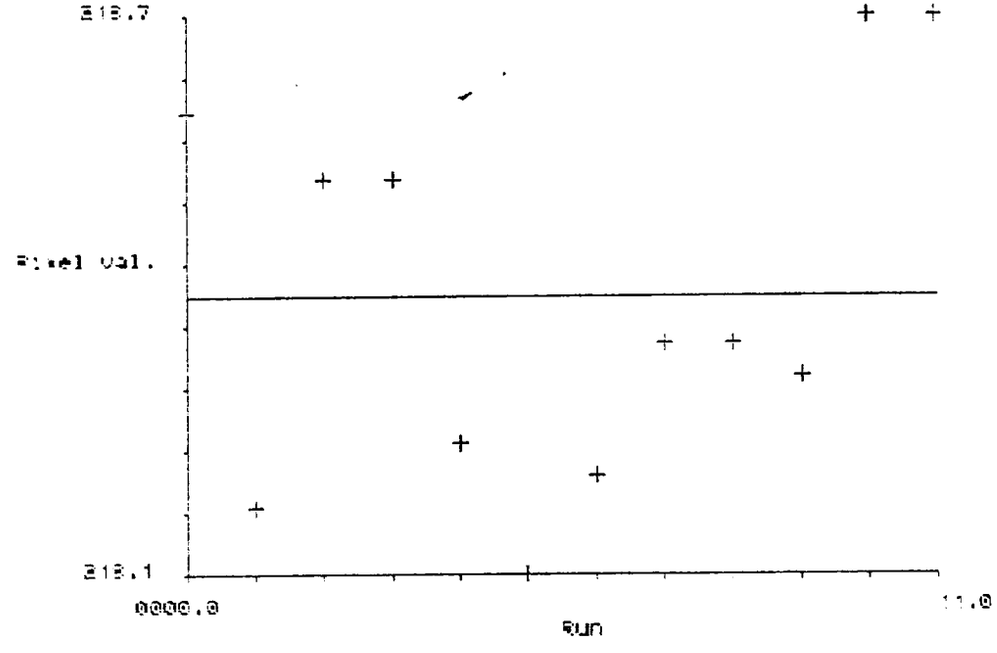

mat.1 35mm f4 mthd 3

Mean of differences= .0788

Standard deviation= .0584

Maximum deviation = .1858

First data point= 00 last data point= 12

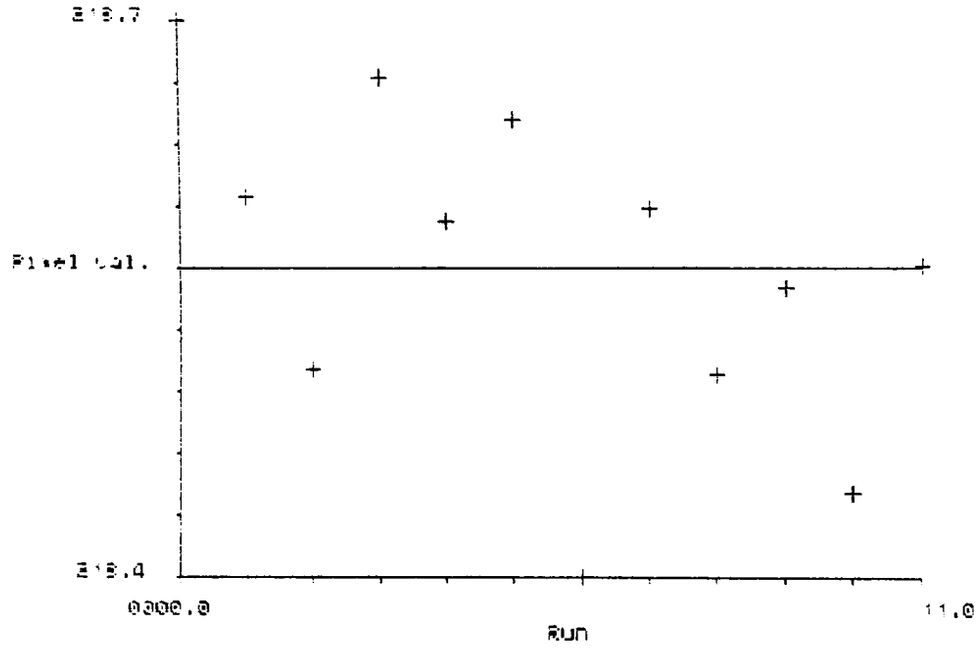

mat.1 35mm f4 mthd 4

Mean of differences= .0989

Standard deviation= .0614

Maximum deviation = .2231

First data point= 00 last data point= 12

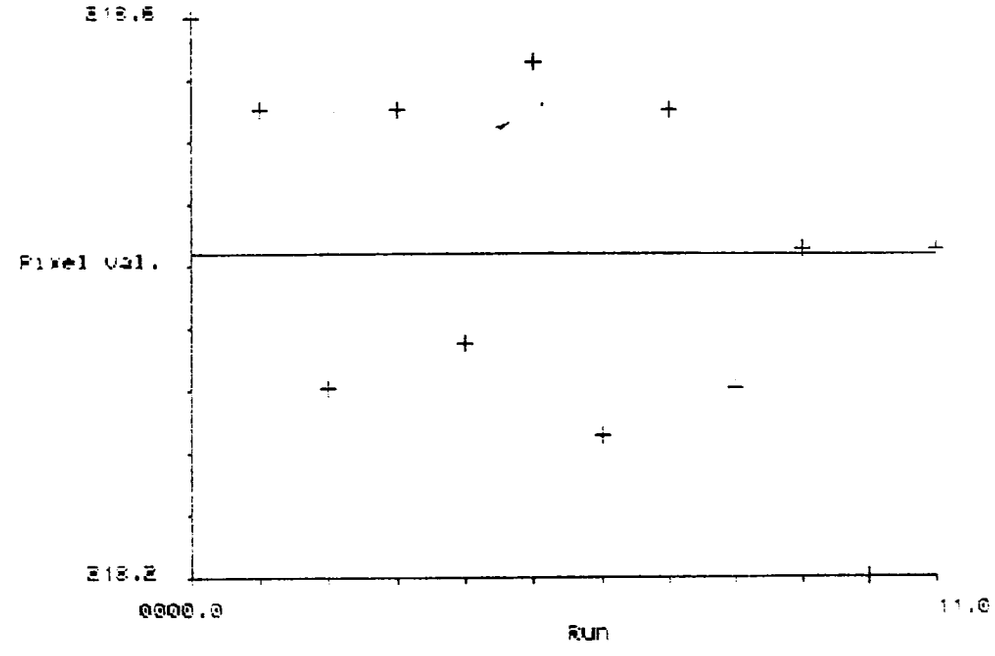

Mat.1 35mm f2 mthd 3
Mean of difference= .0332
Standard deviation= .0230
Maximum deviation = .0630
First data point= 00 last data point= 12

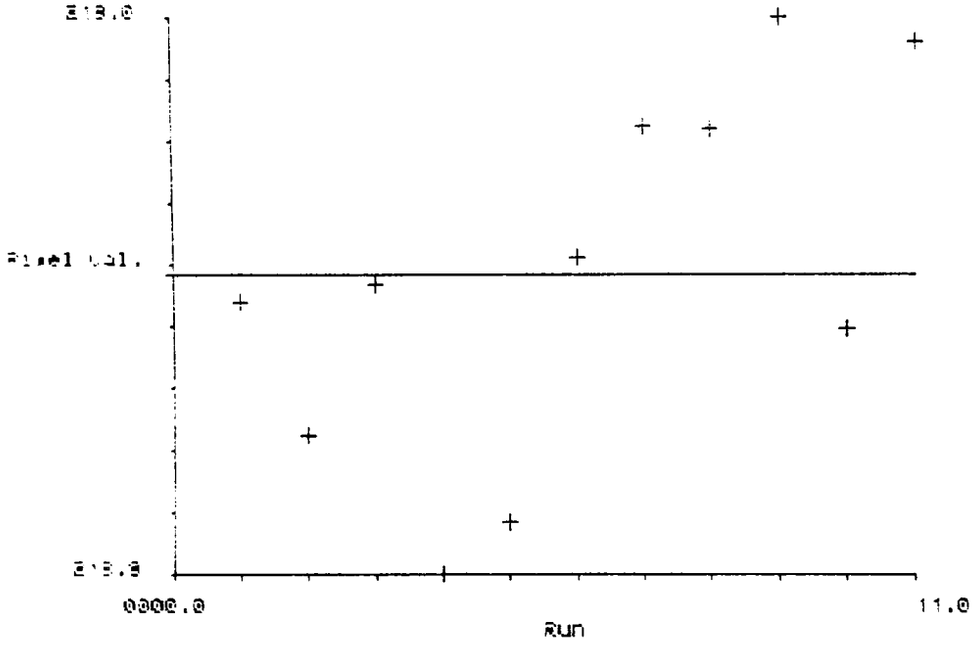

Mat.1 35mm f2 mthd 4
Mean of difference= .0663
Standard deviation= .0581
Maximum deviation = .2204
First data point= 00 last data point= 12

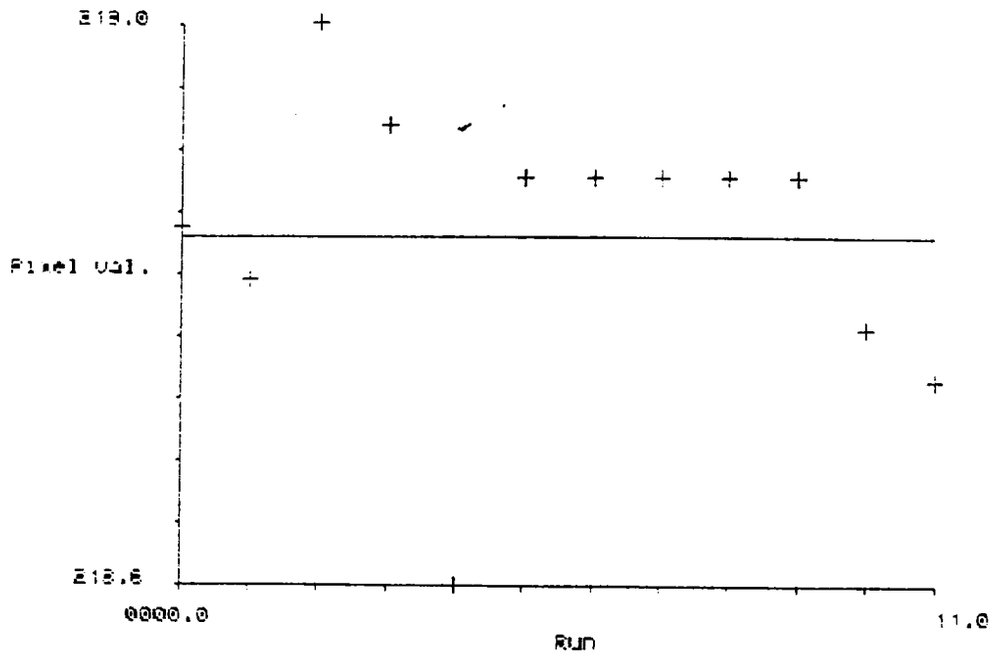

mat.1 50mm f8 mthd 3

Mean of difference= .0052

Standard deviation= .0709

Maximum deviation = .1151

First data point= 00 last data point= 12

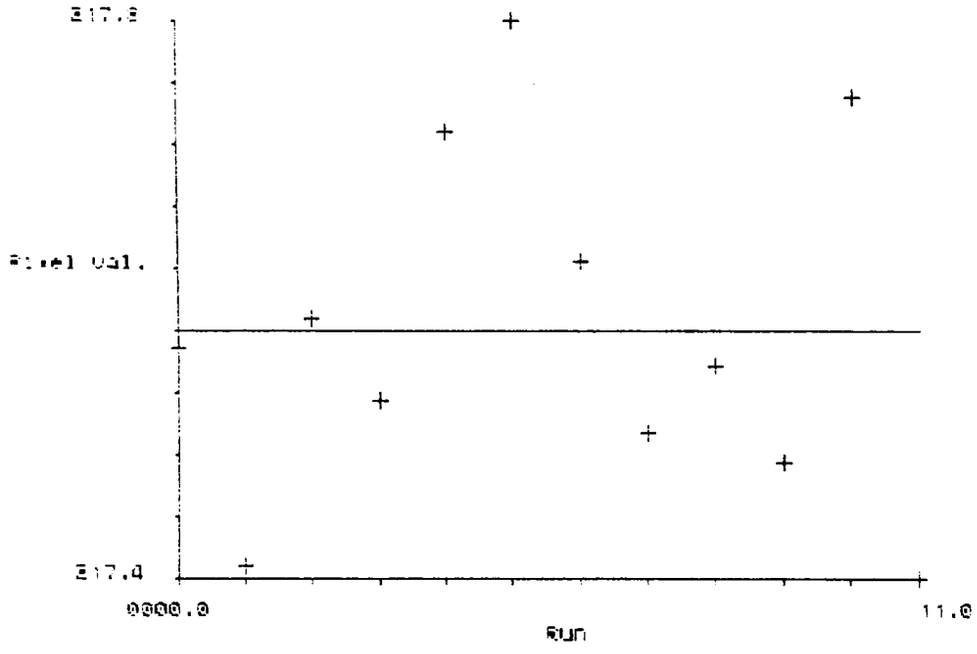

mat.1 50mm f8 mthd 4

Mean of difference= .0014

Standard deviation= .0739

Maximum deviation = .1086

First data point= 00 last data point= 12

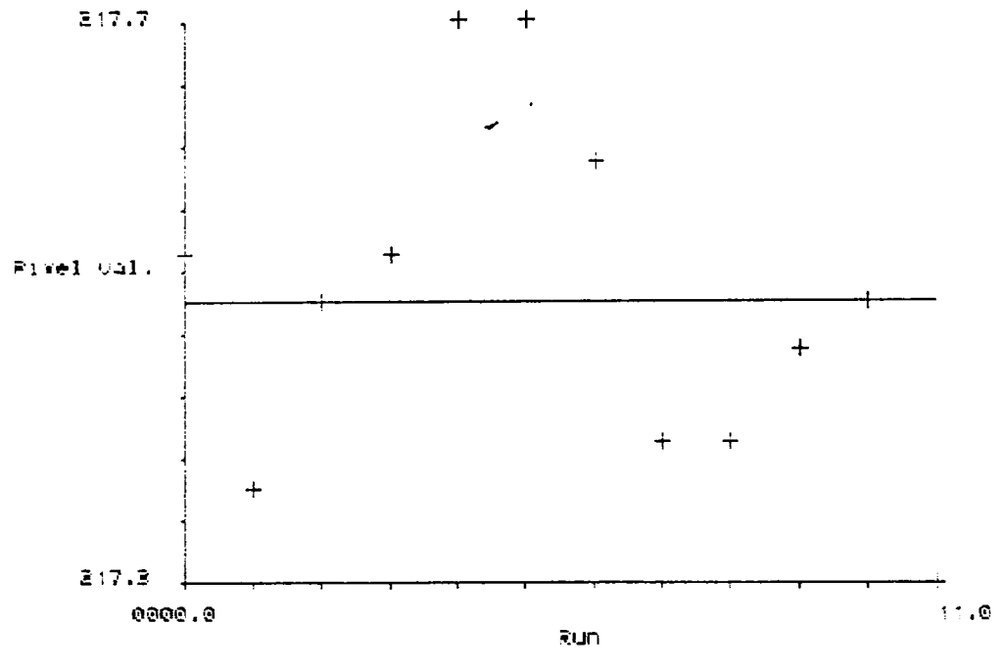

10

mat.1 50mm f4 mind 3

Mean of differences= .0042

Standard deviation= .0610

Maximum deviation = .2017

First data point= 00 last data point= 12

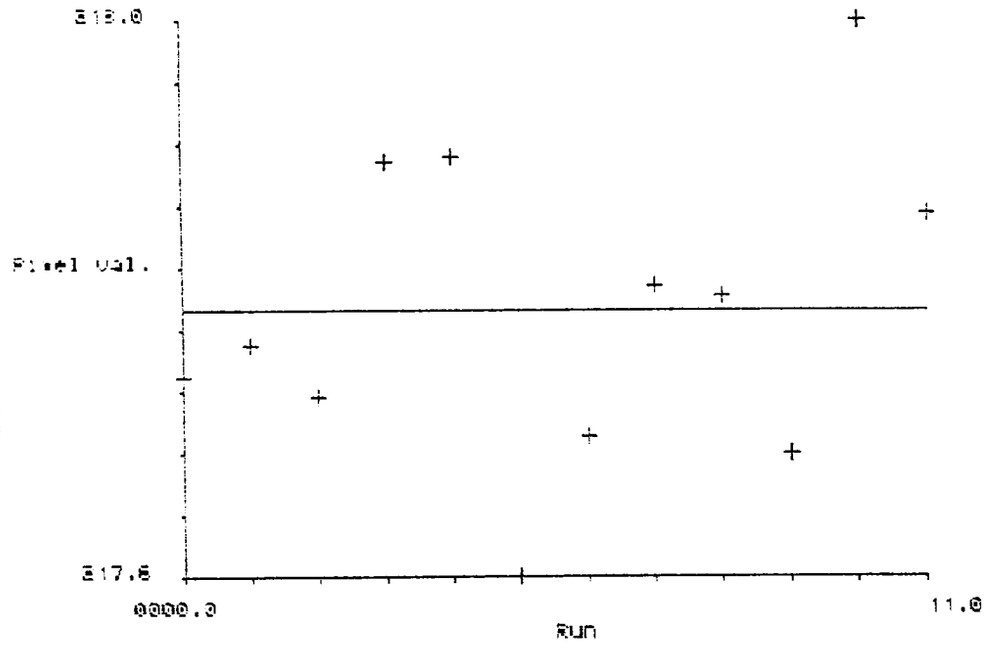

mat.1 50mm f4 mind 4

Mean of differences= .0054

Standard deviation= .0668

Maximum deviation = .2016

First data point= 00 last data point= 12

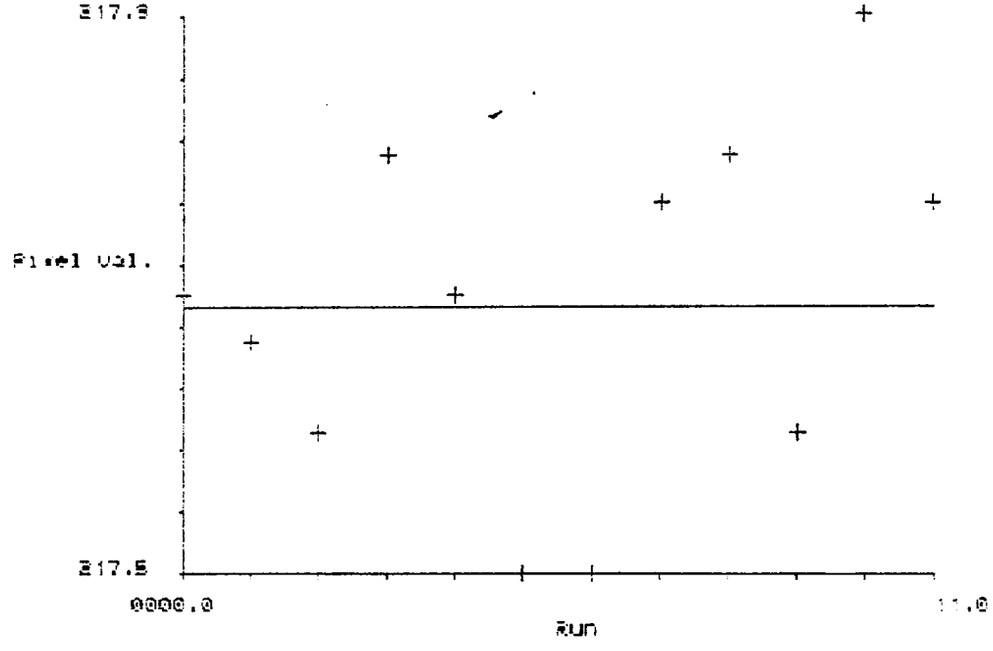

11

mat.1 50mm f2 mthd 3

Mean of difference= .0693

Standard deviation= .0627

Maximum deviation = .2015

First data point= 00 last data point= 12

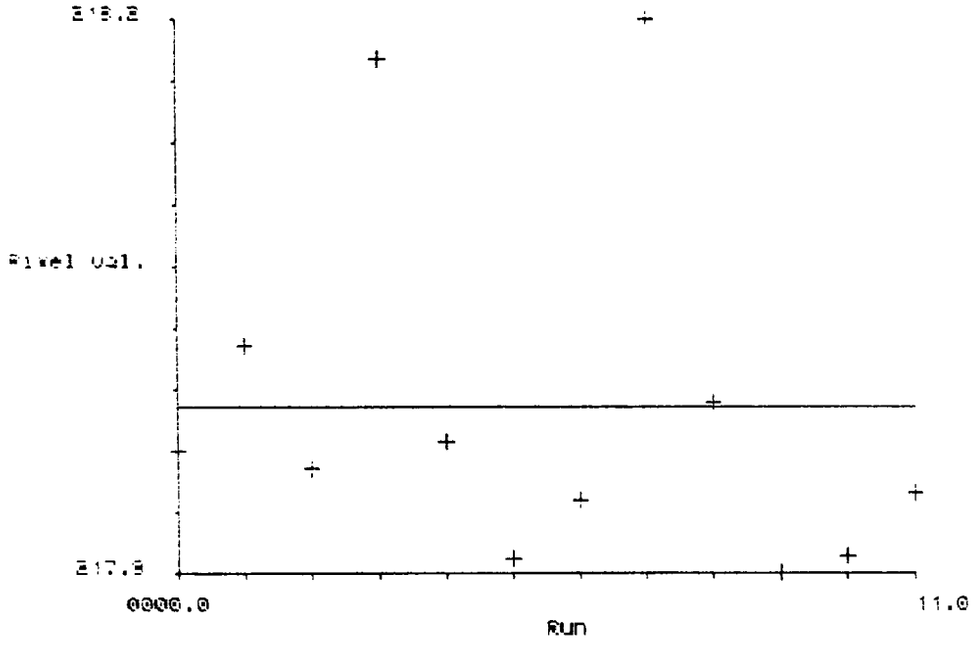

mat.1 50mm f2 mthd 4

Mean of difference= .1075

Standard deviation= .0732

Maximum deviation = .2581

First data point= 00 last data point= 12

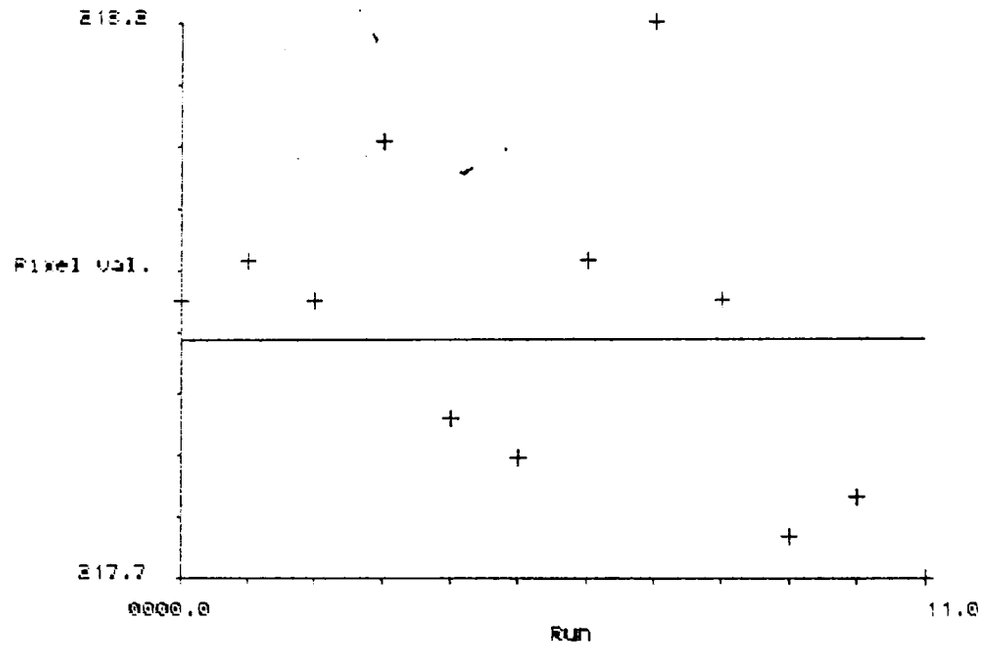

12

mat.2 8mm f8 mthd 3
Mean of difference= .0700
Standard deviation= .0047
Maximum deviation = .0851
First data point= 00 last data point= 12

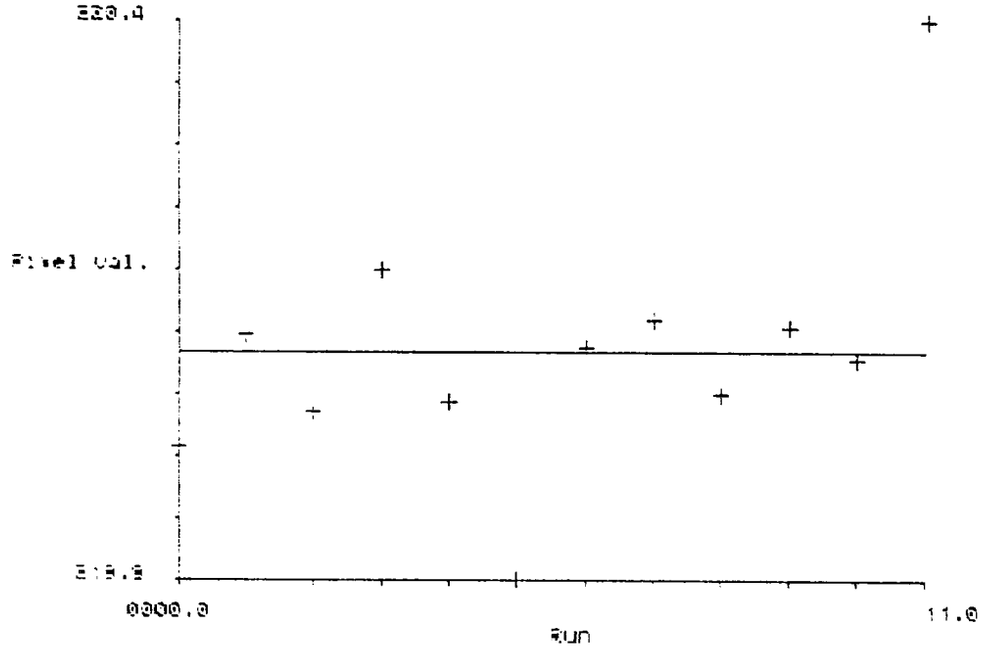

mat.2 8mm f8 mthd 4
Mean of difference= .0006
Standard deviation= .0029
Maximum deviation = .0057
First data point= 00 last data point= 12

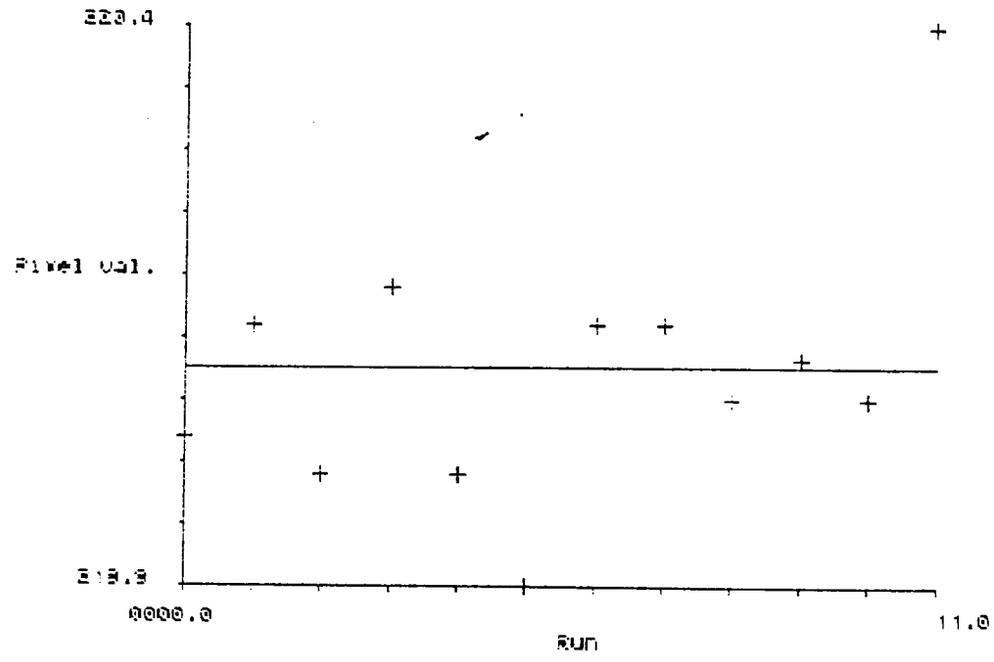

mat.2 6mm #4 mthd 3
Mean of differences= .1403
Standard deviation= .0016
Maximum deviation = .3637
First data point= 00 last data point= 12

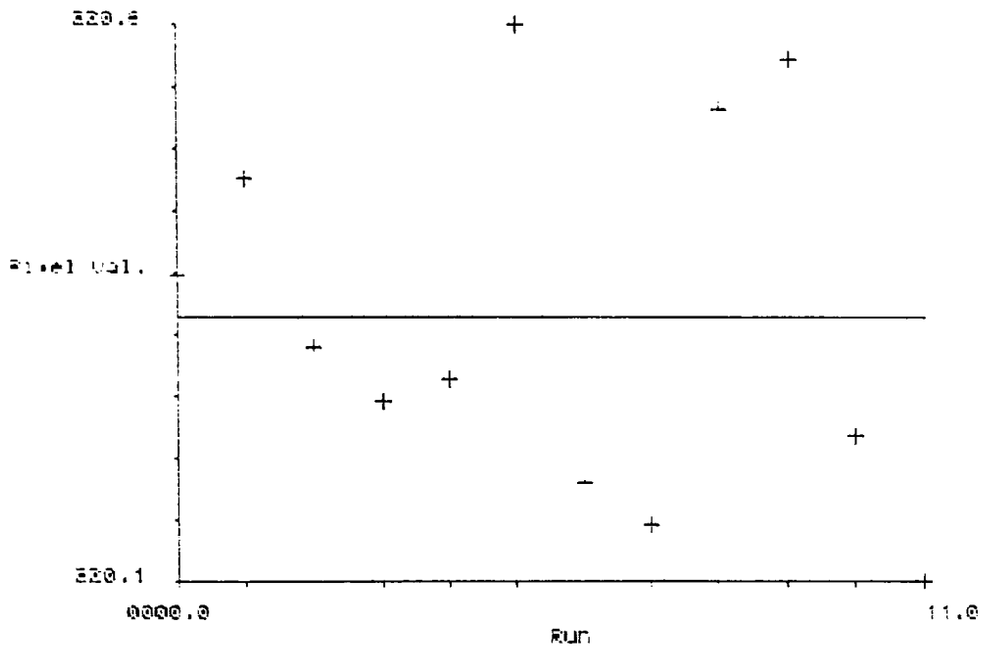

mat.2 6mm #4 mthd 4
Mean of differences= .1585
Standard deviation= .0044
Maximum deviation = .2688
First data point= 00 last data point= 12

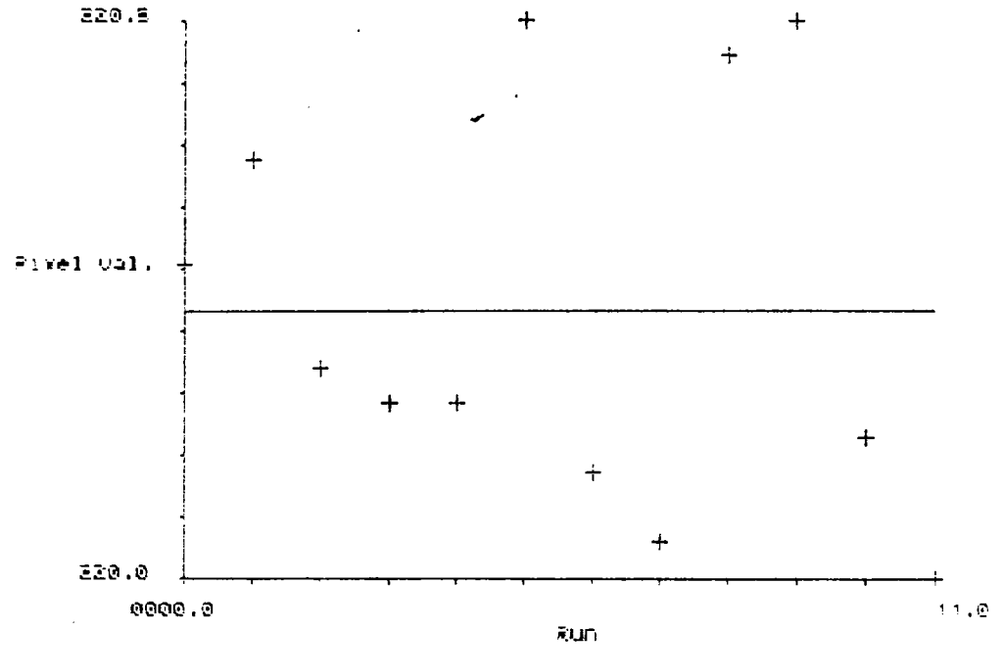

mat.2 8mm f2 mthd 3

Mean of difference= .0787

Standard deviation= .0574

Maximum deviation = .1983

First data point= 00 last data point= 12

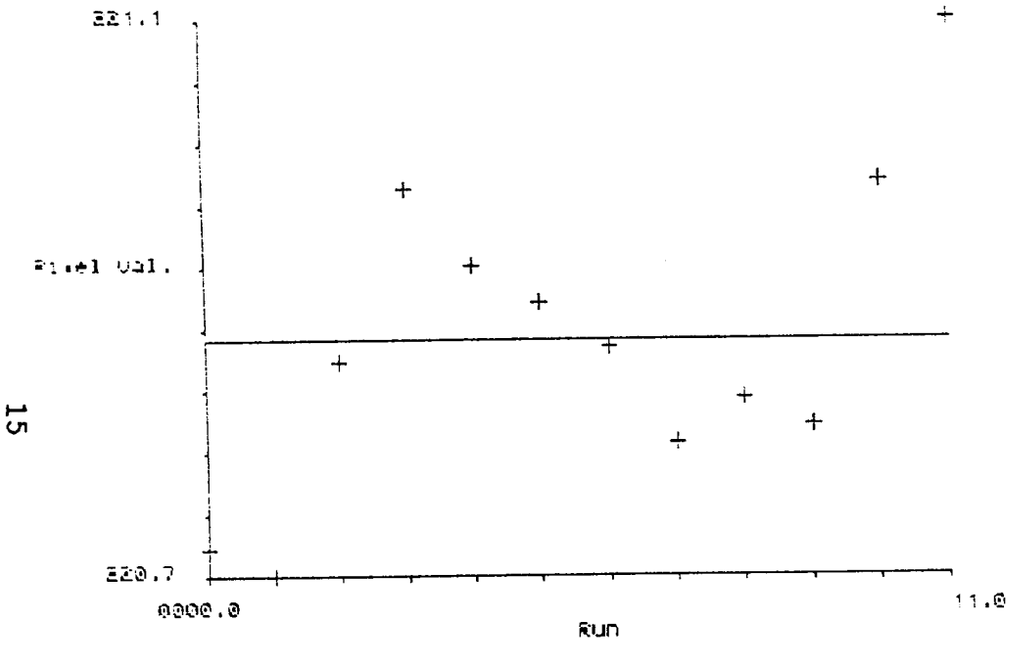

mat.2 8mm f2 mthd 4

Mean of difference= .0535

Standard deviation= .0355

Maximum deviation = .1183

First data point= 00 last data point= 12

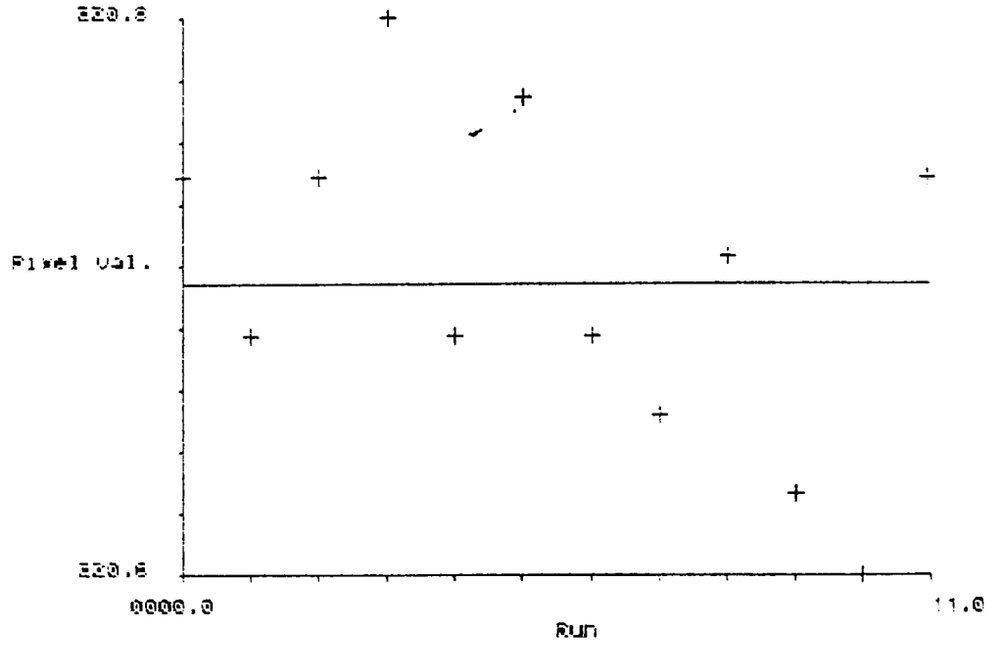

mat.2 25mm f8 mthd 3

Mean of differences= .0983

Standard deviation= .0614

Maximum deviation = .1896

First data point= 00 last data point= 12

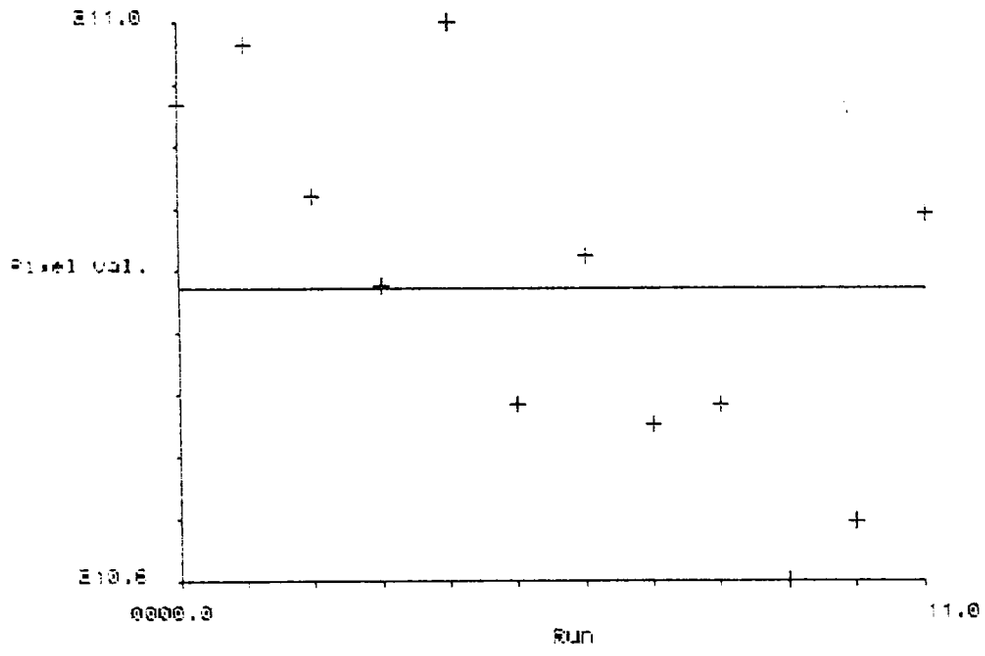

mat.2 25mm f8 mthd 4

Mean of differences= .1075

Standard deviation= .0794

Maximum deviation = .2581

First data point= 00 last data point= 12

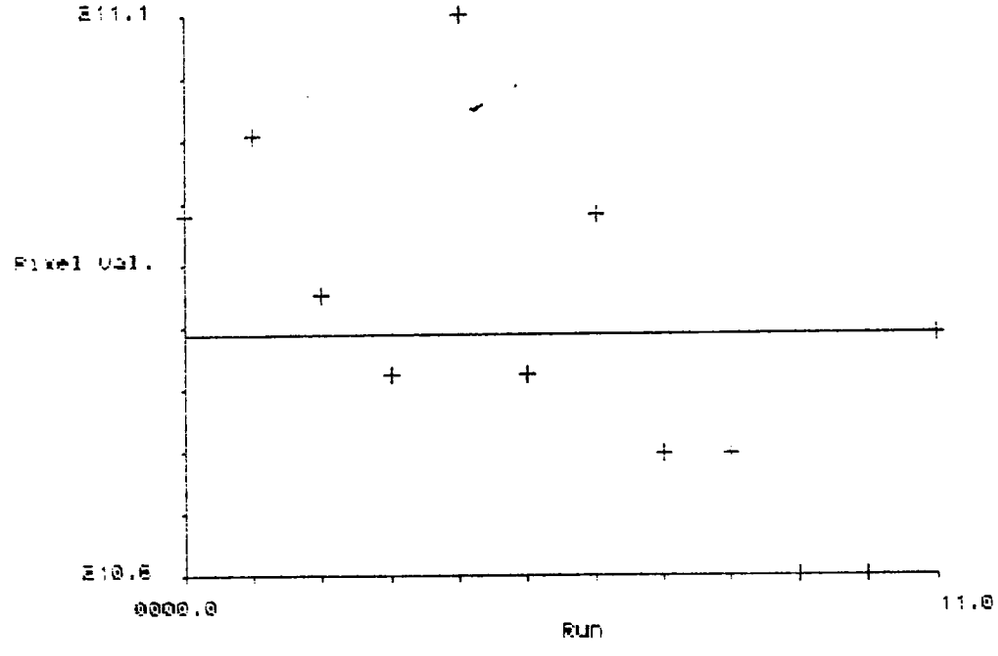

mat.2 25mm f2 mthd 3

Mean of differences= .0334

Standard deviation= .0259

Maximum deviation = .0841

First data point= 00 last data point= 12

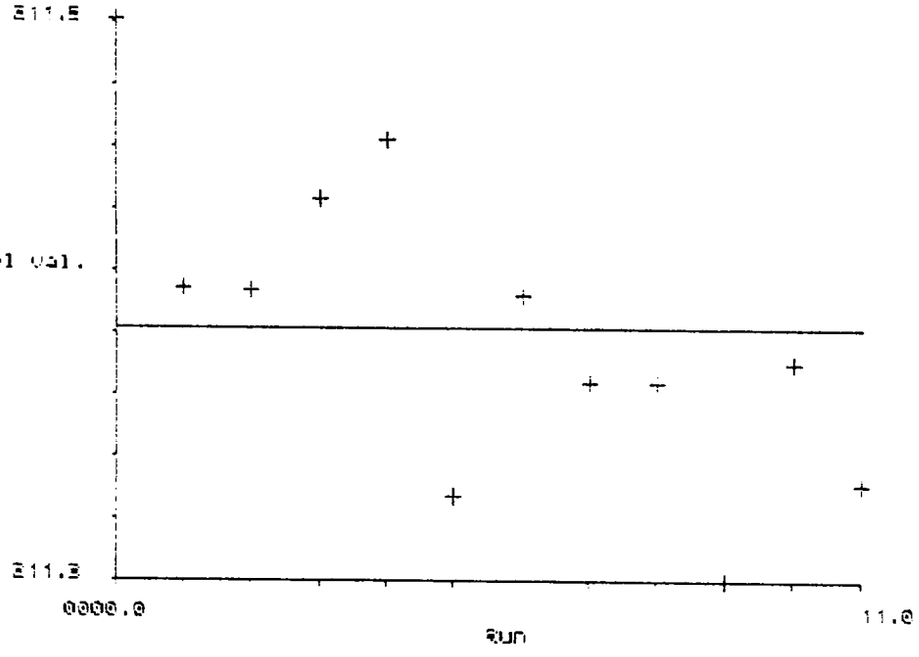

mat.2 25mm f2 mthd 4

Mean of differences= .0497

Standard deviation= .0260

Maximum deviation = .1071

First data point= 00 last data point= 12

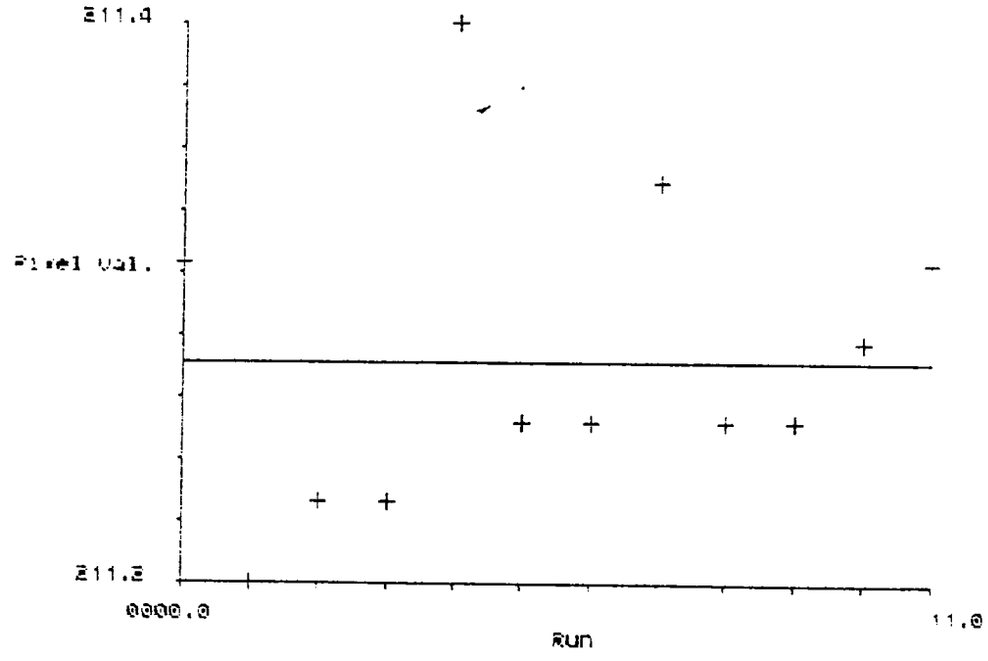

17

B14

mat.2 25mm f4 mthd 3

Mean of difference= .0783

Standard deviation= .0536

Maximum deviation = .1885

First data point= 00 last data point= 12

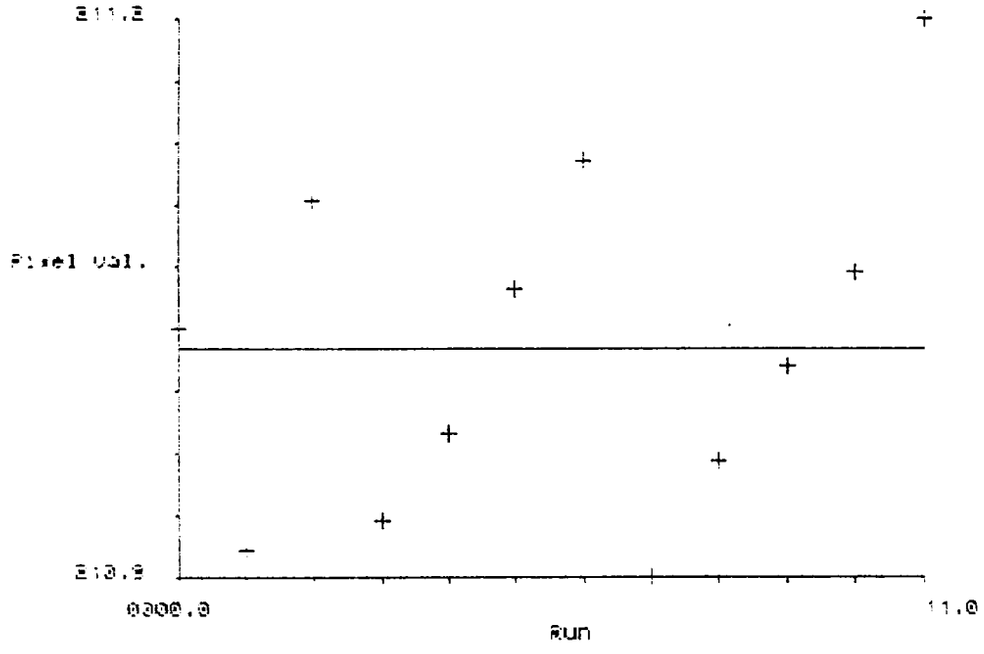

mat.2 25mm f4 mthd 4

Mean of difference= .0784

Standard deviation= .0567

Maximum deviation = .1586

First data point= 00 last data point= 12

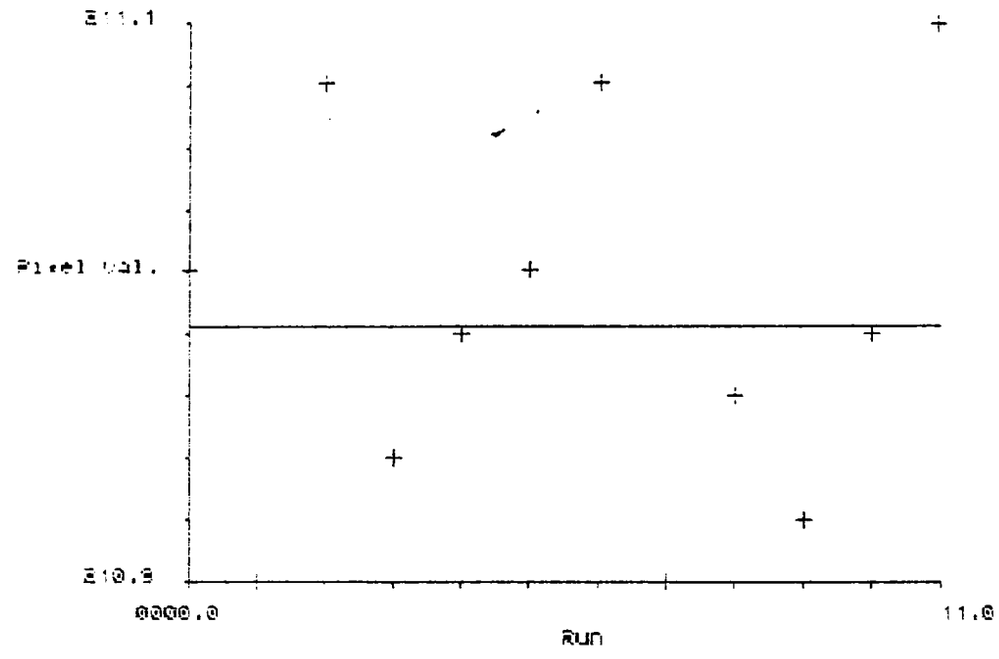

Mat.2 50mm f8 mthd 3

Mean of difference= .3533

Standard deviation= .2460

Maximum deviation = .7867

First data point= 00 last data point= 12

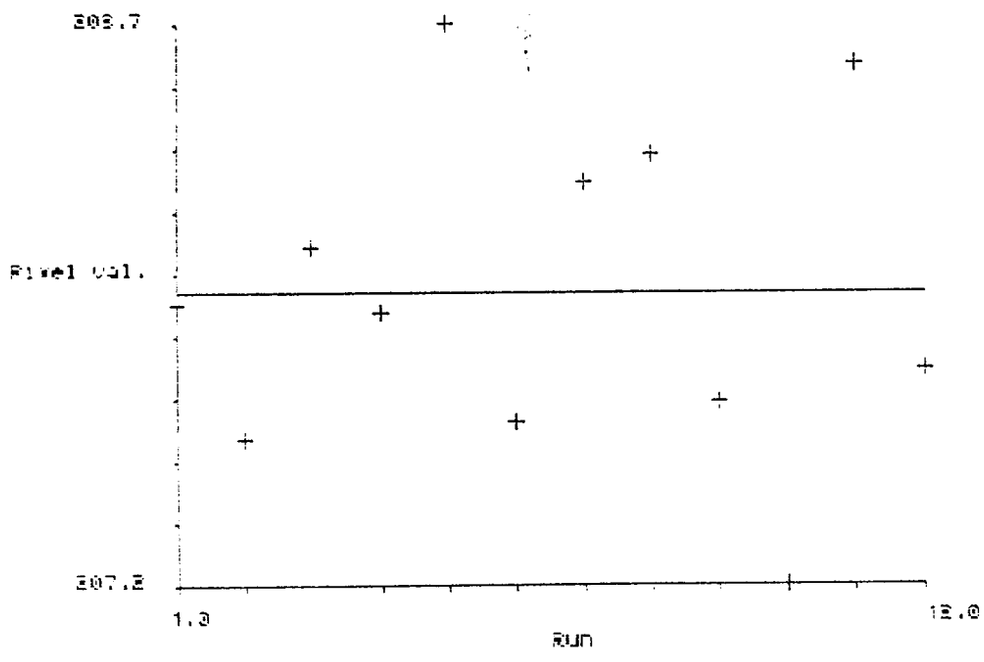

Mat.2 50mm f8 mthd 4

Mean of difference= .3481

Standard deviation= .2725

Maximum deviation = .5790

First data point= 00 last data point= 12

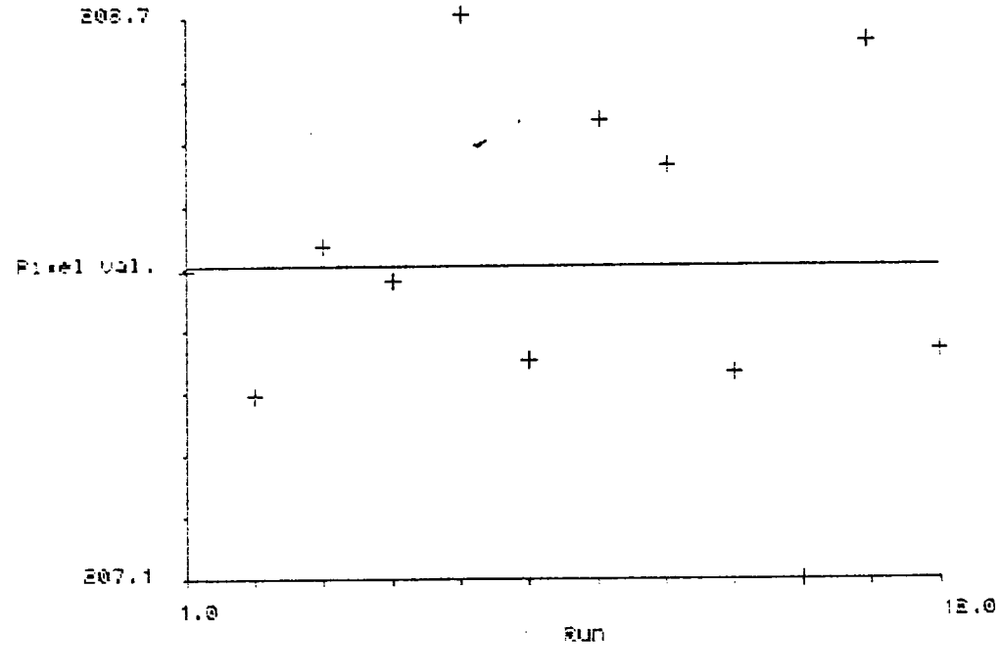

Mat.2 50mm f4 mthd 3

Mean of differences= .1264

Standard deviation= .1052

Maximum deviation = .3711

First data point= 00 last data point= 12

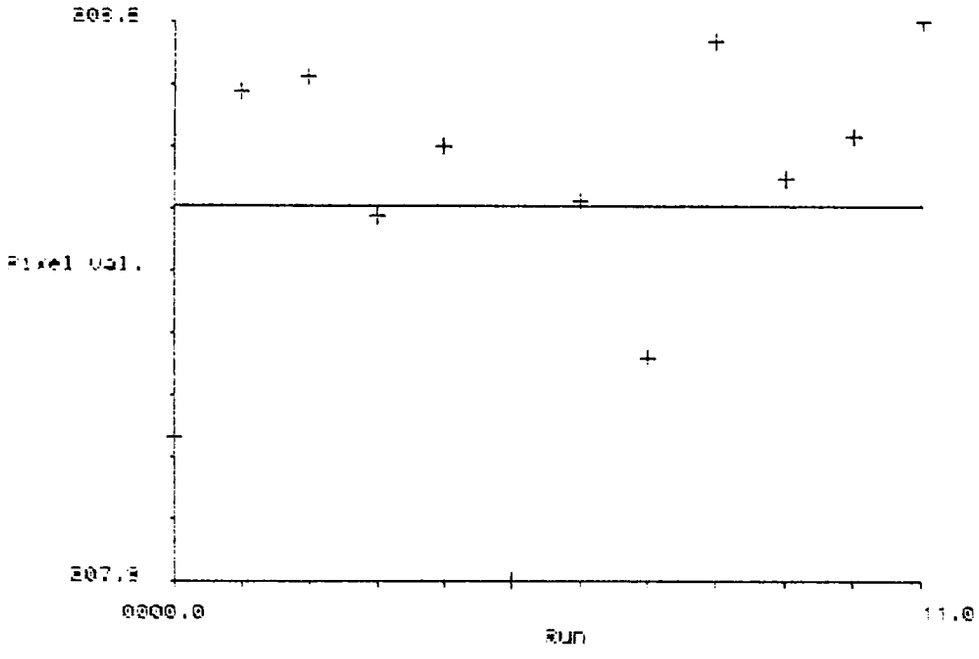

Mat.2 50mm f4 mthd 4

Mean of differences= .1434

Standard deviation= .1091

Maximum deviation = .3804

First data point= 00 last data point= 12

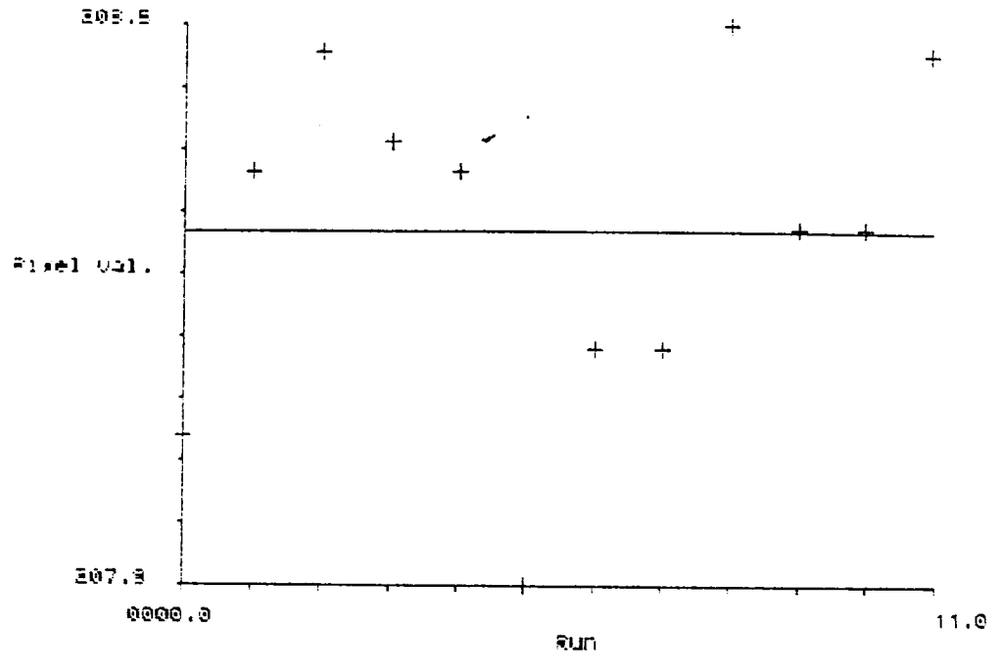

mat.2 50mm f2 mthd 3
Mean of differences= .0489
Standard deviation= .0483
Maximum deviation = .1409
First data point= 00 last data point= 12

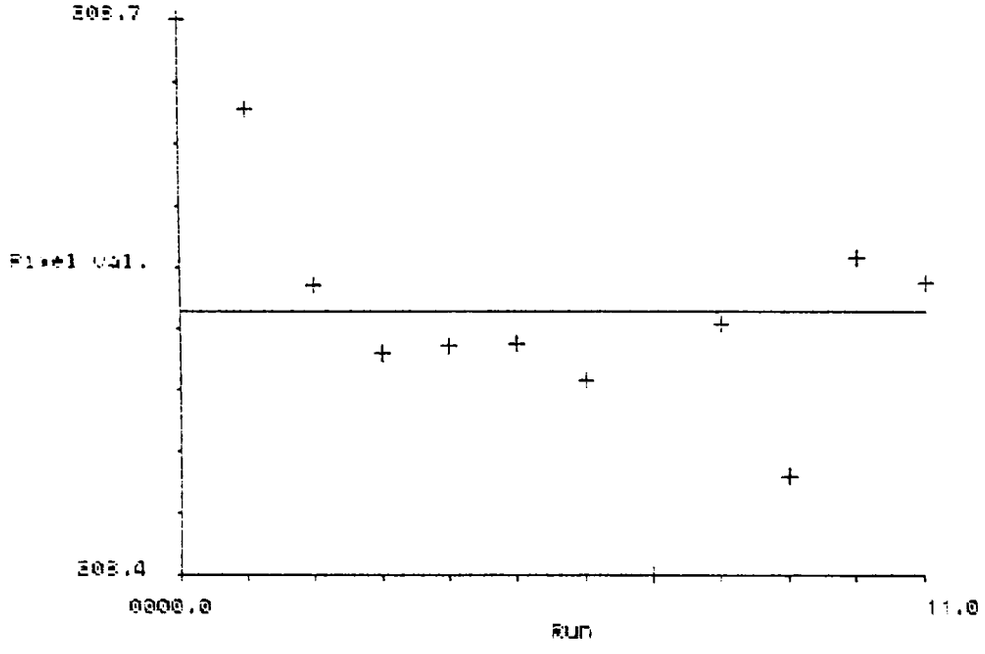

mat.2 50mm f2 mthd 4
Mean of differences= .0860
Standard deviation= .0679
Maximum deviation = .1936
First data point= 00 last data point= 12

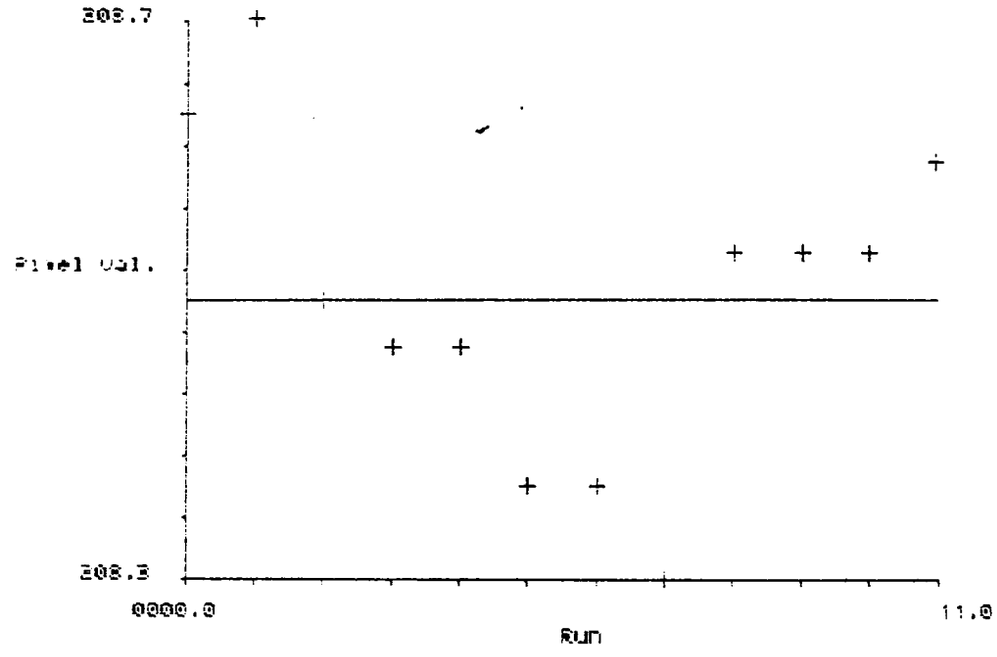

mat.3 8mm f8 mthd 3
Mean of differences= .1265
Standard deviation= .0780
Maximum deviation = .2659
First data point= 00 last data point= 12

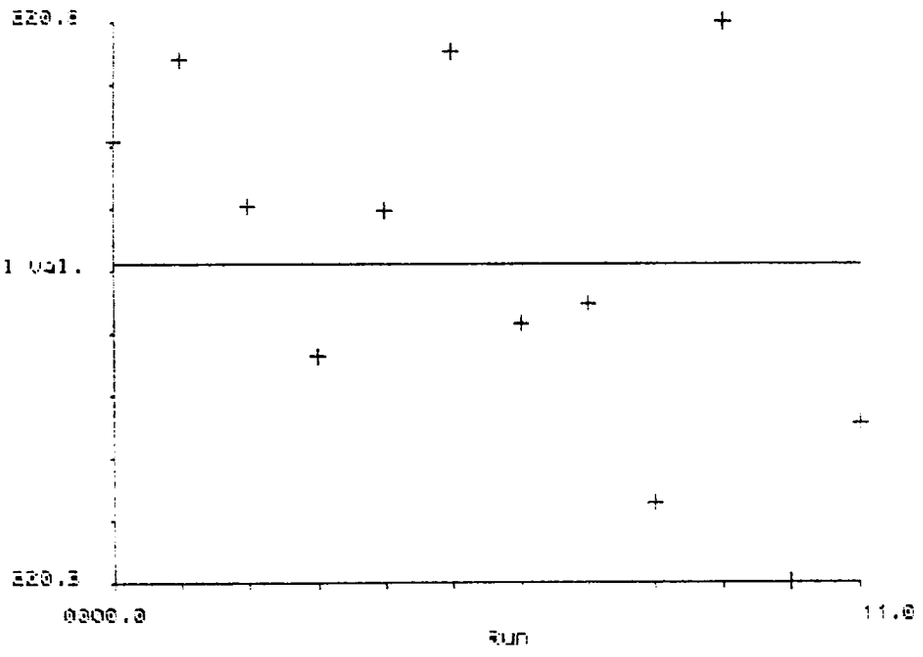

mat.3 8mm f8 mthd 4
Mean of differences= .1344
Standard deviation= .0794
Maximum deviation = .2742
First data point= 00 last data point= 12

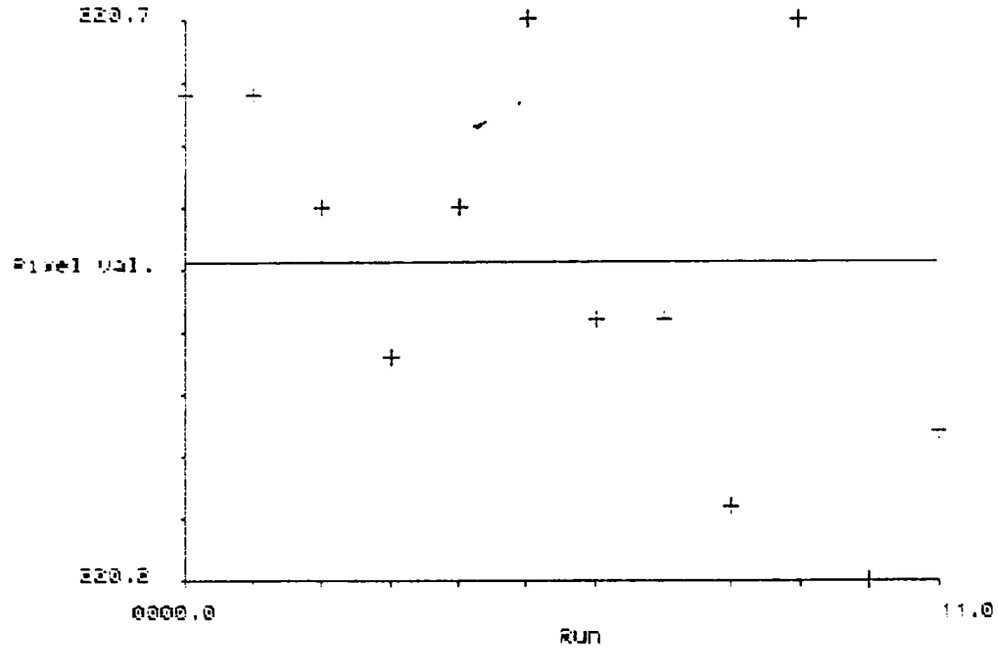

mat.3 8mm f4 mthd 3
Mean of difference= .0788
Standard deviation= .0656
Maximum deviation = .2114
First data point= 00 last data point= 12

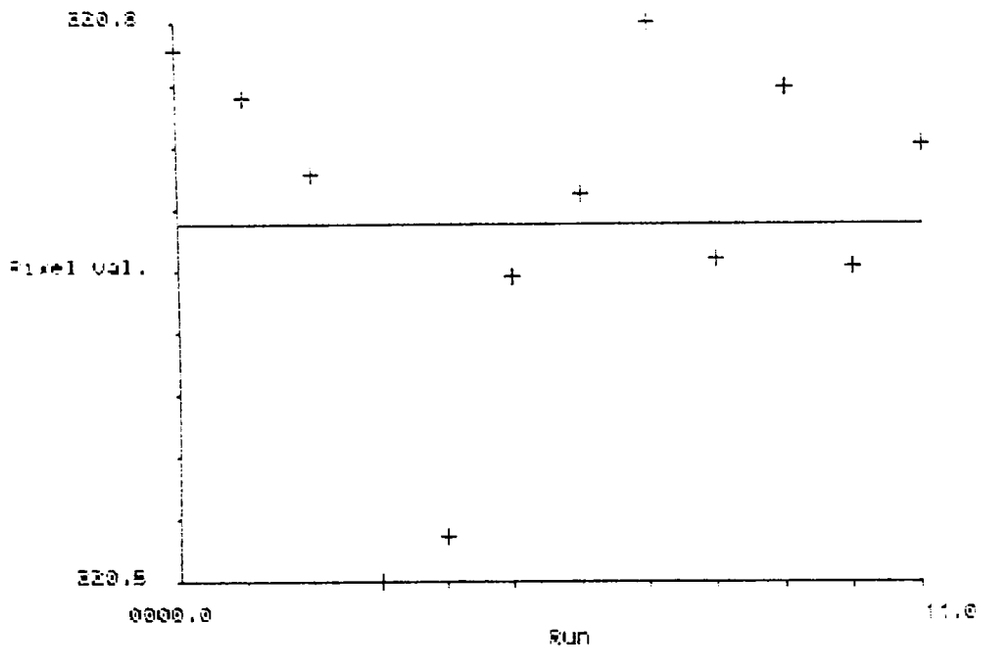

mat.3 8mm f4 mthd 4
Mean of difference= .0712
Standard deviation= .0543
Maximum deviation = .1694
First data point= 00 last data point= 12

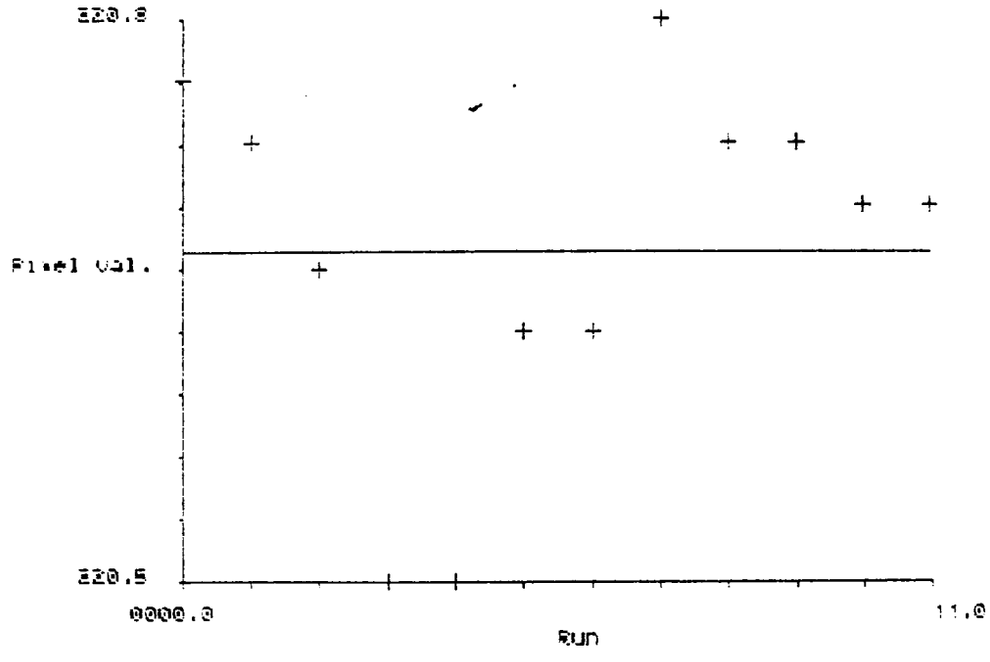

Mat.3 8mm f2 mthd 3

Mean of difference= .0366

Standard deviation= .0224

Maximum deviation = .0889

First data point= 00 last data point= 12

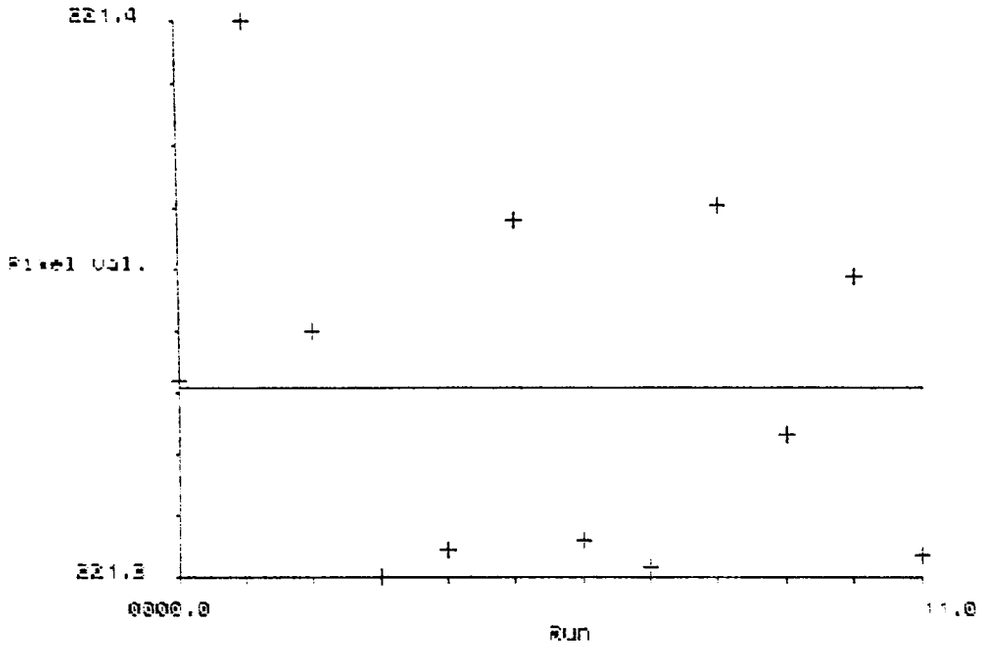

Mat.3 8mm f2 mthd 4

Mean of difference= .0565

Standard deviation= .0391

Maximum deviation = .1425

First data point= 00 last data point= 12

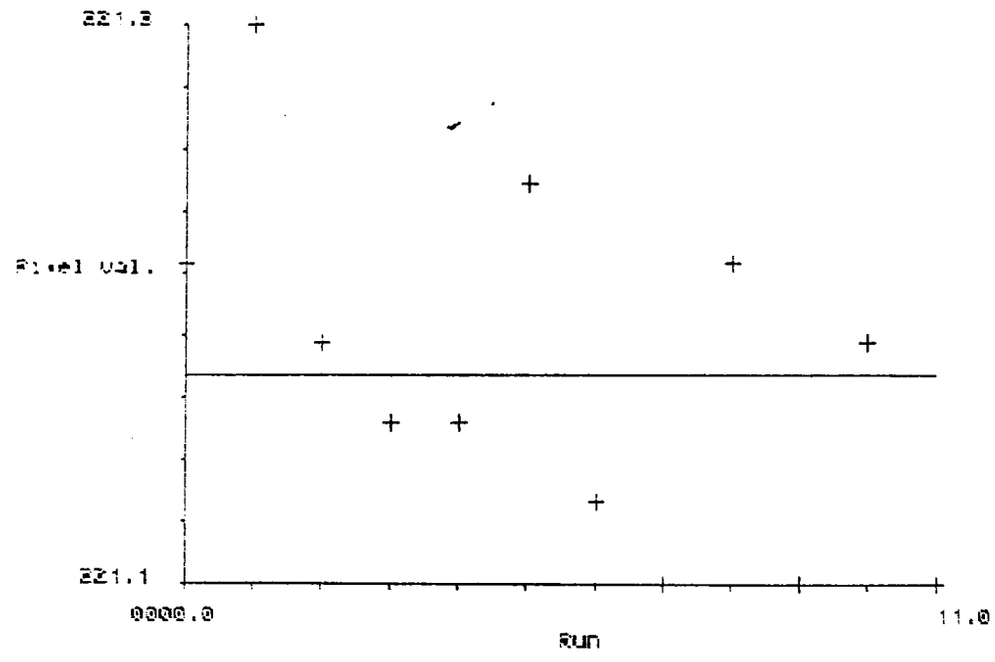

mat.3 35mm f8 mthd 3
Mean of difference= .1041
Standard deviation= .0564
Maximum deviation = .1949
First data point= 00 last data point= 12

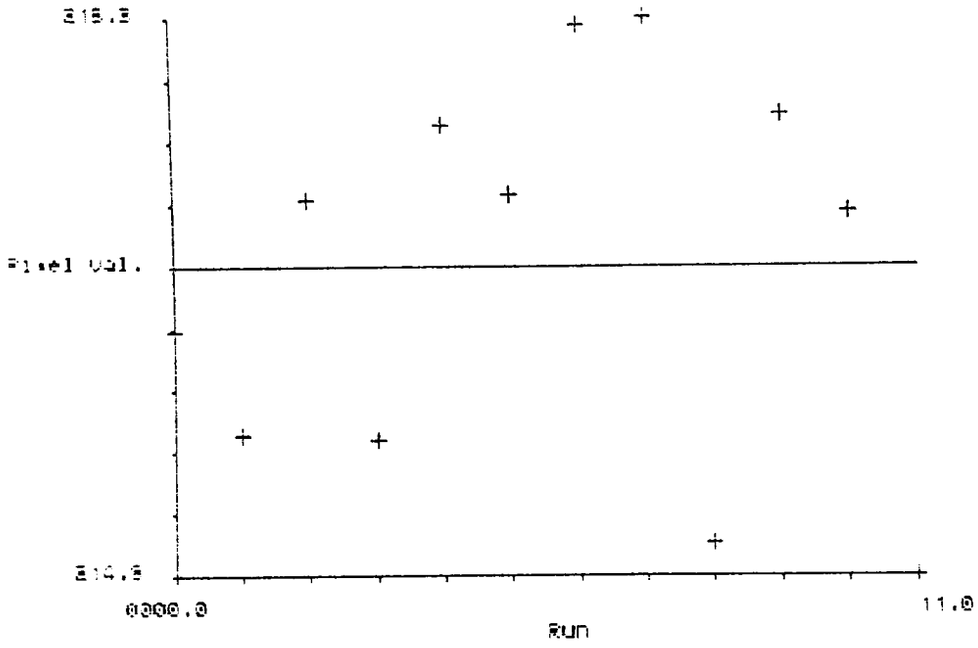

mat.3 35mm f8 mthd 4
Mean of difference= .1246
Standard deviation= .0636
Maximum deviation = .2527
First data point= 00 last data point= 12

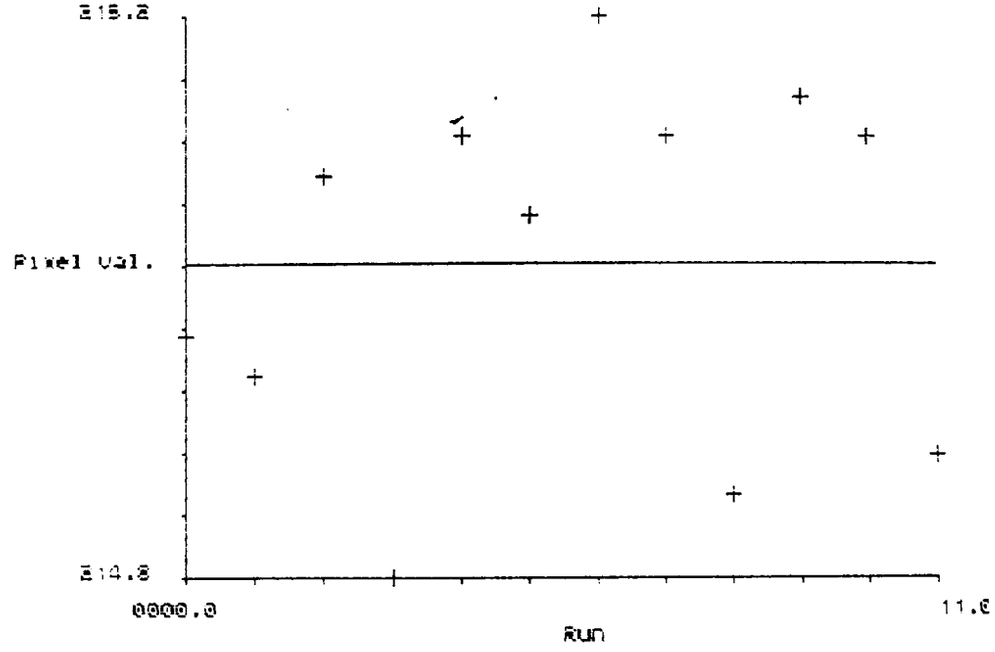

Mat.3 25mm f4 mthd 3

Mean of difference= .0643

Standard deviation= .0393

Maximum deviation = .1319

First data point= 00 last data point= 13

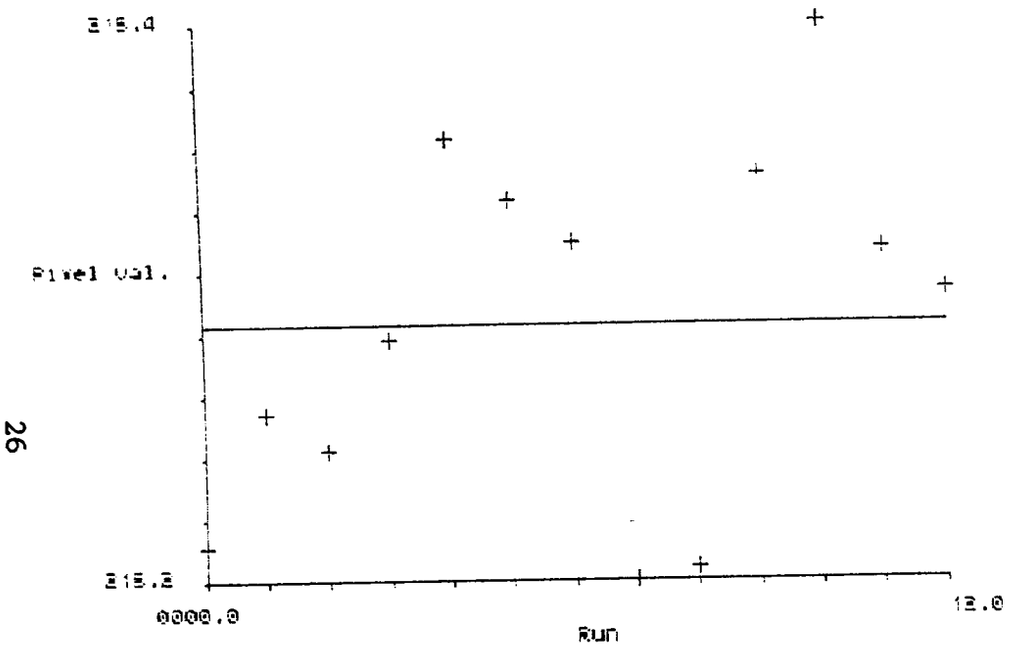

Mat.3 25mm f4 mthd 4

Mean of difference= .0660

Standard deviation= .0568

Maximum deviation = .1588

First data point= 00 last data point= 13

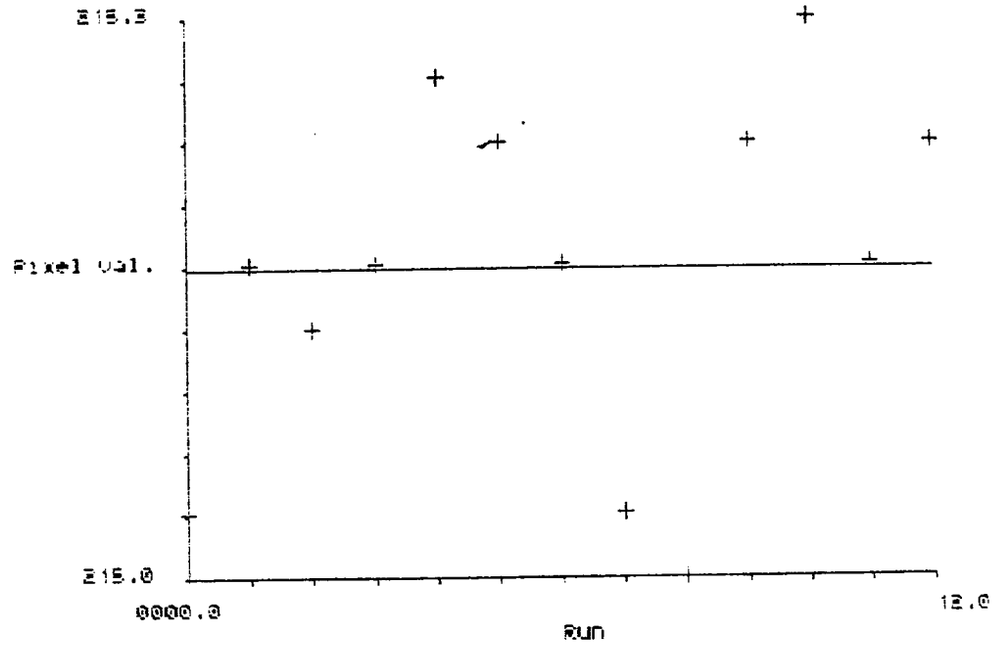

mat.3 25mm f2 mthd 3

Mean of differences= .0328

Standard deviation= .0290

Maximum deviation = .1077

First data point= 00 last data point= 12

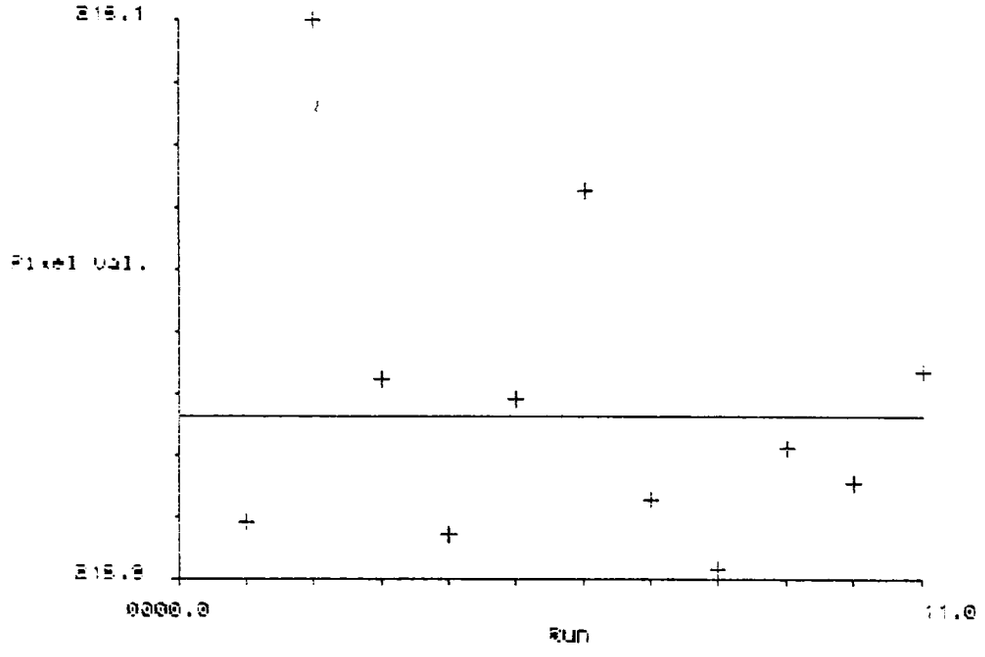

mat.3 25mm f2 mthd 4

Mean of differences= .0511

Standard deviation= .0366

Maximum deviation = .1371

First data point= 00 last data point= 12

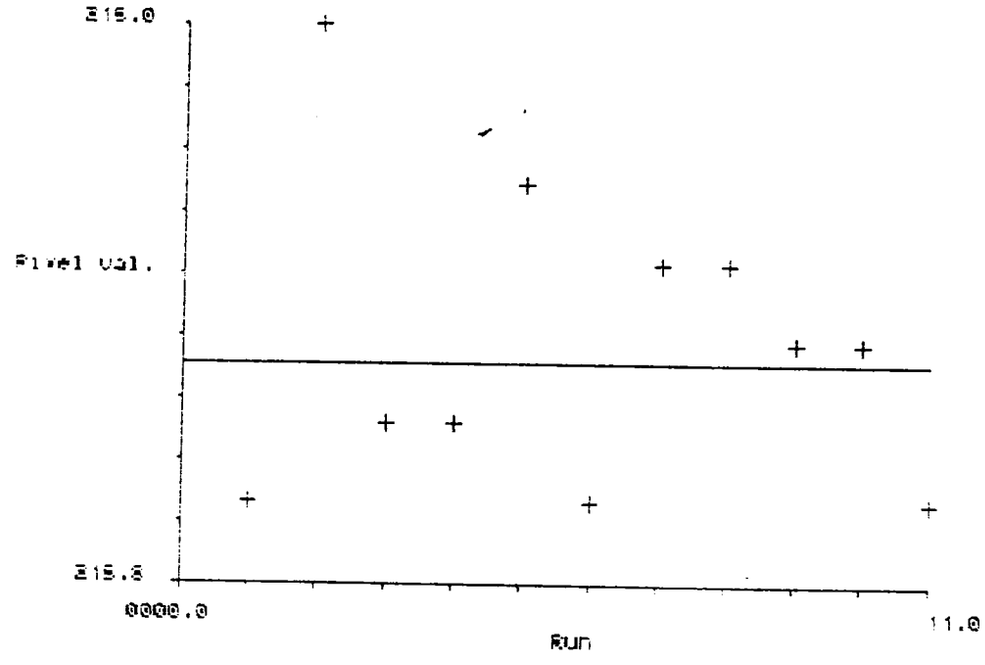

Mat.3 50mm f8 mthd 3

Mean of difference= .1204

Standard deviation= .0987

Maximum deviation = .3662

First data point= 00 last data point= 12

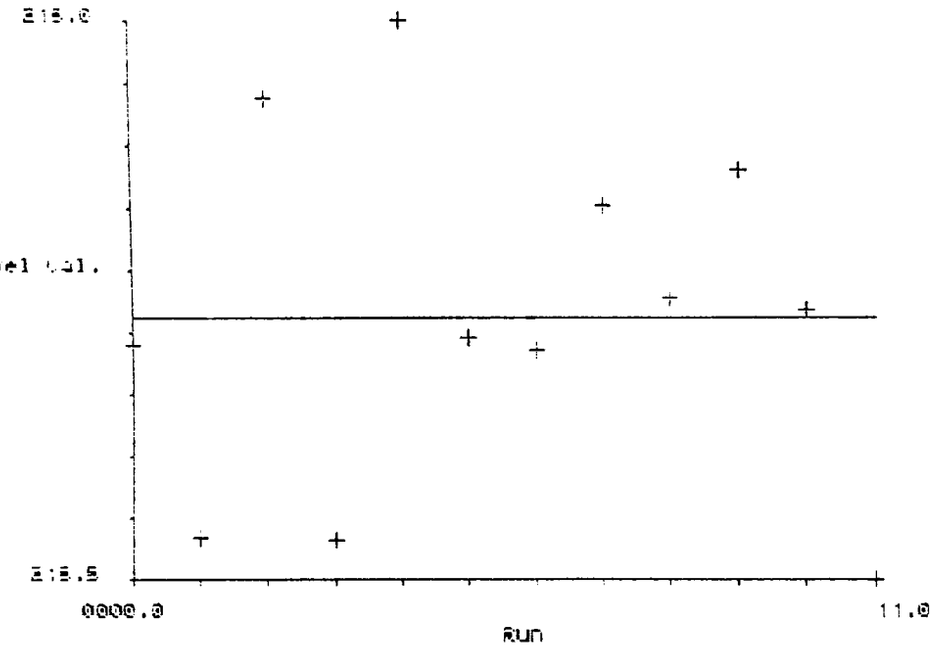

Mat.3 50mm f8 mthd 4

Mean of difference= .1828

Standard deviation= .1431

Maximum deviation = .4883

First data point= 00 last data point= 12

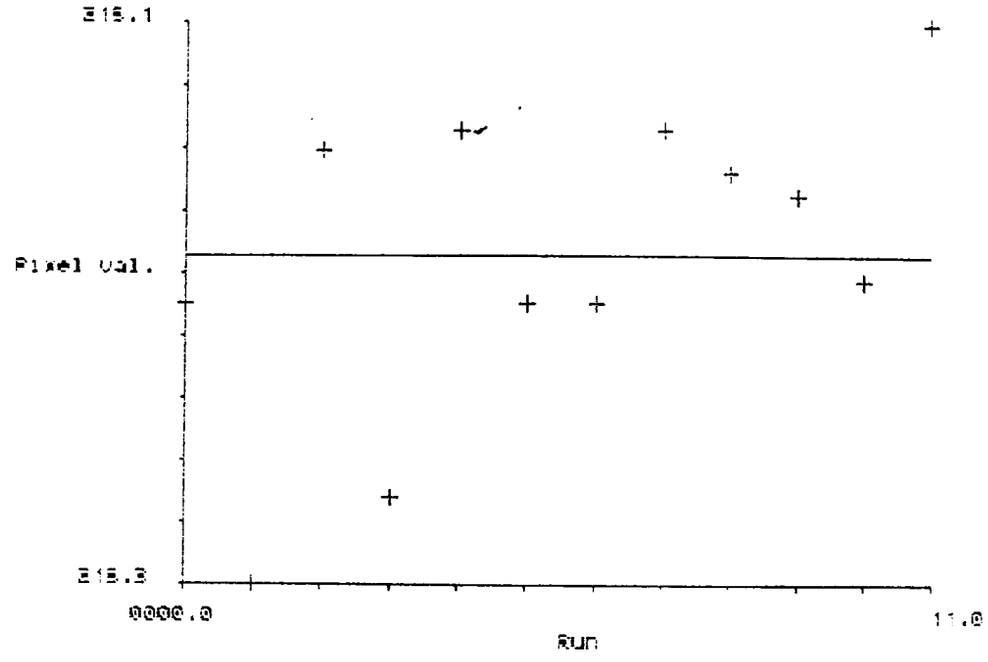

Mat.3 50mm f4 mthd 3
Mean of differences= .0003
Standard deviation= .0582
Maximum deviation = .2276
First data point= 00 last data point= 12

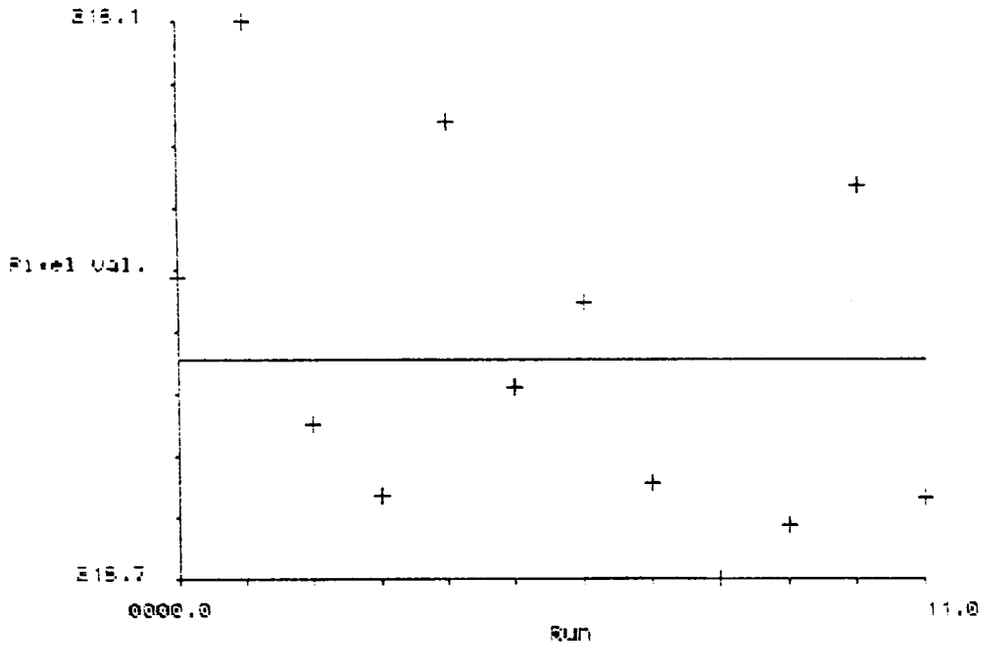

Mat.3 50mm f4 mthd 4
Mean of differences= .1427
Standard deviation= .1064
Maximum deviation = .3360
First data point= 00 last data point= 12

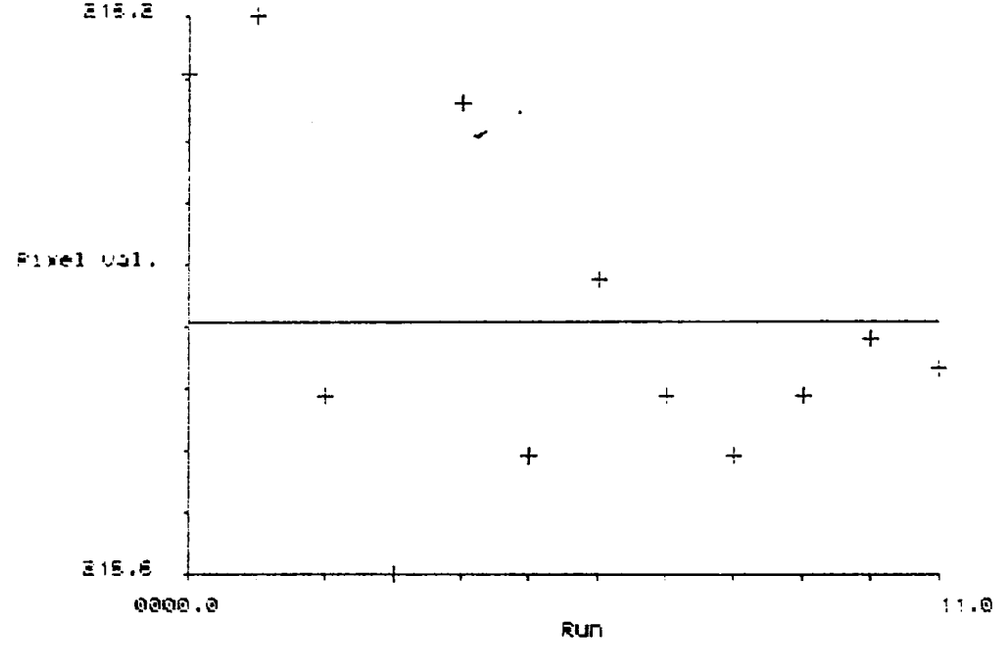

mat.3 50mm f2 mthd 3

Mean of difference= .1477

Standard deviation= .0592

Maximum deviation = .2434

First data point= 00 last data point= 12

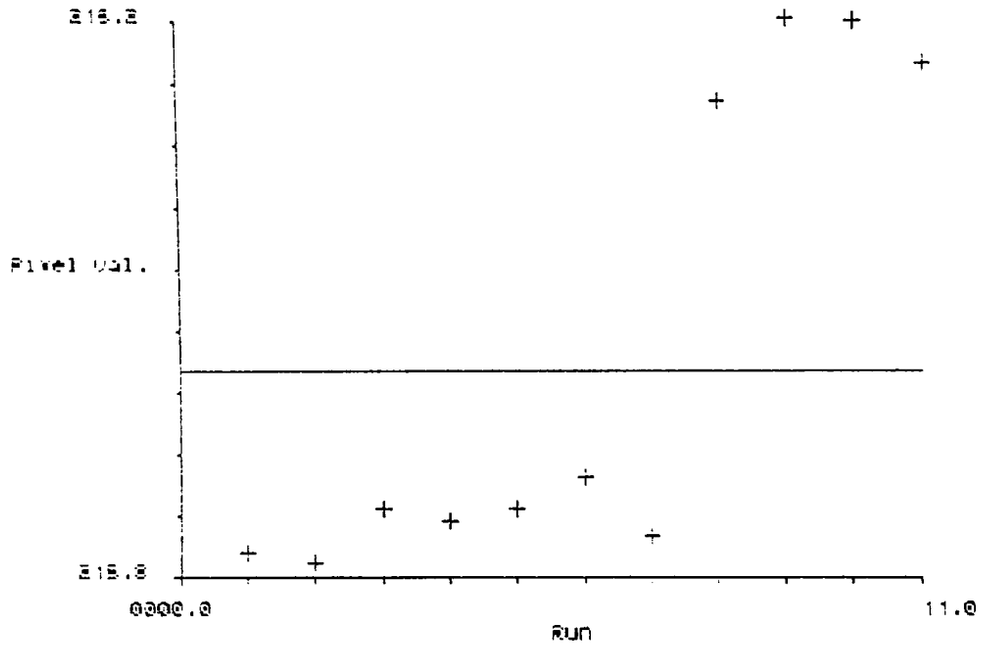

mat.3 50mm f2 mthd 4

Mean of difference= .0753

Standard deviation= .0678

Maximum deviation = .1935

First data point= 00 last data point= 12

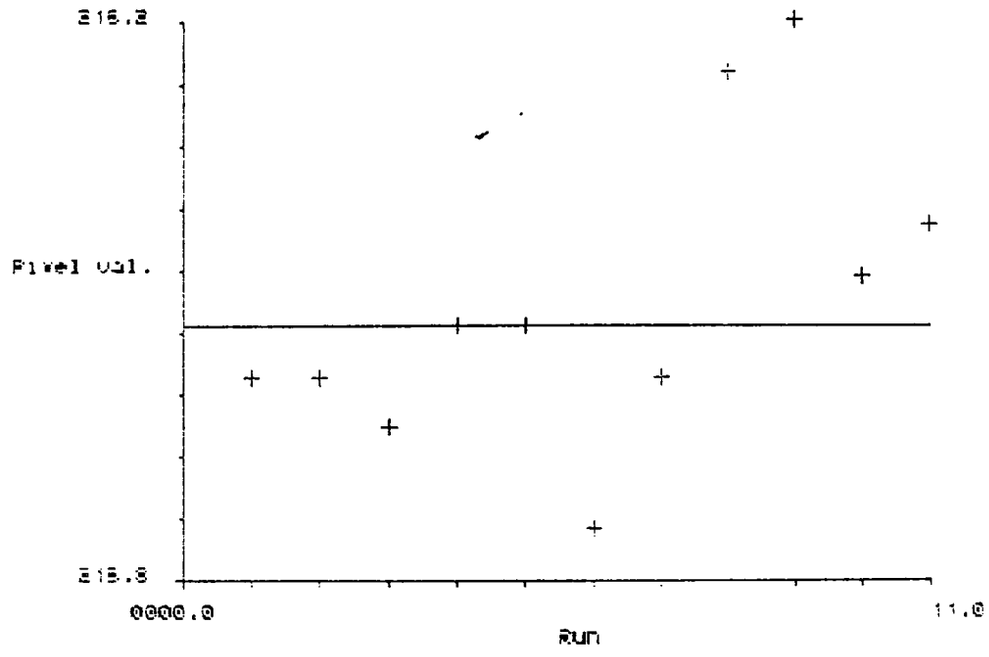

Mat.4 8mm f8 mthd 3
Mean of differences= .2023
Standard deviation= .1777
Maximum deviation = .5062
First data point= 00 last data point= 12

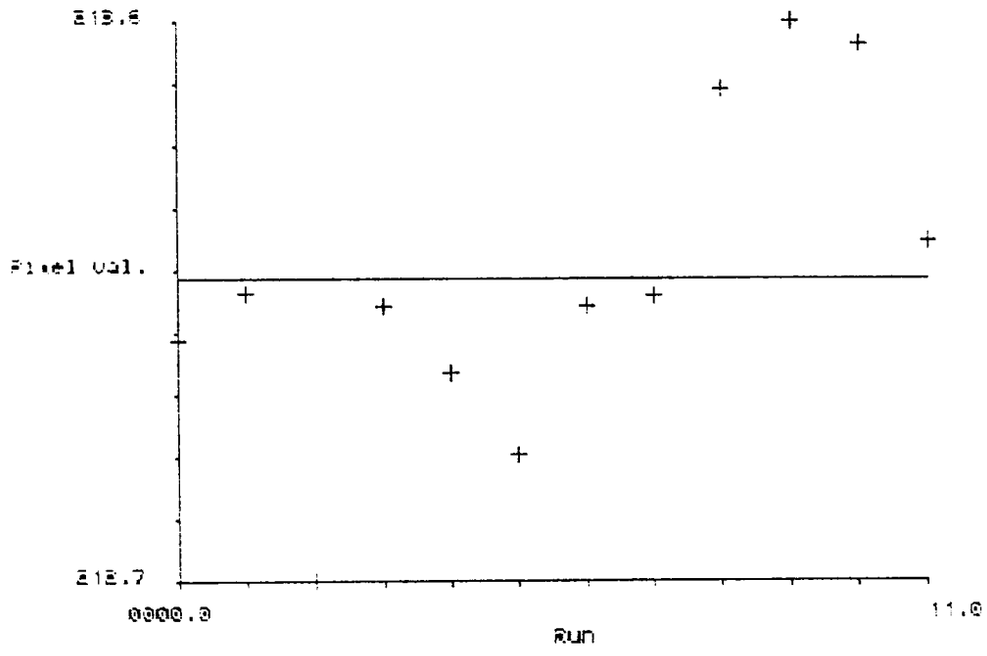

Mat.4 8mm f8 mthd 4
Mean of differences= .2133
Standard deviation= .1640
Maximum deviation = .5054
First data point= 00 last data point= 12

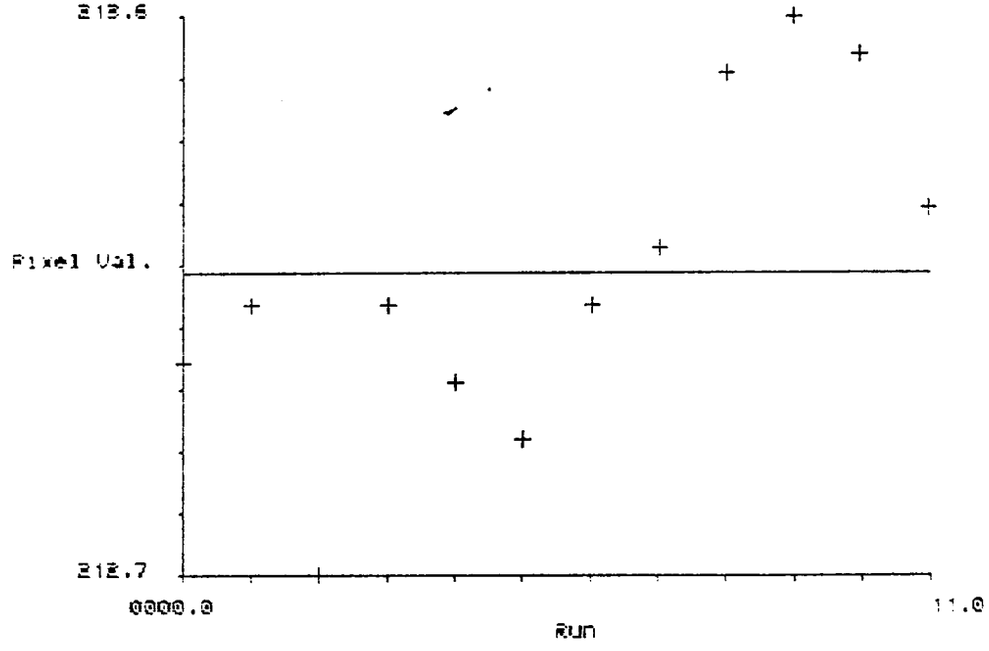

Mat.4 6mm f4 mthd 3
Mean of difference= .1679
Standard deviation= .0062
Maximum deviation = .2980
First data point= 00 last data point= 12

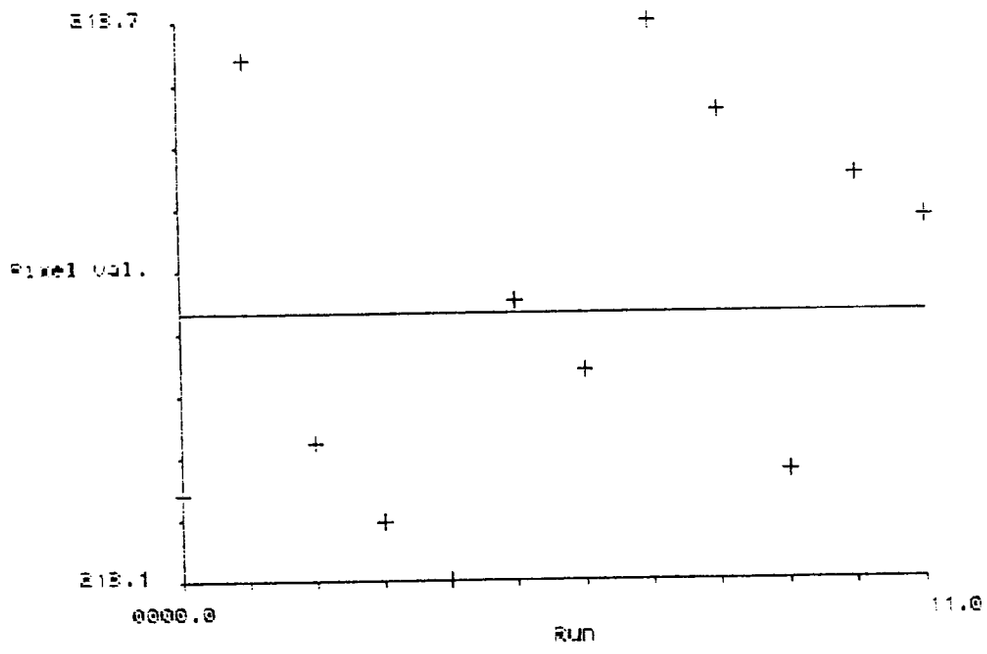

Mat.4 6mm f4 mthd 4
Mean of difference= .1586
Standard deviation= .0007
Maximum deviation = .2930
First data point= 00 last data point= 12

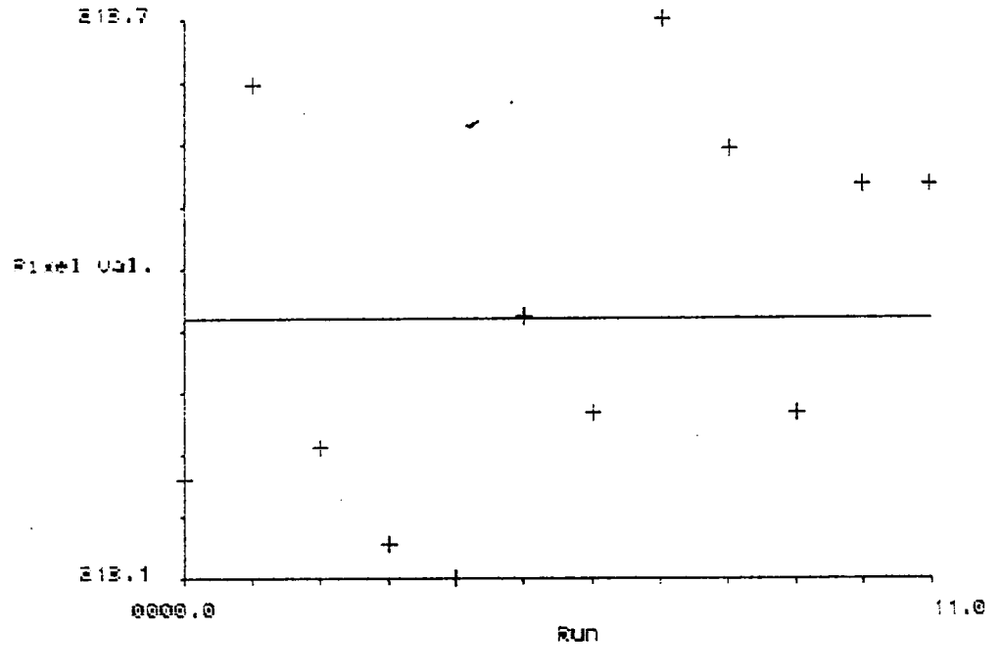

mat.4 5mm f2 mthd 3

Mean of difference= .0888

Standard deviation= .0777

Maximum deviation = .3882

First data point= 00 last data point= 12

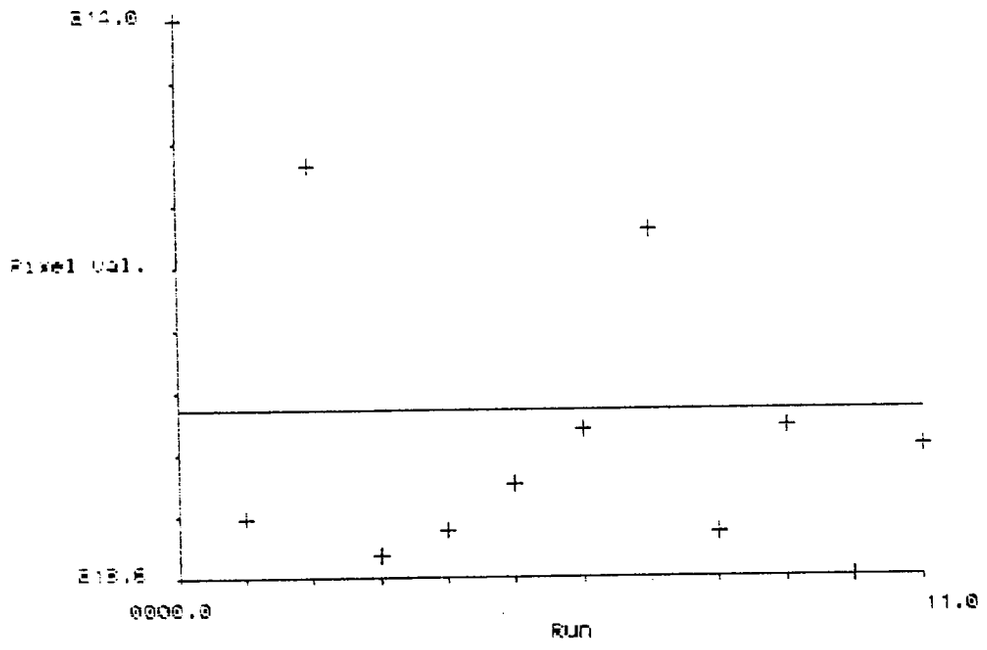

mat.4 5mm f2 mthd 4

Mean of difference= .1474

Standard deviation= .1053

Maximum deviation = .3575

First data point= 00 last data point= 12

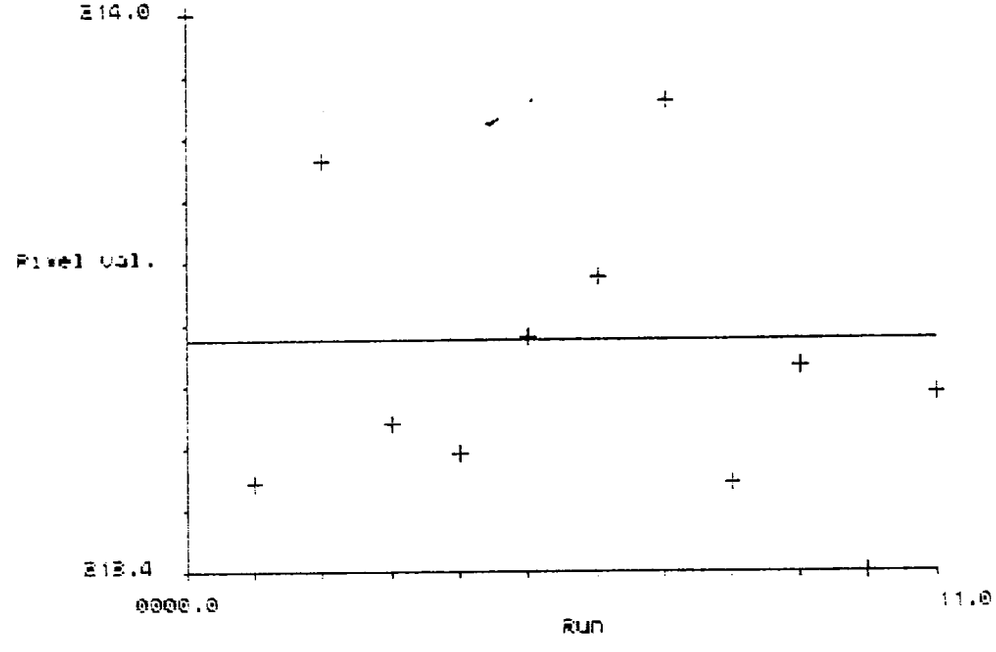

mat.4 25mm f8 mthd 3
Mean of difference= 1.9391
Standard deviation= 3.8484
Maximum deviation = 11.0174
First data point= 00 last data point= 12

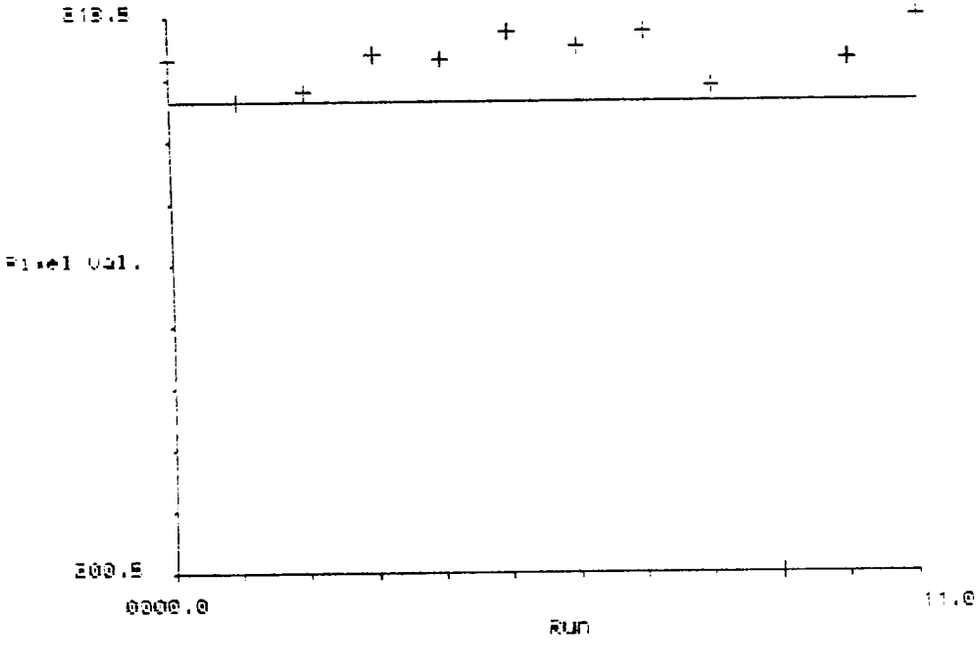

mat.4 25mm f8 mthd 4
Mean of difference= 1.7670
Standard deviation= 3.3236
Maximum deviation = 10.5430
First data point= 00 last data point= 12

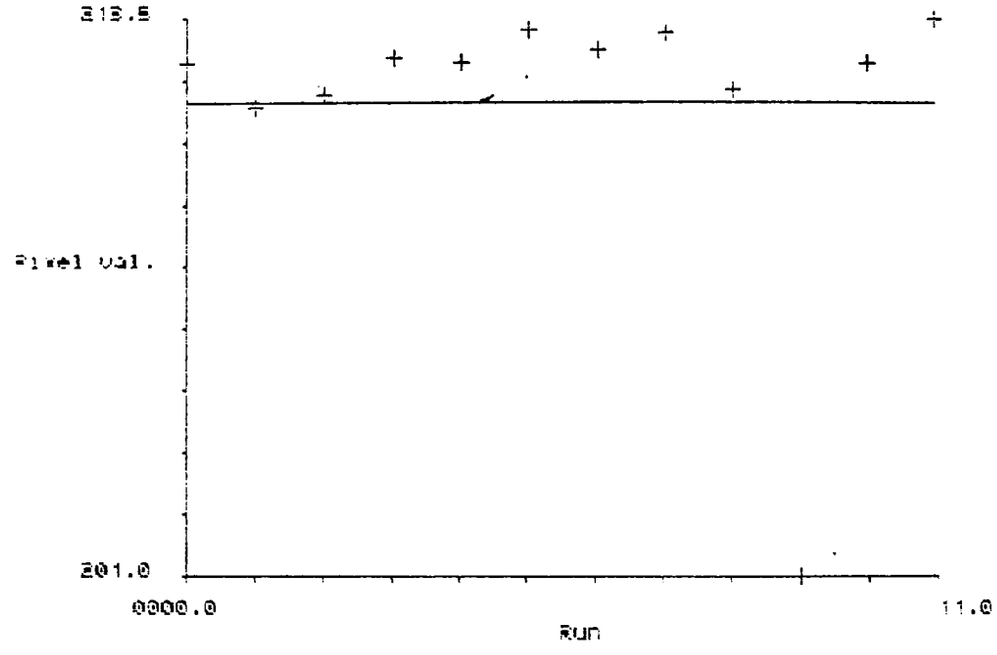

mat.4 25mm f4 mthd 3

Mean of difference= .1466

Standard deviation= .0990

Maximum deviation = .3661

First data point= 00 last data point= 12

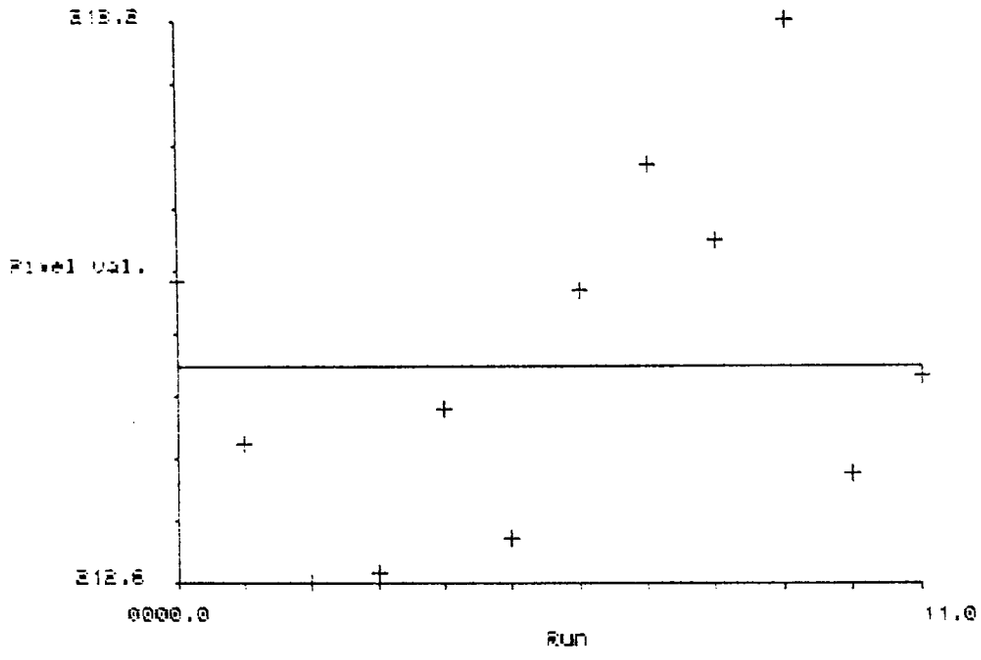

mat.4 25mm f4 mthd 4

Mean of difference= .1694

Standard deviation= .0964

Maximum deviation = .3710

First data point= 00 last data point= 12

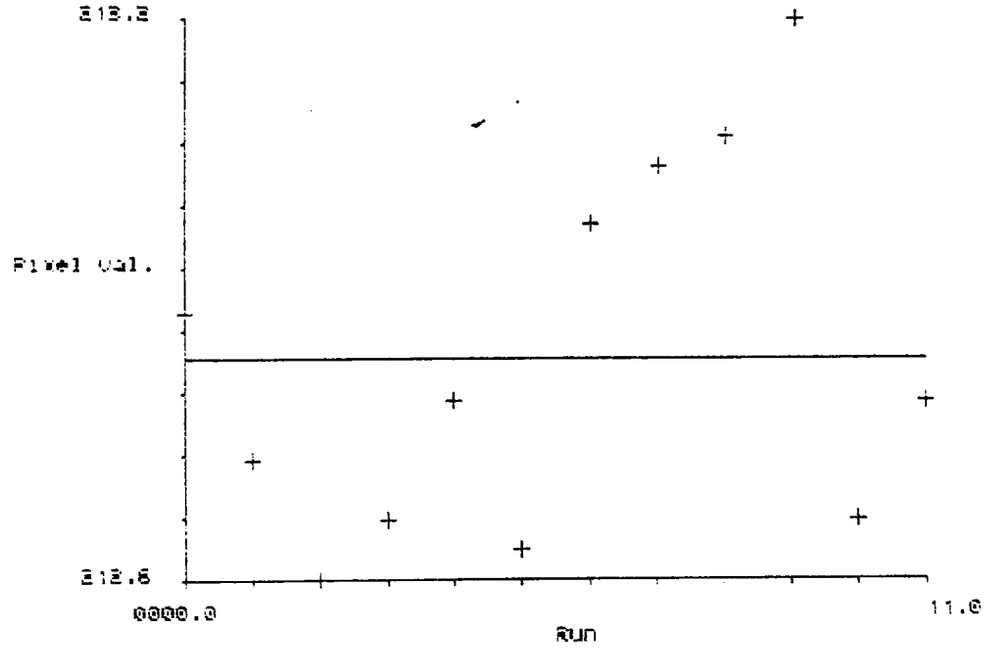

mat.4 25mm f2 mthd 3

Mean of differences= .0587

Standard deviation= .0345

Maximum deviation = .1212

First data point= 00 last data point= 12

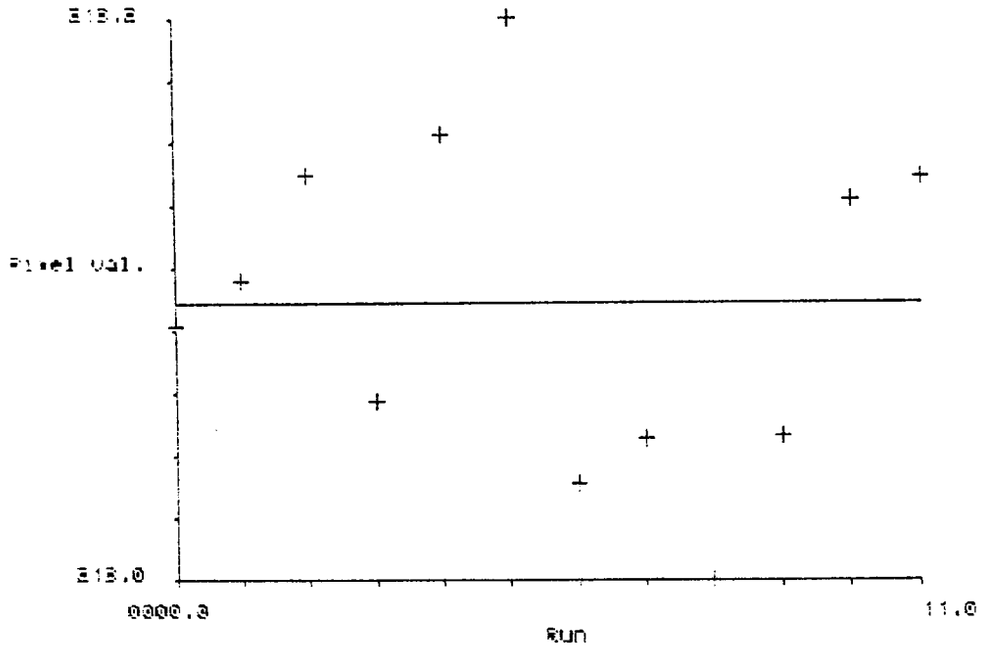

mat.4 25mm f2 mthd 4

Mean of differences= .0600

Standard deviation= .0457

Maximum deviation = .1344

First data point= 00 last data point= 12

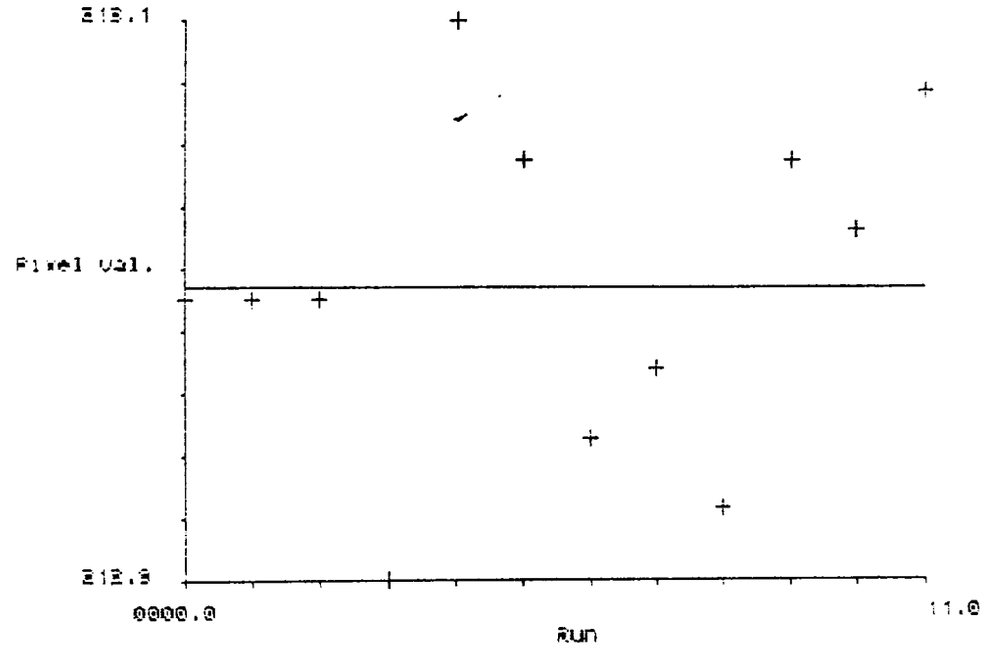

B33

mat.4 50mm f2 mthd 3

Mean of difference= .1809

Standard deviation= .0870

Maximum deviation = .3244

First data point= 00 last data point= 12

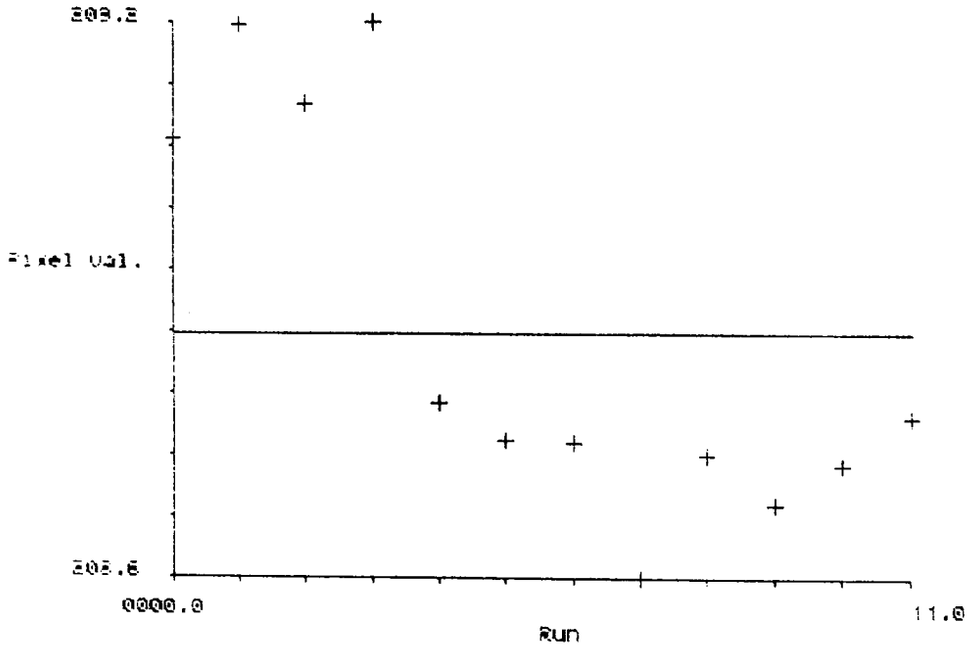

mat.4 50mm f2 mthd 4

Mean of difference= .1962

Standard deviation= .1406

Maximum deviation = .4355

First data point= 00 last data point= 12

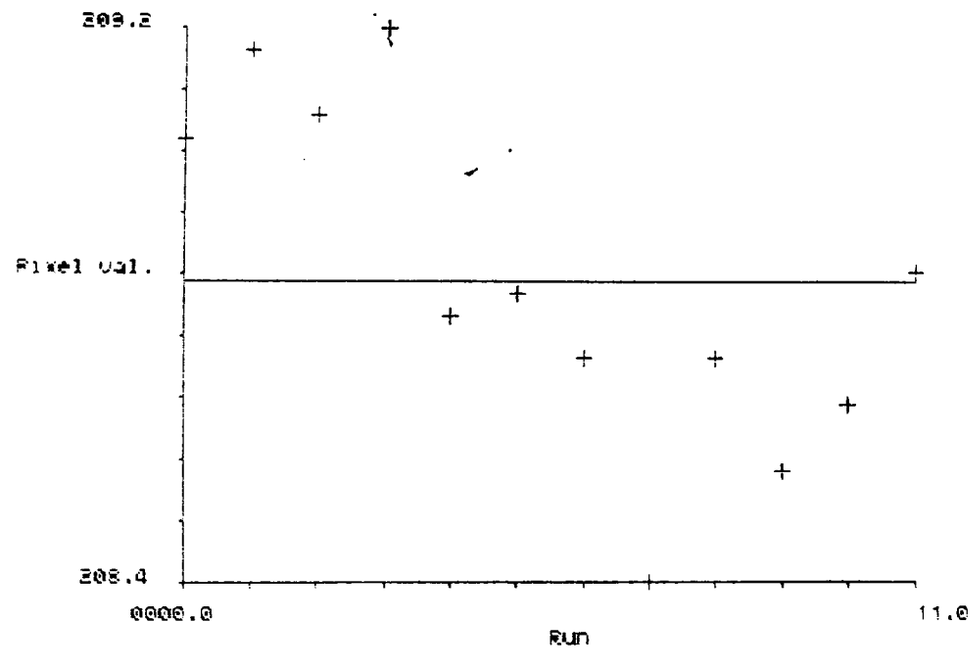

B34

mat.4 50mm f1.2 mthd 3

Mean of differences= .0475

Standard deviation= .0330

Maximum deviation = .1083

First data point= 00 last data point= 12

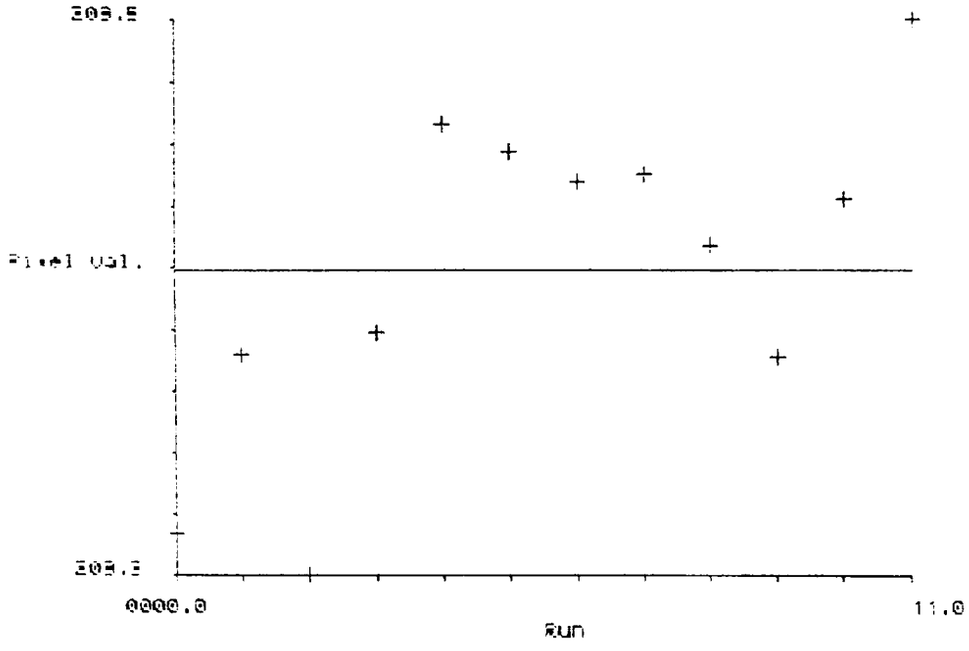

mat.4 50mm f1.2 mthd 4

Mean of differences= .1075

Standard deviation= .0613

Maximum deviation = .2087

First data point= 00 last data point= 12